Title
Ubiquitination and RNA Binding in the Host Antiviral Response to Alphaviruses

Author
Yang, Emily

Publication Date
2022

Peer reviewed|Thesis/dissertation

UNIVERSITY OF CALIFORNIA

Los Angeles

Ubiquitination and RNA Binding in the Host Antiviral Response to Alphaviruses

A dissertation submitted in partial satisfaction of the

requirements for the degree of Doctor of Philosophy

in Molecular Biology

by

Emily Yang

2022

ABSTRACT OF THE DISSERTATION

Ubiquitination and RNA Binding

in the Host Antiviral Response to Alphaviruses

by

Emily Yang

Doctor of Philosophy in Molecular Biology

University of California, Los Angeles, 2022

Professor Melody M. H. Li, Chair

Humanity is plagued by myriad viruses, most of which have no vaccines nor antiviral therapeutics. In order to address this pressing need and stave off future viral pandemics, basic science is required to illuminate both virulence determinants and host defenses. Alphaviruses are arthropod-borne, positive-sense RNA viruses that can cause febrile rashes, debilitating arthritis, and encephalomyelitis, which can prove fatal. The acute phase of their infection is controlled by the type I interferon (IFN) response, wherein host detection of invading pathogens induces expression of IFN and subsequent IFN-stimulated genes (ISGs) to establish an antiviral environment. In this dissertation, I present a study on the roles of ubiquitination and RNA binding in antiviral mechanisms utilized by

two ISGs, the ubiquitin E3 ligase tripartite motif-containing protein 25 (TRIM25) and the RNA CpG sensor zinc finger antiviral protein (ZAP), to restrict alphavirus translation.

While both TRIM25 and ZAP are potent antiviral factors individually, whether through direct or indirect means of viral inhibition, attention has turned in recent years to their cooperative inhibition of varied viruses. Previous work done by our lab suggests that TRIM25-mediated ubiquitination is essential for ZAP inhibition of alphavirus translation, but the exact substrates that mediate this antiviral activity are unknown. Moreover, not only do both TRIM25 and ZAP bind RNA, but also RNA binding is critical to their cellular function. For TRIM25, RNA binding stimulates its ligase activity; for ZAP, RNA binding is required for its detection and inhibition of viral RNA. However, the requirement for ZAP and TRIM25 RNA binding in their synergistic inhibition of viral translation remains unknown.

Here, we utilized a "substrate trapping" approach to elucidate TRIM25 ubiquitination substrates involved in diverse and antiviral cellular processes. We generated a point mutation in the TRIM25 RING catalytic domain that abolishes TRIM25 ligase activity and traps substrates, enabling us to identify and characterize bona fide TRIM25 substrates involved in translation and nucleic acid metabolism. Moreover, our results suggest that several of these substrates contribute to TRIM25 antiviral activity. Together, these findings lay the groundwork for understanding how TRIM25-mediated ubiquitination of diverse substrates may modulate translation, nucleic acid metabolism, and antiviral activity.

We also characterized the effects of ZAP and TRIM25 RNA binding on inhibiting viral translation. We demonstrate that mutations affecting ZAP RNA binding to CpG motifs significantly impact its ability to restrict viral replication and translation, and that the ability of ZAP to bind viral RNA is significantly negatively correlated with its ability to associate with TRIM25. These results suggest that ZAP RNA binding and interaction with TRIM25 may form two distinct determinants for ZAP antiviral mechanisms dependent on the viral context.

Finally, I conclude with our collaborative work in characterizing the ability of novel antifusion peptides induce positive Gaussian curvature, thus remodeling membranes and restricting alphavirus replication. The work presented in this dissertation represents a multifaceted examination of the multiple determinants of TRIM25 and ZAP antiviral activity against alphaviruses, and includes a forward-looking development of antiviral therapeutics.

The dissertation of Emily Yang is approved.

Keriann M. Backus

Douglas L. Black

Oliver I. Fregoso

Jerome A. Zack

Melody M. H. Li, Committee Chair

University of California, Los Angeles

2022

To the only God, who is able to keep us from stumbling,
and presents us blameless before the presence of his glory with great joy

Soli deo gloria

For my uncle, Ji-Hong Hong (洪志宏),

the O.G. 李家人 Ph.D.

TABLE OF CONTENTS

LIST OF FIGURES

Page

LIST OF TABLES

Page

LIST OF SUPPLEMENTARY MATERIALS

Supplemental Figures

Supplementary Tables

Appendices

LIST OF ACRONYMS AND ABBREVIATIONS

PROTEINS

G3BP	*Ras-GTPase-activating protein SH3-domain binding protein*
KHNYN	*KH and NYN domain-containing protein*
NME1	*nucleoside diphosphate kinase 1*
PABPC4	*poly-adenylate binding protein cytoplasmic 4*
TRIM25	*tripartite motif containing protein 25*
UPF1	*up-frameshift protein 1*
ZAP	*zinc finger antiviral protein*

PROTEIN MOTIFS AND DOMAINS

NP	*nucleoprotein*
nsP	*nonstructural protein*
PARP	*poly (ADP-ribose) polymerase*
RBD	*RNA binding domain*
RBM	*RNA binding motif*
RBP	*RNA binding protein*
RdRp	*RNA-dependent RNA polymerase*
RING	*really interesting new gene*
ZnF	*zinc finger*

VIRUSES

CHIKV	*chikungunya virus*
EBOV	*Ebola virus*
HIV	*human immunodeficiency virus*
IAV	*influenza A virus*
JEV	*Japanese encephalitis virus*
ONNV	*o'nyong-nyong virus*
RRV	*Ross river virus*
SINV	*Sindbis virus*
VEEV	*Venezuelan equine encephalitis virus*

NUCLEIC ACID MOTIFS

(-) ssRNA	*negative-sense, single-stranded RNA*
(+) ssRNA	*positive-sense, single-stranded RNA*
CpG	*cytosine-guanidine dinucleotide*
dsRNA	*double-stranded RNA*
gRNA	*genomic RNA*
sgRNA	*subgenomic RNA*
UTR	*untranslated region*

INNATE IMMUNITY

IFN	*interferon*
ISG	*interferon-stimulated gene*
MAVS	*mitochondrial antiviral-signaling protein*
MDA5	*melanoma differentiation-associated protein 5*
PAMP	*pathogen associated molecular pattern*
PRR	*pattern recognition receptor*
RIG-I	*retinoic acid-inducible gene-I*
RLR	*RIG-I like receptor*
SG	*stress granule*

MEMBRANE REMODELING

apoA-I	*apolipoprotein A-I*
NGC	*negative Gausssian curvature*
PGC	*positive Gaussian curvature*
TM	*transmembrane*

MATERIALS AND METHODS

BHK-J	*baby hamster kidney cells*
ePB	*ePiggyBac transposon*
GFP	*green fluorescent protein*
h.p.i.	*hours post infection*
HEK 293T	*human embryonic kidney cells, line 293-transfectable*
IB	*immunoblot*
IP	*immunoprecipitation*
KO	*knockout*
KD	*knockdown*
MD	*molecular dynamics*
MOI	*multiplicity of infection*
MS	*mass spectrometry*
PFU	*plaque forming unit*
RLU	*relative luciferase units*
SAXS	*small-angle X-ray scattering*
shRNA	*short hairpin RNA*
Ub	*ubiquitin*
WT	*wild-type*

ACKNOWLEDGMENTS

I have to begin by thanking my mentor, Dr. Melody Man-Hing Li. It has truly been such a special experience to build the Li Lab from the ground up with you and to figure out what we were doing together; you as a freshly-minted PI with big dreams, me as a bright-eyed, bushy-tailed graduate student with no idea what I was getting into. Through all the highs and lows, you were right there with me in the trenches; remember the time you came back to lab after a faculty dinner to harvest cells with me until 10 pm? Thank you for teaching me everything I know about viruses; for the countless revisions, award-winning letters of rec, texts with cute emojis 😂🤣🙈, infecting me with your contagious nerdy excitement, getting things from the top shelf, letting me tease you mercilessly, pushing me harder when I needed it, and being in my corner every step of the way. Thanks to me, now you get to be in your own corner too, as a life-sized cardboard cutout! You're very welcome. Working with you was easily my favorite, most cherished part of my graduate years. I look forward to following your research, collaborations with you (fingers crossed 🤞) and, God willing, sending talented undergrads your way in the years to come.

Special thanks to everyone else who has supported me through my scientific journey. To my undergraduate PI, Dr. Elissa Hallem, and her lab (special shout out to Drs. Spencer Gang, Michelle Castelletto, and Astra Bryant) for nurturing me in the early stages. To my life twin, Peter Back, for being a steady companion through it all: undergrad MIMG finals, grad school interviews, choosing dissertation labs, the long trudge through grad school; at long last (9 years later!) we part ways. To my thesis committee for their invaluable support and advice, to Drs. Zoran Galić and Tama Hasson for guidance in my teaching aspirations, and to the members of the Li, Fregoso, and Backus labs for

figuring out this science thing with me: my early morning labmate LeAnn, Fregoso friend Carina, Backus buddies José, Maria, and Sunny; and Li lab juniors Serina, Pablo and Sangeetha. And thanks to the best MBI team: Ashley Straight, Stephanie Cuellar, and Helen Houldsworth!

Finally, thank you to my family and friends who reminded me of the truly important things in life and kept me going. To my mom, dad, brother, and the 李家人 clan for raising me to be the person I am today. To Jordan Shiozaki, who keeps me company through late nights of writing by falling asleep on her couch even while the TV is on full volume, who lets me take the most ridiculous pictures of her, and who is the best friend I could ever ask for. To the families that have taken me in as their own and kept this starving graduate student alive through delicious home-cooked meals and life-sustaining company: the Priolos (Michael, Christina, Holland, Agnes, and Noëlle) and the Songs (Rubens, Juni, Ellie, Katie, and Lucy). To faithful friends, for their prayers and shared joys and sorrows: Gwen Silva, Leia Yen, Jess Choi, Phoebe Law, Candice Wu, Prudence Tam, Annie Park, and innumerable others. And to the rest of my church family at Lighthouse Community Church: "As for the saints in the land, they are the excellent ones, in whom is all my delight." (Psalm 16:3)

Last but not least, I would like to acknowledge the following people who contributed to the writing of individual chapters of this dissertation – without them, this work would not exist.

Chapter 2 is adapted from unpublished work currently in production at PLoS Pathogens: "Yang E, Huang S, Jami-Alahmadi Y, McInerney GM, Wohlschlegel JA, and Li MMH (2022). Elucidation of TRIM25 ubiquitination targets involved in diverse and antiviral cellular processes. Accepted." This work was supported in part by NIH grant R01AI158704 (ML), UC CRCC Faculty

Seed Grant (CRN-20-637544; ML), UCLA AIDS Institute and Charity Treks 2019 Seed Grant (ML), Johanna and Joseph H. Shaper Family Chair (ML), Ruth L. Kirschstein MPTG (NRSA AI007323; EY), Warsaw Fellowship (EY), and Whitcome Fellowship (EY). Author contributions were: Conceptualization – EY, GI, JW, ML; Investigation – EY, SH, YJ; Methodology – EY, YJ, JW, ML; Formal analysis, Software – EY, YJ; Project administration – EY, JW, ML; Validation, Visualization, Writing-Original Draft – EY; Writing-Review and Editing – EY, SH, GI, JW, ML; Resources – GI, JW, ML; Supervision – JW, ML; Funding acquisition – ML.

Chapter 3 is adapted from "Yang E[†], Nguyen LP[†], Wisherop CA, Kan RL, and Li MMH (2022). The Role of ZAP and TRIM25 RNA Binding in Restricting Viral Translation. *Frontiers in Cellular and Infection Microbiology*. doi: 10.3389/fcimb.2022.886929." This work was supported in part by NIH R01AI158704 (ML), UCLA AIDS Institute and Charity Treks 2019 Seed Grant (ML), Ruth L. Kirschstein Multidisciplinary Training Grant in Microbial Pathogenesis (NRSA AI007323; EY), Ruth L. Kirschstein Cellular and Molecular Biology Training Program (NRSA GM007185; LN), Warsaw Fellowship (EY), and Whitcome Fellowship (EY, LN). Author contributions were: Conceptualization, Methodology, Project Administration – EY, LN, and ML; Investigation, Validation, Formal Analysis, Visualization – EY, LN; Molecular Cloning – EY, CW, RK; Software – LN; Writing-Original Draft – EY, LN; Writing-Review and Editing – EY, LN, CW, RK, ML; Supervision, Funding acquisition – ML. Co-first authorship indicated by [†].

Chapter 4 is adapted from a manuscript in preparation. I would like to thank everyone who contributed to the work including Yue Zhang, Michelle Lee, Elizabeth Wei-Chia Luo, Jaime De Anda, Gerard Wong, and Melody Man Hing Li. This work was supported in part by National Science

Foundation rapid-response research grant (2032310; GW, ML), the UCLA Broad Stem Cell Research Center COVID-19 Research Award (OCRC #21-104; GW, MML), Johanna and Joseph H. Shaper Family Chair (ML), Warsaw Fellowship (EY), and Whitcome Fellowship (EY). Author contributions were: Conceptualization, Methodology, Writing-Review and Editing, Project Administration – EY, YZ, ML, JDA, EL, GW, MML; Writing-Original Draft – ML, EY; Validation, Formal Analysis, Investigation – EY, YZ, ML, EL, JDA; Supervision, Funding acquisition – GW, MML.

Appendix 1 is a reprint of "Yang E and Li MMH (2020). All About the RNA: Interferon-Stimulated Genes that Interfere with Viral RNA Processes. *Frontiers in Immunology* 11, 3195. doi: 10.3389/fimmu.2020.605024." This work was supported in part by UC Cancer Research Coordinating Committee (UC CRCC) Faculty Seed Grant (CRN-20-637544; ML), UCLA AIDS Institute and Charity Treks 2019 Seed Grant (ML), and Ruth L. Kirschstein Multidisciplinary Training Grant in Microbial Pathogenesis (MPTG, NRSA AI007323; EY). Author contributions were: Writing-Original Draft – EY; Conceptualization, Writing-Review and Editing – EY, ML; Supervision, Funding acquisition – ML.

VITA

EDUCATION

University of California, Los Angeles — 2013–17
Bachelor of Science in Microbiology, Immunology, and Molecular Genetics

RESEARCH EXPERIENCE

Graduate Student Researcher, Laboratory of Dr. Melody Li — July 2018 – 2022
Department of Microbiology, Immunology, and Molecular Genetics, UCLA

Rotation Student, Laboratory of Dr. Keriann Backus — Spring 2018
Department of Biological Chemistry, UCLA

Rotation Student, Laboratory of Dr. Melody Li — Winter 2018
Department of Microbiology, Immunology, and Molecular Genetics, UCLA

Rotation Student, Laboratory of Dr. Manish Butte — Fall 2017
Department of Microbiology, Immunology, and Molecular Genetics, UCLA

Undergraduate Researcher, Laboratory of Dr. Elissa Hallem — 2014–17
Department of Microbiology, Immunology, and Molecular Genetics, UCLA

- Investigation of odor-driven host-seeking behaviors of skin-penetrating parasitic nematodes using quantitative and comparative behavioral analyses

PUBLICATIONS

Yang E[†], Lee M[†], Zhang Y[†], De Anda J, Wong G, & Li MMH. A novel class of positive Gaussian curvature-inducing peptides remodels membranes and inhibits alphavirus replication. *Manuscript in prep.*

Yang E, Huang S, Jami-Alahmadi Y, McInerney GM, Wohlschlegel JA, & Li MMH. Elucidation of TRIM25 ubiquitination targets involved in diverse cellular and antiviral processes. *PLoS Pathog* Accepted (2022). DOI: 10.1371/journal.ppat.1010743

Yang E[†], Nguyen LP[†], Wisherop CA, Kan RL, & Li MMH. The role of ZAP and TRIM25 RNA binding in restricting viral translation. *Front Cell Infect Microbiol* 12, 886929 (2022).
PMID: 35800389 | DOI: 10.3389/fcimb.2022.886929

Yang E & Li MMH. All about the RNA: Interferon-stimulated genes that interfere with viral RNA processes. *Front Immunol* 11, 3195 (2020).
PMID: 33362792 | DOI: 10.3389/fimmu.2020.605024

Gang SS, Castelletto ML, **Yang E**, Ruiz F, Brown TM, Bryant AS, Grant WN, & Hallem EA. Chemosensory mechanisms of host seeking and infectivity in skin-penetrating nematodes. *PNAS* 117, 17913–17923 (2020). PMID: 32651273 | DOI: 10.1073/pnas.1909710117

Gang SS, Castelletto ML, Bryant AS, **Yang E**, Mancuso N, Lopez JB, Pellegrini M, & Hallem EA. Targeted mutagenesis in a human-parasitic nematode. *PLoS Pathog* 13, e1006675 (2017). PMID: 29016680 | DOI: 10.1371/journal.ppat.1006675

† indicates these authors contributed equally to the work

CONFERENCE PRESENTATIONS

Yang E, Jami-Alahmadi Y, Wohlschlegel JA, Li MMH. Talk. "The requirement for ubiquitination in TRIM25-mediated ZAP antiviral activity." Presented at the ASV Virtual Workshop on Innate Effectors (June 2020, July 2021).

SELECTED AWARDS AND HONORS

Grants and Fellowships

- Sidney C. Rittenberg Award, *UCLA* 2021
- Whitcome Fellowship, *UCLA* 2021 – 2022
- Warsaw Fellowship, *UCLA* 2020 – 2021
- Multidisciplinary Training Grant in Microbial Pathogenesis 2018 – 2020
  Ruth L. Kirschstein NRSA AI007323
- Graduate Dean's Scholar Award, *UCLA* 2017 – 2019

Teaching

- Roy and Dorothy John / Fred Eiserling and Judith Lengyel Teaching Excellence Award, *UCLA* 2020
- MIMG Teaching Assistant award, *UCLA* 2019 – 2020

Other

- Summa cum laude, departmental honors, *UCLA* 2017
- Regents Scholar, *UCLA* 2013 – 17
- Undergraduate Research Scholar, *UCLA* 2015 – 2016

MEMBERSHIPS AND OTHER POSITIONS

- Member, *American Society of Virology* 2017 – Present
- Graduate Student Mentor, *Undergraduate Research Center – Sciences* 2019 – 2022
- Amgen Scholar Writing Instructor, *UCLA* 2021

Chapter 1

—

How to TRIM and ZAP alphaviruses

INTRODUCTION

The COVID-19 pandemic highlights the pressing need for basic virology research to identify conserved virus-host interactions that can be readily harnessed to combat emerging viruses (Huang *et al*, 2019; Wang and Anderson, 2019; Pierson and Diamond, 2020). Given the rapid replication and mutation rate of most RNA viruses (Duffy, 2018; Domingo *et al*, 2021), developing therapeutics that target viral factors may not prove to be an effective solution. On the other hand, boosting existing innate antiviral cellular defenses may allow for the development of pan-antiviral therapeutics that target the initial, acute phase of viral infection. Mammalian cells rely on the type I interferon (IFN) response as the first line of defense against all invading pathogens.

This work explores the roles of ubiquitination and RNA binding in combatting alphavirus infection. Specifically, I endeavor to examine the mechanisms by which the IFN-stimulated genes (ISGs) tripartite motif-containing protein 25 (TRIM25) and zinc finger antiviral protein (ZAP) inhibit alphavirus infection. Alphaviruses are ideal for our study of TRIM25 and ZAP antiviral activity given their sensitivity to type I IFN (Ryman *et al*, 2000; Carpentier and Morrison, 2018), their restriction by both TRIM25 and ZAP (Bick *et al*, 2003; Li *et al*, 2017; Zheng *et al*, 2017), and their importance as a class of emerging RNA viruses filled with pandemic potential (Kraemer *et al*, 2019; Messina *et al*, 2019).

The alphavirus section relies heavily on *Fields Virology* (6th ed.) and *Principles of Virology* (4th ed.) (Kuhn, 2013; Flint *et al*, 2015). The antiviral innate immunity, TRIM25, and ZAP sections are adapted from our published review on interferon-stimulated genes that inhibit viral replication in an RNA-centric manner; for more information, see Appendix 1 (Yang and Li, 2020).

ALPHAVIRUSES

Alphaviruses (genus *Alphavirus*, family *Togaviridae*) are enveloped, positive-sense single-stranded RNA ((+) ssRNA) viruses (Flint *et al*, 2015). Alphaviruses are composed of 32 species that infect humans, vertebrates, and fish, broadly grouped into Old World and New World alphaviruses. These include several important human pathogens, wherein the Old World alphaviruses can cause fever, rash, and debilitating arthritis, while the New World alphaviruses can cause encephalomyelitis and in rare occasions, death (Ryman and Klimstra, 2008; Weaver *et al*, 2012). Perhaps more importantly, alphaviruses possess pandemic potential. Completion of infection cycles requires transmission by arthropods such as mosquitos and ticks, whose distributions and spillover potential continue to expand as a result of increasing global temperatures, urbanization, and increased intercontinental travel (Weaver and Lecuit, 2015; Lau *et al*, 2017; Kraemer *et al*, 2019; Messina *et al*, 2019). No antiviral therapeutics for alphavirus infection are currently approved.

Genome organization

Alphavirus genomes are 11.4-11.8 kb in length and consist of two main segments: the nonstructural proteins (nsPs) essential for replication, making up the 5' two-thirds of the genome, and the structural proteins, which make up the last 3' third of the genome (Figure 1A) (Kuhn, 2013). The nonstructural proteins are composed of nsP1 (capping and membrane association), nsP2 (NTPase, helicase, RNA triphosphatase, and protease), nsP3 (mediation of multiple virus-host protein-protein interactions), and nsP4 (RNA-dependent RNA polymerase) (Kuhn, 2013; Götte *et al*, 2018). Many reporter viruses make use of the hypervariable domain within nsP3, which tolerates insertion of large genes such as luciferase and GFP (Götte *et al*, 2018). The structural proteins are composed of the

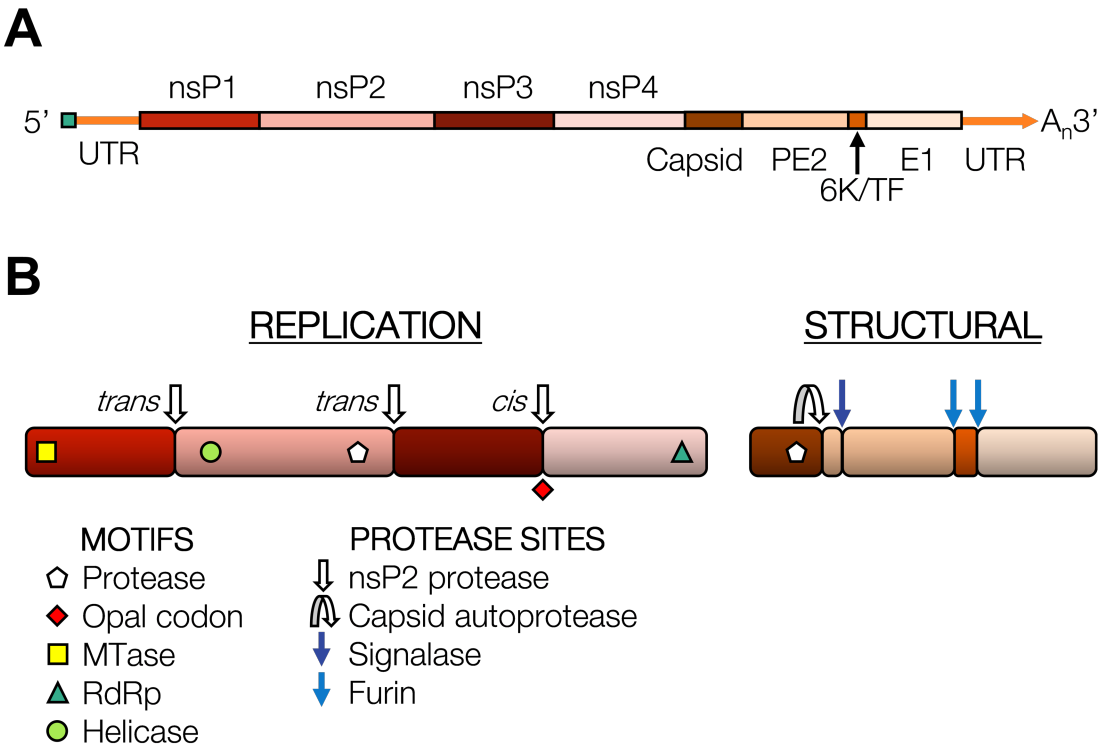

Figure 1. Alphavirus genome and proteins.

(A) Organization of an alphavirus genome. Replication proteins are depicted in shades of red, and structural proteins in shades of orange. PE2 is the precursor E2 protein, composed of E3 and E2. UTR, untranslated region; nsP, nonstructural protein. **(B)** Alphavirus replication and structural polyproteins. MTase, methyl transferase; RdRp, RNA-dependent RNA polymerase. Adapted from *Fields Virology 6th ed., Vol I,* Figure 22.4. Coloring of proteins as denoted in **(A).**

---

capsid (C), followed by E3-E2-6K/TF-E1, where E3, E2, and E1 are glycoproteins. E3 and E2 are grouped together as a precursor to E2, referred to collectively as PE2 (Figure 1). The nonstructural and structural proteins are encoded as two separate open reading frames and translated as polyproteins, which will be discussed in more detail in subsequent sections.

The alphavirus life cycle (Figure 2) broadly consists of: attachment, entry, and uncoating (steps 1-2), translation of non-structural proteins (steps 3-4), transcription and genome replication (steps 5-7), translation and processing of structural proteins (steps 9-10), and finally, assembly, budding, and release (steps 11-14).

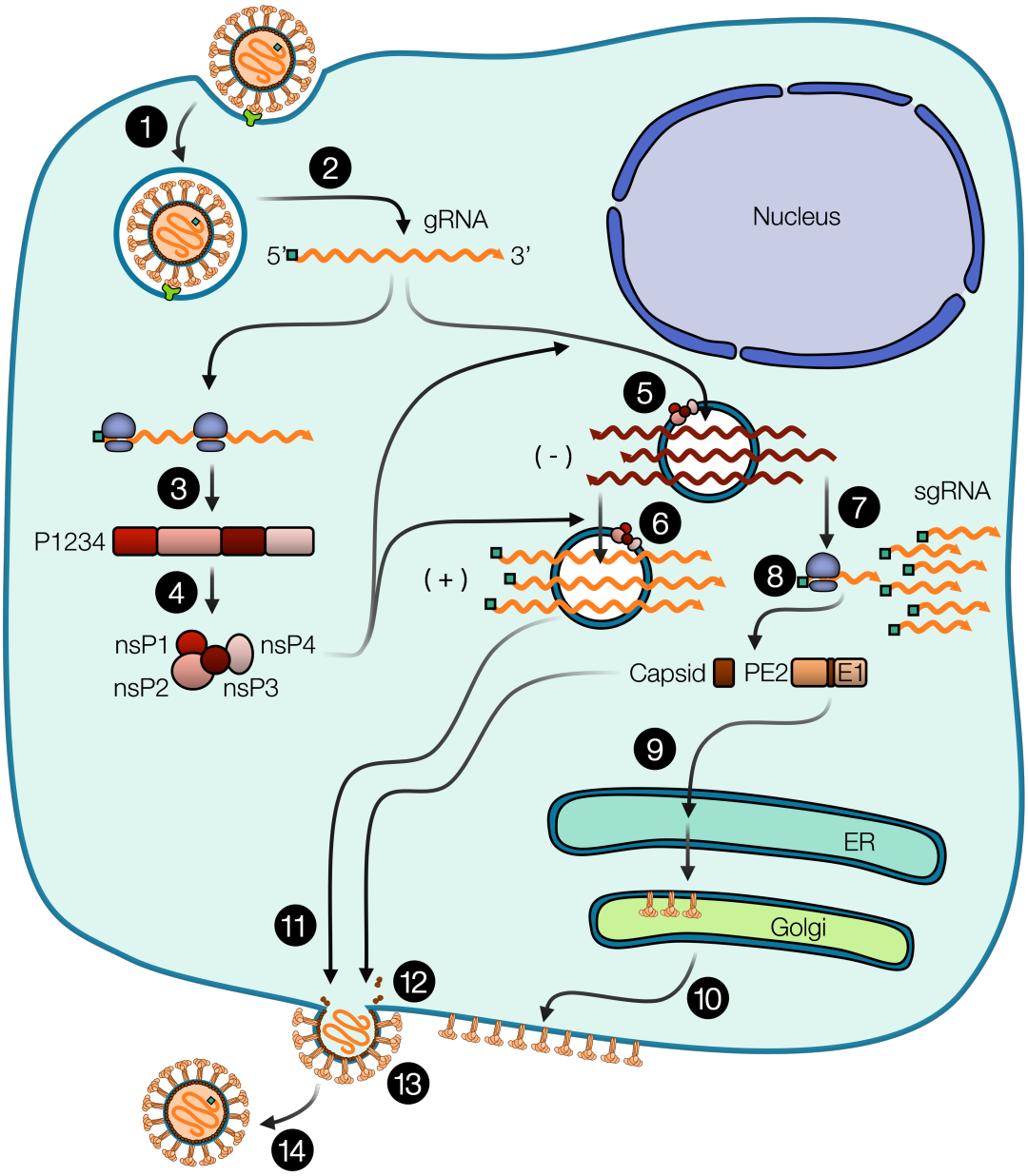

Figure 2. Alphavirus single-cell replication cycle.

(1) The virion binds to a cellular receptor and is endocytosed. **(2)** Acid-mediated fusion results in subsequent uncoating and release of the (+) genomic RNA (gRNA). **(3)** The gRNA is translated to form the replication polyprotein P1234, which is **(4)** sequentially cleaved by the nsP2 protease to form the viral replication complex. Genome replication and transcription occur at cytopathic vacuoles. **(5)** gRNA is first transcribed into full-length (–) RNA, which is then transcribed into **(6)** gRNA and **(7)** subgenomic RNA (sgRNA) from the sg promoter only accessible on the (–) strand. **(8)** sgRNA is translated into the structural polyprotein, including the capsid, which self-cleaves to reveal a hydrophobic ER targeting sequence. **(9)** The remainder PE2-6K-E1 structural polyprotein enters the secretory pathway. **(10)** Processed E2-E1 glycoprotein heterodimers are transported to the plasma membrane. **(11)** The capsid and gRNA form nucleocapsids and migrate to the cell membrane, **(12)** associating with viral glycoproteins. **(13)** An envelope is acquired by the nucleocapsid by budding, resulting in **(14)** final release of viral particles. Adapted from *Principles of Virology 4th ed., Vol I,* Figure 34.

Attachment, entry, and uncoating

The enveloped alphaviruses are arranged with icosahedral symmetry, displaying the glycoproteins E1 and E2 on their surfaces. These are arranged as 80 trimer spikes of E1-E2 heterodimers, with the 240 total proteins interacting with 240 capsid proteins (Griffin, 2013). The E1-E2 spikes are responsible for interacting with host cell receptors to mediate attachment and entry. Several alphavirus receptors have been identified, including NRAMP2, Mxra8, LDLRAD3, VLDLR and ApoER2 (Rose *et al*, 2011; Zhang *et al*, 2018; Ma *et al*, 2020; Clark *et al*, 2022). The E2 glycoprotein functions in receptor attachment, while E1 functions in membrane fusion.

Following receptor-mediated attachment to the host cell, alphaviruses undergo clathrin-dependent endocytosis to enter the cell. The acidic pH within endocytic vesicles destabilizes the E1-E2 heterodimer, dissociating the two proteins and exposing the E1 fusion peptide. Mechanisms of viral fusion are categorized into three classes of viral fusion proteins; alphaviruses employ class II viral fusion proteins (Rey and Lok, 2018). Prefusion class II proteins are primarily composed of β-sheets and form a multimeric assembly that encases the entire viral membrane, in contrast to the class I prefusion independent trimers composed of long α-helices (Rey and Lok, 2018). Cholesterol-dependent insertion of the E1 fusion peptide into the host membrane induces membrane curvature and subsequent fusion, resulting in release of the nucleocapsid core into the host cytoplasm. Mechanisms of core disassembly and genome uncoating remain largely uncharacterized.

Translation of non-structural proteins

The (+) ssRNA alphavirus genome resembles host mRNA, possessing a 5’ cap, and is able to be immediately translated. The nsPs are translated first as two different polyproteins, P123 and P1234;

an opal stop codon between nsP3 and nsP4 is read through 10-20% of the time, resulting in a smaller proportion of P1234, which contains the RdRp nsP4. The nsP2 protease cleaves P1234 between nsP3 and nsP4 in *cis*, generating a preliminary replication complex composed of P123 and nsP4 (Figure 3).

Transcription and genome replication

The replication complex P123 + nsP4 preferentially synthesizes full length negative-sense (-) strands (Figure 3). However, once enough copies of P123/P1234 have been translated, nsP2 is able to cleave at the nsP1-nsP2 and nsP2-nsP3 junctions in *trans*. These cleavages generate the mature replication complex of completely processed nsP1, nsP2, nsP3, and nsP4, which is able to efficiently synthesize (+) strands (Figure 3). Replication complexes form initially on the plasma membrane, inducing spherule formation, and are found on cytopathic vacuoles later in infection.

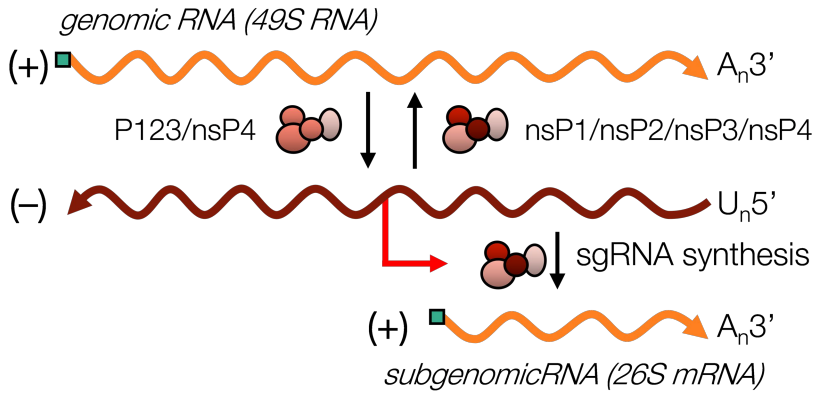

Figure 3. Synthesis of alphavirus RNA.

Alphavirus (+) gRNA is transcribed to the full-length (–) RNA by the partially processed replication complex (RC) P123/nsP4. As more nonstructural proteins are translated, cleavages by nsP2 in *trans* completely process the nonstructural polyprotein, producing the mature nsP1/nsP2/nsP3/nsP4 RC. The mature RC preferentially synthesizes (+) RNA, transcribing both the full-length gRNA and the shorter sgRNA from the 3' third of the genome. Synthesis of sgRNA utilizes the sg promoter (red arrow), which is only accessible from the (–) strand intermediate. Adapted from *Principles of Virology 4th ed., Vol I,* Figure 33.

Translation and processing of structural proteins

Structural proteins are translated as a single polyprotein from the subgenomic RNA (sgRNA), whose promoter is only accessible from the (-) strand (Figure 3, red arrow). Synthesis of sgRNA occurs at approximately three times the level of the genomic RNA (gRNA). Due to the carefully regulated availability of differing replication complexes, sgRNA synthesis and subsequent translation of structural proteins only occur late within the alphavirus life cycle. The capsid self-cleaves from the remainder of the structural polyprotein, exposing an endoplasmic reticulum (ER) signal sequence which translocates the envelope proteins (PE2-6K-E1) into the ER for further processing and post-translational modifications. Within the ER, PE2 and E1 are glycosylated and heterodimerize with one another. Oligomerization of PE2 and E1 allow them to exit the ER and traverse the trans-Golgi network to reach the plasma membrane. E3 is cleaved from PE2 by furin within the trans-Golgi network to generate the completely processed E2-E1 heterodimer, which embeds into the plasma membrane.

Assembly, budding, and release

Following its self-cleavage, the capsid associates with gRNA to assemble viral nucleocapsids. These nucleocapsids migrate to the plasma membrane where E2-E1 spikes are embedded, facilitating the interaction of capsid proteins with E2 cytoplasmic tails for final assembly. Budding of the nucleocapsid at the E2-E1 studded plasma membrane provides an envelope for new virions, which are subsequently released.

Reporter viruses

Many different reporter alphaviruses have already been developed, facilitating our examination of viral replication and translation. A reporter virus contains insertion of a foreign gene into the viral genome, expression of which is easily visualized or measured. As the virus replicates itself, the foreign gene is copied alongside the viral genome, thereby providing a direct measure of, and "reporting" on, the amount of ongoing viral replication within the cell. In alphaviruses, reporter genes are typically inserted into the nsP3 hypervariable C-terminal domain which readily tolerates large insertions (Götte *et al*, 2018).

Our study utilizes reporter viruses containing firefly luciferase, which emits bioluminescence, or green fluorescent protein. We also utilize a replication-deficient, temperature-sensitive luciferase reporter virus that is unable to replicate at the non-permissive temperature of 40˚C (Rice *et al*, 1987; Bick *et al*, 2003). For this virus, all luciferase activity represents translation of the incoming viral genome, making it an ideal tool to study TRIM25 and ZAP inhibition of viral translation.

ANTIVIRAL INNATE IMMUNITY

Alphavirus infections are controlled by host innate immune defenses; specifically, by the type I interferon (IFN) response (Carpentier and Morrison, 2018). The type I IFN response can largely be split into two phases: pathogen sensing and IFN-stimulated gene (ISG) production (Figure 4).

Hosts possess sensors which recognize pathogen-associated molecular patterns (PAMPs) of invading viruses. The primary PAMP for alphaviruses is its RNA, distinguished from host RNA primarily via its 5'-triphosphate motifs and long double-stranded RNA (dsRNA) intermediates. RNA-based PAMPs are sensed by Toll-like receptors (TLRs), RIG-I-like receptors (RLRs), Nod-like

receptors (NLRs), and C-type lectin receptors (CLRs) (Bottermann and James, 2018; Carpentier and Morrison, 2018). The RLRs retinoic acid-inducible gene I (RIG-I) and melanoma differentiation-associated gene 5 (MDA5) are RNA helicases able to sense foreign RNA in the cytoplasm (for a comprehensive review on distinguishing self from non-self nucleic acid, see Schlee and Hartmann, 2016). Upon activation, RIG-I and MDA5 interact with and activate the mitochondrial antiviral signaling protein (MAVS), which multimerizes and initiates downstream activation of the transcription factors IFN-regulatory factors 3 or 7 (IRF3/7) and nuclear factor kappa-light-chain-

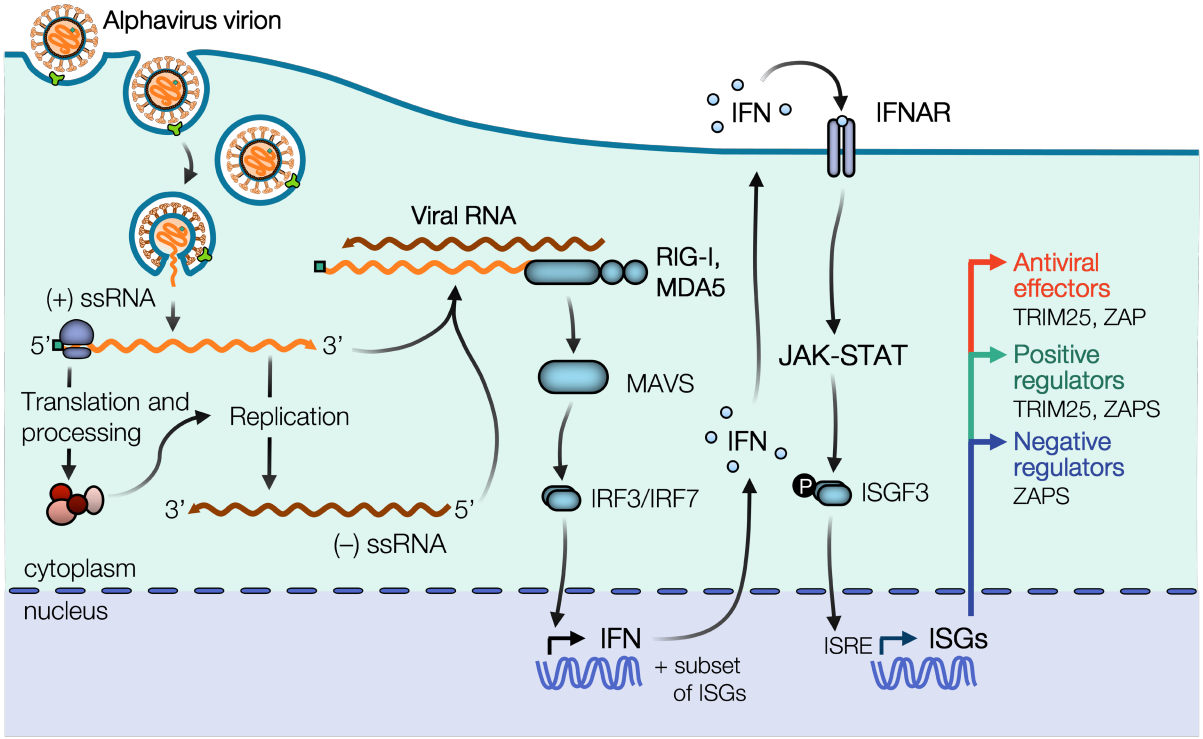

Figure 4. Alphavirus infection is controlled by the type I interferon response.

Upon entry of the host cell, alphavirus virions uncoat and translate their genomic RNA, which is positive-sense single-stranded ((+) ssRNA). Replication proteins generate a full-length negative-sense copy of the viral genome ((–) ssRNA). Viral RNA is sensed by the RNA sensors RIG-I and MDA5, which signal through MAVS to activate the transcription factors interferon regulatory factor (IRF) 3 / IRF7. These factors translocate to the nucleus to induce expression of interferon (IFN) and a subset of IFN-stimulated genes (ISGs). IFN traffics out of the cell, signaling in an autocrine and paracrine fashion through the type I IFN receptor, IFNAR. Subsequently, IFNAR signals through the JAK-STAT pathway, inducing formation of the phosphorylated transcription factor complex IFN-stimulated gene factor 3 (ISGF3). ISGF3 binds to IFN-stimulated response elements (ISREs) to induce expression of IFN-stimulated genes (ISGs).

enhancer of activated B cells (NFκB). As a result, these transcription factors translocate to the nucleus to activate expression of type I IFN and other proinflammatory cytokines.

Type I interferon response

The type I IFN receptor is expressed ubiquitously on almost all cell types, allowing for IFN signaling in both infected and neighboring cells that are uninfected. Janus kinase-signal transducer and activator of transcription (JAK-STAT) is the predominant, canonical pathway that regulates ISG transcription. IFN binding to its cell surface receptor, comprised of IFN-α receptor 1 (IFNAR1) and IFN-α receptor 2 (IFNAR2), leads to phosphorylation of the pre-associated JAKs, JAK1 and tyrosine kinase 2 (TYK2). Phosphorylated JAK1 and TYK2 then phosphorylate IFNAR1/2, which recruits STAT1/2 to be phosphorylated themselves. Phosphorylated STAT1/2 recruit IRF9 to form the transcription factor complex IFN-stimulated gene factor 3 (ISGF3). ISGF3 translocates to the nucleus where STAT1 is further phosphorylated for full activation. Within the nucleus, ISGF3 binds to IFN-stimulated response elements (ISREs) present in ISG promoters, which then effect an antiviral cellular environment (for a comprehensive review on IFN signaling, see Au-Yeung and Horvath, 2018).

Interferon-stimulated genes

Broadly speaking, an ISG is any gene whose expression is induced by IFN signaling. Advances in RNA-sequencing (RNA-seq) technology have enabled the identification of ISGs across varied cell lines by measuring changes in the transcriptome in response to IFN stimulation. The online database INTERFEROME continues to catalog the results of such gene profiling studies (Rusinova *et al*, 2013). However, ISG expression is more nuanced in reality. A subset of ISGs are direct targets of IRF3/7 and can be induced with or without downstream IFN signaling (Au-Yeung and Horvath, 2018). Other

ISGs are both basally expressed and IFN-inducible, while still others are cell-type specific (Schneider *et al*, 2014; Schoggins, 2019). Moreover, there are three types of IFN, wherein type I and III are the classic antiviral IFNs. Though type I and III IFNs bind to different receptors, they signal through the same JAK-STAT pathway, thus inducing a shared array of ISGs. Still, type I and III IFN signaling pathways are differentiated by expression kinetics and cell-type specific receptor expression (for a comprehensive review, see Lazear *et al*, 2019). Tight regulation of ISG expression is necessary because dysregulation of the type I IFN response results in interferonopathies or deleterious systemic inflammation (Melki and Frémond, 2020).

In addition to regulating their own expression, ISGs are well known for their inhibition of viral replication. They employ diverse mechanisms to block virtually every step of viral replication, though ISGs have been shown to target different viral life cycle stages for different viruses (for a comprehensive review on a broad range of antiviral ISGs, see Schoggins, 2019). For example, the IFITM family blocks viral entry of diverse viruses (Liao *et al*, 2019) while the Mx GTPases recognize diverse nucleocapsids and block their nuclear import (Haller *et al*, 2015). TRIM5α disrupts retrovirus uncoating and targets several viral proteins for proteasomal degradation (Ganser-Pornillos and Pornillos, 2019). However, these only represent the tip of the iceberg.

Recent advances in systematic approaches have allowed for the unbiased discovery of ISGs with previously uncharacterized antiviral activity. Compiled ISG libraries have facilitated focused loss-of-function or gain-of-function screens of hundreds of ISGs, illuminating the contribution of individual ISGs in varied viral contexts (Schoggins *et al*, 2011; Li *et al*, 2013; OhAinle *et al*, 2018; Subramanian *et al*, 2018). Furthermore, as advances in omics approaches allow examination of cellular

changes on a systemic level, attention is shifting to how ISGs interact and even synergize with one another (Schoggins *et al*, 2011; Karki *et al*, 2012; Hubel *et al*, 2019). Moreover, detailed mechanistic studies are still needed in order to unravel their mode of action. As ISGs may employ different antiviral mechanisms against different viruses, studies in varied viral systems will illuminate how ISGs might recruit different cellular pathways or factors.

Given that this dissertation focuses on the ISGs TRIM25 and ZAP, I will now present a brief overview of each protein, discussing their history, cellular roles, and antiviral determinants and mechanisms.

TRIM25

TRIM25, also known as estrogen-responsive finger protein (EFP), was first identified as an estrogen-responsive gene via its binding to a genomic probe consisting of an estrogen receptor-binding fragment (Inoue *et al*, 1993, 1995). Subsequent studies focused on its role as a primary estrogen-responsive gene in breast cancer, capable of mediating cell and tumor growth (Ikeda *et al*, 2000; Urano *et al*, 2002; Suzuki *et al*, 2005). One potential mechanism for EFP in mediating cell growth is its ubiquitination of the negative cell cycle regulator 14-3-3σ, thus targeting it for degradation (Urano *et al*, 2002). TRIM25 was then found to not only contain an ISRE but also to be stimulated by IFN, sparking interest in its role in antiviral innate immunity (Nakasato *et al*, 2006). Shortly thereafter, TRIM25 was demonstrated to ubiquitinate the dsRNA sensor RIG-I (Gack *et al*, 2007), thus setting off a series of studies examining the role of TRIM25 in viral infections. Two aspects of TRIM25 biology critical for its control of viral replication are its ligase activity and its ability to bind RNA.

TRIMs and ubiquitination

TRIM25 is a RING E3 ligase, a member of the largest class of E3 ligases which share an N-terminal catalytic RING domain. E3 ligases occupy the final step in cellular ubiquitination, a post-translational modification which ligates ubiquitin, a ~7 kDa protein, to an acceptor lysine on the substrate. Monoubiquitination occurs if the ubiquitin C terminus is ligated to the substrate lysine; modifying the N terminus or one of the seven lysines of a substrate-attached ubiquitin (Figure 5A) can lead to polyubiquitination, wherein a polymeric ubiquitin chain is formed. Ubiquitination of a protein can alter its cellular fate depending on the type of linkage (e.g. K48, K63), ranging from proteasomal degradation to scaffold formation for assembly of cellular signaling complexes (Komander and Rape, 2012). In order for ubiquitin to be ligated to an acceptor lysine, it must be sequentially

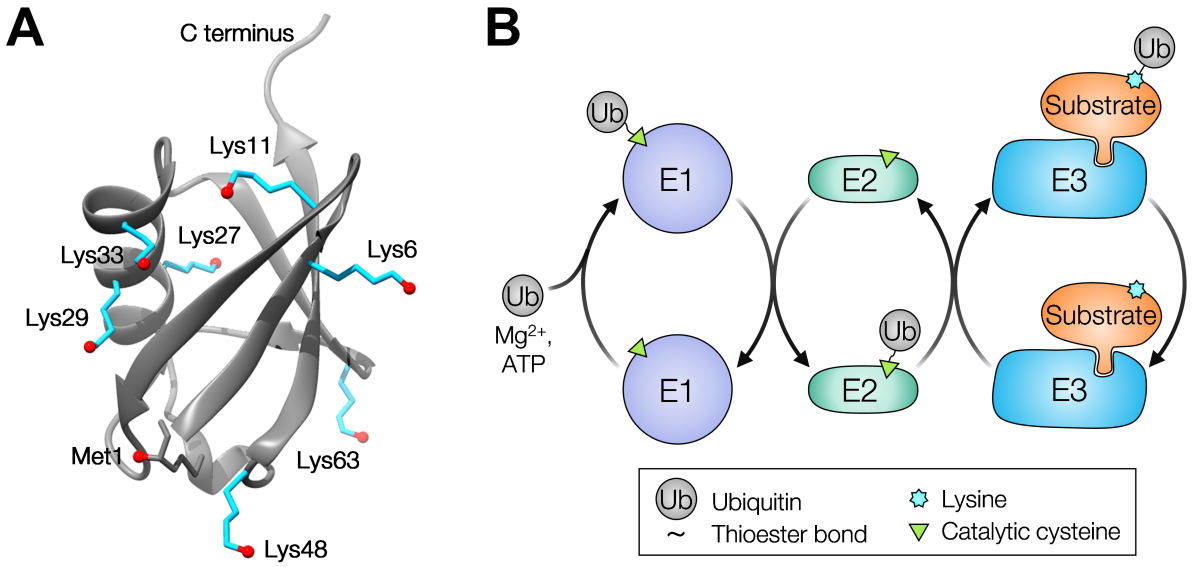

Figure 5. The ubiquitin conjugation system.

(A) Structure of ubiquitin (PDB: 1UBQ) showing the seven Lys residues (blue) and Met1. Red spheres indicate amino groups used in ubiquitin chain formation. **(B)** A ubiquitin forms a thioester bond (~) with the catalytic cysteine (green) of a ubiquitin-activating enzyme (E1). E1 binds a ubiquitin-conjugating enzyme (E2) and transfers its ubiquitin to the E2 catalytic cysteine to form E2~ubiquitin. A ubiquitin ligase (E3) recruits E2~ubiquitin and substrate to transfer ubiquitin from E2 to a substrate lysine. E2 disengages from E3 upon transfer, and E3 can bind another E2~ubiquitin to catalyze additional round(s) of substrate ubiquitination.

activated by the E1 ubiquitin-activating enzyme, carried by the E2 ubiquitin-conjugating enzyme, and finally ligated to an acceptor lysine by one of over 600 human E3 ligases (Figure 5B).

TRIMs are the largest group of RING E3 ligases and constitute an important family of proteins in the type I IFN response (Rajsbaum *et al*, 2014; Bottermann and James, 2018). There are over 70 human TRIM proteins, many of which are induced by type I IFN (Rajsbaum *et al*, 2014; Vunjak and Versteeg, 2019). Interestingly, the rapid expansion of the TRIM family coincides with the development of adaptive immunity, suggesting that TRIMs may have evolved to play a role in immune regulation (Rajsbaum *et al*, 2014). These proteins typically possess three conserved domains at the N-terminus: the catalytic RING domain, one to two B-box domains thought to function in higher order oligomerization, and a coiled-coil (CC) domain that allows TRIMs to dimerize and potentially oligomerize (Esposito *et al*, 2017). The C-terminal domain of the TRIM family varies by subgroup; TRIM25 is a member of the largest subgroup, IV, which possesses a PRY-SPRY domain thought to mediate protein-protein interactions (Figure 6) (Rajsbaum *et al*, 2014). Most TRIMs either directly inhibit viral replication by targeting viral components for degradation or indirectly inhibit by modulating innate immune signaling (van Gent *et al*, 2018; Hage and Rajsbaum, 2019).

TRIM25 RNA binding contributes to its ligase and antiviral activity

While well characterized as a ubiquitin E3 ligase, more attention has turned in recent years to elucidating the role of RNA binding in TRIM25 ligase and antiviral activity (for a comprehensive review, see Choudhury *et al*, 2020). TRIM25 was first identified as an RNA binding protein in mRNA interactome captures performed in HeLa cells (Castello *et al*, 2012) and embryonic stem cells (Kwon *et al*, 2013). Several groups have attempted to elucidate the TRIM25 RNA binding domain,

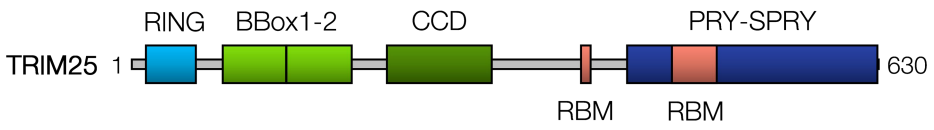

Figure 6. TRIM25 domain structure.

Structural domains indicated as colored in rectangles. Grey line indicates unstructured regions. CCD, coiled-coil domain; RBM, RNA-binding motif.

---

independently mapping it to a 39-amino acid sequence in the C-terminal PRY-SPRY domain (Castello *et al*, 2016; Choudhury *et al*, 2017) and to a lysine-rich 7K motif in the linker between the CC and PRY-SPRY domains (Figure 6, RBM) (Sanchez *et al*, 2018). Analysis of TRIM25-bound RNA revealed its preference for G- and C-rich sequences and for mRNAs and long intergenic noncoding RNAs (Choudhury *et al*, 2017). Furthermore, not only is TRIM25 RNA binding stimulated upon alphavirus infection, but also TRIM25 binds directly to SINV gRNA (Garcia-Moreno *et al*, 2019).

Importantly, RNA binding is thought to stimulate TRIM25 ligase activity (Choudhury *et al*, 2017; Sanchez *et al*, 2018), which is required for many of its antiviral mechanisms (discussed in the following section). It remains unclear how RNA binding stimulates TRIM25-mediated ubiquitination. RNA may function as a scaffold to recruit substrates to TRIM25, or by inducing allosteric changes in TRIM25 to directly increase catalytic activity (Williams *et al*, 2019).

TRIM25 antiviral mechanisms

TRIM25 utilizes both ubiquitin-dependent and -independent measures to antagonize viral replication. TRIM25 antiviral mechanisms can be broadly classified into three categories: stimulating antiviral signaling, direct antagonism of viral components, and synergizing with ZAP (for comprehensive reviews on TRIM25 antiviral mechanisms, see Martín-Vicente *et al*, 2017; Choudhury

et al, 2020). It is worth noting that many viruses possess anti-TRIM25 measures, highlighting the effectiveness of TRIM25 to induce a hostile antiviral cellular environment (for a comprehensive review on viral antagonism of TRIM25, see Zhang *et al*, 2021).

TRIM25 is perhaps best characterized for its role in regulating the RIG-I–MAVS signaling axis. TRIM25 mediates K63-linked ubiquitination of the RIG-I 2CARD domain, required for the initiation of antiviral signaling in response to viral RNA PAMPs (Gack *et al*, 2007, 2008). TRIM25 can also synthesize unanchored K63-linked polyubiquitin chains to activate RIG-I signaling (Zeng *et al*, 2010). These polyubiquitin chains promote the interaction of RIG-I with MAVS by tetramerizing the RIG-I 2CARD domain, which subsequently nucleates MAVS filament formation and recruitment of downstream signaling molecules (Hou *et al*, 2011; Jiang *et al*, 2012; Peisley *et al*, 2014). TRIM25 may also play a role in activating NF-κB downstream of MAVS signaling (Lee *et al*, 2015a; Liu *et al*, 2020a). However, the critical role of TRIM25 in ubiquitinating RIG-I has been called into question in recent years, with some studies purporting that a second E3 ligase, Riplet, is sufficient for RIG-I activation (Oshiumi *et al*, 2013; Shi *et al*, 2017; Cadena *et al*, 2019; Hayman *et al*, 2019; for comprehensive reviews on the TRIM25/Riplet controversy, see Okamoto *et al*, 2018; Oshiumi, 2020). Finally, TRIM25 is also able to negatively regulate IFN signaling by targeting MAVS for proteasomal degradation (Castanier *et al*, 2012).

Moreover, TRIM25 is able to antagonize viral replication by targeting varied viral components for degradation or by sequestering viral proteins, similar to other TRIM proteins. TRIM25 inhibits replication of infectious bursal disease virus, a chicken dsRNA virus, by mediating K27-linked polyubiquitination of the viral structural protein VP3 and subsequent proteasomal degradation (Wang

et al, 2021). TRIM25 inhibits influenza A virus (IAV) RNA synthesis by interacting with IAV ribonucleoproteins, blocking mRNA elongation by preventing the viral RNA from moving into the polymerase complex (Meyerson *et al*, 2017).

The varied antiviral roles of TRIM25 as a ZAP co-factor, including its ubiquitination of the Ebola virus (EBOV) nucleoprotein (Galão *et al*, 2022) and other putative host proteins (Li *et al*, 2017; Zheng *et al*, 2017), will be discussed following the next section on ZAP.

ZAP

ZAP, also known as zinc finger CCCH-type containing antiviral 1 (ZC3HAV1) or poly (ADP-ribose) polymerase 13 (PARP13), was first identified in a cDNA screen for genes that prevent retrovirus infection. In this study, overexpression of the rat N-terminal region of ZAP (NZAP) resulted in specific loss of cytoplasmic Moloney murine leukemia viral mRNA (Gao *et al*, 2002). Subsequent studies assessed ZAP antiviral potential, finding NZAP able to inhibit replication of broad range of viruses, including but not limited to Sindbis virus (SINV, *Togaviridae* (Bick *et al*, 2003)), Ebola virus (EBOV, *Filoviridae* (Muller *et al*, 2007)), human immunodeficiency virus-1 (HIV-1, *Retroviridae* (Zhu *et al*, 2011)), Hepatitis B virus (HBV, *Hepadnaviridae* (Mao *et al*, 2013)), coxsackievirus B3 (CVB3, *Picornaviridae* (Li *et al*, 2015)), IAV (*Orthomyxoviridae* (Liu *et al*, 2015)), and Japanese encephalitis virus (JEV, *Flaviviridae* (Chiu *et al*, 2018)). ZAP antiviral activity can be selective within viral families and genera, as not all flaviviruses and picornaviruses tested are sensitive to ZAP (Bick *et al*, 2003; Chiu *et al*, 2018). ZAP also post-transcriptionally regulates expression of cellular mRNA (Todorova *et al*, 2014) and restricts retrotransposition of human retrotransposons (Goodier *et al*, 2015; Moldovan and Moran, 2015).

ZAP domain structure

ZAP possesses four N-terminal CCCH zinc fingers (Chen *et al*, 2012) that directly bind to CpG-containing viral RNA, are required for antiviral activity, and dictate its mostly cytoplasmic and stress granule localization (Guo *et al*, 2004; Goodier *et al*, 2015; Youn *et al*, 2018; Law *et al*, 2019). Solving the crystal structure of NZAP in complex with RNA confirmed ZAP preference for single-stranded nucleic acids and CpG dinucleotides, revealing the presence of a CpG-dinucleotide specific binding pocket (Meagher *et al*, 2019; Luo *et al*, 2020). ZAP preference for CpG-rich substrates could explain in part why many RNA viruses infecting mammals and other vertebrates, such as IAV and SARS-CoV-2, exhibit CpG suppression (Greenbaum *et al*, 2008; Cheng *et al*, 2013; Gioacchino *et al*, 2020; Nchioua *et al*, 2020). ZAP can even sense CpG dinucleotides within individual viral mRNA transcripts of DNA viruses, as in the case of human cytomegalovirus (Lin *et al*, 2020). Here, CpG suppression within the major immediate early transcript 1 confers ZAP resistance (Lin *et al*, 2020). However, CpG suppression does not always confer resistance to ZAP as in the case of SARS-CoV-2 (Nchioua *et al*, 2020).

Alternative splicing results in multiple splice variants which differ from one another in expression, localization, and antiviral activity. The long splice variant, ZAPL, includes a catalytically inactive C-terminal PARP-like domain missing from the short splice variant, ZAPS (Figure 7). Alternative splicing of a 121 aa extension of exon 4 results in two additional splice variants ZAPM and ZAPXL, whose antiviral activities are similar to ZAPS and ZAPL, respectively (Li *et al*, 2019). All splice variants include a central domain composed of a fifth CCCH zinc finger motif and two WWE modules, which bind to poly(ADP-ribose) (PAR) through the second WWE module (Figure 7). PAR

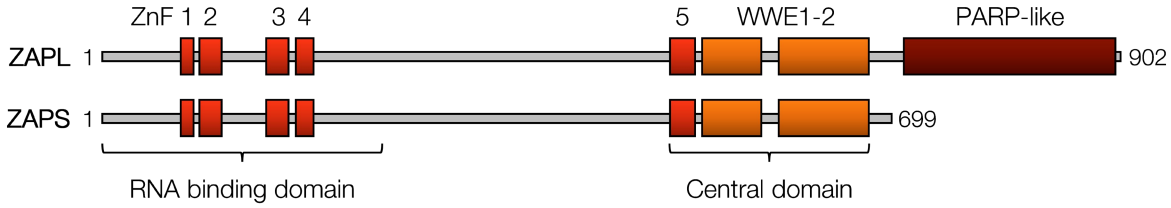

Figure 7. ZAP domain structure.

Structural domains indicated as colored in rectangles. Grey line indicates unstructured regions. ZnF, zinc finger.

---

binding is thought to potentiate ZAP antiviral activity by coordinating the stable association of ZAP and its co-factors, which could occur either by clustering of multivalent ZAP-RNA complexes or by localizing ZAP to stress granules (Xue *et al*, 2022).

ZAPL vs ZAPS

ZAPL is more antiviral than ZAPS (Kerns *et al*, 2008; Li *et al*, 2019). This boost to antiviral activity is attributed to its PARP-like domain, which contains a prenylation motif at its C-terminus that targets ZAPL to endolysosomes (Charron *et al*, 2013; Schwerk *et al*, 2019). Addition of this prenylation motif to ZAPS increases its antiviral activity, though not to the same extent as ZAPL (Schwerk *et al*, 2019). Curiously enough, ZAPL's catalytically dead PARP triad motif is required for its antiviral activity; its replacement with the canonical active PARP motif abolishes ZAPL antiviral activity, though it remains unclear how this inactive motif is required (Gläsker *et al*, 2014). Furthermore, ZAPL is constitutively expressed in several cell types, while ZAPS expression is induced by innate immune signaling (Li *et al*, 2019; Schwerk *et al*, 2019).

Studies conflict as to how ZAPS contributes to innate immune signaling. Though one group showed that ZAPS stimulates RIG-I dependent IFN response upon stimulation with a RIG-I RNA

agonist (Hayakawa *et al*, 2011), others found that ZAP mediates a RIG-I-independent antiviral response to retroviruses and HBV (Wang *et al*, 2012; Lee *et al*, 2013; Mao *et al*, 2013). More recently, ZAPS was shown to negatively regulate the type I IFN response by binding to and stimulating the degradation of *IFN* mRNAs; ZAP-deficient Huh7 cells had a higher and more prolonged IFN response upon treatment with a RIG-I agonist (Schwerk *et al*, 2019). On the other hand, ZAPS was found to synergize with other ISGs, wherein 31 ISGs have a statistically significant increase in antiviral activity in its presence (Karki *et al*, 2012).

ZAP antiviral mechanisms

ZAP targets viruses primarily by two distinct antiviral mechanisms, namely viral translation inhibition (for the (+) ssRNA viruses SINV and JEV) and viral RNA degradation (for HIV-1, HBV, the (-) ssRNA virus EBOV, and the (+) ssRNA viruses CVB3 and JEV). These disparate mechanisms can be explained in part by recruitment of co-factors and differing viral contexts (for a comprehensive review on ZAP antiviral mechanisms, see Ficarelli *et al*, 2021).

ZAP inhibition of SINV translation has been linked to its disruption of the interaction between translation initiation factors eIF4A and eIF4G (Zhu *et al*, 2012). This disruption does not affect global translation seeing as polysome profiles were unchanged when ZAP was overexpressed (Zhu *et al*, 2012). ZAP is also able to repress translation of a luciferase reporter containing the minimal ZAP responsive fragment in the SINV genome without promoting degradation of the reporter (Zhu *et al*, 2012).

Apart from inhibiting viral translation, ZAP also induces viral RNA degradation by recruiting an array of RNA helicases, the endonuclease KHNYN, and exosome components (Guo *et al*, 2007;

Chen *et al*, 2008; Ye *et al*, 2010; Ficarelli *et al*, 2019). ZAP selectively affects cellular transcripts, as it destabilizes the TRAILR4 mRNA and inhibits retrotransposition of endogenous retroelements such as long interspersed element-1 and Alu (Todorova *et al*, 2014; Goodier *et al*, 2015). ZAP substrate specificity determinants largely remained a mystery until it was demonstrated to inhibit HIV-1 with synonymous, elevated CpG dinucleotide mutations (HIV^{CG}) but not wild-type HIV-1 (Takata *et al*, 2017).

TWO ARE BETTER THAN ONE: TRIM25 AND ZAP, TOGETHER 🤝

While TRIM25 and ZAP are rightfully both counted as potent antiviral factors when examined individually, a growing body of evidence suggests that their collaborative inhibition of viral replication is both long-lasting and far-reaching. TRIM25-ZAP antiviral complexes not only are likely evolutionary conserved but also have been implicated in varied antiviral mechanisms.

Both TRIM25 and ZAP were identified among 62 'core' vertebrate ISGs in a screen of the chicken and nine mammalian interferomes, wherein their expression was induced by IFN in all species (Shaw *et al*, 2017). Moreover, both TRIM25 and ZAP display signatures of positive selection (Kerns *et al*, 2008; Malfavon-Borja *et al*, 2013; Judd *et al*, 2021). Together, these studies strongly suggest that TRIM25 and ZAP have both been historically involved in host-virus interactions (Daugherty and Malik, 2012). A recent study examining the origin and evolution of ZAP took these observations one step further, finding that chicken and alligator ZAP antiviral activity was dependent on the co-expression of their cognate TRIM25 (Gonçalves-Carneiro *et al*, 2021), suggesting that ZAP-TRIM25 pairing displays species-specific functional compatibility.

Interest in the ZAP and TRIM25 partnership piqued with work from our lab identifying TRIM25 as a critical ZAP co-factor in inhibiting alphavirus translation (Figure 8A) (Li *et al*, 2017). These results were concurrently corroborated by another group (Zheng *et al*, 2017). TRIM25 is absolutely required for inhibition of viral translation by ZAP, as ZAP is unable to inhibit translation of replication-deficient SINV in TRIM25-deficient cells (Li *et al*, 2017). Not only is TRIM25 putatively required for ZAP recognition of its RNA substrates, as TRIM25 knockdown decreases ZAP association with luciferase reporter RNA, but also TRIM25 ubiquitin ligase activity is essential for ZAP antiviral activity (Li *et al*, 2017; Zheng *et al*, 2017). Curiously, though TRIM25 ubiquitinates ZAP, TRIM25 still contributes to ZAP antiviral activity in the presence of a ubiquitination-deficient ZAP mutant (Li *et al*, 2017), suggesting that TRIM25-mediated ubiquitination of host factors other than ZAP is critical for the inhibitory effects (Figure 8A, question marks). Moreover, it is likely that K63-linked ubiquitination is required for ZAP antiviral activity, as overexpression of a ubiquitin K63R mutant unable to form K63 linkages reduced ZAP inhibition of SINV replication (Zheng *et al*, 2017).

Since our initial identification of TRIM25 and ZAP working together to inhibit alphavirus replication, TRIM25-ZAP complexes have been demonstrated to inhibit replication of the retrovirus HIV-1, the DNA virus human cytomegalovirus (HCMV), and the (-) ssRNA virus EBOV through disparate mechanisms (Ficarelli *et al*, 2019; Lin *et al*, 2020; Galão *et al*, 2022). In all three of these contexts, viral inhibition appears to depend on ZAP's ability to sense CpG dinucleotides, though the exact antiviral mechanisms differ.

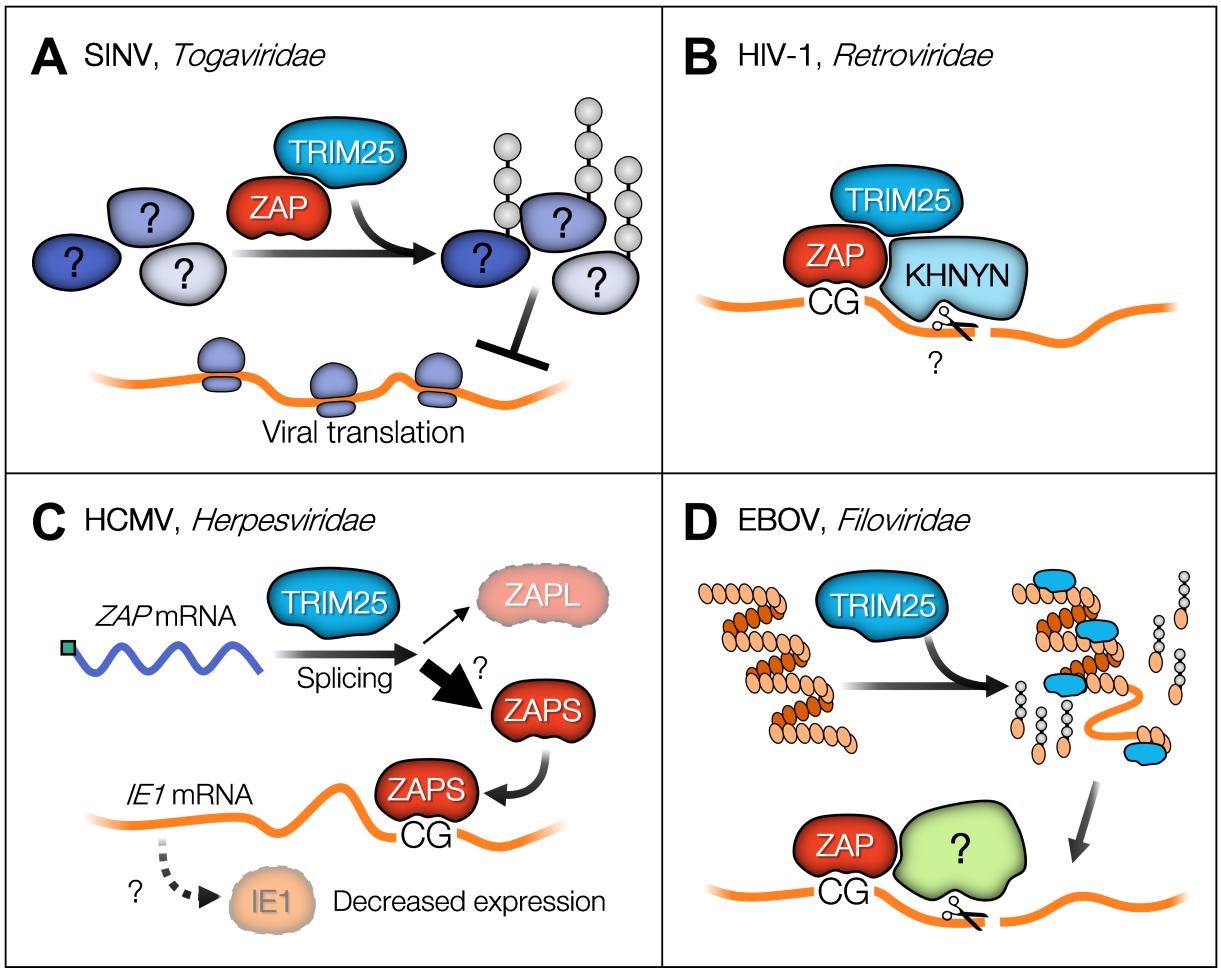

Figure 8. TRIM25 and ZAP inhibit replication of diverse viruses.

(A) ZAP recruits TRIM25 to ubiquitinate other host proteins, which inhibit viral translation. **(B)** ZAP complexes with TRIM25 and the putative endoribonuclease KHNYN to degrade viral RNA. **(C)** TRIM25 induces splicing and expression of ZAPS, which senses CpG in HCMV *IE1* mRNA and results in decreased IE1 expression. **(D)** TRIM25 interacts with and ubiquitinates EBOV nucleoprotein (orange oval), resulting in its dissociation to expose the viral genome to ZAP CpG sensing and RNA degradation. Orange line, viral RNA; gray circle, ubiquitin; large question mark, unknown protein identity; small question mark, unknown mechanism.

In the context of HIV-1 infection, ZAP and TRIM25 complex with a third host factor, the putative endoribonuclease KHNYN, to inhibit HIV^{CG} replication by targeting viral RNA for degradation (Figure 8B). Knockdown of KHNYN abolishes HIV^{CG} sensitivity to ZAP (Ficarelli *et al*, 2019). Interestingly, ZAP sensitivity among primate lentiviruses does not correlate with overall CpG genomic frequency; only elevation of CpG dinucleotides in the 5' third of the HIV-1 *env* gene causes

ZAP susceptibility (Ficarelli *et al*, 2020; Kmiec *et al*, 2020). Moreover, introducing CpGs into the HIV-1 genome in the 5' end of the *gag* gene can change pre-mRNA splicing, inhibiting virion production. Altered pre-mRNA splicing is likely due to utilization of a cryptic splice donor, incorporating the Gag initiation codon in all spliced viral RNAs and likely resulting in inefficient translation of all HIV-1 proteins. This antiviral effect is thought to be at least partially ZAP-independent, given that virion production is not rescued in ZAP knockout (KO) cells (Ficarelli *et al*, 2020).

In contrast, TRIM25 and ZAP work together more indirectly during HCMV infection. In this context, TRIM25 regulates ZAP alternative splicing, and is required for efficient upregulation of ZAPS which in turn recognizes CpG motifs within the HCMV major immediate early transcript (IE1), resulting in its decreased expression (Figure 8C) (Lin *et al*, 2020). Curiously, RNA levels of ZAP target transcripts do not decrease (Lin *et al*, 2020); exact mechanisms for ZAP-mediated decrease of HCMV gene expression and TRIM25 induction of ZAPS alternative splicing remain unclear (Figure 8C, question marks). It is worth noting that a second study found that ZAP recognizes not only CpG motifs but also other cytosine-rich sequences in the context of HCMV infection, specifically destabilizing viral mRNAs expressed from the *UL4-UL6* gene locus (Gonzalez-Perez *et al*, 2021).

Finally, during EBOV infection TRIM25 exposes the viral genome to ZAP CpG detection and RNA degradation (Figure 8D) (Galão *et al*, 2022). This is accomplished by TRIM25 interacting with and mediating the ubiquitination of the EBOV nucleoprotein (NP) in an RNA-independent manner, resulting in NP dissociation from viral RNA. The authors of this study utilized an EBOV

replicon system (trVLP). TRIM25 RING, PRY-SPRY, and RNA binding motifs are all required for EBOV restriction, given that deletion or mutation of any of these significantly impairs TRIM25 antiviral activity. Endogenous ZAPL but not ZAPS could be detected in TRIM25-NP co-precipitates, but this effect could be due to low levels of ZAPS basal expression. Furthermore, ZAP association with the EBOV trVLP genome is dependent on the presence of TRIM25. Notably, TRIM25 likely functions outside of its role as a stimulator of RLR signaling, given that TRIM25 and ZAP were still able to inhibit EBOV replication in RIG-I KO cells. Moreover, the identity of the ZAP-associated ribonuclease responsible for EBOV RNA degradation remains unknown (Figure 8D, question mark), given that depletion of KHNYN did not rescue viral RNA levels (Galão *et al*, 2022).

SIGNIFICANCE AND DISSERTATION OVERVIEW

In summary, the study of TRIM25 and ZAP antiviral activity has raised many questions concerning the ways these two ISGs are able to inhibit a wide range of viruses with a variety of mechanisms. For example, the identity of these TRIM25 substrates that function in ZAP antiviral activity remains to be discovered, as does how they contribute to suppression of alphavirus translation. Furthermore, while it is known that both TRIM25 and ZAP bind RNA, that RNA binding is crucial for their antiviral activity, and that TRIM25 and ZAP interact with one another, it remains unexplored how their individual RNA binding capability affects their cooperative antiviral mechanisms. In the following chapters, I will present my work on the identification and characterization of TRIM25 ubiquitination targets (Chapter 2), the elucidation of the role of ZAP and TRIM25 RNA binding in restricting viral translation (Chapter 3), and conclude with a forward-looking characterization of novel antifusion peptides that remodel membranes and inhibit alphavirus replication (Chapter 4).

Chapter 2

—

Elucidation of TRIM25 ubiquitination targets involved in diverse and antiviral cellular processes

ABSTRACT

The tripartite motif (TRIM) family of E3 ubiquitin ligases is well known for its roles in antiviral restriction and innate immunity regulation, in addition to many other cellular pathways. In particular, TRIM25-mediated ubiquitination affects both carcinogenesis and antiviral response. While individual substrates have been identified for TRIM25, it remains unclear how it regulates diverse processes. Here we characterized a mutation, R54P, critical for TRIM25 catalytic activity, which we successfully utilized to "trap" substrates. We demonstrated that TRIM25 targets proteins implicated in stress granule formation (G3BP1/2), nonsense-mediated mRNA decay (UPF1), nucleoside synthesis (NME1), and mRNA translation and stability (PABPC4). The R54P mutation abolishes TRIM25 inhibition of alphaviruses independently of the host interferon response, suggesting that this antiviral effect is a direct consequence of ubiquitination. Consistent with that, we observed diminished antiviral activity upon knockdown of several TRIM25-R54P specific interactors including NME1 and PABPC4. Our findings highlight that multiple substrates mediate the cellular and antiviral activities of TRIM25, illustrating the multi-faceted role of this ubiquitination network in modulating diverse biological processes.

AUTHOR SUMMARY

Ubiquitin E3 ligases each interact with and ubiquitinate a subset of cellular proteins, thereby regulating specific cellular processes. Tripartite motif containing protein 25 (TRIM25) is one such E3 ligase involved in carcinogenesis and antiviral innate immunity. TRIM25 catalytic activity is indispensable for the host antiviral response against alphaviruses, an arthropod-borne group of RNA viruses possessing expanding distributions and pandemic potential. However, it remains poorly

understood which TRIM25 substrates mediate viral inhibition. To complicate the matter, identification of E3 ligase substrates is technically challenging, given the transient nature of ligase-substrate interactions. Here, we present the first comprehensive ubiquitinome study utilizing a novel "substrate trapping" approach to identify TRIM25 target proteins. We found that TRIM25 ubiquitinates key players in translational and nucleic acid metabolic processes, specifically involving stress granule formation, nonsense-mediated mRNA decay, nucleotide synthesis, and translation initiation. In addition, TRIM25 ligase activity is critical for its inhibition of diverse alphaviruses through viral translation suppression, highlighting the importance of ubiquitination in driving antiviral activity in this context. Our study both provides new insights into understanding the innate immune and cell biology roles of TRIM25 and paves the way forward for identification of novel TRIM substrates at large.

BACKGROUND

Addition of ubiquitin, or ubiquitination, is a post-translational modification that is highly conserved in eukaryotic organisms and operates in myriad cellular pathways. Ubiquitin is a small, 76 amino acid protein that must be activated by E1 enzymes, passed to E2 carrier enzymes, and finally covalently attached to lysines on substrates by E3 ligases. Though only one enzyme is needed at each step, their numbers vary widely. Humans encode 2 E1 enzymes, about 40 E2 enzymes, and upwards of 600 E3 ligases (Li *et al*, 2008; Metzger *et al*, 2012). This vast number of E3 ligases is needed because they determine substrate specificity; however, the means by which E3 ligases identify their substrates and the array of substrates ubiquitinated by any given E3 ligase remain largely unknown.

The tripartite motif containing protein (TRIM) family is one of the largest families of E3 ligases, with over 70 *TRIM* genes in humans (Vunjak and Versteeg, 2019). TRIMs share three common domains at their N-terminus – the catalytic RING domain, 1 to 2 B-Box domains, and a coiled-coil domain – but differ in their C-termini (Vunjak and Versteeg, 2019). These varied C-termini determine TRIM substrate specificity, allowing this large family of proteins to regulate diverse cellular processes, including but not limited to viral restriction, immune signaling, stress responses, proliferation, and differentiation (Ozato *et al*, 2008; Rajsbaum *et al*, 2014; Hatakeyama, 2017; Hage and Rajsbaum, 2019). Mutations in *TRIM* genes have been associated with rare genetic diseases, including developmental, muscular, and neurological disorders (Meroni, 2020; Meroni and Desagher, 2022). However, development of targeted therapeutic approaches has been hindered by not only the lack of knowledge on their specific substrates, but also the frequent involvement of TRIMs in multiple cellular processes. One prime example is TRIM25, which functions in both cancer and antiviral innate immunity (Heikel *et al*, 2016; Martín-Vicente *et al*, 2017). When examined in the context of cancer, TRIM25-mediated ubiquitination primarily targets varied proteins for proteolytic degradation, which can either enhance or hinder carcinogenesis (Urano *et al*, 2002; Dong *et al*, 2012; Zang *et al*, 2017; Sato *et al*, 2018; Liu *et al*, 2020).

Many of the TRIM proteins are upregulated by interferon (IFN) and play significant roles in the host innate immune response (Hage and Rajsbaum, 2019). Upon detection of viral infection by the host cell, type I IFN is produced, inducing expression of hundreds of IFN-stimulated genes (ISGs) to establish an antiviral environment (Schneider *et al*, 2014; Schoggins, 2019). TRIM25 is one such ISG which not only stimulates innate immune signaling by ubiquitinating and activating the dsRNA

sensor RIG-I, but also functions as a critical co-factor of another ISG, zinc finger antiviral protein (ZAP) (Gack *et al*, 2007; Li *et al*, 2017; Zheng *et al*, 2017). While TRIM25 has been shown to complex with ZAP in the context of several different viral infections (Yang and Li, 2020), its ligase activity has only been tied to its participation in blocking translation of incoming RNA genomes of alphavirus (family *Togaviridae*) (Li *et al*, 2017). Given that ubiquitination of ZAP or lack thereof fails to affect its viral translation inhibition (Li *et al*, 2017), it is likely that TRIM25 antiviral involvement depends on its ubiquitination of other cellular proteins. Interestingly, both TRIM25 and ZAP not only bind viral RNA but also interact with other RNA binding proteins, implying that proteins involved in RNA processes may feature prominently among TRIM25 substrates (Goodier *et al*, 2015; Choudhury *et al*, 2017; Garcia-Moreno *et al*, 2019; Ficarelli *et al*, 2021).

In light of this question, we set out to identify novel TRIM25 substrates that may play a role in translation and RNA processes. Because identification of E3 ligase substrates is technically challenging due to the transient nature of ligase-substrate interactions, we utilized a "substrate trapping" approach similar to previously reported (Decorsière *et al*, 2016) to capture TRIM25 interactors in a co-immunoprecipitation (IP)/mass spectrometry (MS) experiment. We sought to generate a TRIM25 mutant that would be unable to interact with the upstream E2 carrier enzyme, thus simultaneously rendering it incapable of ubiquitination and prolonging its interactions with substrates. We identified a point mutation, R54P, in the TRIM25 RING catalytic domain, which almost completely abolishes its autoubiquitination in cells.

While almost all of the more highly enriched interactors are shared by both TRIM25-wild-type (WT) and -R54P, we found that TRIM25-R54P enriches for additional interactors as compared

to TRIM25-WT. Further characterization of some of the most highly enriched interactors, Ras-GTPase-activating protein SH3-domain binding proteins (G3BP) 1 and 2, RNA helicase up-frameshift protein 1 (UPF1), nucleoside diphosphate kinase 1 (NME1), and poly-adenylate binding protein cytoplasmic 4 (PABPC4), has validated their identification as novel TRIM25 substrates. We identified NME1 and PABPC4 as TRIM25-R54P specific interactors during viral infection. Moreover, upon characterization of its antiviral activity, the TRIM25-R54P mutant demonstrates a complete loss of inhibition against a panel of Old World and New World alphaviruses despite higher IFN and ISG expression compared to WT, suggesting that ubiquitination of TRIM25 substrates directly leads to activation of an antiviral state. Altogether, we have identified both known and novel interactors as TRIM25 substrates, and demonstrated the validity of this "substrate trapping" approach in identifying bona fide E3 ligase substrates. We have shed light on the ways that TRIM25-mediated ubiquitination might target substrates to modulate translation, nucleic acid metabolism, and antiviral response, paving the way for further work characterizing the critical role of TRIMs in diverse cellular and viral processes.

RESULTS

Point mutations in TRIM25 RING domain almost completely abolish TRIM25 auto-ubiquitination

It is technically challenging to identify E3 ligase-substrate interactions as they are often transient, resulting in proteasomal degradation or a change in localization or activity of the substrates. In order to enrich for transient E3 ligase-substrate interactions, we turned to a less conventional co-IP approach that makes use of E3 mutants unable to interact with E2 conjugating enzymes. This prevents ubiquitin transfer to E3 substrates and their subsequent targeting to other cellular pathways and as a

result, "trapping" these substrates. This approach successfully identified the cellular 'structural maintenance of chromosomes' (Smc) complex Smc5/6 as being targeted by hepatitis B virus X protein for ligase-mediated degradation (Decorsière *et al*, 2016). We hypothesized that a similar approach would serve to identify TRIM25 substrates, which will be immunoprecipitated more robustly with a TRIM25 E2 binding mutant than with TRIM25-WT, as the former is unable to mediate transfer of ubiquitin from E2 to substrates.

Residues important for the RING-E2 interaction and thus necessary for ligase activity have already been identified in the RING E3 ligase MDM2 (Nomura *et al*, 2017). We aligned the structure of the TRIM25 RING domain complexed to E2-ubiquitin (Ub) to the analogous MDM2-E2-Ub structure and identified two conserved critical E2 interaction residues in the TRIM25 RING domain, I15 and R54 (Figure 9A). To assess loss of ligase activity, we transfected HA-tagged Ub and FLAG-tagged TRIM25 into 293T cells and immunoprecipitated TRIM25 in denaturing conditions. We then blotted for HA-Ub, wherein polyubiquitination manifests as a ladder of bands. These TRIM25 E2 binding mutants (I15K and R54P), are deficient in auto-polyubiquitination, suggesting successful crippling of ligase activity (Figure 9B). Individual E2 binding mutants retain a mono-Ub band (Figure 9B), so we generated the double mutant I15K/R54P, which did not display further reduction in ligase activity (Figure 9B). Therefore, we selected the R54P mutant for future co-IP/MS studies since this mutation has previously been shown to reduce TRIM25 catalytic activity and polyubiquitin chain formation (Koliopoulos *et al*, 2016).

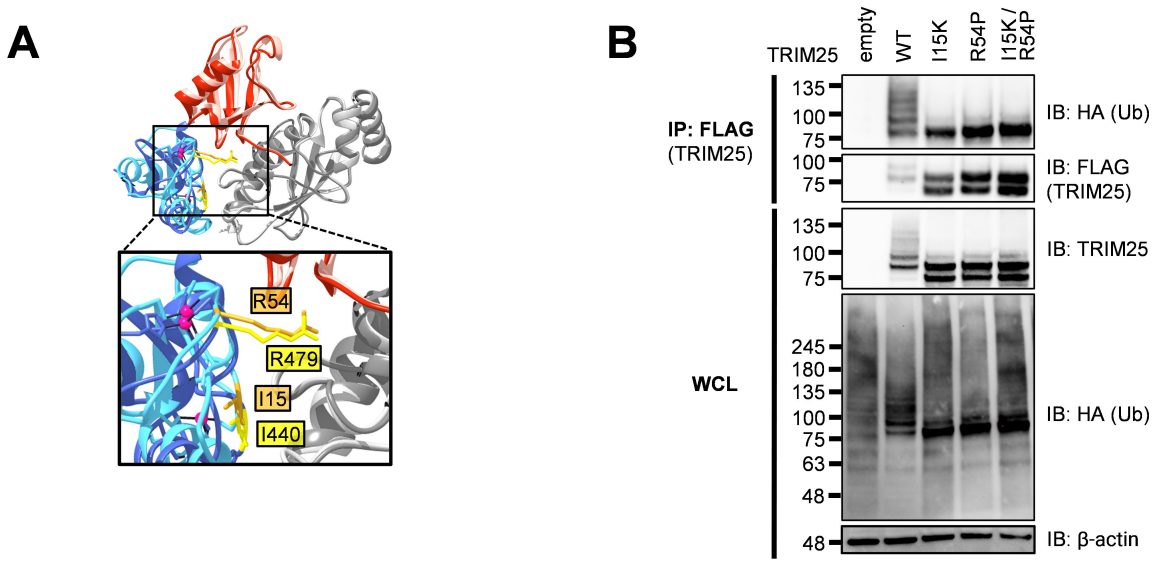

Figure 9. Individual TRIM25 RING residues required for TRIM25 autoubiquitination.

(A) Alignment of the RING E3 ligases MDM2 (dark blue) and TRIM25 (light blue) in complex with ubiquitin (red) and the E2 UbcH5 (gray), performed using UCSF Chimera (Pettersen *et al*, 2004). Highlighted in gold (TRIM25) and yellow (MDM2) are homologous residues. PDB: 5MNJ (MDM2), 5EYA (TRIM25). **(B)** Western blot of lysates of 293T cells transfected with FLAG-TRIM25 mutants and HA-ubiquitin (Ub). Data representative of three independent experiments.

Substrate trapping approach enriches for novel TRIM25 interactors

Next, we asked what proteins are modified by TRIM25, as identification of these substrates will elucidate how ubiquitination facilitates TRIM25-mediated cellular and antiviral activities. We first used CRISPR-Cas9 to generate a TRIM25 KO 293T cell line (Supplemental Figure 2.1). We then stably integrated doxycycline (dox) inducible FLAG-tagged TRIM25-WT and mutant -R54P using the ePiggyBac (ePB) transposon system (Woodard and Wilson, 2015), where both TRIM25-WT and -R54P are similarly induced in a dose-dependent manner (Figure 10A). TRIM25 protein levels are comparable upon detection using a FLAG or TRIM25-specific antibody (Figure 10A). To capture TRIM25 substrates, we performed two independent co-IP/MS experiments using our reconstituted TRIM25 KO 293T cell lines (Figure 10B). We induced TRIM25-WT or -R54P

expression in the presence or absence of the prototype alphavirus Sindbis virus (SINV), performed a FLAG IP to enrich for TRIM25, and analyzed the resultant protein mixture using MS. TRIM25 KO 293T cells with dox added were used as a control, since previous work by our lab found that dox treatment nonspecifically affects viral replication in other systems (Luu *et al*, 2021). We found that this "substrate trapping" approach enriches for interactors specific to TRIM25-R54P under both mock and infected conditions (Figure 10C-D, red circles). These TRIM25-R54P specific interactors tend to have lower fold change in abundance over background than interactors common to both TRIM25-WT and TRIM25-R54P (Figure 10C-D, blue circles), suggesting that the TRIM25-R54P co-IP/MS captures weaker interactions not identified with TRIM25-WT. After filtering for interactors enriched in both independent experiments, we found that TRIM25-R54P enriches for 14 unique interactors under mock conditions (Table 1) and that almost all TRIM25-WT interactors (25 of 30) are also present as TRIM25-R54P interactors (Table 2), indicating that TRIM25-R54P is otherwise functionally similar to TRIM25-WT. During viral infection, TRIM25-R54P enriches for all TRIM25-WT interactors in addition to 16 unique interactors (Tables 3-4), suggesting an effective "substrate trap." Interestingly, we found that the number of TRIM25 interactors drastically decreases during viral infection for both TRIM25-WT (29 to 7 interactors; Tables 2 and 4) and TRIM25-R54P (38 to 23 interactors; Tables 1 and 3). We used DAVID bioinformatics resources (Huang *et al*, 2009) to find that TRIM25 interactors are highly enriched in GO terms involved in translation, RNA metabolism, and viral transcription (Figure 9E). This is in line with our hypothesis that TRIM25 substrates mediate diverse cellular and viral processes as a consequence of ubiquitination.

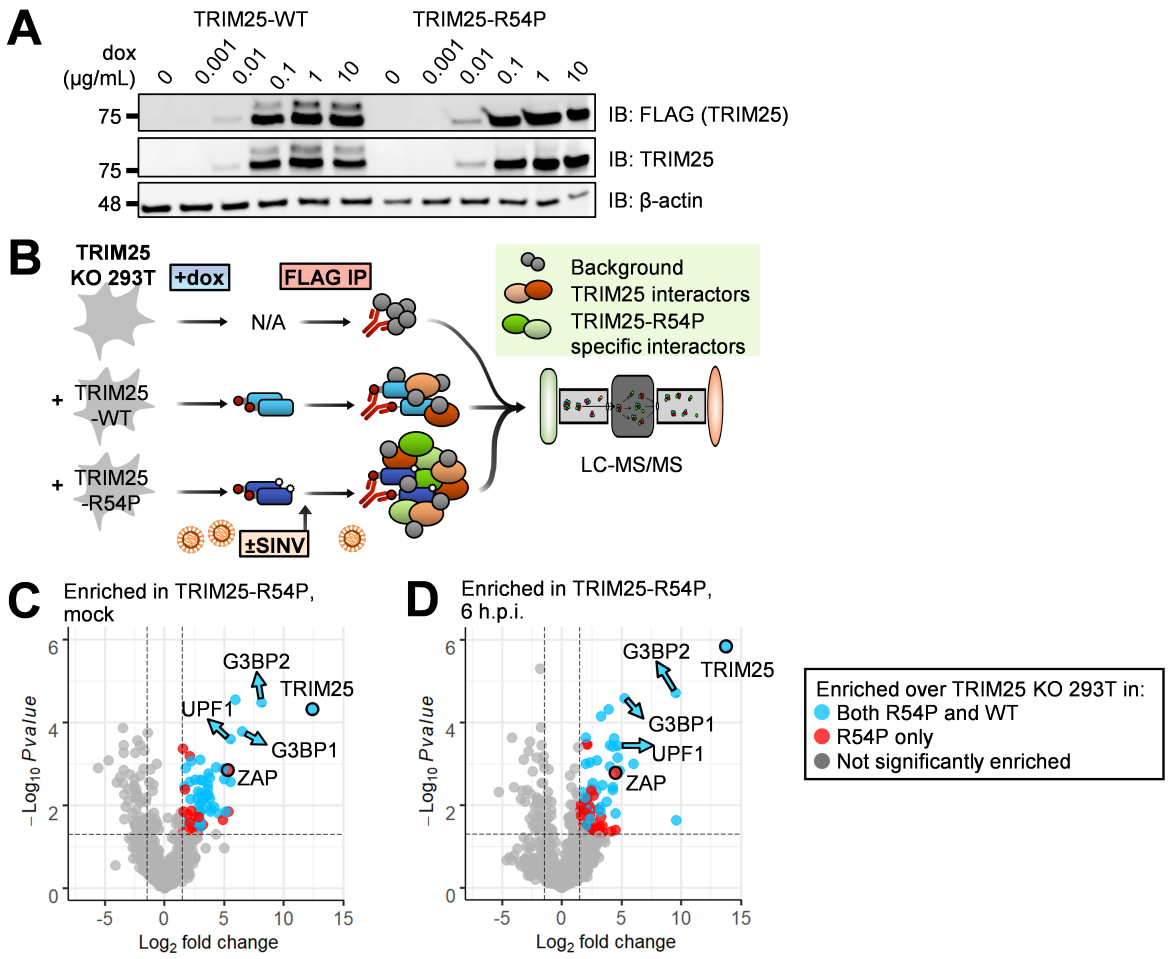

E

	P value	
Gene Ontology Term	**mock**	**6 h.p.i.**
Nuclear-transcribed mRNA catabolic process, NMD	9.17E-26	5.55E-09
SRP-dependent cotranslational protein targeting to membrane	3.68E-23	5.12E-06
Translational initiation	1.03E-22	1.30E-08
Viral transcription	4.96E-22	1.03E-05
Translation	2.41E-20	4.95E-07
rRNA processing	1.00E-19	1.29E-04

Figure 10. TRIM25 co-IP/MS identifies TRIM25 interactors.

(A) Western blot of TRIM25 inducible 293T cell lines in the presence of increasing amount of dox (0, 0.001, 0.01, 0.1, 1, and 10 µg/mL). Data are representative of two independent experiments. **(B)** Schematic of co-IP/MS experiment to identify TRIM25 interactors. **(C-D)** Volcano plots of proteins significantly enriched over TRIM25 KO background in TRIM25-R54P co-IP/MS in the **(C)** absence or **(D)** presence of viral infection. Data representative of two independent experiments. Blue dots represent proteins that were also significantly enriched in TRIM25-WT co-IP and red dots represent proteins that were only enriched in TRIM25-R54P co-IP. Proteins were counted as enriched when log2FC>1.5 and -log10Pvalue>1.3 (Pvalue<0.05). The R package EnhancedVolcano (Blighe *et al*, 2021) was used to generate volcano plots. **(E)** Gene ontology terms significantly enriched in all unique TRIM25-WT and TRIM25-R54P interactors. Analysis performed for GO terms in biological processes using DAVID (Huang *et al*, 2009).

Table 1. TRIM25-R54P interactors in the absence of virus.

Interactors pulled down in both independent experiments shown here; proteins also enriched in TRIM25-WT co-IP are italicized and bolded. Fold change = FC. In EXP #2, the "i" prefacing log2FC and Pvalue refers to how missing data values were imputed.

Protein	EXP #1 log2FC	EXP #2 ilog2FC	EXP #1 -log10Pvalue	EXP #2 -log10iPvalue
TRIM25	***12.39***	***7.51***	***4.29***	***2.12***
G3BP2	8.11	5.55	4.48	1.50
G3BP1	***6.50***	***4.03***	***3.78***	***1.73***
PABPC1	***5.93***	***5.10***	***4.55***	***3.28***
UPF1	***5.50***	***4.79***	***3.60***	***1.44***
RPL27	5.34	3.69	1.84	1.55
ZC3HAV1	5.32	5.31	2.83	1.42
ZCCHC3	***5.12***	***3.75***	***1.85***	***1.78***
RPL36	4.98	3.48	2.88	1.79
MOV10	4.91	4.49	1.64	1.80
RPLP2	***4.13***	***5.86***	***1.96***	***1.55***
SSB	***3.89***	***4.48***	***1.91***	***1.71***
RPS3A	***3.79***	***2.69***	***2.16***	***1.89***
MRPL11	***3.77***	***5.47***	***2.66***	***1.40***
RPL3	3.66	2.15	2.24	1.79
RPS12	***3.66***	***3.49***	***2.76***	***1.89***
NME1	***3.61***	***4.79***	***2.39***	***1.79***
IGF2BP3	***3.56***	***3.28***	***1.98***	***1.50***
RPS8	***3.26***	***3.27***	***2.19***	***1.75***
DNAJA1	3.17	3.92	2.61	1.91
RPL21	3.06	2.39	1.48	1.47
DDX21	***3.05***	***1.89***	***1.59***	***1.73***
RPL7A	***3.04***	***2.52***	***2.05***	***1.73***
DDX50	***3.03***	***3.66***	***1.48***	***1.53***
RPL14	***3.01***	***2.79***	***1.83***	***1.79***
HSPA9	***2.98***	***2.54***	***3.10***	***1.73***
RPL8	***2.95***	***2.64***	***2.62***	***1.50***
RPL4	***2.95***	***1.93***	***1.80***	***1.50***
RPL30	***2.92***	***4.99***	***1.86***	***1.81***
RPL6	2.88	1.95	1.97	1.50
RPL19	2.77	5.27	1.34	1.36
CXorf56	2.62	2.59	1.71	1.34
MRPS25	***2.56***	***3.34***	***2.61***	***1.54***
POLDIP2	2.24	2.45	3.07	1.64
IGF2BP2	***2.20***	***3.23***	***2.15***	***1.46***
HSPA5	***2.10***	***2.61***	***2.56***	***1.79***
NCL	1.95	2.58	1.78	2.63
HSPA8	***1.64***	***2.01***	***2.45***	***1.79***
RTRAF	1.60	1.76	1.84	1.31

Table 2. TRIM25-WT interactors in the absence of virus.

Interactors pulled down in both independent experiments shown here; proteins also enriched in TRIM25-R54P co-IP in both independent experiments are italicized and bolded. Fold change = FC. In EXP #2, the "i" prefacing log2FC and Pvalue refers to how missing data values were imputed.

Protein	EXP #1 log2FC	EXP #2 ilog2FC	EXP #1 -log10Pvalue	EXP #2 -log10iPvalue
TRIM25	***12.35***	***7.21***	***4.29***	***2.36***
NME1	***5.89***	***5.69***	***3.19***	***2.11***
PABPC1	***5.18***	***4.36***	***4.32***	***2.65***
UPF1	***4.15***	***4.99***	***3.13***	***1.56***
G3BP1	***3.84***	***4.38***	***2.89***	***2.08***
SSB	***3.67***	***5.28***	***1.82***	***1.67***
RPS12	***3.52***	***3.02***	***2.70***	***2.24***
DDX21	***3.52***	***1.60***	***1.79***	***2.07***
ZCCHC3	***3.41***	***2.47***	***1.50***	***1.50***
MRPL11	***3.11***	***4.50***	***2.36***	***1.83***
MRPS25	***3.11***	***5.37***	***2.93***	***1.81***
RPS3A	***3.02***	***1.92***	***1.82***	***2.11***
RPL14	***2.91***	***2.56***	***1.78***	***1.71***
RPS8	***2.86***	***3.07***	***1.99***	***2.11***
RPL23A	2.83	2.50	1.42	2.29
LARP1	2.82	2.72	1.75	1.65
HSPA9	***2.78***	***2.55***	***2.98***	***1.98***
DDX50	***2.78***	***5.52***	***1.38***	***1.87***
RPLP2	***2.71***	***5.81***	***1.37***	***1.36***
RPL7A	***2.68***	***2.05***	***1.87***	***2.11***
RPL8	***2.67***	***1.91***	***2.46***	***1.46***
IGF2BP3	***2.67***	***3.65***	***1.56***	***1.66***
HSPA5	***2.36***	***2.77***	***2.75***	***2.05***
FMR1	2.16	2.14	1.38	1.56
RPL4	***2.09***	***1.96***	***1.33***	***2.08***
RPL30	***1.98***	***4.99***	***1.33***	***2.66***
RPL32	1.91	2.10	1.44	2.05
IGF2BP2	***1.73***	***2.16***	***1.80***	***1.45***
HSPA8	***1.66***	***2.26***	***2.46***	***1.65***
FXR1	1.52	4.86	2.66	1.59

Table 3. TRIM25-R54P interactors during viral infection.

Interactors pulled down in both independent experiments shown here; proteins also enriched in TRIM25-WT co-IP in both independent experiments are italicized and bolded. Fold change = FC. In EXP #2, the "i" prefacing log2FC and Pvalue refers to how missing data values were imputed.

Protein	EXP #1 log2FC	EXP #2 ilog2FC	EXP #1 -log10Pvalue	EXP #2 -log10iPvalue
TRIM25	***13.82***	***6.87***	***5.83***	***1.28***
G3BP2	9.50	7.66	4.71	1.40
G3BP1	5.25	2.51	4.58	1.92
NME1	4.81	3.43	2.84	1.40
H1FX	***4.65***	***4.49***	***3.14***	***1.46***
UPF1	***4.64***	***5.24***	***3.44***	***1.94***
ZC3HAV1	4.47	2.77	2.77	1.42
RPL8	4.26	2.98	2.36	1.80
PABPC4	4.25	2.67	3.42	1.42
PABPC1	4.24	3.54	2.44	1.44
HP1BP3	***4.00***	***4.09***	***3.44***	***1.50***
LARP1	***3.93***	***4.59***	***4.32***	***1.61***
DDX50	***3.74***	***4.14***	***2.08***	***1.47***
RPL21	3.40	3.45	1.50	1.44
RPL29	3.38	2.53	2.48	2.06
HSPA9	***3.28***	***2.04***	***4.15***	***2.05***
ZCCHC3	***3.23***	***4.49***	***1.95***	***1.54***
RPS3A	3.18	1.53	1.36	1.38
GLYR1	3.01	2.59	1.43	1.59
YBX1	2.61	1.73	1.44	1.44
GNL3L	2.47	5.28	2.35	1.58
RPL19	2.44	2.90	2.39	1.75
MRPS26	1.98	1.90	1.49	1.31
MRPS9	1.58	2.56	2.02	1.38

Table 4. TRIM25-WT interactors during viral infection.

Interactors pulled down in both independent experiments shown here; proteins also enriched in TRIM25-R54P co-IP in both independent experiments are italicized and bolded. Fold change = FC. In EXP #2, the "i" prefacing log2FC and Pvalue refers to how missing data values were imputed.

Protein	EXP #1 log2FC	EXP #2 ilog2FC	EXP #1 -log10Pvalue	EXP #2 -log10iPvalue
TRIM25	***13.19***	***6.43***	***5.75***	***1.15***
H1FX	***3.95***	***3.23***	***2.87***	***1.74***
UPF1	***3.86***	***5.51***	***3.13***	***1.62***
HP1BP3	***2.75***	***3.84***	***2.82***	***1.75***
ZCCHC3	***2.65***	***4.90***	***1.78***	***1.41***
HSPA9	***2.63***	***2.35***	***3.77***	***1.41***
LARP1	***2.62***	***4.61***	***3.63***	***1.42***
DDX50	***2.44***	***5.21***	***1.47***	***1.46***

TRIM25 interacts with G3BP1 and 2 through a conserved binding motif and modifies them with predominantly K63 polyubiquitin chains

Among the most enriched TRIM25-R54P interactors in the presence and/or absence of SINV infection (Tables 1 and 3), we identified the core stress granule proteins G3BP1 and 2, RNA helicase UPF1 (Figure 10C-D, blue arrows), metastatic suppressor and nucleoside kinase NME1, and poly(A) binding protein PABPC4 as high priority candidates given our interest in RNA metabolic and translation processes (G3BP1 and 2, UPF1, PABPC4) and TRIM25's role in regulating carcinogenesis (NME1). Next, we asked whether any of these are TRIM25 ubiquitination substrates.

Both G3BP1 and G3BP2, hereafter collectively referred to as G3BP, associate very strongly with TRIM25 in the co-IP/MS (Tables 1-4, G3BP1, log2FoldChange 2.5–6.5; G3BP2, log2FoldChange 5.5–9.5). G3BP normally function in stress granule (SG) assembly, interacting with RNA and other cellular proteins to induce SG formation (Tourrière *et al*, 2003; Kang *et al*, 2021). Interestingly, the Old World alphaviruses exploit G3BP to promote their own replication (Cristea *et al*, 2006, 2010; Scholte *et al*, 2015; Kim *et al*, 2016). These viruses utilize their non-structural protein 3 (nsP3) to recruit G3BP into viral replication complexes, which disrupts antiviral SG formation (Panas *et al*, 2015), clusters viral replication complexes (Kim *et al*, 2016), and recruits translation initiation machinery (Götte *et al*, 2019). By doing so, alphaviruses enhance viral replication at the cost of endogenous G3BP function.

Previous work identified an FGDF peptide motif in alphavirus nsP3 which binds with high affinity to G3BP (Panas *et al*, 2015; Schulte *et al*, 2016). More recent work characterizing viral-host interaction motifs has uncovered a conserved G3BP-binding motif, ΦxFG (where Φ is a hydrophobic

residue) (Kruse *et al*, 2021). This G3BP interaction motif is present in both viral and host proteins, such as the cellular SG protein and known G3BP interactor USP10, and is remarkably similar to the alphavirus nsP3-G3BP interaction motif, FGDF, but likely binds with lower affinity (Kruse *et al*, 2021). Moreover, TRIM25 was identified as a G3BP1 interaction partner (Kruse *et al*, 2021). Mutating the latter two amino acids in the TRIM25-specific motif (404-PTFG-407), to alanine (404-PTAA-407) was sufficient to abolish TRIM25-G3BP1 interaction (Kruse *et al*, 2021). Meanwhile, TRIM25 and G3BP2 have previously been shown to interact in the context of prostate cancer (Takayama *et al*, 2018). To examine whether this motif is also necessary for TRIM25-G3BP2 interaction, we co-transfected myc-tagged G3BP into TRIM25 KO 293T cells along with FLAG-tagged TRIM25-WT, -R54P, or -PTAA, and performed a FLAG IP to pull down TRIM25. While both TRIM25-WT and -R54P robustly associate with both G3BP1 and -2, TRIM25-PTAA does not associate with either G3BP1 or 2 (Figure 11A), validating our co-IP/MS identification of G3BP as TRIM25 interactors.

We then used the ePB transposon system to reconstitute TRIM25 KO 293T cells with dox inducible TRIM25-PTAA. To establish that TRIM25 ubiquitinates G3BP and that the TRIM25-G3BP interaction is necessary for ubiquitination, we co-transfected myc-tagged G3BP with HA-Ub into TRIM25-WT, -R54P, and -PTAA inducible cell lines. After inducing TRIM25 expression, we performed a myc IP and probed for the presence of ubiquitinated G3BP. We found that both G3BP1 and 2 are robustly polyubiquitinated only in the presence of TRIM25-WT (Figure 11B), again validating our co-IP/MS identification of G3BP as TRIM25 substrates. No ubiquitination is detected in the presence of ligase-deficient TRIM25-R54P, whereas ubiquitination is dramatically diminished

in the presence of G3BP-interaction deficient TRIM25-PTAA (Figure 11B). Interestingly, TRIM25 appears to more robustly ubiquitinate G3BP2 as compared to G3BP1 (Figure 11B). Given the TRIM25-mediated polyubiquitination of G3BP1 and 2, we then characterized G3BP ubiquitination linkage type. To do so, we transfected our TRIM25-WT inducible cell line with myc-G3BP1 or -2 and different forms of HA-Ub: -WT, -K48, and -K63. Ub-K48 and -K63 have all lysines mutated to arginine except -K48 and -K63, respectively, such that only K48 or K63 polyubiquitin chains are able to be formed (Lim *et al*, 2005). We found that both G3BP1 and 2 are most robustly ubiquitinated in the presence of Ub-K63, suggesting that TRIM25 primarily mediates K63-linked ubiquitination of both proteins (Figure 11C). Interestingly, while both G3BP1 and 2 exhibit a lower level of ubiquitination in the presence of Ub-K48, G3BP1 possesses more K48-linked polyubiquitin chains as compared to G3BP2 (Figure 11C), indicating that TRIM25 is able to distinguish between and differentially ubiquitinate these related proteins.

We then asked whether TRIM25-G3BP interaction and G3BP ubiquitination are required for TRIM25 antiviral activity. We found that overexpression of TRIM25-PTAA suppresses SINV replication (Supplemental Figure 2.2A) and translation (Supplemental Figure 2.2B) similarly to TRIM25-WT, suggesting that loss of TRIM25-G3BP interaction or G3BP ubiquitination is not sufficient to restore SINV infection. It has been demonstrated that different alphaviruses display differing degrees of dependency on G3BP for their replication, wherein SINV is partially reliant and chikungunya virus (CHIKV) is completely reliant on G3BP (Kim *et al*, 2016; Götte *et al*, 2020). We hypothesized that a more G3BP-reliant virus such as CHIKV might be more sensitive to any antiviral mechanisms that are dependent on G3BP. In such a system, TRIM25-PTAA, which is unable to

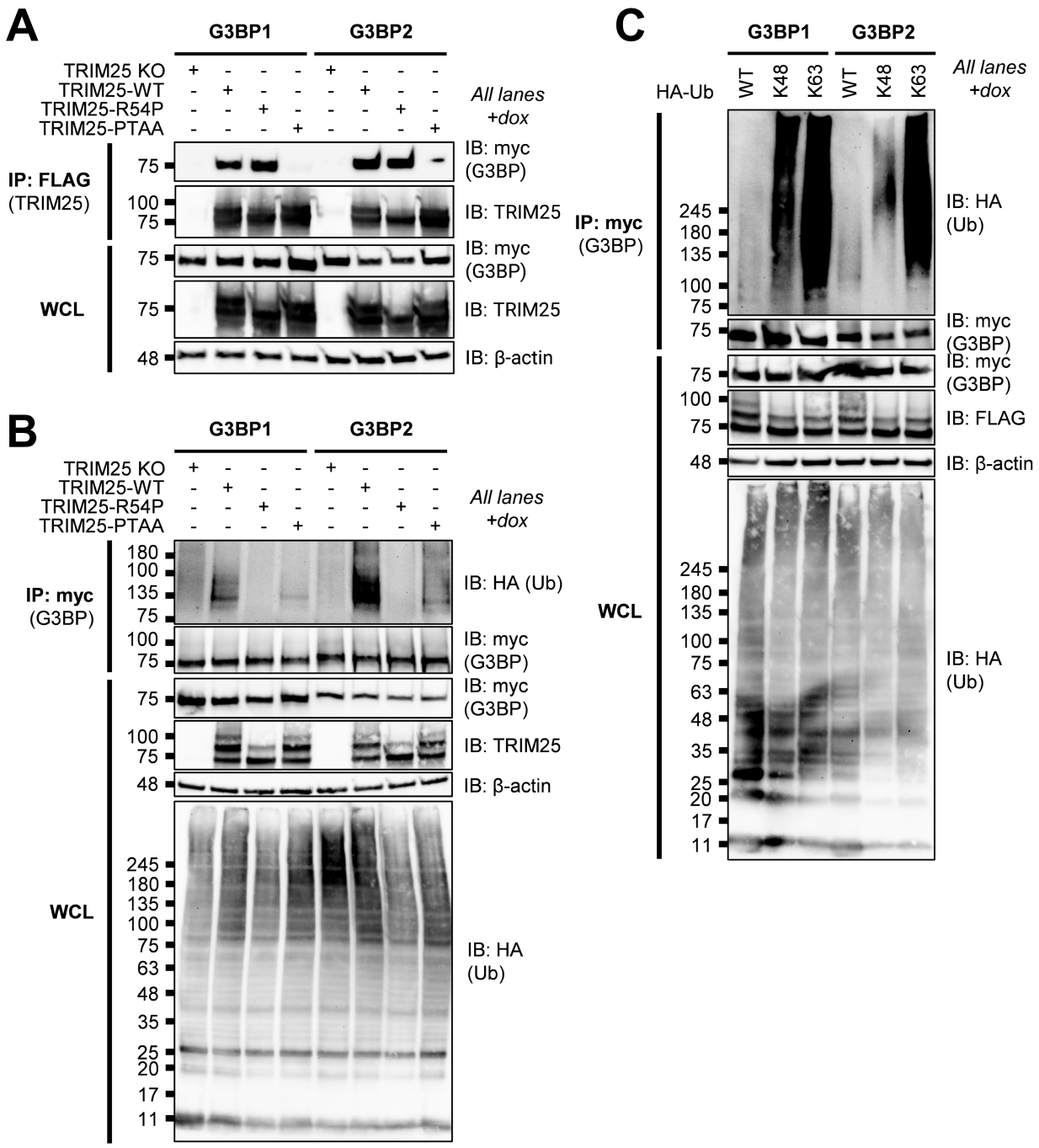

Figure 11. TRIM25 interacts with and polyubiquitinates G3BP.

(A) Western blot of TRIM25 KO 293T cells transfected with myc-G3BP1/2 and FLAG-TRIM25-WT, -R54P, or -PTAA. Lysates were subjected to FLAG IP. Data are representative of three independent experiments. (B-C) Western blot of TRIM25 inducible cells transfected with myc-G3BP1/2 and HA-Ub-WT, or (C) -K48, or -K63. Lysates were subjected to myc IP. Data are representative of three independent experiments.

interact with and efficiently ubiquitinate G3BP to potentially disrupt their pro-viral functions, may not be as antiviral as TRIM25-WT. Interestingly, inhibition of CHIKV infection is also dependent on TRIM25 with functional ligase activity, as TRIM25-R54P restores virion production to similar levels as TRIM25 KO (Supplemental Figure 2.2C). However, we found no significant difference between TRIM25-WT and TRIM25-PTAA in their ability to suppress virion production (Supplemental Figure 2.2C). Overall, though we validated G3BP interaction with and ubiquitination by TRIM25, we did not find that the TRIM25-G3BP axis is sufficient for TRIM25 antiviral activity.

TRIM25 interacts with and mono-ubiquitinates UPF1 at K592

Moreover, UPF1 associates very strongly with TRIM25 in the co-IP/MS (Tables 1-4, log2FoldChange 3.9–5.5), supporting a role for UPF1 as a novel TRIM25 interactor. UPF1 is best known for its central role in nonsense-mediated mRNA decay (NMD), where it is recruited to premature termination codons to catalyze the NMD pathway, inhibiting further translation and recruiting other RNA-degrading enzymes (Kim and Maquat, 2019). UPF1 has also been implicated in serving an antiviral role in the context of alphavirus infection (Balistreri *et al*, 2014). The authors of this study found that depletion of NMD components, including UPF1, promotes viral replication; further investigation revealed that UPF1 likely destabilizes incoming viral RNA genomes (Balistreri *et al*, 2014).

We first validated that TRIM25 interacts with UPF1. To do so, we transfected V5-tagged UPF1 into TRIM25 inducible cell lines, then induced for TRIM25-WT or -R54P expression with dox, and performed a FLAG IP to pull down TRIM25. We found that UPF1 is robustly detected only when TRIM25 is induced (Figure 12A), validating the TRIM25-UPF1 interaction identified in our

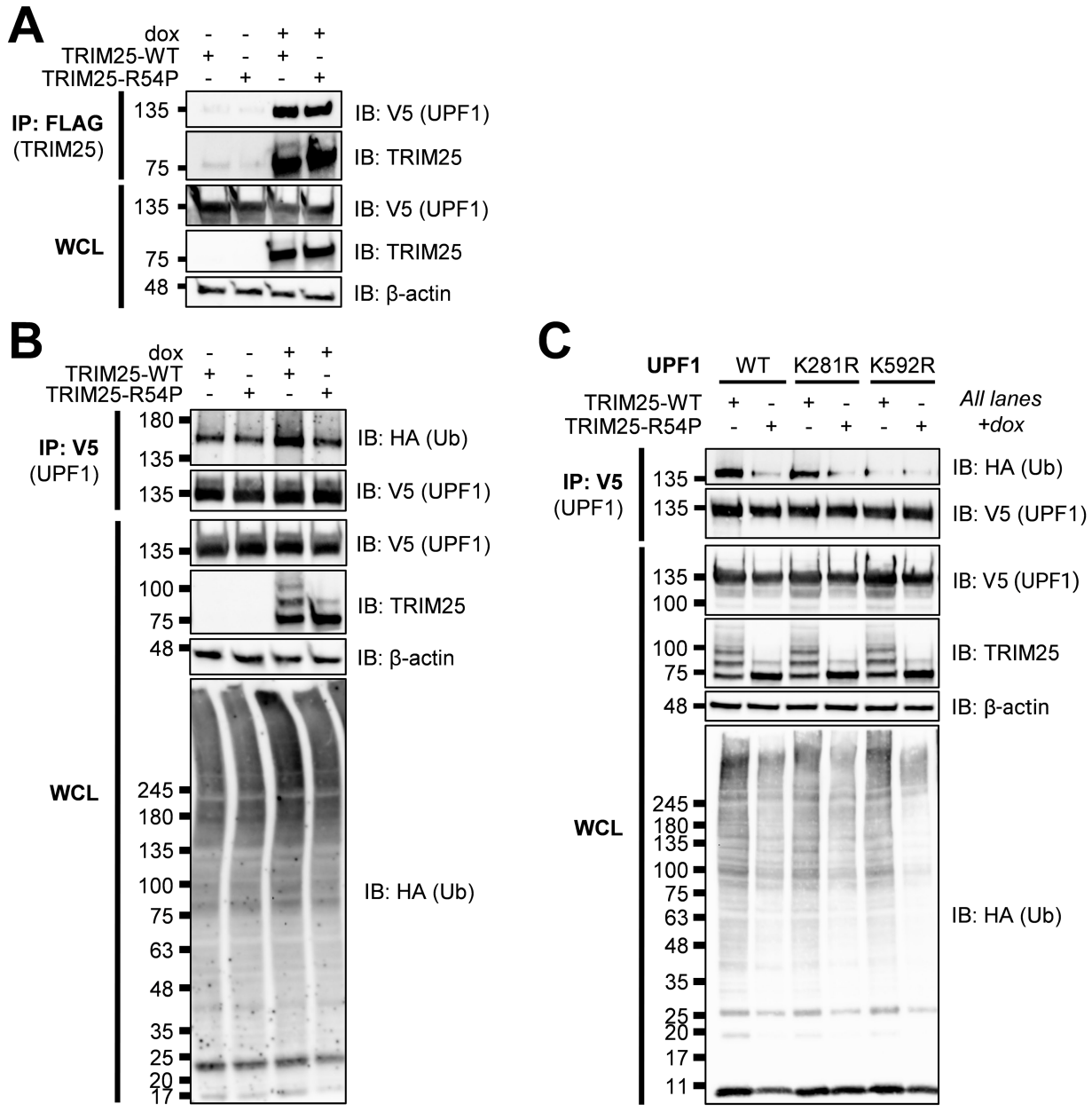

Figure 12. TRIM25 interacts with and mono-ubiquitinates UPF1.

(A) Western blot of TRIM25 inducible cells transfected with V5-tagged UPF1 in the presence or absence of 1 µg/mL dox. Lysates were subjected to FLAG IP. Data are representative of three independent experiments. **(B-C)** Western blot of TRIM25 inducible cells transfected with **(B)** V5-UPF1 or **(C)** V5-UPF1 mutants (K281R, K592R) and HA-Ub in the presence of 1 µg/mL dox. Lysates were subjected to V5 IP. Data are representative of two independent experiments for **(B)** and of three independent experiments for **(C)**.

co-IP/MS. To test the hypothesis that TRIM25 ubiquitinates UPF1, we co-transfected V5-tagged UPF1 with HA-Ub into our TRIM25 inducible cell lines and induced TRIM25 expression. We then performed a V5 IP and probed for the presence of ubiquitinated UPF1. We found that UPF1 is more robustly mono-ubiquitinated only in the presence of TRIM25-WT and not ligase-deficient TRIM25-R54P (Figure 12B, ~50% more by ImageJ quantification), suggesting that TRIM25 mono-ubiquitinates UPF1. We then identified putative ubiquitination sites by selecting residues that are both identified in a previously published ubiquitinome (Kim *et al*, 2011) and predicted via UbPred to be ubiquitinated (Score > 0.70) (Radivojac *et al*, 2010), and mutated these sites to arginine (K281R, K592R). Whereas ubiquitination is unchanged in UPF1 K281R, the introduction of K592R abolishes UPF1 ubiquitination in the presence of TRIM25-WT (Figure 12C). Together, these results validate our co-IP/MS identification of UPF1 as a novel TRIM25 substrate.

Next, we asked whether UPF1 plays a role in TRIM25 antiviral activity. We tested several UPF1 siRNAs and selected the one with the most efficient knockdown (Supplemental Figure 2.2D). We observed that UPF1 knockdown only has a significant effect on SINV replication when TRIM25 is absent, though trends toward an effect when TRIM25-WT is induced (Supplemental Figure 2.2E-F). Together, these data suggest that UPF1 could be antiviral independent of TRIM25 and that it is not critical for the TRIM25 antiviral response.

TRIM25 polyubiquitinates NME1 but only interacts with endogenous, not ectopically expressed NME1

Finally, we asked whether TRIM25-R54P specific interactors identified in our co-IP/MS were bona fide TRIM25 substrates. We identified NME1 as one of the most enriched TRIM25-R54P

interactors in the presence of SINV infection (Table 3, log2FoldChange 3.4–4.8). NME1 is a nucleoside diphosphate kinase and a major synthesizer of non-ATP nucleoside triphosphates, perhaps best characterized in its role in inhibiting cell migration and proliferation of tumor cells via inhibition of MAPK signaling (Mátyási *et al*, 2020). However, the role of NME1 in viral replication is not well studied (Yan *et al*, 2009).

Given its well-characterized role as a metastatic suppressor, we decided to validate NME1 as a TRIM25 ubiquitination substrate. We first set out to validate TRIM25 interaction with NME1 as identified in our co-IP/MS (Tables 1-3). To do so, we transfected myc-tagged NME1 or UPF1 to serve as a positive control in our TRIM25 inducible lines, induced for TRIM25-WT or -R54P expression, and performed a FLAG IP to pull down TRIM25. We then probed for any associated UPF1 or NME1. While we saw robust association of UPF1 with both TRIM25-WT and -R54P in line with our previous results (Figures 12A and 13A, MW ~135 kDa), we did not identify NME1 (Figure 13A, MW 20-25 kDa). We also performed the reverse IP where we pulled down myc-tagged NME1, but were unable to find any TRIM25 interacting with NME1 (Figure 13B). We hypothesized that this lack of TRIM25-NME1 interaction could be due to functional differences between ectopically expressed myc-NME1 and endogenous NME1, given our successful validation of the other robust TRIM25 interactors from our co-IP/MS, G3BP and UPF1 (Figures 11 and 12). To test this hypothesis, we performed a FLAG IP using our TRIM25 inducible lines and probed for co-IP of endogenous NME1 along with endogenous G3BP and UPF1 as positive controls. In line with our co-IP/MS results, endogenous G3BP, UPF1, and NME1 enrich robustly with TRIM25 pulldown,

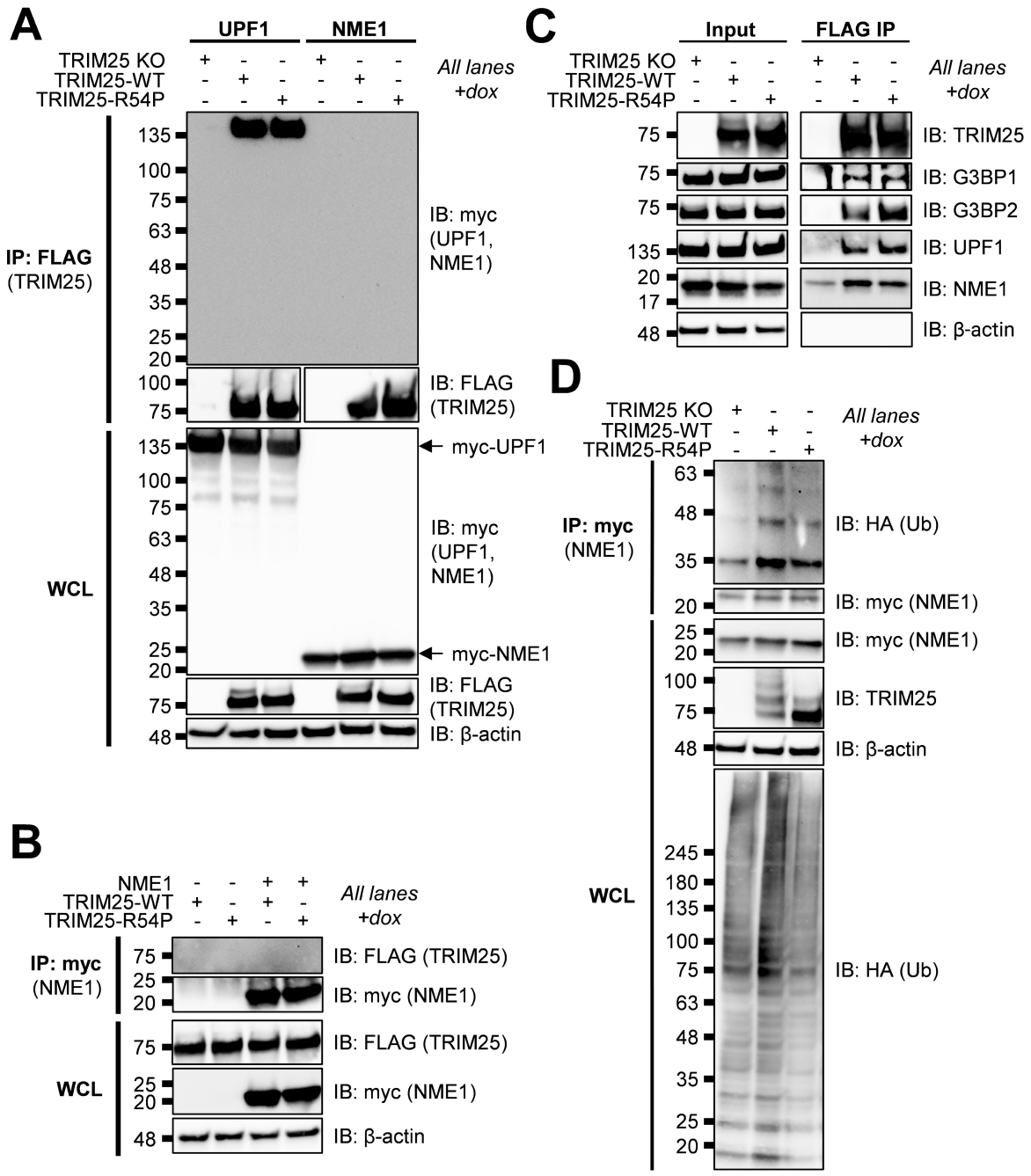

Figure 13. TRIM25 interacts with and polyubiquitinates NME1.

(A) Western blot of TRIM25 KO and TRIM25 inducible cells transfected with myc-tagged UPF1 or NME1 in the presence of 1 µg/mL dox. Lysates were subjected to a FLAG IP. Data are representative of two independent experiments. (B) Western blot of TRIM25 inducible cells transfected with myc-NME1 in the presence or absence of 1 µg/mL dox. Lysates were subjected to a myc IP. Data are representative of two independent experiments. (C) Western blot of TRIM25 KO and TRIM25 inducible cells in the presence of 1 µg/mL dox. Lysates were subjected to a FLAG IP. Data are representative of two independent experiments. (D) Western blot of TRIM25 KO and TRIM25 inducible cells treated with 1 µg/mL dox and transfected with myc-NME1 and HA-Ub. Lysates were subjected to myc IP. Data are representative of three independent experiments.

despite a low level of non-specific binding of NME1 to the FLAG IP in TRIM25 KO 293T cells (Figure 13C).

To test whether TRIM25 ubiquitinates NME1, we transfected myc-tagged NME1 into TRIM25-WT and -R54P inducible cells, induced for TRIM25 expression, and performed a myc IP. We found that NME1 is more robustly polyubiquitinated in the presence of TRIM25-WT as compared to TRIM25-R54P, although we cannot yet rule out the possibility that TRIM25 might mono-ubiquitinate NME1 at multiple sites (Figure 13D).

TRIM25 interacts with PABPC4 and predominantly modifies it with K63 polyubiquitin chains

We chose PABPC4 as a second example of TRIM25-R54P specific substrates. We identified PABPC4 as a TRIM25-R54P interactor in the presence of SINV infection (Table 3). PABPC4 is a member of the poly(A) binding protein (PABP) family, which functions in translation initiation by binding the mRNA poly(A) tail, thus regulating mRNA translation and stability (Wigington *et al*, 2014). PABPs have been shown to localize to SGs and to inhibit recruitment of UPF1 to 3'UTRs (Burgess *et al*, 2011; Wigington *et al*, 2014). Given their key roles in translation and mRNA metabolism, PABPs are frequently targeted and manipulated by viruses during infection (Gao *et al*, 2022). Interestingly, PABPC4 was recently found to broadly inhibit coronavirus replication by recruiting an E3 ligase to ubiquitinate the viral nucleocapsid protein and target it for degradation (Jiao *et al*, 2021).

We first validated the TRIM25-PABPC4 interaction by transfecting myc-tagged PABPC4, inducing for TRIM25-WT or -R54P expression, and pulling down TRIM25 via FLAG IP. We then probed for any associated PABPC4. We found that PABPC4 is robustly detected when either TRIM25

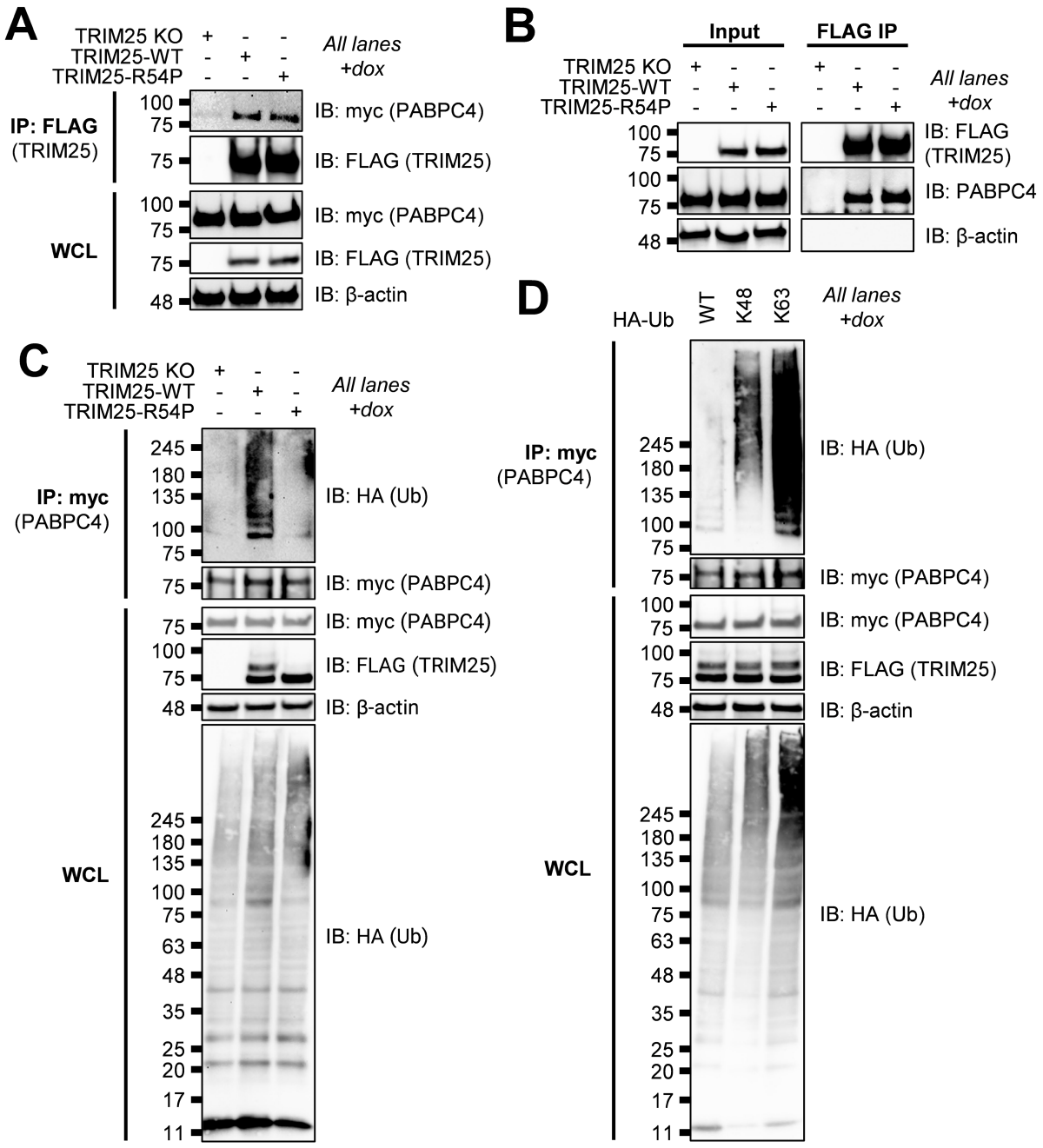

Figure 14. TRIM25 interacts with and polyubiquitinates PABPC4.

(A) Western blot of TRIM25 KO and TRIM25 inducible cells transfected with myc-tagged PABPC4 in the presence of 1 µg/mL dox. Lysates were subjected to a FLAG IP. Data are representative of two independent experiments. (B) Western blot of TRIM25 KO and TRIM25 inducible cells in the presence of 1 µg/mL dox. Lysates were subjected to a FLAG IP. Data are representative of two independent experiments. (C) Western blot of TRIM25 KO and TRIM25 inducible cells treated with 1 µg/mL dox and transfected with myc-PABPC4 and HA-Ub-WT. Lysates were subjected to myc IP. Data are representative of two independent experiments. (D) Western blot of TRIM25-WT inducible cells treated with 1 µg/mL dox and transfected with myc-PABPC4 and HA-Ub-WT, HA-Ub-K48, or HA-Ub-K63. Lysates were subjected to myc IP. Data are representative of two independent experiments.

-WT or TRIM25-R54P is induced (Figure 14A), validating the TRIM25-PABPC4 interaction identified in our co-IP/MS. We also found that both TRIM25-WT and -R54P interact with endogenous PABPC4 (Figure 14B).

We then asked whether TRIM25 ubiquitinates PABPC4. We transfected myc-PABPC4 into TRIM25-WT and -R54P inducible cells, induced for TRIM25 expression, and performed a myc IP. We found that PABPC4 is more robustly polyubiquitinated in the presence of TRIM25-WT as compared to TRIM25-R54P (Figure 14C). Upon characterizing ubiquitination via transfection of Ub-K48 or -K63, we found that like G3BP, PABPC4 is most robustly ubiquitinated in the presence of Ub-K63, suggesting that TRIM25 primarily mediates K63-linked ubiquitination of PABPC4 (Figure 14D).

Taken together, these results suggest that TRIM25-R54P specific interactors identified in our co-IP/MS, such as NME1 and PABPC4, function as bona fide TRIM25 substrates, and that TRIM25 is able to utilize a range of ubiquitin linkages dependent on the substrate context.

TRIM25 antiviral activity is dependent on its ligase activity

Given our identification of diverse host factors as TRIM25 substrates (Figures 11-14), many of which function in translational and RNA processes (Figure 10E) and several of which have known roles in alphavirus replication, we hypothesized that TRIM25 ligase activity is critical for orchestrating an antiviral response.

We used TRIM25 inducible cell lines in the KO background (Figure 10A) to characterize the requirement of ligase activity in TRIM25-mediated viral inhibition. We found that TRIM25-WT,

which retains ligase activity, represses SINV replication, whereas ligase mutant TRIM25-R54P does not (Figure 15A). Overexpression of TRIM25-WT (Figure 15A, solid light blue line) dramatically represses SINV replication by 7-15 fold at earlier timepoints (6-12 hours post infection (h.p.i.)) to 43-52 fold at later timepoints (24-40 h.p.i.) compared to TRIM25 KO 293T cell lines (Figure 15A, dotted lines). Interestingly, some replicates fail to initiate infection in the presence of TRIM25-WT, causing seemingly large variability in viral replication. In contrast, overexpression of ligase-deficient TRIM25-R54P (Figure 15A, solid dark blue line) restores SINV replication to levels even higher than the TRIM25 KO background (Figure 15A, dotted lines). Overexpressed TRIM25-R54P may act in a dominant negative manner by binding to and sequestering ZAP, preventing ZAP from interacting with its other co-factors. Similarly, we found that overexpression of TRIM25-WT robustly represses virion production by approximately 36-250 fold at 24-40 h.p.i., whereas overexpression of TRIM25-R54P restores virion production to comparable levels as the TRIM25 KO background (Figure 15B, compare solid light blue line to solid dark blue line).

We then investigated at which step TRIM25 may be acting to inhibit SINV infection. Previous work done by our lab showed that TRIM25 synergized with ZAP in blocking SINV translation (Li *et al*, 2017). We utilized a temperature-sensitive replication-deficient SINV luciferase reporter virus to characterize the requirement of ligase activity in TRIM25-mediated inhibition of viral translation, since luciferase activity for this virus represents translation of the incoming viral genome. Overexpressed TRIM25-WT inhibits viral translation by 6 fold at 6 h.p.i. (Figure 15C), supporting our hypothesis that TRIM25 blocks alphavirus replication by inhibiting translation of incoming viral genomes.

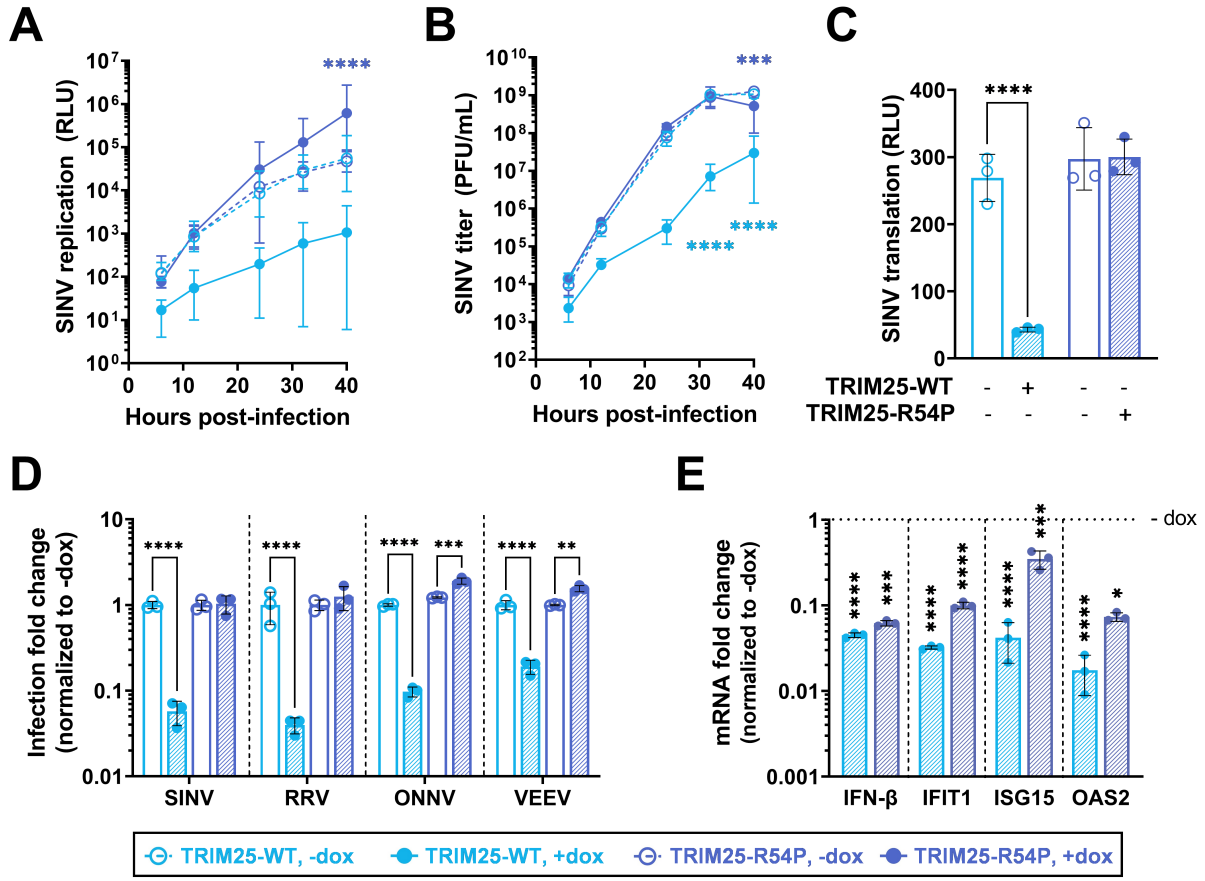

Figure 15. Point mutation in TRIM25 RING domain cripples TRIM25 antiviral activity.

(**A-C**) Dox inducible TRIM25-WT or -R54P were integrated into TRIM25 KO 293T cells using the ePiggyBac (ePB) transposon, and induced for TRIM25-WT or -R54P expression at 1 µg/mL dox. Cells were infected with (**A**) SINV Toto1101/Luc at an MOI of 0.01 plaque forming unit (PFU)/cell, and lysed at 6, 12, 24, 32, and 40 hours post infection (h.p.i.); data combined from three independent experiments, error bars indicate range; or (**B**) Sindbis virus (SINV) Toto1101 at an MOI of 0.01 PFU/cell, harvesting supernatant at 6, 12, 24, 32, and 40 h.p.i. for plaque assays; data representative of two independent experiments, error bars indicate range; or (**C**) SINV Toto1101/Luc:ts6 at an MOI of 1 PFU/cell and lysed at 6 h.p.i. for measurement of luciferase activity; data representative of two independent experiments, error bars indicate standard deviation. (**D**) Percent infected cells (GFP+) at MOI of 0.01 PFU/cell (SINV 24 h.p.i.; Ross River virus (RRV) 24 h.p.i.; o'nyong-nyong virus (ONNV) 22 h.p.i.; Venezuelan equine encephalitis virus (VEEV) 10 h.p.i.) were normalized to that of the respective cell line without dox (set to one-fold). Asterisks indicate statistically significant differences, calculated using (**A-B, D**) Two-way ANOVA and Tukey's multiple comparisons test: **, $p<0.01$; ***, $p<0.001$; ****, $p<0.0001$; (light blue compares WT +/- dox, dark blue compares R54P +/- dox) or (**C**) Two-way ANOVA and Sidak's multiple comparisons test: ****, $p<0.0001$. Data for each virus (demarcated by dashed lines) was statistically analyzed independently. (**E**) TRIM25 inducible cells were treated with poly(I:C) in the presence or absence of dox, and RNA was harvested for RT-qPCR analysis. mRNA levels of IFN/ISGs in TRIM25-WT or R54P were normalized to that of the respective cell line without dox (set to one-fold, horizontal dotted line). Data representative of two independent experiments. mRNA fold change for each gene (demarcated by vertical dashed lines) was statistically analyzed independently. Asterisks indicate statistically significant differences as compared to the -dox condition (Two-way ANOVA and Sidak's multiple comparisons test: *, $p<0.05$; ***, $p<0.001$; ****, $p<0.0001$).

While we already examined TRIM25 antiviral activity against the Old World alphavirus CHIKV, wherein TRIM25-WT inhibits robustly and TRIM25-R54P fails to inhibit (Supplemental Figure 2.2C), we then asked whether ligase-deficient TRIM25-R54P remains active against other alphaviruses. We tested other Old World (Ross River virus, RRV; o'nyong-nyong virus, ONNV) and New World (Venezuelan equine encephalitis virus, VEEV) alphaviruses. TRIM25-WT remains potently antiviral against all alphaviruses tested, while overexpression of TRIM25-R54P either has no effect on or restores viral replication to levels higher than the TRIM25 KO background (Figure 15D, light blue and dark blue shaded bars). Taken together, these data clearly demonstrate that TRIM25-dependent ubiquitination is required for inhibition of alphavirus replication, specifically through a block in viral translation.

TRIM25-mediated viral inhibition is independent of changes in the type I IFN response

To exclude the complementary possibility that TRIM25 is exerting antiviral effects through affecting type I IFN or ISG production, we quantified the mRNA of IFN-β and the prominent ISGs IFIT1, ISG15, and OAS2 in the presence of poly(I:C), a dsRNA mimetic and stimulator of innate immune signaling. If TRIM25 antiviral activity is mediated through a strengthened IFN response, we would expect that both IFN and ISG production will increase when TRIM25-WT is induced and to be lower in the presence of TRIM25-R54P due to its defective antiviral activity. Poly(I:C) stimulation works well, inducing IFN-β robustly both in the presence and absence of TRIM25 induction (Supplemental Figure 2.3). Surprisingly, we found that overexpression of either TRIM25-WT or TRIM25-R54P significantly suppresses production of IFN-β, IFIT1, ISG15, and OAS2 mRNA in the presence of poly(I:C) (Figure 15E). We also observed that induction of TRIM25-WT results in a

more drastic suppression of the ISGs as compared to TRIM25-R54P (Figure 15E, compare light blue to dark blue shaded bar), leading to a higher type I IFN response in the TRIM25-R54P inducible cell line. Together, these data support our hypothesis that TRIM25 antiviral activity is not mediated through the IFN response.

Identification of TRIM25-R54P specific interactors as critical for viral inhibition

As we showed that the loss of antiviral activity of TRIM25-R54P does not correlate with the levels of IFN and ISG expression, suggesting a direct consequence of TRIM25-mediated ubiquitination of target proteins, we then decided to examine TRIM25-R54P interactors identified in our co-IP/MS that are not consistently present in the TRIM25-WT enrichment (Tables 1 and 3, non-bolded and non-italicized proteins). These candidate proteins likely exhibit weaker or more transient interactions with TRIM25 and are ubiquitinated by TRIM25. We hypothesized that if any of these interactors are critical for TRIM25 antiviral activity, loss of their expression would result in increased viral replication even in the presence of overexpressed TRIM25-WT. While we initially also assessed a subset of ribosomal proteins identified as TRIM25-R54P interactors, their knockdown results in high cytotoxicity and therefore are excluded from subsequent analyses. We validated most of the TRIM25-R54P interactors that are not present on the TRIM25-WT lists (Tables 1-4) in the absence (Table 1, Figure 16A, Supplemental Figure 2.4A) or presence of viral infection (Table 3, Figure 16B, Supplemental Figure 2.4B). While knockdown of multiple interactors trends towards restoring SINV replication, only loss of RTRAF (Table 1, log2FoldChange 1.6–1.8) and NME1 (Table 3, log2FoldChange 3.4–4.8) significantly restores SINV replication (Figure 16A-B).

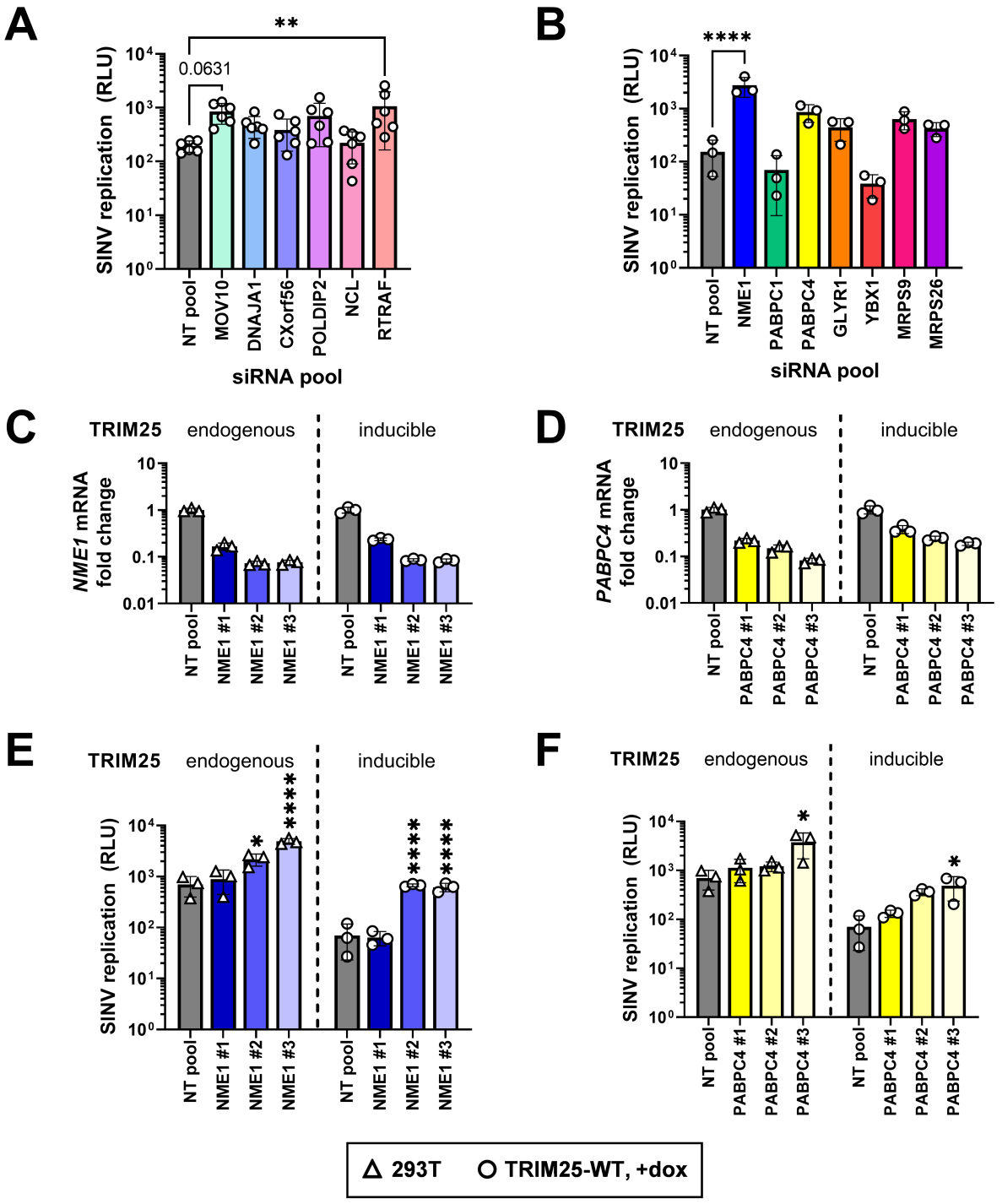
A
**
0.0631
SINV replication (RLU)
NT pool
MOV10
DNAJA1
CXorf56
POLDIP2
NCL
RTRAF
siRNA pool
B
****
SINV replication (RLU)
NT pool
NME1
PABPC1
PABPC4
GLYR1
YBX1
MRPS9
MRPS26
siRNA pool
C
TRIM25
endogenous
inducible
NME1 mRNA fold change
NT pool
NME1 #1
NME1 #2
NME1 #3
D
TRIM25
endogenous
inducible
PABPC4 mRNA fold change
NT pool
PABPC4 #1
PABPC4 #2
PABPC4 #3
E
TRIM25
endogenous
inducible
SINV replication (RLU)
F
TRIM25
endogenous
inducible
SINV replication (RLU)
293T
TRIM25-WT, +dox

Figure 16. Knocking down TRIM25-R54P specific interactors identifies essential substrates for TRIM25 antiviral activity.

(A-B) TRIM25 inducible cells were transfected with pooled siRNAs for either **(A)** hits specific to TRIM25-R54P in the absence of viral infection or **(B)** hits specific to TRIM25-R54P in the presence of viral infection. Cells were induced for TRIM25-WT expression at 1 µg/mL dox, infected with Toto1101/Luc at an MOI of 0.01 PFU/cell, and lysed at 24 h.p.i. for measurement of luciferase activity. Asterisks indicate statistically significant differences as compared to the NT pool siRNA (One-way ANOVA, Dunnett's multiple comparison test; **, $p<0.01$; ****, $p<0.0001$). Unlabeled comparisons are not significant. Data are either **(A)** pooled from or **(B)** representative of two independent experiments. **(C-F)** Parental 293T cells (TRIM25: endogenous) or TRIM25 inducible (TRIM25: inducible) cells were transfected with individual siRNAs for **(C,E)** *NME1* or **(D,F)** *PABPC4*, induced for TRIM25-WT expression at 1 µg/mL dox, and **(C-D)** had RNA extracted for RT-qPCR analysis or **(E-F)** infected with Toto1101/Luc at an MOI of 0.01 PFU/cell. Cells were lysed at 24 h.p.i. for measurement of luciferase activity. Asterisks indicate statistically significant differences as compared to the NT pool for each cell line. 293T and TRIM25-WT cell lines were statistically analyzed independently from one another (One-way ANOVA, Dunnett's multiple comparison test; *, $p<0.05$; ****, $p<0.0001$). Data are representative of two independent experiments for each cell line.

We decided to de-convolute the siRNA pools for both NME1 and PABPC4, given our verification of them as bona fide TRIM25 interactors and substrates (Figures 13 and 14). Moreover, loss of NME1 results in the most significant restoration of SINV replication (Figure 16B). We hypothesized that siRNAs that induced greater knockdown of *NME1* or *PABPC4* expression would also result in greater SINV replication. Therefore, we de-convoluted both *NME1* and *PABPC4* siRNA pools in both our inducible TRIM25-WT cell line and in the parental 293T cell line, which retains endogenous TRIM25 and ZAP expression. There, we observed that the degree of both *NME1* and *PABPC4* mRNA expression (Figure 16C-D) significantly and negatively correlate with increase of viral replication (Figure 16E-F), supporting a role for both NME1 and PABPC4 in TRIM25-dependent alphavirus inhibition. This correlation is more robust in the presence of inducible TRIM25-WT (NME1: $r = -0.83$, $p<0.001$; PABPC4: $r = -0.87$, $p<0.001$) than in the presence of endogenous TRIM25 (NME1: $r = -0.82$, $p<0.01$; PABPC4: $r = -0.74$, $p<0.01$). Altogether, these results suggest that the antiviral activity of TRIM25 is mediated by multiple substrates. Though knockdown of most individual interactors on their own does not significantly restore SINV replication, the fact that several

have demonstrated a phenotype implies that together they may have a larger impact on viral replication. Further studies need to be performed to determine their synergistic effects on viral infection and functional consequences of their ubiquitination by TRIM25.

DISCUSSION

Many TRIMs are involved in and ubiquitinate components of multiple cellular and antiviral processes (Ozato *et al*, 2008; Rajsbaum *et al*, 2014; Hatakeyama, 2017; Vunjak and Versteeg, 2019). In this study, we set out to identify TRIM25 substrates by generating a point mutation in the TRIM25 RING domain, R54P, which is predicted to abolish its interaction with E2 carrier enzymes and is sufficient to cripple TRIM25 ligase activity (Figure 9). We reported identification of TRIM25 substrates involved in nucleic acid metabolism and translation (Figure 10), in line with its role in blocking viral translation (Li *et al*, 2017). We characterized the ubiquitination of the most enriched TRIM25 interactors, G3BP (Figure 11) and UPF1 (Figure 12), as well as two TRIM25-R54P specific interactors during infection, NME1 (Figure 13), and PABPC4 (Figure 14). These represent proteins with essential cellular functions, some of which with prior involvement in alphavirus infection (Balistreri *et al*, 2014; Götte *et al*, 2019). We also used the TRIM25-R54P mutant to definitively show the critical role of ubiquitination in TRIM25 antiviral activity that is independent of IFN production and signaling (Figure 15). We then examined proteins that display a preference for association with TRIM25-R54P under mock and viral infection conditions, and found that several of these are necessary for TRIM25 antiviral activity (Figure 16), identifying them as potential TRIM25 substrates mediating viral inhibition. Our results suggest that targeting of any single substrate by TRIM25 is

insufficient to mediate the entirety of its cellular and antiviral activities, illustrating the powerful, multi-faceted role of this ubiquitination network in diverse biological processes.

We propose that the success of this "substrate trapping" approach in identifying TRIM25 ubiquitination substrates hinges on preservation of protein structure. Previous reports that unearthed the importance of TRIM25 ligase activity in the ZAP antiviral response depended on either deleting the entire TRIM25 RING catalytic domain or disrupting formation of the RING zinc finger motif, potentially having an adverse effect on protein folding overall thereby affecting other TRIM25 cellular functions or interactions (Li *et al*, 2017; Zheng *et al*, 2017). The R54P point mutation we generated has been demonstrated to preserve protein structure and cognate interactions in other contexts (Nomura *et al*, 2017), instilling greater credibility in our identification of novel TRIM25 substrates. Moreover, this mutation is predicted to abolish the E3 ligase-E2 conjugating enzyme interaction (Koliopoulos *et al*, 2016), preventing any downstream ubiquitination events and thus prolonging transient ligase-substrate interactions. The TRIM25-R54P specific hits may have weaker, more transient, or infection-specific interactions not easily detected by the conventional co-IP/MS approach. Other "substrate trapping" approaches depend on fusing a polyubiquitin binding domain to the ligase of interest (Mark *et al*, 2016), which may either disrupt native protein-protein interactions or result in false-positive identification of ubiquitinated proteins. Moreover, this type of approach would fail to identify substrates that are not polyubiquitinated, given that ligases can mono or multi-monoubiquitinate their substrates (Komander and Rape, 2012).

For the first time, we identified G3BP1/2, UPF1, NME1, and PABPC4 as bona fide TRIM25 substrates (Figures 11-14). Furthermore, we were able to characterize TRIM25 polyubiquitination of

G3BP and PABPC4 as primarily utilizing K63 linkages (Figures 11C and 14D). This type of linkage is commonly used to build signaling scaffolds, as TRIM25 does to activate RIG-I (Gack *et al*, 2007), and could potentially play a role in either SG assembly or disassembly by recruiting SG components in the former or generating steric hindrance in the latter. Additionally, our validation of K592 as a mono-ubiquitination site on UPF1 (Figure 12C) overlaps with a predicted acetylation site on the same residue, and neighbors a predicted phosphorylation site at T595, potentially modulating these other post-translational modifications of UPF1 (Hornbeck *et al*, 2015). These residues lie within the AAA ATPase domain of UPF1, suggesting that ubiquitination of UPF1 by TRIM25 might affect its ATP hydrolysis, thus hindering UPF1 in its NMD target discrimination and efficient translation termination (Lee *et al*, 2015b; Serdar *et al*, 2016). Interestingly enough, G3BP1 and UPF1 cooperate to mediate structure-mediated RNA decay (Fischer *et al*, 2020). It is entirely possible that TRIM25-mediated ubiquitination could affect this process by modulating their interaction with one another, though further experiments are required to explore this hypothesis.

Though UPF1 and G3BP have previously been implicated as antiviral and pro-viral factors in alphavirus replication, respectively (Balistreri *et al*, 2014; Götte *et al*, 2019), we did not find a role for either in the TRIM25-ZAP antiviral response (Supplemental Figure 2.2). UPF1 may have an antiviral role independent of TRIM25, given that its knockdown only rescued viral replication when TRIM25 was absent (Supplemental Figure 2.2E). This hypothesis is supported by a previous report which found that UPF1 was involved in regulating half-life stability of viral RNA (Balistreri *et al*, 2014), which TRIM25 does not affect (Li *et al*, 2017). On the other hand, G3BP is known to cluster replication complexes and recruit translation initiation machinery (Götte *et al*, 2019), which might be disrupted

through G3BP ubiquitination by TRIM25, resulting in translational suppression. Alternatively, Given that the G3BP interaction motifs in TRIM25 and nsP3 are similar (Kruse *et al*, 2021; Götte *et al*, 2018), it is tempting to speculate that TRIM25 may compete with the viral nsP3 for G3BP interaction and recruitment, resulting in diminishment of G3BP pro-viral effects. However, the pro-viral roles of G3BP did not seem to be affected by TRIM25 ubiquitination or lack thereof, given that abolishing TRIM25-G3BP interaction through overexpression of the TRIM25-PTAA mutant did not rescue SINV replication and translation nor CHIKV virion production (Supplemental Figure 2.2A-C). Nevertheless, we noted that the TRIM25-PTAA mutant still preserves some ubiquitination of G3BP despite completely abolishing the TRIM25-G3BP interaction (Figure 11A-B). Further studies are warranted to fully elucidate the role of G3BP ubiquitination in TRIM25 antiviral activity.

TRIM25-mediated ubiquitination of NME1 and PABPC4 may interfere with RNA metabolic processes by altering their stability or ability to bind RNA. Both of these proteins have previously been demonstrated to be ubiquitinated by other E3 ligases. Ubiquitination of NME1 by the E3 ligase SCF-FBXO24 targets it for degradation (Chen *et al*, 2015). The ability of TRIM25 to modify another substrate, G3BP, with both proteolytic K48- and non-proteolytic K63-polyubiquitin linkages, implies that TRIM25 may also be targeting NME1 for degradation, thereby hindering nucleotide synthesis and general RNA metabolic processes. On the other hand, ubiquitination of PABPC4 by the E3 ligase MKRN decreases its affinity for binding mRNA poly(A) tails (Li *et al*, 2021b). It is interesting to speculate that TRIM25-mediated polyubiquitination of PABPC4 could regulate PABPC4 binding to the poly(A) tail on viral RNAs, thus modulating the stability of the RNA and reducing its ability to form translation initiation complexes.

We also utilized the TRIM25-R54P mutant to define the requirement for ligase activity in TRIM25 inhibition of alphavirus replication. We found that TRIM25 ligase activity is absolutely required for its inhibition of diverse alphaviruses through a block in viral translation (Figure 15A-D). Interestingly, overexpression of both TRIM25-WT and -R54P results in a dampened IFN response in our hands (Figure 15E), contrasting with the previously established role of TRIM25 in activating RIG-I signaling and implicating TRIM25 as a negative regulator of the type I IFN response (Koepke *et al*, 2021). Moreover, TRIM25-R54P with a complete loss of antiviral activity actually exhibits relatively more production of IFN and a subset of ISG mRNAs (Figure 15E). Still, these data together suggest that the robust TRIM25 antiviral activity against alphaviruses is not mediated through an augmented IFN response, but through its ligase activity and subsequent ubiquitination network.

Our examination of the contribution of a subset of TRIM25-R54P specific interactors to TRIM25 antiviral activity has yielded several hits, namely RTRAF, NME1, and PABPC4 (Figure 16). Though only pooled siRNA knockdown for *RTRAF* and *NME1* gave statistically significant restored viral replication, pooled siRNA knockdown of PABPC4 still restored viral replication by approximately 5 fold (Figure 16B). Additionally, both NME1 and PABPC4 expression significantly and negatively correlated with viral replication (Figure 16C-F). RTRAF, also known as hCLE or C14orf166, is an RNA binding protein involved in cellular transcription, translation, and RNA transport, and is required for influenza virus replication (Pérez-González *et al*, 2014; Pazo *et al*, 2019; Rodriguez *et al*, 2011). Notably, RTRAF is a member of a cap-binding complex that activates mRNA translation (Pazo *et al*, 2019). Given RTRAF's role in facilitating translation of mRNAs, it is therefore tempting to speculate that RTRAF may be required for translation of alphavirus RNA, and TRIM25-

mediated ubiquitination of RTRAF may affect its ability to do so. The novel bona fide TRIM25 substrate NME1, which functions as a major synthesizer of non-ATP nucleoside triphosphates, upon ubiquitination may inhibit alphavirus replication via a similar mechanism as the potent restriction factor SAMHD1, which depletes deoxynucleotide pools, effectively preventing replication of varied DNA viruses and reverse transcription of HIV-1 (Deutschmann and Gramberg, 2021). On the other hand, TRIM25-mediated ubiquitination of NME1 may inhibit its metastatic suppressor activities, potentially serving as a novel mechanism for TRIM25's previously described roles in carcinogenesis. Finally, TRIM25-mediated ubiquitination of PABPC4 could inhibit translation initiation by interfering with necessary protein-protein interactions to form the mRNA closed loop structure for ribosomal recruitment. Alternatively, it is possible that PABPC4 could inhibit alphavirus replication in a manner similar to its general block of coronavirus replication by recruiting TRIM25 to target alphavirus proteins for degradation (Jiao *et al*, 2021). Further studies need to be carried out to elucidate the functional consequences of these TRIM25 substrates in blocking viral translation and other cellular processes.

The novelty of this work lies within our innovative approach to uncover the multifaceted TRIM25 ubiquitination network, which is likely involved in mediating TRIM25 cellular and antiviral functions. Many questions remain unanswered as to how TRIM25-mediated ubiquitination modulates the activity of these substrates. In contrast to the more binary consequences of K48-linked dependent degradation, other types of ubiquitin linkage may effect more nuanced cellular changes by modulating substrate activity and localization (Komander and Rape, 2012). Given TRIM25 proclivity for K63 linkages in the context of alphavirus infection and innate immunity (Gack *et al*, 2007; Li *et*

al, 2017; Zheng *et al*, 2017), we are tempted to speculate that TRIM25 eschews a simple degradation approach in favor of a more nuanced modulation of substrate activity and localization. Current therapeutics that harness E3 ligases focus on their degradative power, generating compounds that bring ligases in close proximity to a target protein for degradation (Liang *et al*, 2020). Further research is warranted to explore the utility of alternate modes of ubiquitination in biological therapeutics.

ACKNOWLEDGMENTS

We thank Dr. Bill Schneider (Rockefeller University) for help with alignment of TRIM25 KO sequences and Drs. Douglas Black, Irvin Chen, and Oliver Fregoso (UCLA) for critical reading of the manuscript. We want to especially thank Drs. Oliver Fregoso and Michael Emerman (Fred Hutchinson Cancer Center) for their valuable input during the manuscript submission and review process. We also thank the UCLA Proteome Research Center for their services. RT-qPCR and flow cytometry was performed in the UCLA AIDS Institute that is supported by the James B. Pendleton Charitable Trust and the McCarthy Family Foundation. Molecular graphics and analyses performed with UCSF Chimera, developed by the Resource for Biocomputing, Visualization, and Informatics at the University of California, San Francisco, with support from NIH P41-GM103311.

MATERIALS AND METHODS

Cell culture, viruses, and infections

ZAP KO 293T cells (clone 89) and its respective parental 293T cells were generously provided by Dr. Akinori Takaoka at Hokkaido University (Hayakawa *et al*, 2011). 293T (parental, ZAP KO, and TRIM25 KO (see below) with or without inducible expression of TRIM25) were cultured in Dulbecco's Modified Eagle Medium (DMEM; Thermo Fisher Scientific, Waltham, MA) supplemented with 10% fetal bovine serum (FBS; Avantor Seradigm, Radnor, PA). Baby hamster kidney 21 (BHK-21; American Type Culture Collection, Manasass, VA) cells were cultured in Minimal Essential Media (Thermo Fisher Scientific) supplemented with 7.5% FBS.

Wild-type SINV (Toto1101), temperature-sensitive SINV (Toto1101/Luc:ts6), SINV expressing firefly luciferase (Toto1101/Luc), SINV expressing EGFP (TE/5'2J/GFP), CHIKV vaccine strain 181/clone 25 (generously provided by Scott Weaver, The University of Texas Medical Branch at Galveston), ONNV expressing EGFP (generously provided by Dr. Steve Higgs, Kansas State University), RRV expressing EGFP (generously provided by Dr. Mark Heise, University of North Carolina), and VEEV vaccine strain TC-83 (generously provided by Dr. Ilya Frolov, University of Alabama at Birmingham) have been previously described (Bick *et al*, 2003; Rice *et al*, 1987; Frolova *et al*, 2002; Gorchakov *et al*, 2012; Brault *et al*, 2004; Morrison *et al*, 2006; Atasheva *et al*, 2010). Viral stocks and titers for multiplicity of infection (MOI) calculations were generated in BHK-21 cells as previously described (Bick *et al*, 2003). Viral infections and plaque assays were performed as previously described (Bick *et al*, 2003). TRIM25 inducible cells (see below) were induced for TRIM25 expression and infected with EGFP expressing viruses at an MOI of 0.01 plaque forming unit

(PFU)/cell, harvested at 10-24 hours post infection (h.p.i.), and fixed in 1% paraformaldehyde for flow cytometry analysis. Data was acquired using a MACSQuant Analyzer 10 (Miltenyi Biotec, Auburn, CA) and analyzed using FlowJo (BD Biosciences, Franklin Lakes, NJ). Percent infected (GFP+) cells was calculated and normalized to the -dox condition of each respective cell line.

Plasmids and transfections

See Supplementary Table 2.1: Cloning primers. Addgene plasmids for HA-tagged ubiquitin (pRK5-HA-Ubiquitin-WT, #17608; pRK5-HA-Ubiquitin-K48, #17605; pRK5-HA-Ubiquitin-K63, #17606), UPF1 (pCW57.1-Tet-UPF1WT, #99146), and PABPC4 (pDESTmycPABPC4, #19877) were used (Lim *et al*, 2005; Landthaler *et al*, 2008; Feng *et al*, 2017). Full-length TRIM25 was generously provided by Dr. Jae U. Jung at the University of Southern California (Gack *et al*, 2007). Dr. Gerald McInerney at the Karolinska Institutet, Sweden, generously provided pGFP-G3BP1 and pGFP-G3BP2a (Götte *et al*, 2019). The coding sequence of NME1 isoform a (NM_198175.1) was synthesized as a gene fragment (Integrated DNA Technologies, Coralville, IA), where the ends were flanked by restriction enzyme sites *NotI* and *XbaI*, and random nucleotides were incorporated to maintain the open reading frame. Dr. Oliver Fregoso kindly gifted us a pcDNA3.1-3XFLAG plasmid. The 3XFLAG tag was swapped out for a V5 tag or a myc tag using *BamHI* and *HindIII* restriction sites to generate V5-pcDNA3.1 or myc-pcDNA3.1, respectively. The plasmid pcDNA3.1-3XFLAG was used as an expression vector for TRIM25, pcDNA3.1-V5 for UPF1, and pcDNA3.1-myc for G3BP1, G3BP2, NME1, and PABPC4. TRIM25 was cloned into pcDNA3.1-3XFLAG using *XhoI* and *XbaI* restriction sites, while UPF1, G3BP, NME1, and PABPC4 were cloned into either pcDNA3.1-V5 (UPF1) or pcDNA3.1-myc (G3BP, NME1, and PABPC4) using the *NotI* and *XbaI*

restriction sites. TRIM25 RING domain mutants (I15K, R54P, I15K/R54P) were generated by mutagenesis of pcDNA-3XFLAG-TRIM25 using the QuikChange II XL Site-Directed Mutagenesis Kit (Agilent Technologies, Santa Clara, CA), while the TRIM25-PTAA mutant was generated using the Q5 Site-Directed Mutagenesis Kit (New England Biolabs, Ipswich, MA), by performing sequential mutagenesis reactions to individually mutate each residue to alanine. TRIM25 was cloned into a 3XFLAG expressing ePiggyBac transposon plasmid at the *ClaI* and *NotI* restriction sites. All plasmids were verified by sequencing (Genewiz, South Plainfield, NJ).

Cells were transfected using X-tremeGENE9 DNA Transfection Reagent (Roche Life Science, Basel, Switzerland) at a ratio of 3 µL to1 µg DNA according to the manufacturer's instructions. Empty vectors (pcDNA3.1-3XFLAG, V5, or myc) were transfected as necessary to keep total plasmid amount in co-transfections constant.

TRIM25 *targeting by CRISPR*

The MIT Optimized CRISPR Design portal (crispr.mit.edu) and CHOPCHOP (Labun *et al*, 2016) (chopchop.cbu.uib.no) were used to design guide RNAs targeting exon 1 of the human *TRIM25* gene (Supplemental Figure 2.1A). The guide with the highest ranking in both scoring programs (5'-CGGCGCAACAGGTCGCGAACGGG-3') was selected for cloning into the PX459 vector (Addgene, #62988), a non-lentiviral construct that also delivers Cas9 (Ran *et al*, 2013). Oligos containing the guide RNA sequences (5'- CACCGCGGCGCAACAGGTCGCGAAC-3' and 5'-AAACGTTCGCGACCTGTTGCGCCGC-3') were ligated and cloned into PX459 linearized with *BbsI*. 293T cells were transiently transfected with PX459 expressing TRIM25 guide RNA and selected with 1 µg/mL puromycin the next day to eliminate untransfected cells. Following two days of

puromycin selection, surviving cells were counted, diluted to 0.3 cell/well in a 96-well plate, and seeded in 10% FBS DMEM. Single cell clones were expanded and treated with or without puromycin. Clones sensitive to puromycin, indicating failure to integrate guide RNA expressing vector, were harvested for immunoblot analysis to assess TRIM25 expression. Five clones (3, 6, 8, 9, and 10) were selected based on western blotting results indicating complete loss of TRIM25 protein expression (Supplemental Figure 2.1B). Viral replication within these clones was characterized by infection with a luciferase-expressing SINV (Toto1101/Luc). Clone #8 was selected for generation of TRIM25 inducible cell lines based on its intermediate viral replication phenotype (Supplemental Figure 2.1C), similar to previous TRIM25 siRNA data (Li *et al*, 2017). A 600-bp amplicon flanking the gRNA targeting site was amplified from genomic DNA isolated from each clonal population using a Quick-DNA Miniprep Plus kit (Zymo Research, Irvine, CA) and KOD Hot Start Master Mix (Millipore Sigma). Amplicons from clone #8 were sent to Massachusetts General Hospital Center for Computational and Integrative Biology DNA Core for Complete Amplicon Sequencing, confirming that CRISPR targeting results in deletions in exon 1 of *TRIM25*, leading to frameshift mutations and premature stop codons in both alleles (Supplemental Figure 2.1D).

Generation of TRIM25 inducible cell lines

To reconstitute TRIM25 expression (WT and R54P) in our TRIM25 KO 293T cell line (clone #8; see above for details), we used the enhanced PiggyBac (ePB) transposable element system provided by the Brivanlou laboratory at the Rockefeller University, as previously described (Lacoste *et al*, 2009; Li *et al*, 2019). TRIM25 KO 293T cells were transfected with 1:1 ePB transposon vector encoding TRIM25-WT or TRIM25-R54P and the transposase plasmid. Two days post-transfection,

1.5 µg/mL of puromycin was used to select a population of TRIM25 KO 293T cells inducible for TRIM25-WT, -R54P, or -PTAA, which were then expanded and treated with different amounts of dox (0.01, 0.1, 1, and 10 µg/mL) to confirm TRIM25 inducible expression by immunoblotting.

Mass spectrometry (MS)

To identify TRIM25 substrates, three 15-cm dishes per condition were seeded with $7.5x10^6$ TRIM25 inducible or TRIM25 KO 293T cells each in the presence of 1 µg/mL dox. Two days later, cells were mock infected or infected with Toto1101 at an MOI of 1 PFU/cell. Six hours post infection, cells were trypsinized, spun down, and lysed in 3 mL of FLAG IP buffer. Supernatant was transferred to a new 15 mL tube and supplemented with 5 mL of FLAG IP buffer before incubating with 80 µL of anti-FLAG beads for 45 min at 4˚C, rotating. Immunoprecipitates were washed three times in FLAG IP buffer before elution with 130 µL of 8M urea in 100 mM Tris-HCl, pH 8, shaken for 10 min at 1200 rpm, room temperature. Supernatant was carefully transferred to a new tube and proteins were precipitated by addition of 4 volumes of -20˚C acetone and incubation at 4˚C overnight. After centrifugation at 16,100g for 30 min at 4˚C, pellets were washed with -20˚C acetone and centrifuged again.

Dried pellets were processed at the UCLA Proteomics Core. Protein samples were reduced and alkylated using 5mM Tris (2-carboxyethyl) phosphine and 10mM iodoacetamide, respectively, and then proteolyzed by the sequential addition of trypsin and lys-C proteases at 37˚C as described (Mayank *et al*, 2019). Digested peptides were resuspended in 5% formic acid and fractionated online using a 25cm long, 75 µM inner diameter fused silica capillary packed in-house with bulk C18 reversed phase resin (length, 25 cm; inner diameter, 75 µM; particle size, 1.9 µm; pore size, 100 Å; Dr. Maisch

GmbH) (Jami-Alahmadi *et al*, 2021). The 140-minute water-acetonitrile gradient was delivered using a Dionex Ultimate 3000 UHPLC system (Thermo Fisher Scientific) at a flow rate of 300 nL/min (Buffer A: water with 3% DMSO and 0.1% formic acid and Buffer B: acetonitrile with 3% DMSO and 0.1% formic acid). Fractionated peptides were ionized and analyzed by tandem mass spectrometry (MS/MS) Orbitrap Fusion Lumos mass spectrometer (Thermo Fisher Scientific). Label-free quantitation was performed using the MaxQuant software package (Cox and Mann, 2008). The mass spectrometry proteomics data have been deposited to the ProteomeXchange Consortium via the PRIDE (Perez-Riverol *et al*, 2022) partner repository with the dataset identifier PXD034024.

The EMBL Human reference proteome (UP000005640 9606) was utilized for all database searches. Statistical analysis of MaxQuant output data was performed with the artMS Bioconductor package (Jimenez-Morales *et al*, 2019) which performs the relative quantification of protein abundance using the MSstats Bioconductor package (default parameters). Intensities were normalized across samples by median-centering the log2-transformed MS1 intensity distributions. The abundance of proteins missing from one condition but found in more than 2 biological replicates of the other condition for any given comparison were estimated by imputing intensity values from the lowest observed MS1-intensity across samples and p-values were randomly assigned to those between 0.05 and 0.01 for illustration purposes. Significant hits were defined as interactors that possessed a log2FoldChange of >1.5 and a -log10Pvalue > 1.3 (Pvalue < 0.05).

TRIM25 autoubiquitination and co-immunoprecipitation (co-IP) assay

To assess TRIM25 autoubiquitination or co-immunoprecipitation with proteins of interest, transfected or untransfected cells in 6-well plates were collected and lysed by rotating for 30 min at

4˚C in FLAG IP buffer (100 mM Tris-HCl 8.0, 150 mM NaCl, 5 mM EDTA, 1 mM DTT, 5% glycerol, 0.1% NP-40) supplemented with a complete protease inhibitor cocktail (Roche), before spinning down at 14000 rpm for 15 min at 4˚C. Anti-FLAG beads (EZview Red ANTI-FLAG M2 Affinity Gel, Sigma-Aldrich, St. Louis, MO) or anti-myc beads (EZview Red ANTI-MYC M2 Affinity Gel, Sigma-Aldrich) were equilibrated by washing 3 times in FLAG IP buffer. Three hundred µL of whole cell lysate (WCL) were incubated with 30 µL of anti-FLAG beads for 45 minutes at 4˚C, rotating. Immunoprecipitates were washed 3 times with the FLAG IP buffer. Bound proteins were eluted with SDS loading buffer and boiled for 5 minutes for immunoblot analysis.

Ubiquitination IP assay

To assess TRIM25 ubiquitination of putative substrates, immunoprecipitation was performed essentially as previously described (Li *et al*, 2017). Briefly, cells were collected and lysed in 0.5% SDS buffer supplemented with complete protease inhibitor cocktail (Roche Life Science). Three hundred µL of WCL were diluted into 1X TNA buffer (0.25% Triton, 50 mM Tris-HCl, pH 7.5; 200 mM NaCl, 1 mM EDTA) + 2 mg/mL BSA. WCL containing V5-tagged substrates were then incubated with 1 µg of anti-V5 antibody overnight at 4˚C. The next morning, 40 µL Protein A Dynabeads (Invitrogen, Waltham, MA) were added and incubated for 2 h at 4˚C. WCL containing myc-tagged substrates were incubated with anti-myc beads directly following lysis for 45 minutes at 4˚C, rotating. Following incubation with beads, both myc-tagged and V5-tagged immunoprecipitates were washed 3 times with 1X TNA buffer + 2 mg/mL BSA. Myc-tagged NME1 underwent an additional two washes with 1X TNA buffer only. Bound proteins were eluted with SDS loading buffer and boiled for 5 minutes for immunoblot analysis.

Immunoblot analysis

Proteins were resolved through SDS-PAGE using 4-15% precast Mini-PROTEAN TGX Gels (Bio-Rad, Hercules, CA) and NuPAGE MOPS SDS running buffer (Thermo Fisher Scientific) before transferring to a PVDF membrane (Bio-Rad). Immunodetection was achieved with 1:5,000 anti-ZAP (Abcam, Cambridge, United Kingdom); 1:5,000 anti-TRIM25 (BD Biosciences), 1:1,000 anti-HA (Roche Life Sciences), 1:5,000 anti-V5 (Invitrogen), 1:2,500 anti-myc (Cell Signaling Technology, Danvers, MA), 1:20,000 anti-FLAG (Sigma-Aldrich), 1:500 anti-G3BP1 (Santa Cruz, Dallas, TX), 1:1,000 anti-G3BP2 (Assay Biotech, Fremont, CA), 1:1,000 anti-UPF1 (Cell Signaling Technology), 1:10,000 anti-NME1 (Abcam), 1:2,000 anti-PABPC4 (Proteintech, Rosemont, IL), and 1:20,000 anti-actin-HRP (Sigma-Aldrich). Primary antibodies were detected with 1:20,000 goat anti-mouse HRP (Jackson ImmunoResearch, West Grove, PA), 1:20,000 goat anti-rabbit HRP (Thermo Fisher Scientific), or 1:20,000 donkey anti-rat HRP (Jackson ImmunoResearch). Blots were visualized using ProSignal Pico ECL Reagent (Genesee Scientific, San Diego, CA) on a ChemiDoc (Bio-Rad). Quantification of western blots was performed using ImageJ.

siRNA knockdown

See Supplementary Table 2.2: siRNAs. Ambion Silencer siRNAs and nontargeting controls (Thermo Fisher Scientific) were reverse transfected with DharmaFECT 1 Transfection Reagent (Horizon Discovery, Cambridge, United Kingdom) according to manufacturer protocols. Briefly, siRNAs were mixed with DharmaFECT 1 Transfection Reagent (1:100 dilution in HBSS) and 50 µL of siRNA mix were added to each well in a 24 well plate, or 100 µL in a 12 well plate. 1.2 x 10^5 cells were added per well in 250 µL in a 24 well plate or 2.4 x 10^6 in 500 µL in a 12 well plate, for a final

concentration of 25 nM siRNA and total volume of 300 µL or 600 µL. Plates that would be subjected to SINV infection were first poly-L-lysine treated. Cells were induced for TRIM25 expression using a final concentration of 1 µg/mL dox one day post-transfection, as applicable. Cells were harvested for RNA extraction for RT-qPCR to quantify gene knockdown (see below) or subjected to SINV infection 48 h post-transfection. To assess ISG induction in TRIM25 inducible cells upon poly(I:C) treatment, one day post-transfection cells were treated with 1 µg poly(I:C) HMW (InvivoGen, San Diego, CA) and 1 µg/mL dox per well. RT-qPCR data were normalized to the -dox condition for each cell line.

Quantitative reverse transcription PCR (RT-qPCR)

See Supplementary Table 2.3: RT-qPCR primers. Total RNA was isolated from siRNA-treated cells using the RNeasy mini kit (Qiagen, Hilden, Germany) or the Quick-RNA kit (Zymo Research). 400 ng to 1 µg of input RNA was used as a template for RT using Protoscript II First Strand cDNA Synthesis Kit (New England Biolabs) and random hexamers, following manufacturer instructions. RT-qPCR was performed using 5 µL of 4 to 10-fold-diluted cDNA, and Luna Universal qPCR Master Mix (New England Biolabs) in the CFX Real-Time PCR system (Bio-Rad), courtesy of the UCLA Virology Core. qPCR conditions were as follows: initial denaturation step at 95 ˚C for 1 min, 40 cycles of 95˚C for 15 sec followed by 60˚C for 30 sec, concluding with a final 10 sec at 60˚C. A melt curve was calculated by heating to 95˚C incrementally by 0.5˚C/s for 10 sec at each temperature. Transcript levels of ISGs and R54P specific interactors were determined by normalizing the target transcript CT value to the CT value of the RPS11 transcript, an endogenous housekeeping gene. Fold change was calculated using this normalized value relative to the average of cells treated with the NT siRNA control (CT method).

SUPPLEMENTARY MATERIAL

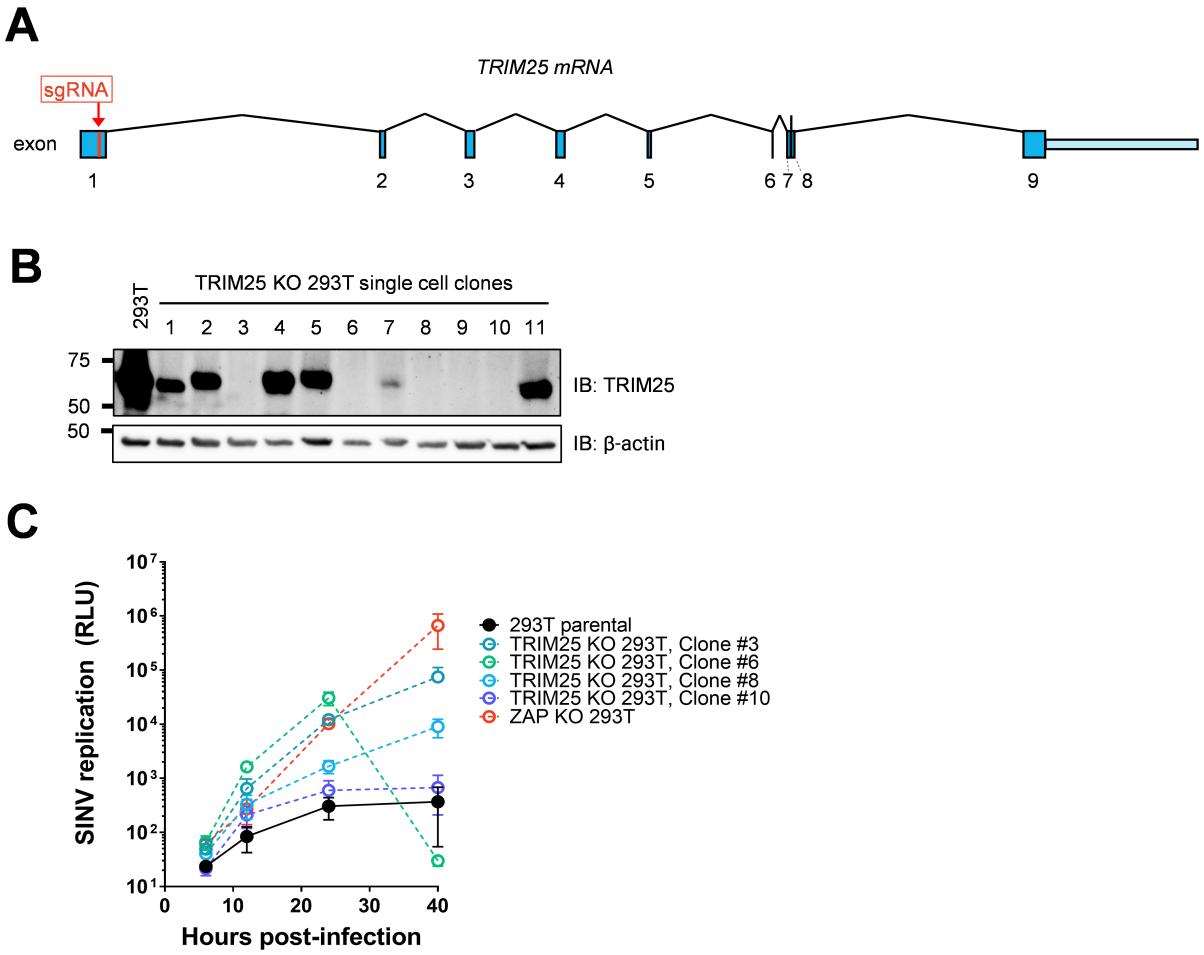

Supplemental Figure 2.1. Validation of TRIM25 KO in CRISPR clones.

(A) Schematic of where TRIM25 sgRNA targets exon 1. (B) Western blot of TRIM25 KO CRISPR single cell clones. (C) Cells were infected with SINV Toto1101/Luc at an MOI of 0.01 PFU/cell and lysed at 6, 12, 24, and 40 h.p.i. for measurement of luciferase activity. (D) CRISPR-targeting region in the genomic sequence of TRIM25 is shown in clone 8. The alignment shown is in the same reading frame of the wild-type TRIM25 protein. A red dash represents a deletion when compared to the wild-type TRIM25 sequence.

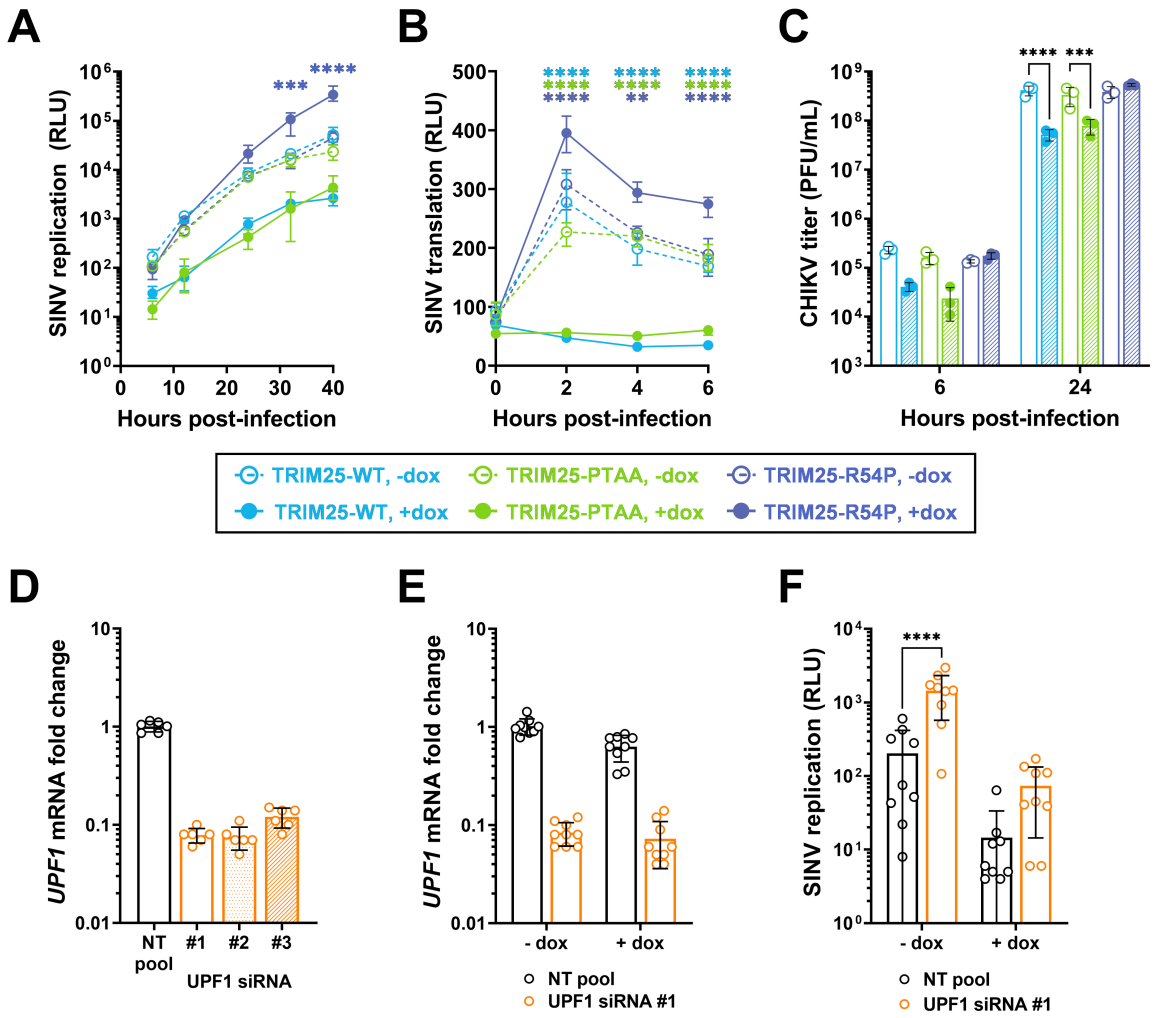

Supplemental Figure 2.2. G3BP and UPF1 are insufficient to mediate TRIM25 antiviral activity.

(A-C) TRIM25-inducible cells were induced for TRIM25-WT, -R54P, or -PTAA expression at 1 µg/mL dox, infected with (A) SINV Toto1101/Luc at an MOI of 0.01 PFU/cell, and lysed at 6, 12, 24, 32, and 40 h.p.i.; or with (B) SINV Toto1101/Luc:ts6 at an MOI of 1 PFU/cell and lysed at 0, 2, 4, and 6 h.p.i. for measurement of luciferase activity; or (C) CHIKV at an MOI of 0.01 PFU/cell, harvesting supernatant at 6 and 24 h.p.i. for plaque assays. Open circles and dashed lines indicate absence of TRIM25 induction. Data are representative of two independent experiments. Error bars represent (A-B) range or (C) standard deviation. Asterisks indicate statistically significant differences (Two-way ANOVA and Tukey's multiple comparisons test: **, p<0.01; ***, p<0.001; ****, p<0.0001). Light blue compares WT +/- dox, dark blue for R54P +/- dox, and green for PTAA +/- dox. Unlabeled comparisons are not significant. (D) TRIM25-WT inducible cells were transfected with NT pool siRNA or UPF1 siRNAs in the absence of dox. RNA was extracted 24 hours post-transfection for RT-qPCR analysis. Data are combined from two independent experiments. (E-F) TRIM25-WT inducible cells were transfected with NT pool siRNA or UPF1 siRNA #1, induced for TRIM25-WT expression at 1 µg/mL dox, and infected with Toto1101/Luc at an MOI of 0.01 PFU/cell. Cells were lysed at 24 h.p.i. for (E) measurement of luciferase activity or (F) quantification of UPF1 knockdown via RT-qPCR. Data are combined from three independent experiments. Asterisks indicate statistically significant differences (Two-way ANOVA and Šídák's multiple comparisons test: ****, p<0.0001). Unlabeled comparisons are not significant.

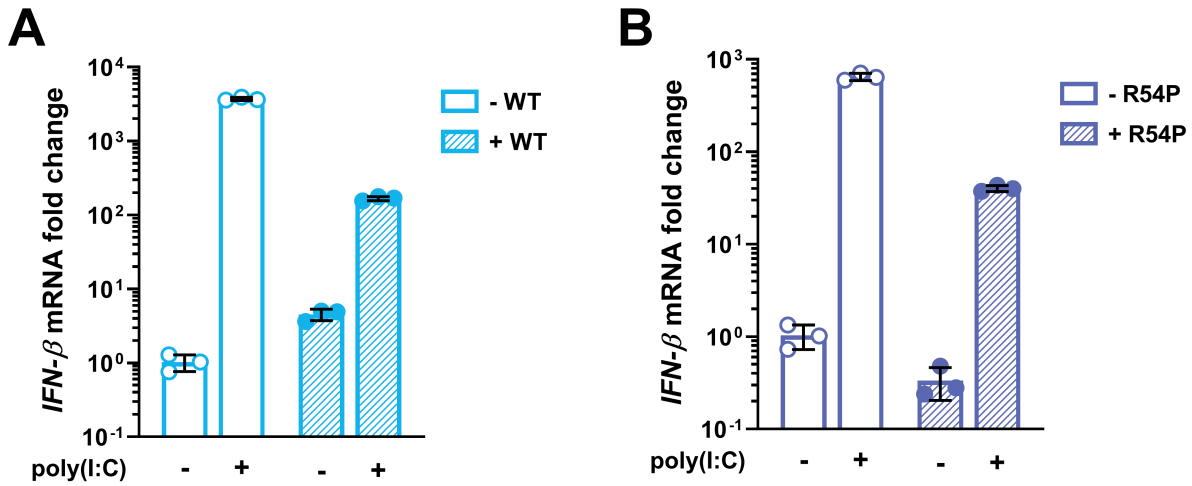

Supplemental Figure 2.3. Poly(I:C) treatment robustly induces *IFN-β* mRNA expression.

(**A-B**) TRIM25 inducible cells were treated with poly(I:C) in the presence or absence of (**A**) TRIM25-WT or (**B**) TRIM25-R54P induction. RNA was harvested for RT-qPCR analysis. Data are representative of two independent experiments.

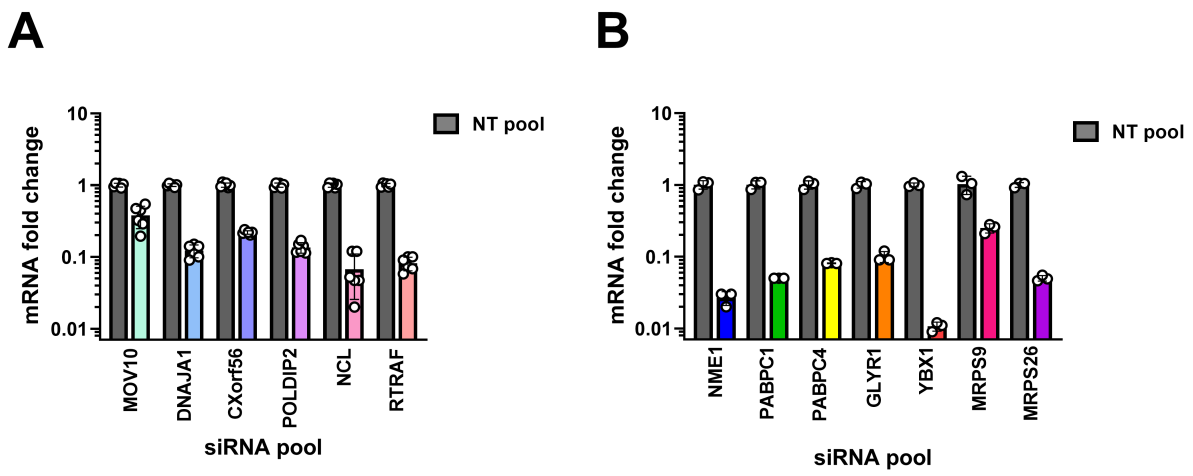

Supplemental Figure 2.4. Validation of pooled siRNA knockdown.

(**A-B**) TRIM25 inducible cells were transfected with pooled siRNAs for either (**A**) hits specific to TRIM25-R54P in the absence of viral infection or (**B**) hits specific to TRIM25-R54P in the presence of viral infection. Cells were induced for TRIM25-WT expression at 1 µg/mL dox. RNA was extracted for RT-qPCR analysis.

Supplementary Table 2.1. Cloning primers.

Primers used for mutagenesis and cloning of all DNA constructs.

Name	Primer sequence (5'-3')	Construction
XhoI-ClaI-TRIM25 F1 (EY-47)	gtttCTCGAGgtATCGATATGGCAGAGCTGTGCCCC	pcDNA-3XFLAG-TRIM25, ePiggyBac-3XFLAG-TRIM25
XbaI-NotI-TRIM25 R1 (EY-48)	gtttTCTAGAGCGGCCGCCTACTTGGGGGAGCAGATGGAG	pcDNA-3XFLAG-TRIM25, ePiggyBac-3XFLAG-TRIM25
TRIM25-I15K F1 (EY-10)	AGGAGCTGTCGTGCTCCAagTGCCTGGAGC	pcDNA-3XFLAG-TRIM25-I15K
TRIM25-I15K R1 (EY-11)	GCTCCAGGCActTGGAGCACGACAGCTCCT	pcDNA-3XFLAG-TRIM25-I15K
TRIM25-R54P F1 (EY-12)	CCCGCAGTGCCcCGCCGTCTACC	pcDNA-3XFLAG-TRIM25-R54P
TRIM25-R54P R1 (EY-13)	GGTAGACGGCGgGGCACTGCGGG	pcDNA-3XFLAG-TRIM25-R54P
TRIM25-PTAG F1 (EY-172)	GCTTCCCACGgcTGGAGCCCCG	pcDNA-3XFLAG-TRIM25-PTAA
TRIM25-PTAA F1 (EY-173)	CCCACGGCTGcAGCCCCGGAA	pcDNA-3XFLAG-TRIM25-PTAA
TRIM25-PTAA R2 (EY-174)	AAGCTTGCTGGGTAAGGCAGGG	pcDNA-3XFLAG-TRIM25-PTAA
NotI-UPF1 F1 (EY-91)	gtttGCGGCCGCaGTGGAAGCCTATGGGCC	pcDNA-V5-UPF1
XbaI-UPF1 R1 (EY-92)	gtttTCTAGAGCCACGTTGCTTAGCTCTTC	pcDNA-V5-UPF1
NotI-G3BP1 F1 (EY-119)	gtttGCGGCCGCaGTGATGGAGAAGCCTAGTCCCC	pcDNA-myc-G3BP1
XbaI-G3BP1 R1 (EY-120)	gtttTCTAGATTACTGCCGTGGCGCAAG	pcDNA-myc-G3BP1
NotI-G3BP2 F1 (EY-121)	gtttGCGGCCGCaGTTATGCAGAAGCCCAGTCCG	pcDNA-myc-G3BP2
XbaI-G3BP2 R1 (EY-97)	gtttTCTAGAtcagcgacgctgtcctgtg	pcDNA-myc-G3BP2
NotI-NME1 F1 (SH-08)	gtctGCGGCCGCTGTGCTACTGTCTACTTTAGG	pcDNA-myc-NME1
XbaI-NME1 R1 (SH-09)	ggtaTCTAGATTATTCATAGATCCAGTTCTGAGC	pcDNA-myc-NME1
NotI-PABPC4 F1 (SH-45)	gtttGCGGCCGCtAACGCTGCGGCCAG	pcDNA-myc-PABPC4
XbaI-PABPC4 R1 (SH-46)	ggtaTCTAGACTAAGAGGTAGCAGCAGCAACA	pcDNA-myc-PABPC4

Supplementary Table 2.2. siRNAs.

Gene Symbol	Full Gene Name	Gene ID	siRNA ID	Exon(s) Targeted	Sense siRNA Sequence
CXorf56	chromosome X open reading frame 56	63932	29642	3	GGCAUUGAACGACAGUACAtt
CXorf56	chromosome X open reading frame 56	63932	29736	3	GGAAGAAAUGUGCAAAGUGtt
CXorf56	chromosome X open reading frame 56	63932	127302	7	GCAUUUAGAUCAGGAGGCAtt
DNAJA1	DnaJ (Hsp40) homolog, subfamily A, member 1	3301	10092	2	GGAGAGAAGUUUAAACAGAtt
DNAJA1	DnaJ (Hsp40) homolog, subfamily A, member 1	3301	10180	3	GGGAAUUAUAUGACAAAGGtt
DNAJA1	DnaJ (Hsp40) homolog, subfamily A, member 1	3301	144744	5	GCGGAUCAGUCCUAAAGAUtt
GLYR1	glyoxylate reductase 1 homolog	84656	109777	15	GGAUCUCCGCUUAGCCAUUtt
GLYR1	glyoxylate reductase 1 homolog	84656	109778	15	GGUGUACAAAAGAGCCAAGtt
GLYR1	glyoxylate reductase 1 homolog	84656	113776	4	GCCAUAUCAUGCUCAUAAAtt
MOV10	Mov10, Moloney leukemia virus 10, homolog (mouse)	4343	28823	2	GGGCUGAGUAUCUUCAUGGtt
MOV10	Mov10, Moloney leukemia virus 10, homolog (mouse)	4343	28919	4	GGAGCCGGCACAUUCUACAtt
MOV10	Mov10, Moloney leukemia virus 10, homolog (mouse)	4343	29008	20	GGAAGAAAACUCUGAAAACtt
MRPS26	mitochondrial ribosomal protein S26	64949	32714	3	GGAAGAGGUGAAAAACUUCtt
MRPS26	mitochondrial ribosomal protein S26	64949	130988	4	CCAUGUAUGUAUCAUGGCGtt
MRPS26	mitochondrial ribosomal protein S26	64949	130989	4	GGAAGGUUCAGCCUUAUCCtt
MRPS9	mitochondrial ribosomal protein S9	64965	131876	6	CCAGAGACGUGAUUGGCAGtt
MRPS9	mitochondrial ribosomal protein S9	64965	131877	10	GCAAUACGACUGGCAAUGGtt
MRPS9	mitochondrial ribosomal protein S9	64965	131878	10	GCUGGACUACUUACUACUGtt
NCL	nucleolin	4691	16052	2	GGAGGUAGAAGAAGAUAGUtt
NCL	nucleolin	4691	16225	7	GGAAAAGACAGUAAGAAAGtt
NCL	nucleolin	4691	144014	2	GGUCGUCAUACCUCAGAAGtt
NME1	NME/NM23 nucleoside diphosphate kinase 1	4830	41	2,3	GGAUUCCGCCUUGUUGGUCtt
NME1	NME/NM23 nucleoside diphosphate kinase 1	4830	42	3,4	GGAACACUACGUUGACCUGtt
NME1	NME/NM23 nucleoside diphosphate kinase 1	4830	43	5,6	GGCUGUAGGAAAUCUAGUUtt
PABPC1	poly(A) binding protein, cytoplasmic 1	26986	11745	8	GGUUACUUCAUGGCAGCUAtt
PABPC1	poly(A) binding protein, cytoplasmic 1	26986	11834	15	GGGACCAUGAAAAGAAACUtt
PABPC1	poly(A) binding protein, cytoplasmic 1	26986	216913	8	GCUGUUCCCAACCCUGUAAtt
PABPC4	poly(A) binding protein, cytoplasmic 4 (inducible form)	8761	13771	1	GGCCAUGCUGUACGAAAAGtt
PABPC4	poly(A) binding protein, cytoplasmic 4 (inducible form)	8761	13867	2	GGGAAAGCCAAUCCGCAUCtt

PABPC4	poly(A) binding protein, cytoplasmic 4 (inducible form)	8761	13959	6	GGAGAGAAUUAGUCGAUAUtt
POLDIP2	polymerase (DNA-directed), delta interacting protein 2	26073	147585	6	GGUUCCCAUCCAACAUGAAtt
POLDIP2	polymerase (DNA-directed), delta interacting protein 2	26073	147586	11	GCUUUAGGUAUGGAUUGAUtt
POLDIP2	polymerase (DNA-directed), delta interacting protein 2	26073	147587	11	CGUGAGGUUUGAUCAGUAAtt
RTRAF	RNA transcription, translation, and transport factor	51637	23656	2	GGGAAUUUAAGAAACAUCCtt
RTRAF	RNA transcription, translation, and transport factor	51637	134783	8	GGCAAUUAUUGCUGAUCCAtt
RTRAF	RNA transcription, translation, and transport factor	51637	134784	8	CCUACUUAGUACAGUUGGGtt
UPF1	UPF1 regulator of nonsense transcripts homolog (yeast)	5976	12197	2	GGAAGAUGAAGAAGACACCtt
UPF1	UPF1 regulator of nonsense transcripts homolog (yeast)	5976	12290	4	GGGCAAAAUGCAAAGAGGUtt
UPF1	UPF1 regulator of nonsense transcripts homolog (yeast)	5976	12379	24	GGAAAAAAAACUUCGCAUUtt
YBX1	Y box binding protein 1	4904	5109	2	GGUUUUGGGAACAGUAAAAtt
YBX1	Y box binding protein 1	4904	5291	3	GGAAGAUGUAUUUGUACACtt
YBX1	Y box binding protein 1	4904	115541	5	GGCAGCAAAUGUUACAGGUtt

Supplementary Table 2.3. RT-qPCR primers.

Primers used to quantify target gene mRNA levels by RT-qPCR analysis.

Target gene	Name	Primer sequence (5'-3')
CXorf56	CXorf56 RT-qPCR F1 (EY-181)	CGGTCCCGTGTGATTGATG
CXorf56	CXorf56 RT-qPCR R1 (EY-182)	CCGCAGATACATAGTCTCCTCAT
DNAJA1	DNAJA1 RT-qPCR F1 (EY-183)	ACTGGAGCCAGGCGATATTAT
DNAJA1	DNAJA1 RT-qPCR R1 (EY-184)	CTTCAACGAGCTGTATGTCCAT
GLYR1	GLYR1 RT-qPCR F1 (EY-185)	AGAAACCTCGCGGAAAGAAAT
GLYR1	GLYR1 RT-qPCR R1 (EY-186)	GACAGCATCTACCGCTTGC
IFIT1	IFIT1 RT-qPCR F1 (EY-134)	TTGATGACGATGAAATGCCTGA
IFIT1	IFIT1 RT-qPCR R1 (EY-135)	CAGGTCACCAGACTCCTCAC
IFN-β	IFN-β RT-qPCR F1 (EY-98)	GTCAGAGTGGAAATCCTAAG
IFN-β	IFN-β RT-qPCR R1 (EY-99)	ACAGCATCTGCTGGTTGAAG
ISG15	ISG15 RT-qPCR F1 (YD-09)	GGCTGGGAGCTGACGGTGAAG
ISG15	ISG15 RT-qPCR R1 (YD-10)	GCTCCGCCCGCCAGGCTCTGT
MOV10	MOV10 RT-qPCR F1 (EY-151)	GGGCCAGTGTTTCGAGAGTTT
MOV10	MOV10 RT-qPCR F1 (EY-152	TCTTGGTGACGTAGGCCAGA
MRPS26	MRPS26 RT-qPCR F1 (EY-189)	CCAAATCCAAGATCGAGCGAG
MRPS26	MRPS26 RT-qPCR R1 (EY-190)	GGCGGTAGTGCTGGTAACG
MRPS9	MRPS9 RT-qPCR F1 (EY-191)	TGTAACCAGAGACGTGATTGGC
MRPS9	MRPS9 RT-qPCR R1 (EY-192)	TAGCAGCCGAATGAACTGCAT
NCL	NCL RT-qPCR F1 (EY-193)	GCACCTGGAAAACGAAAGAAGG
NCL	NCL RT-qPCR R1 (EY-194)	GAAAGCCGTAGTCGGTTCTGT
NME1	NME1 RT-qPCR F1 (EY-159)	AAGGAGATCGGCTTGTGGTTT
NME1	NME1 RT-qPCR R1 (EY-160)	CTGAGCACAGCTCGTGTAATC
OAS2	OAS2 RT-qPCR F1 (YD-11)	CGGTGTATGCCTGGGAACAGG
OAS2	OAS2 RT-qPCR R1 (YD-12)	GGGTCAACTGGATCCAAGATTAC
PABPC1	PABPC1 RT-qPCR F1 (EY-195)	CAGGCTCACCTCACTAACCAG
PABPC1	PABPC1 RT-qPCR R1 (EY-196)	GGTAGGGGTTGATTACAGGGT
PABPC4	PABPC4 RT-qPCR F1 (EY-197)	TGGTAAGACCCTAAGTGTCAAGG
PABPC4	PABPC4 RT-qPCR R1 (EY-198)	TCCTCGTGTTTTTCGTAACTCAC
POLDIP2	POLDIP2 RT-qPCR F1 (EY-199)	CACCTCTCGTCCCGAAACC
POLDIP2	POLDIP2 RT-qPCR R1 (EY-200)	CCATTCTGTTTTGGCACCTCAA
RPS11	RPS11 RT-qPCR F1	GCCGAGACTATCTGCACTAC
RPS11	RPS11 RT-qPCR R1	ATGTCCAGCCTCAGAACTTC
RTRAF	RTRAF RT-qPCR F1 (EY-221)	TTCCGACGCAAGTTGACGG
RTRAF	RTRAF RT-qPCR R1 (EY-222)	CTGTCTTCAATCTTGTAGTGCCT
UPF1	UPF1 RT-qPCR F1 (EY-149)	CTGCAACGGACGTGGAAATAC
UPF1	UPF1 RT-qPCR R1 (EY-150)	ACAGCCGCAGTTGTAGCAC
YBX1	YBX1 RT-qPCR F1 (EY-223)	GGGGACAAGAAGGTCATCGC
YBX1	YBX1 RT-qPCR R1 (EY-224)	CGAAGGTACTTCCTGGGGTTA

Chapter 3

—

The role of ZAP and TRIM25 RNA binding in restricting viral translation

ABSTRACT

The innate immune response controls the acute phase of virus infections; critical to this response is the induction of type I interferon (IFN) and resultant IFN-stimulated genes to establish an antiviral environment. One such gene, zinc finger antiviral protein (ZAP), is a potent antiviral factor that inhibits replication of diverse RNA and DNA viruses by binding preferentially to CpG-rich viral RNA. ZAP restricts alphaviruses and the flavivirus Japanese encephalitis virus (JEV) by inhibiting translation of their positive-sense RNA genomes. While ZAP residues important for RNA binding and CpG specificity have been identified by recent structural studies, their role in viral translation inhibition has yet to be characterized. Additionally, the ubiquitin E3 ligase tripartite motif-containing protein 25 (TRIM25) has recently been uncovered as a critical co-factor for ZAP's suppression of alphavirus translation. While TRIM25 RNA binding is required for efficient TRIM25 ligase activity, its importance in the context of ZAP translation inhibition remains unclear. Here, we characterized the effects of ZAP and TRIM25 RNA binding on translation inhibition in the context of the prototype alphavirus Sindbis virus (SINV) and JEV. To do so, we generated a series of ZAP and TRIM25 RNA binding mutants, characterized loss of their binding to SINV genomic RNA, and assessed their ability to interact with each other and to suppress SINV replication, SINV translation, and JEV translation. We found that mutations compromising general RNA binding of ZAP and TRIM25 impact their ability to restrict SINV replication, but mutations specifically targeting ZAP CpG-mediated RNA binding have a greater effect on SINV and JEV translation inhibition. Interestingly, ZAP-TRIM25 interaction is a critical determinant of JEV translation inhibition. Taken

together, these findings illuminate the contribution of RNA binding and co-factor interaction to the synergistic inhibition of viral translation by ZAP and TRIM25.

BACKGROUND

The type I interferon (IFN) response is one of the first lines of cellular defense against invading pathogens. The IFN-induced zinc finger antiviral protein (ZAP) is a potent inhibitor of diverse RNA and DNA viruses (Yang and Li, 2020; Ficarelli *et al*, 2021). ZAP encodes at least four splice isoforms, two of which, ZAPS (short) and ZAPL (long) are well characterized (Charron *et al*, 2013; Li *et al*, 2019; Schwerk *et al*, 2019). ZAPS and ZAPL share the N-terminal CCCH zinc fingers (ZnFs) that mediate RNA binding while ZAPL has an additional C-terminal catalytically inactive poly(ADP-ribose) polymerase (PARP)-like domain, which contributes to its greater antiviral activity compared to the IFN-inducible ZAPS (Yang and Li, 2020; Ficarelli *et al*, 2021). Two primary mechanisms of ZAP antiviral activity include targeting viral RNA for degradation and suppressing viral translation (Yang and Li, 2020). However, it remains largely unclear how ZAP is able to coordinate multiple means of viral antagonism while lacking enzymatic activity on its own. These mechanisms appear to be dependent on viral context. For example, ZAP is thought to inhibit human immunodeficiency virus-1 (HIV-1) primarily by targeting its RNA for degradation (Zhu *et al*, 2011, 2012). On the other hand, ZAP inhibits alphavirus replication by suppressing translation of incoming viral genomes, and inhibits replication of Japanese encephalitis virus (JEV) by both RNA degradation and translation suppression (Bick *et al*, 2003; Chiu *et al*, 2018). In addition to inhibiting viral replication by binding directly to viral RNA, ZAP also recruits cellular co-factors, such as exosome components, the putative

endonuclease KHNYN, and the E3 ligase tripartite motif containing protein 25 (TRIM25) (Guo *et al*, 2007; Li *et al*, 2017; Zheng *et al*, 2017; Ficarelli *et al*, 2019).

Earlier efforts to elucidate ZAP RNA binding activity showed that ZAP binds RNA with its four N-terminal CCCH ZnFs, and mutations of ZnFs 2 and 4 most dramatically reduce ZAP antiviral activity (Guo *et al*, 2004). The first structural study of only the N-terminal region of ZAP (NZAP) posited that the four ZnFs form two distinct RNA binding cavities; however, this study did not directly show ZAP bound to RNA (Chen *et al*, 2012). In recent years, much focus has been given to the discovery of ZAP as a CpG dinucleotide sensor in the context of HIV-1 infection (Takata *et al*, 2017; Ficarelli *et al*, 2019). Since then, two studies have elucidated the structure of ZAP complexed with CpG-containing RNA and identified critical residues responsible for its CpG binding specificity (Meagher *et al*, 2019; Luo *et al*, 2020). While several studies characterized ZAP RNA binding activity, they have done so in the context of only NZAP or only ZAPL and not ZAPS, and primarily focused on the mechanism of RNA degradation (Chen *et al*, 2012; Meagher *et al*, 2019; Luo *et al*, 2020; Gonçalves-Carneiro *et al*, 2021). Moreover, most did not utilize full-length viral RNA for measuring ZAP RNA binding activity, instead assaying with only a ZAP-sensitive fragment (Chen *et al*, 2012; Luo *et al*, 2020). Meanwhile, it has been suggested that translation inhibition may be preceded by and required for ZAP-mediated mRNA degradation (Zhu *et al*, 2012). Furthermore, these ZAP RNA binding studies have mostly expressed RNA binding mutants against the background of endogenous ZAP and TRIM25.

While much attention has been given to characterizing ZAP RNA binding, less has been given to its critical co-factors such as TRIM25. TRIM25 was identified as a ZAP co-factor in the context of inhibiting alphavirus translation (Li *et al*, 2017; Zheng *et al*, 2017). However, it remains unclear whether TRIM25 modulates the RNA binding activity or specificity of ZAP. Like ZAP, TRIM25 is an RNA binding protein (Choudhury *et al*, 2017; Sanchez *et al*, 2018; Garcia-Moreno *et al*, 2019). TRIM25 RNA binding has been mapped to two separate motifs: a 39-amino acid stretch in the C-terminal PRY-SPRY domain (Choudhury *et al*, 2017), and a lysine-rich sequence (7K) within the L2 linker connecting the coiled-coil and PRY-SPRY domains (Sanchez *et al*, 2018). TRIM25 also appears to preferentially bind G- and C-rich sequences, and prefers mRNAs and long intergenic non-coding RNAs (Choudhury *et al*, 2017). TRIM25 RNA binding is required for its ubiquitin ligase activity (Choudhury *et al*, 2017), which in turn is required for its function in ZAP antiviral activity (Li *et al*, 2017; Zheng *et al*, 2017). Both TRIM25 and ZAP directly bind SINV RNA, and have been demonstrated to associate more strongly with SINV RNA during infection (Guo *et al*, 2004; Garcia-Moreno *et al*, 2019). TRIM25 and ZAP also associate with one another, with the ZAP interaction motif within TRIM25 mapped to its C-terminal PRY-SPRY domain (Li *et al*, 2017). Meanwhile, the TRIM25 interaction motif for ZAP is thought to reside within its N-terminal ZnFs (Gonçalves-Carneiro *et al*, 2021), though the additional PARP-like domain within ZAPL may contribute to TRIM25 binding as well by modulating proper localization (Kmiec *et al*, 2021).

While some have attempted to illuminate the contribution of ZAP or TRIM25 RNA binding to the ZAP-TRIM25 interaction, these studies have focused on only a few select mutations. Still, most agree that RNA binding in either ZAP or TRIM25 is not required for the ZAP-TRIM25 interaction.

One group demonstrated not only that RNase A treatment has little effect on the ZAPL-TRIM25 interaction, but also that an example ZAPL RNA binding mutant retains and even increases its interaction with TRIM25 (Gonçalves-Carneiro *et al*, 2021). Another showed the TRIM25 mutant in which the 7K motif is replaced with alanines (abbreviated as 7KA) associates more strongly with ZAP (Gonçalves-Carneiro *et al*, 2021), while a third found that the TRIM25 mutant with a deletion of the 39-amino acid sequence in the PRY-SPRY domain (abbreviated as ΔRBD) fails to bind ZAP at all (Choudhury *et al*, 2017). Still, it is important to note that the RNA binding motif deleted in TRIM25 ΔRBD is located within the same PRY-SPRY domain that TRIM25 uses to interact with ZAP, complicating these findings, and that the same study corroborated previous findings that RNase A treatment has little impact on the ZAP-TRIM25 interaction (Choudhury *et al*, 2017).

In light of the recent novel structural insights, we asked how different ZAP and TRIM25 RNA binding mutations affect the ability of ZAP and TRIM25 to interact with one another and to restrict SINV and JEV translation. We curated a panel of ZAP and TRIM25 RNA binding mutants from prior studies, including mutants with a range of RNA binding and antiviral capabilities (Guo *et al*, 2004; Chen *et al*, 2012; Meagher *et al*, 2019; Luo *et al*, 2020). We first characterized these ZAP and TRIM25 mutants' direct binding to SINV RNA. We then asked how their ability to bind RNA affects their ability to interact with one another. Generally, we observed that ZAP mutants that fail to bind SINV RNA interact more strongly with TRIM25. In contrast, we observed that the TRIM25 7KA mutant binds both SINV RNA and ZAP more strongly than TRIM25 wild-type (WT), and that the TRIM25 ΔRBD mutant is too unstable to have any detectable interaction with ZAP. Moreover, we generally found that mutants that fail to bind SINV RNA also fail to inhibit SINV replication and

translation, with residues important for CpG recognition playing a critical role in ZAP translation inhibition. Surprisingly, when we tested the ability of ZAP and TRIM25 RNA binding mutants to inhibit translation of a JEV replicon, some mutants demonstrate increased antiviral activity, while those with mutations in residues important for CpG recognition have reduced activity. We then performed a correlation analysis to determine which ZAP properties are necessary for its antiviral activity against SINV and JEV. We found a significant negative correlation between ZAP SINV RNA binding and ZAP-TRIM25 interaction. We also found a significant positive correlation between ZAP SINV RNA binding and SINV replication inhibition, as well as between ZAP-TRIM25 interaction and JEV translation inhibition. These data together suggest that ZAP RNA binding and interaction with TRIM25 may form two distinct determinants for ZAP antiviral mechanisms in different viral contexts, even while they appear to be inversely correlated in the context of binding to SINV RNA. Altogether, this study furthers our understanding of how viral RNA binding and interaction with co-factors might modulate translation inhibition by ZAP.

RESULTS

ZAP and TRIM25 RNA binding mutants show a range of binding to SINV genomic RNA

To investigate the role of ZAP and TRIM25 RNA binding in the context of viral translation, we generated a panel of constructs with mutations previously demonstrated to impact RNA binding. For ZAP, each of the following mutations was introduced both in ZAPS and ZAPL to probe potential isoform differences in RNA binding and antiviral function. These mutations fall into two general categories: 1) ZnF mutants that individually disrupt each CCCH motif and 2) CpG RNA binding cavity mutants. We made four individual mutations to disrupt each N-terminal CCCH ZnF: H86K,

C88R, C168R, and H191R, which are located in ZnF 1, 2, 3, and 4, respectively (Guo *et al*, 2004). Two putative RNA binding cavities were previously identified based on a crystallized NZAP structure without bound RNA (Chen *et al*, 2012). Therefore, we also made two triple mutations in the two RNA binding cavities contained within the ZnFs: V72A/Y108A/F144A (abbreviated as VYF), found within ZnFs 2-3, and H176A/F184A/R189A (abbreviated as HFR), found within ZnF 4 (Chen *et al*, 2012). More recent studies have elucidated structures of NZAP bound to CpG-containing RNA (Meagher *et al*, 2019; Luo *et al*, 2020). Building on this work, we made two double mutations and one triple mutation within the ZnFs that mediate CpG dinucleotide-specific binding. These mutations are C96A/Y98A (abbreviated as CY) and K107A/Y108A (abbreviated as KY) within ZnF 2, and E148A/K151A/R170A (abbreviated as EKR) within ZnF 3, which demonstrate a range of RNA binding and antiviral activities (Meagher *et al*, 2019; Luo *et al*, 2020). NZAP mutants CY, KY, and EKR previously demonstrated loss of antiviral activity against a SINV NanoLuc luciferase reporter virus, with EKR exhibiting the least defect as compared to NZAP WT (Luo *et al*, 2020). Notably, the individual mutations Y108A/F and F144A/Y appear to be critical for ZAP recognition of CpG-rich RNA, wherein they completely and partially abolish ZAP's ability to discriminate between CpG-rich and CpG-deficient strains of HIV-1, respectively (Meagher *et al*, 2019; Luo *et al*, 2020).

For TRIM25, we generated two constructs, one in which we replaced the lysine-rich motif in the L2 linker with alanines (TRIM25 7KA) (Sanchez *et al*, 2018) and one in which we deleted the RNA binding domain in the PRY-SPRY domain (TRIM25 ΔRBD) (Choudhury *et al*, 2017).

We cloned each of these ZAP and TRIM25 WT or RNA binding mutants into a pcDNA3.1-3XFLAG and/or -myc plasmid, allowing for transient expression of each construct following transfection into ZAP or TRIM25 KO 293T cells. We titrated the amount of plasmid to transfect for each construct to ensure even expression across constructs and with ZAPS, ZAPL, and TRIM25 WT (Supplemental Figure 3.1). Because the ZAP CpG RNA binding cavity mutants generally express at higher levels than the ZnF mutants, we decided to transfect two amounts of ZAPS and ZAPL WT in our assays to match these two expression patterns. We then assessed the ability of the ZAP and TRIM25 mutants to bind SINV genomic RNA by an *in vitro* RNA pull-down assay. We incubated lysates of cells transfected with ZAP or TRIM25 mutants with biotin-labeled SINV (Toto1101 strain) genomic RNA, allowing for RNA and bound protein to be immunoprecipitated using streptavidin beads and probed for the presence of bound ZAP or TRIM25. As a negative control, we also assessed the ability of the WT constructs to bind firefly luciferase (Fluc) RNA. We quantified the resultant ZAP and TRIM25 bound to RNA and normalized to input ZAP and TRIM25 protein levels with ImageJ. The ZnF mutations in both ZAPS and ZAPL drastically reduce all SINV RNA binding, with only the ZAPS and ZAPL ZnF 1 mutant (H86K) and the ZAPS ZnF 3 mutant (C168R) showing low levels of binding (Figure 17A). In contrast, mutations in the CpG RNA binding cavities result in a range of binding phenotypes. For both ZAPS and ZAPL, the VYF, CY, and KY mutants show complete to near complete loss of SINV RNA binding, while the HFR and EKR mutants show similar to increased RNA binding relative to ZAPS and ZAPL WT (Figure 17B).

The TRIM25 mutants demonstrate diverging RNA binding phenotypes. The 7KA mutant not only has gained binding to SINV RNA relative to WT, but also to the Fluc negative control

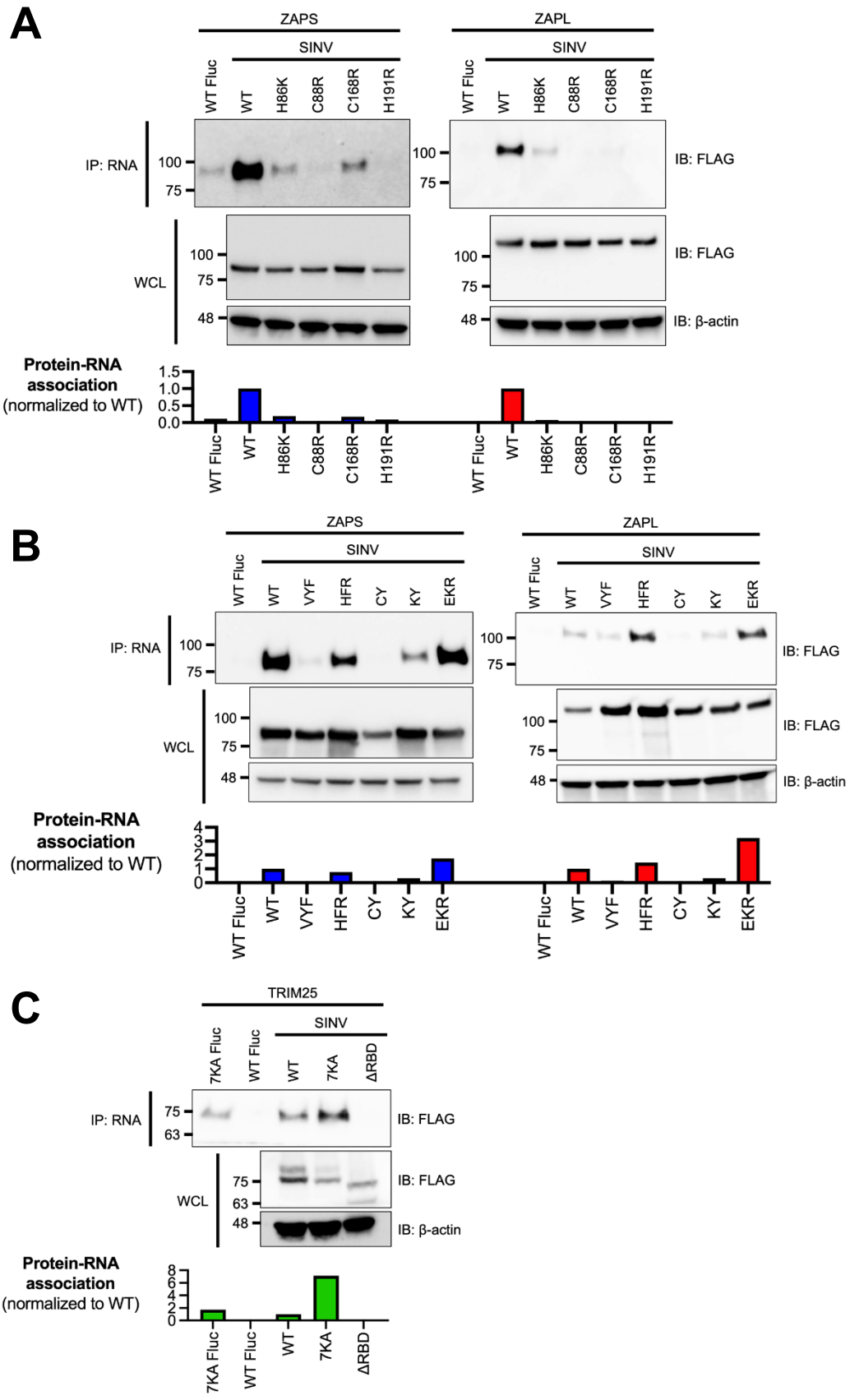
A
ZAPS
SINV
WT Fluc
WT
H86K
C88R
C168R
H191R
ZAPL
IP: RNA
WCL
100
75
48
IB: FLAG
IB: β-actin
Protein-RNA association (normalized to WT)
1.5
1.0
0.5
0.0
B
EKR
CY
KY
VYF
HFR
4
3
2
1
0
C
TRIM25
7KA Fluc
7KA
ΔRBD
63
8
6
4
2

Figure 17. Association of ZAP and TRIM25 RNA binding mutants with SINV RNA.

(A-B) ZAP KO or (C) TRIM25 KO 293T cells were transfected with (A) ZAP zinc finger mutants, (B) ZAP CpG RNA binding cavity mutants, or (C) TRIM25 mutants. ZAP or TRIM25 pulled down (IP) with Sindbis virus (SINV) or firefly luciferase (Fluc) RNA and in whole cell lysate (WCL) were assayed by immunoblot (IB). Blots were quantified with ImageJ. Data are representative of two independent experiments.

(Figure 17C). Consistent with previous findings, the ΔRBD mutation abolishes binding to SINV RNA (Figure 17C). Together, our findings indicate that the different RNA binding residues of ZAP and TRIM25 contribute in varying degrees to viral RNA binding.

RNA binding mutations generally increase ZAP-TRIM25 association

Given that TRIM25 RNA binding has been purported to stimulate its interaction with ZAP (Choudhury *et al*, 2017), and that the ZAP ZnFs responsible for RNA binding are also thought to mediate its interaction with TRIM25 (Gonçalves-Carneiro *et al*, 2021), we hypothesized that abolishing ZAP RNA binding would negatively impact ZAP association with TRIM25, and vice versa. We also aimed to capture any ZAP isoform-specific characteristics for association with TRIM25, given previous reports that TRIM25 preferentially interacts with ZAPL (Li *et al*, 2017; Kmiec *et al*, 2021). Therefore, we expected that ZAP RNA binding mutants would display decreased enrichment in the presence of TRIM25 co-immunoprecipitation (co-IP) compared to ZAP WT. In concordance with prior work and our observation of different RNA binding activities of the TRIM25 mutants (Figure 17C), we also expected that TRIM25 7KA and ΔRBD would behave differently.

To test this hypothesis, we transfected ZAP KO 293T cells with either FLAG-tagged ZAPS or ZAPL RNA binding mutants and myc-tagged TRIM25 WT. Given that the ZAP ZnFs 2-4 display approximately equal, near complete loss of RNA binding (Figure 17A), and that ZnFs 2 and 4 are more important for mediating ZAP antiviral activity against alphaviruses and for CpG specificity (Bick

et al, 2003; Meagher *et al*, 2019; Luo *et al*, 2020), we proceeded with testing only ZnF mutants 2 and 4 in addition to the complete panel of CpG RNA binding cavity mutants. We then performed a myc IP to enrich for TRIM25 and probed for the presence of associated ZAPS or ZAPL, quantifying resultant ZAP pulldown with ImageJ. Surprisingly, we found that both ZnF mutants (C88R and H191R) in both ZAPS and ZAPL display increased association with TRIM25 (Figure 18A-B). Of the remaining RNA binding mutants, VYF, CY, and KY with near complete loss of RNA binding (Figure 17B) display similar to increased TRIM25 association for both ZAPS and ZAPL, though to a lesser extent than the ZnF mutants (Figure 18A-B). Only HFR with relatively unaffected RNA binding (Figure 17B) exhibits diminished interaction with TRIM25 as compared to ZAPS and ZAPL WT (Figure 18A-B), while EKR which mostly retains or even gains binding to SINV RNA (Figure 17B) binds to TRIM25 to a similar degree as compared to ZAP WT (Figure 18A-B).

To test the ability of TRIM25 RNA binding mutants to interact with ZAP, we transfected TRIM25 KO 293T cells with myc-tagged TRIM25 RNA binding mutants and FLAG-tagged ZAPS or ZAPL WT. When we transfected amounts that would yield similar levels of TRIM25 expression (Figure 18C), we found that these levels are too low to visualize previously demonstrated interactions between TRIM25 WT and ZAPS or ZAPL (data not shown). In our hands, the TRIM25 ΔRBD mutant is markedly less stable than the other TRIM25 constructs. Therefore, we maximized the transfected amounts of all TRIM25 forms to better visualize any differences in TRIM25 association with ZAP, normalizing the TRIM25 co-IP to input lysates and quantifying with ImageJ. As expected, we observed that TRIM25 7KA binds more robustly than TRIM25 WT to both ZAPS and ZAPL, while the TRIM25 ΔRBD levels are likely too low to be detected in the ZAP co-IP (Figure 18C).

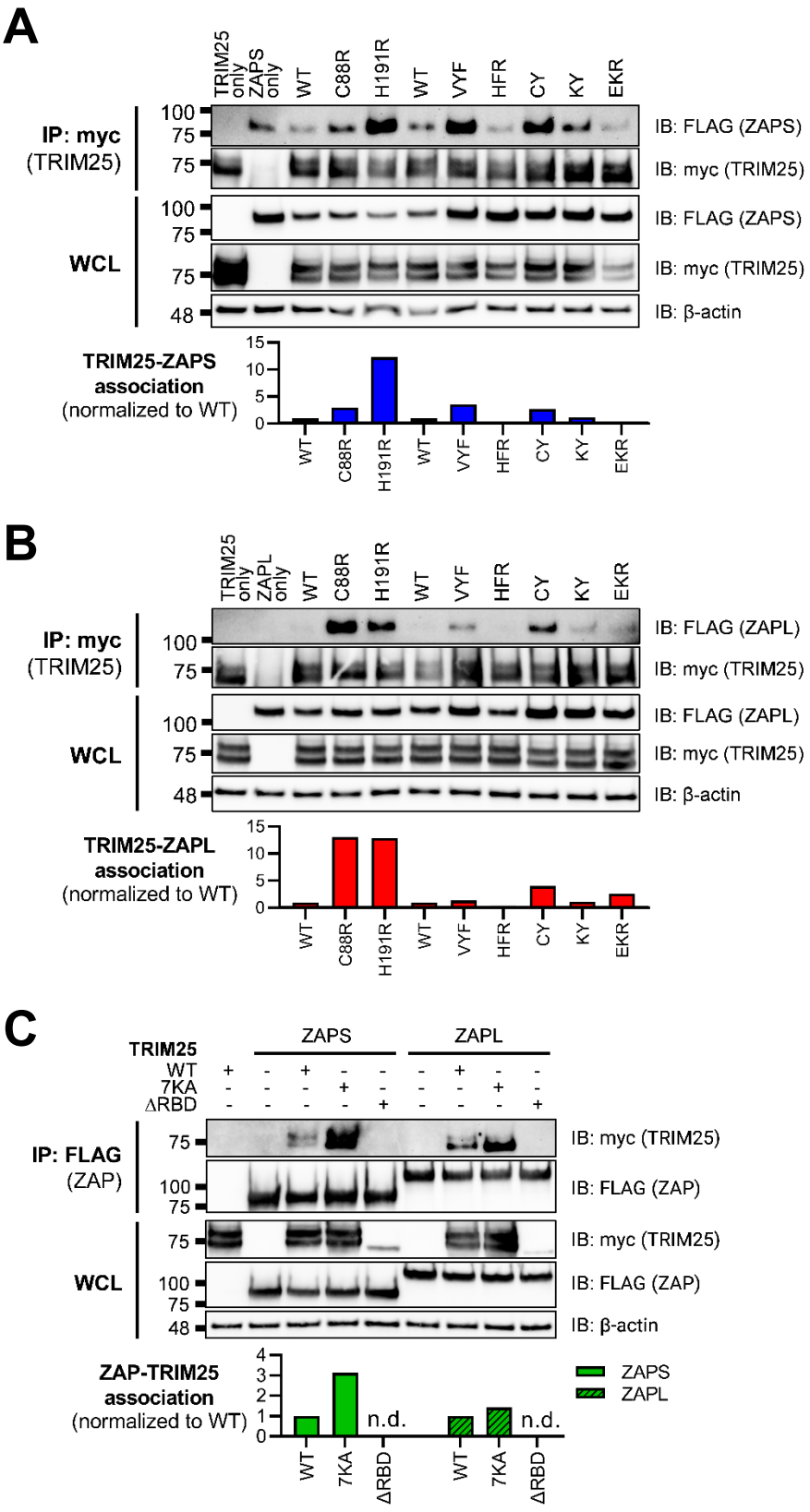
A
TRIM25 only
ZAPS only
WT
C88R
H191R
WT
VYF
HFR
CY
KY
EKR
IP: myc (TRIM25)
IB: FLAG (ZAPS)
IB: myc (TRIM25)
WCL
IB: FLAG (ZAPS)
IB: myc (TRIM25)
IB: β-actin
100
75
75
100
75
75
48
TRIM25-ZAPS association (normalized to WT)
15
10
5
0
B
TRIM25 only
ZAPL only
IP: myc (TRIM25)
IB: FLAG (ZAPL)
IB: myc (TRIM25)
WCL
IB: FLAG (ZAPL)
IB: myc (TRIM25)
IB: β-actin
TRIM25-ZAPL association (normalized to WT)
C
TRIM25
ZAPS
ZAPL
WT
7KA
ΔRBD
IP: FLAG (ZAP)
IB: myc (TRIM25)
IB: FLAG (ZAP)
WCL
IB: myc (TRIM25)
IB: FLAG (ZAP)
IB: β-actin
ZAP-TRIM25 association (normalized to WT)
n.d.
n.d.
ZAPS
ZAPL

Figure 18. Interaction of ZAP or TRIM25 RNA binding mutants with TRIM25 or ZAP WT.

(A-B) Western blot of ZAP KO 293T cells transfected with myc-tagged TRIM25 and (A) FLAG-tagged ZAPS RNA binding mutants or (B) FLAG-tagged ZAPL RNA binding mutants. Different amounts of (A) ZAPS and (B) ZAPL WT were transfected to match protein expression levels for each subset of ZnF mutants and CpG RNA binding cavity mutants. Blots were quantified with ImageJ. Data are representative of two independent experiments. (C) Western blot of TRIM25 KO 293T cells transfected with FLAG-tagged ZAPS or ZAPL and myc-tagged TRIM25 RNA binding mutants; n.d. stands for not detectable by western blot. Blots were quantified with ImageJ. Data are representative of two independent experiments.

Together, these data suggest that ZAP RNA binding may compete with ZAP-TRIM25 interaction likely because ZAP interacts with TRIM25 through its N-terminal ZnFs. Moreover, there do not appear to be ZAP isoform-specific differences for the RNA binding mutants as a whole, with trends of increased or decreased TRIM25 association holding true for each mutant in ZAPS and ZAPL.

RNA binding is required for both ZAP and TRIM25 inhibition of SINV replication

Next, we asked how loss of RNA binding would affect the ability of ZAP and TRIM25 to inhibit SINV replication. Given the centrality of RNA binding to ZAP antiviral activity and to TRIM25 ligase activity, we hypothesized that mutations with near complete loss of RNA binding would abolish antiviral activity completely, while mutations with moderate loss of RNA binding would exhibit an intermediate phenotype. We transfected ZAP KO 293T cells with ZAP RNA binding mutants and infected with the SINV luciferase reporter virus Toto1101/Luc. As expected, the mutant EKR which retains its ability to bind SINV RNA as compared to ZAPS and ZAPL WT (Figure 17B) also remains capable of inhibiting SINV replication (Figure 19A-B). Both ZAPS and ZAPL ZnF mutants display reduced antiviral activity, and all other CpG RNA binding cavity mutants display differing degrees of loss of antiviral activity (Figure 19A-B). We observed significant differences in viral replication between ZnF mutants and WT for ZAPL (Figure 19B) but not for ZAPS (Figure 19A), likely due to ZAPL's greater viral inhibition. In ZAPS, mutants CY and KY have the most

significant increase in viral replication compared to ZAPS WT (Figure 19A), while ZAPL HFR has the most significant increase in viral replication compared to ZAPL WT (Figure 19B).

Meanwhile, we transfected TRIM25 KO 293T cells with TRIM25 RNA binding mutants to assess their ability to inhibit SINV replication. TRIM25 7KA, which binds SINV RNA more robustly than TRIM25 WT (Figure 17C) exhibits a similar degree of SINV inhibition (Figure 19C). On the other hand, TRIM25 ΔRBD, which fails to bind SINV RNA at all, restores viral replication to TRIM25 KO levels (Figure 19C). Finally, we asked whether the observed loss of antiviral activity for any of the ZAP and TRIM25 RNA binding mutants tested was due to a decrease in protein expression. To test this, we assayed protein expression both before and after SINV infection and found that with the exception of the ZAPL ZnF mutants, protein expression for all ZAP and TRIM25 variants

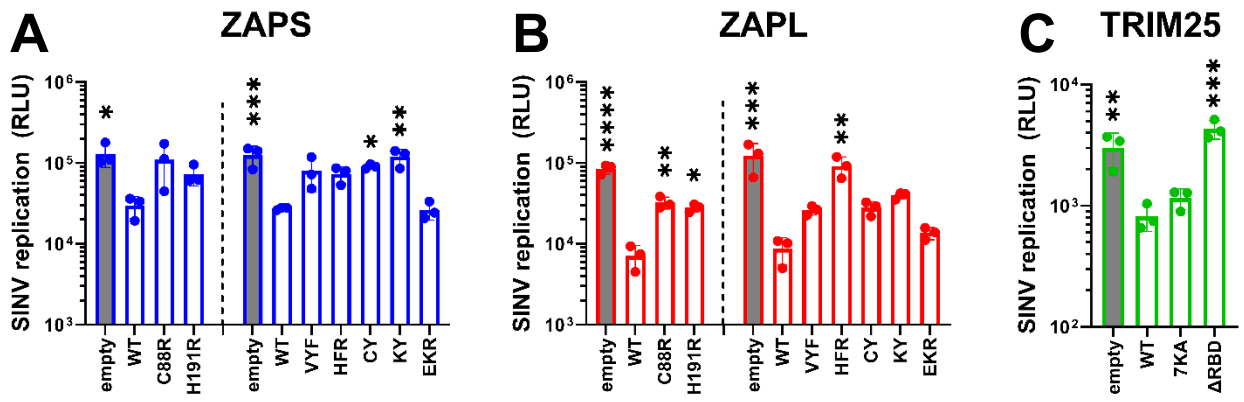

Figure 19. Inhibition of SINV replication by ZAP and TRIM25 RNA binding mutants.

(A-B) ZAP KO 293T cells or **(C)** TRIM25 KO 293T cells were transfected with **(A)** ZAPS RNA binding mutants, **(B)** ZAPL RNA binding mutants, or **(C)** TRIM25 RNA binding mutants, infected with SINV Toto1101/Luc at an MOI of 0.01 PFU/cell, and lysed 24 hours post infection (h.p.i.) for measurement of luciferase activity. Different amounts of **(A)** ZAPS and **(B)** ZAPL WT were transfected to match protein expression levels for each subset of ZnF mutants and CpG RNA binding cavity mutants. Data from triplicate wells are representative of two independent experiments. Asterisks indicate statistically significant differences as compared to **(A-B)** ZAP WT or **(C)** TRIM25 WT within each subset of RNA binding mutants (by one-way ANOVA and Dunnett's multiple comparisons test: *, $p<0.05$; **, $p<0.01$; ***, $p<0.001$; ****, $p<0.0001$). Unlabeled comparisons are not significant.

increases to varying degrees during infection (Supplemental Figure 3.2). Still, almost all of the ZAP RNA binding mutants express more highly than ZAP-WT (Supplemental Figure 3.2A-B), supporting our hypothesis that it is mutation of these RNA binding residues and not overall protein levels that determines degree of antiviral activity. Together, these data point strongly to the primacy of RNA binding in both ZAP and TRIM25 inhibition of SINV replication.

ZAP CpG-mediated RNA binding but not TRIM25 RNA binding is required for inhibition of SINV translation

Following our characterization of ZAP and TRIM25 RNA binding mutants' ability to inhibit SINV replication, we asked whether this antiviral activity stems from a block in alphavirus translation, given that ZAP blocks SINV translation and that TRIM25 is absolutely required for this inhibition (Li *et al*, 2017). These prior studies readily measure SINV translation with a replication-deficient temperature-sensitive luciferase reporter virus, Toto1101/Luc:ts6, such that any luciferase activity would reflect translation of the incoming viral genome (Rice *et al*, 1987; Bick *et al*, 2003). Here, we decided to omit the ZnF 4 mutant (H191R) due to its similarity in behavior to the ZnF 2 mutant (C88R), and the CpG RNA binding mutant EKR due to its lack of antiviral activity (Figure 19A-B). We transfected ZAP KO 293T cells with ZAPS or ZAPL ZnF 2 and CpG RNA binding cavity mutants and infected with Toto1101/ Luc:ts6.

Here, we found that while transfection of mutants VYF and KY significantly restores SINV translation in both ZAPS and ZAPL (Figure 20A-B), HFR only significantly restores SINV translation in the context of ZAPL (Figure 20B), in line with its antiviral activity against SINV replication (Figure 19B). Given that the residue Y108 is mutated in both VYF and KY and has previously been implicated

in determining ZAP CpG specificity (Meagher *et al*, 2019), our data suggest that Y108 is very important for ZAP inhibition of SINV translation. Moreover, given that HFR largely retains RNA binding in both ZAPS and ZAPL (Figure 17B), these data suggest that mechanisms in addition to RNA binding may modulate ZAP translation inhibition. No dramatic restoration of viral translation is seen for the ZnF 2 mutant (C88R) in either isoform (Figure 20A-B), nor does any TRIM25 RNA binding mutant impact TRIM25 inhibition of viral translation when transfected into TRIM25 KO cells (Figure 20C), though the lack of effect could be attributed to low protein expression of TRIM25 ΔRBD. Interestingly, we observed that there appear to be two distinct translation phenotypes in the presence of the TRIM25 ΔRBD mutant in two independent experiments, wherein half of the replicate wells exhibit inhibited translation similar to TRIM25 WT and the other half have partially restored

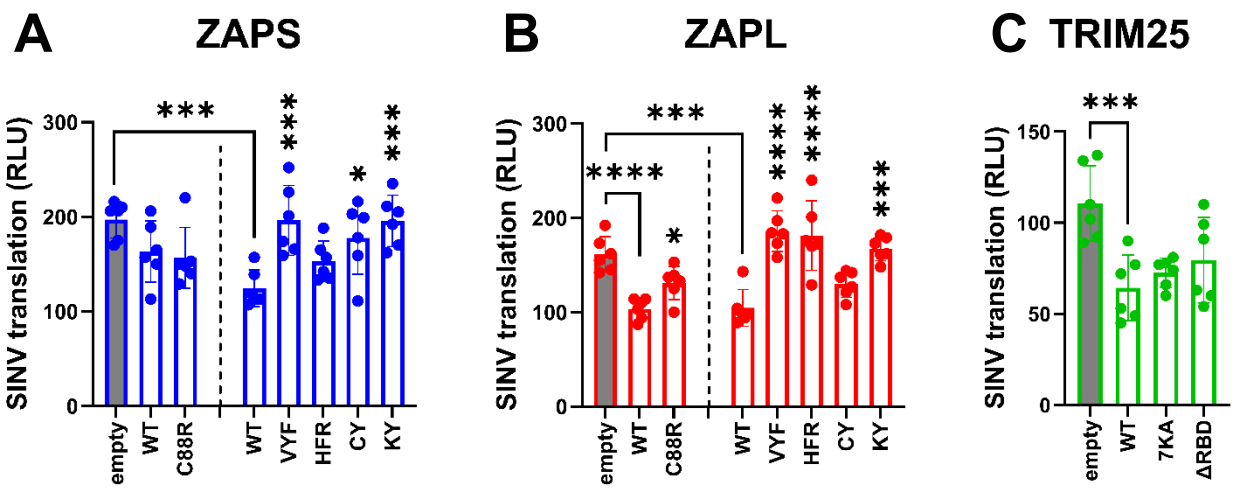

Figure 20. Inhibition of SINV translation by ZAP and TRIM25 RNA binding mutants.

(A-B) ZAP KO 293T cells or **(C)** TRIM25 KO 293T cells were transfected with **(A)** ZAPS RNA binding mutants, **(B)** ZAPL RNA binding mutants, or **(C)** TRIM25 RNA binding mutants, infected with SINV Toto1101/Luc:ts6 at an MOI of 1 PFU/cell, and lysed 6 h.p.i. for measurement of luciferase activity. Data from triplicate wells are combined from two independent experiments. Asterisks indicate statistically significant differences as compared to **(A-B)** ZAP WT, wherein different amounts of **(A)** ZAPS and **(B)** ZAPL WT were transfected to match protein expression levels for each subset of ZnF mutants and CpG RNA binding cavity mutants, or **(C)** TRIM25 WT within each subset of RNA binding mutants (by one-way ANOVA and Dunnett's multiple comparisons test: *, $p<0.05$; ***, $p<0.001$; ****, $p<0.0001$). Unlabeled comparisons are not significant.

SINV translation (Figure 20C).

We also asked here whether the observed loss of inhibition of viral translation for any of the ZAP and TRIM25 RNA binding mutants tested was due to a decrease in protein expression. Similar to the replication competent SINV Toto1101/Luc, infection with the replication-deficient SINV Toto1101/Luc:ts6 generally results in higher expression of ZAP and TRIM25 variants (Supplemental Figure 3.3), though the phenotype for a 6 hour infection is not as robust as a 24 hour infection. Interestingly, we observed a mild decrease in expression for ZAPS CY, ZAPS VYF and ZAPL ZnF 2 mutant (C88R) (Supplemental Figure 3.3A-B). Still, most ZAP and TRIM25 RNA binding mutants exhibit similar, if not slightly higher protein expression as compared to ZAP and TRIM25-WT. Together, these data suggest that CpG recognition by ZAP is critical for its alphavirus translation inhibition and this is independent of ZAP isoforms.

ZAP CpG-mediated RNA binding but not TRIM25 RNA binding is required for inhibition of JEV translation, while ZAP ZnF mutations enhance JEV translation inhibition

Because we observed that specific residues involved in ZAP CpG recognition are more important for SINV translation inhibition, rather than RNA binding in general, we next asked if this trend holds true for ZAP translation inhibition of other viruses. JEV is another virus that is translationally inhibited by ZAP (Chiu *et al*, 2018). To assess if ZAP and TRIM25 RNA binding plays a similar role in blocking JEV translation as they do in blocking alphavirus translation, we assessed the ability of our constructs to inhibit a replication-defective JEV replicon expressing *Renilla* luciferase (Rluc) (Li *et al*, 2016). Because ZAP can also mediate degradation of JEV RNA, we measured luciferase activity 4 hours after transfecting the JEV replicon reporter to capture a time point that is early enough

to see ZAP primarily functioning through translation inhibition, but also long enough to see significant luciferase expression from the replicon. Previous work has shown that there is a minimal decrease in JEV replicon RNA at this time (Chiu *et al*, 2018). We attempted to co-transfect the JEV replicon with Fluc RNA as a transfection control, but found that ZAPL also restricts Fluc expression (Supplemental Figure 3.4), as previously demonstrated (Li *et al*, 2019).

We found that the ZAP and TRIM25 RNA binding mutants inhibit JEV translation to varying degrees (Figure 21). Surprisingly, we observed that the ZAPS and ZAPL ZnF 4 mutants (H191R) are significantly more inhibitory than their WT counterparts, while the ZAPL ZnF 2 mutant (C88R) is more inhibitory than ZAPL WT (Figure 21A-B). Given that these mutants show increased association with TRIM25 (Figure 18B), these data suggest a positive relationship between ZAP-TRIM25 interaction and JEV translation inhibition. The ZAP CpG RNA binding cavity mutants either show similar inhibition to ZAPS and ZAPL WT or, in the case of the ZAPS KY and ZAPL HFR and KY mutants, decreased inhibition (Figure 21A-B). Taken together with the SINV translation inhibition data, these data further point to the importance of the RNA binding cavities in ZAP inhibition of viral translation, including CpG-specific binding by the residue Y108.

Upon assaying TRIM25 variants, we found that the TRIM25 ΔRBD mutant inhibits JEV translation similarly to TRIM25 WT (Figure 21C), as we observed with SINV translation inhibition (Figure 20C). Surprisingly, the TRIM25 7KA mutant loses its ability to inhibit JEV translation (Figure 21C), in contrast to its ability to inhibit SINV translation similarly to TRIM25 WT (Figure 20C). Given the diverging phenotypes of the 7KA mutant, we were curious if the TRIM25 mutants

show a different pattern of binding to SINV versus JEV replicon RNA that would explain the differences in translation inhibition. We found that the TRIM25 7KA mutant binds JEV replicon RNA to a greater degree than TRIM25 WT, while the TRIM25 ΔRBD mutant loses the ability to bind JEV replicon RNA (Figure 21D). These findings recapitulate the TRIM25 SINV RNA binding

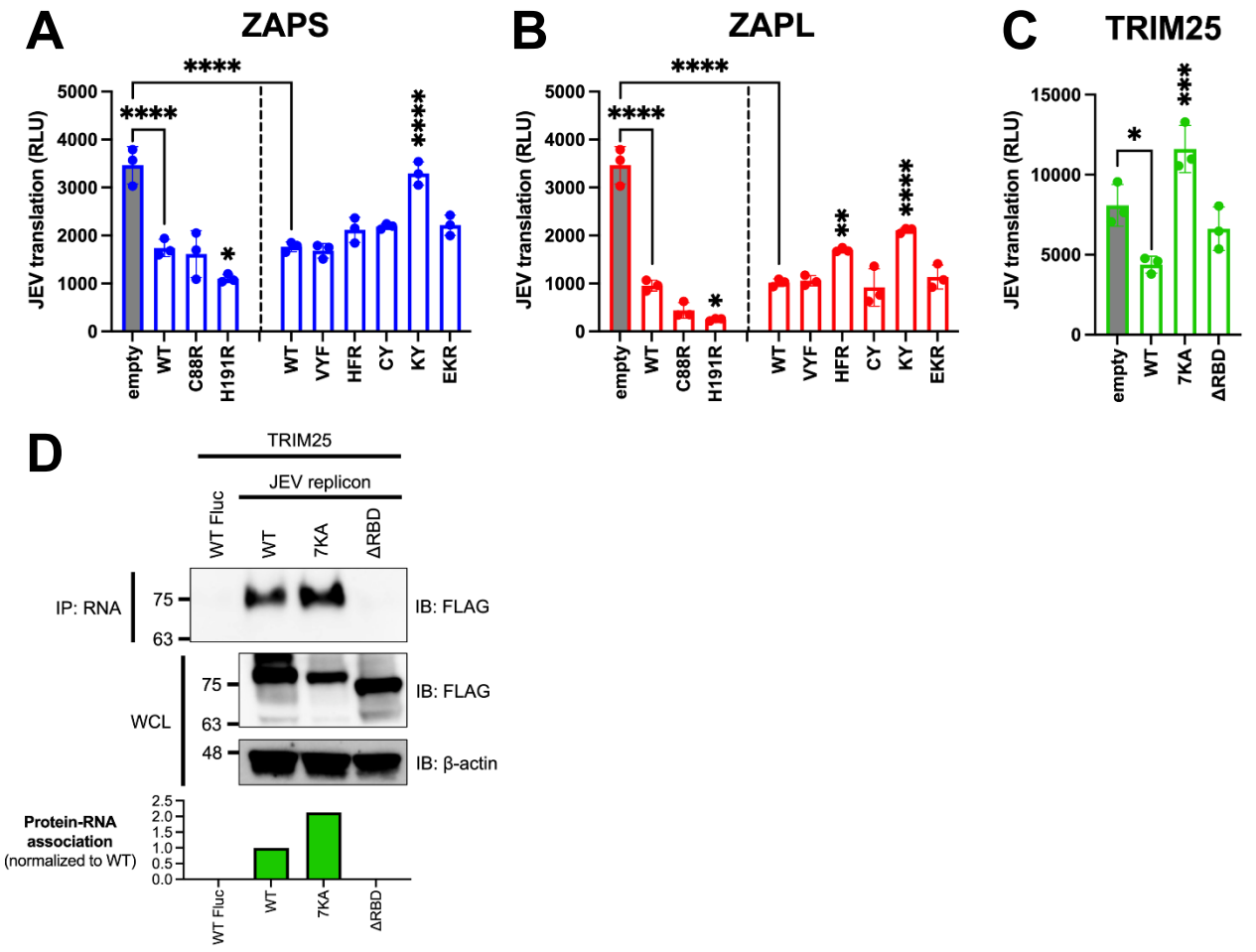

Figure 21. Inhibition of Japanese encephalitis virus (JEV) translation by ZAP and TRIM25 RNA binding mutants.

(A-B) ZAP KO 293T cells or **(C)** TRIM25 KO 293T cells were transfected with **(A)** ZAPS RNA binding mutants, **(B)** ZAPL RNA binding mutants, or **(C)** TRIM25 RNA binding mutants, transfected with a replication-defective JEV replicon RNA reporter, and lysed 4 hours post-reporter transfection for measurement of luciferase activity. Data from triplicate wells are representative of two independent experiments. Asterisks indicate statistically significant differences as compared to **(A-B)** ZAP WT or **(C)** TRIM25 WT within each subset of RNA binding mutants (by one-way ANOVA and Dunnett's multiple comparisons test: *, $p<0.05$; **, $p<0.01$; ***, $p<0.001$; ****, $p<0.0001$). Unlabeled comparisons are not significant. **(D)** TRIM25 KO 293T cells were transfected with TRIM25 mutants. TRIM25 pulled down with RNA and in WCL were assayed by western blot and quantified with ImageJ. Data are representative of two independent experiments.

phenotypes (Figure 17C), and suggest that RNA binding by TRIM25 is not an important determinant for its ability to inhibit JEV translation.

ZAP SINV RNA binding negatively correlates with ZAP-TRIM25 interaction and positively correlates with SINV replication inhibition, while ZAP-TRIM25 interaction positively correlates with JEV translation inhibition

Given our wide panel of ZAPS and ZAPL RNA binding mutants, we sought to look for significant correlations between any pairs of ZAP phenotypes. To facilitate this, we quantified the immunoblots for ZAP SINV RNA binding and ZAP-TRIM25 co-IPs and calculated fold inhibition relative to empty plasmid transfection for the viral inhibition assays (Table 5). Using these values, we calculated Pearson correlation coefficients and p-values for each pairwise phenotype comparison. When analyzing our data for the ZnF 2 and 4 mutants and the complete panel of CpG RNA binding cavity mutants (Figure 22A), we found a significant negative correlation ($r = -0.63$, $p<0.01$) between ZAP SINV RNA binding and ZAP-TRIM25 interaction (Figure 22B), lending further support to the idea that ZAP RNA binding competes with its ability to associate with TRIM25. We also observed a significant positive correlation ($r = 0.78$, $p<0.001$) between ZAP SINV RNA binding and SINV replication inhibition (Figure 22C), but interestingly, no correlation between ZAP SINV RNA binding and SINV translation inhibition (Table 5). This suggests that while general ZAP RNA binding is important for its antiviral activity, it is not as critical for the specific step of translation inhibition, although we did observe a significant positive correlation ($r = 0.64$, $p<0.05$) between SINV replication inhibition and SINV translation inhibition (Figure 22D). Finally, we found a significant positive correlation ($r = 0.54$, $p<0.05$) between ZAP-TRIM25 interaction and JEV translation inhibition (Figure 22E), further suggesting that ZAP interaction with TRIM25 potentiates its ability

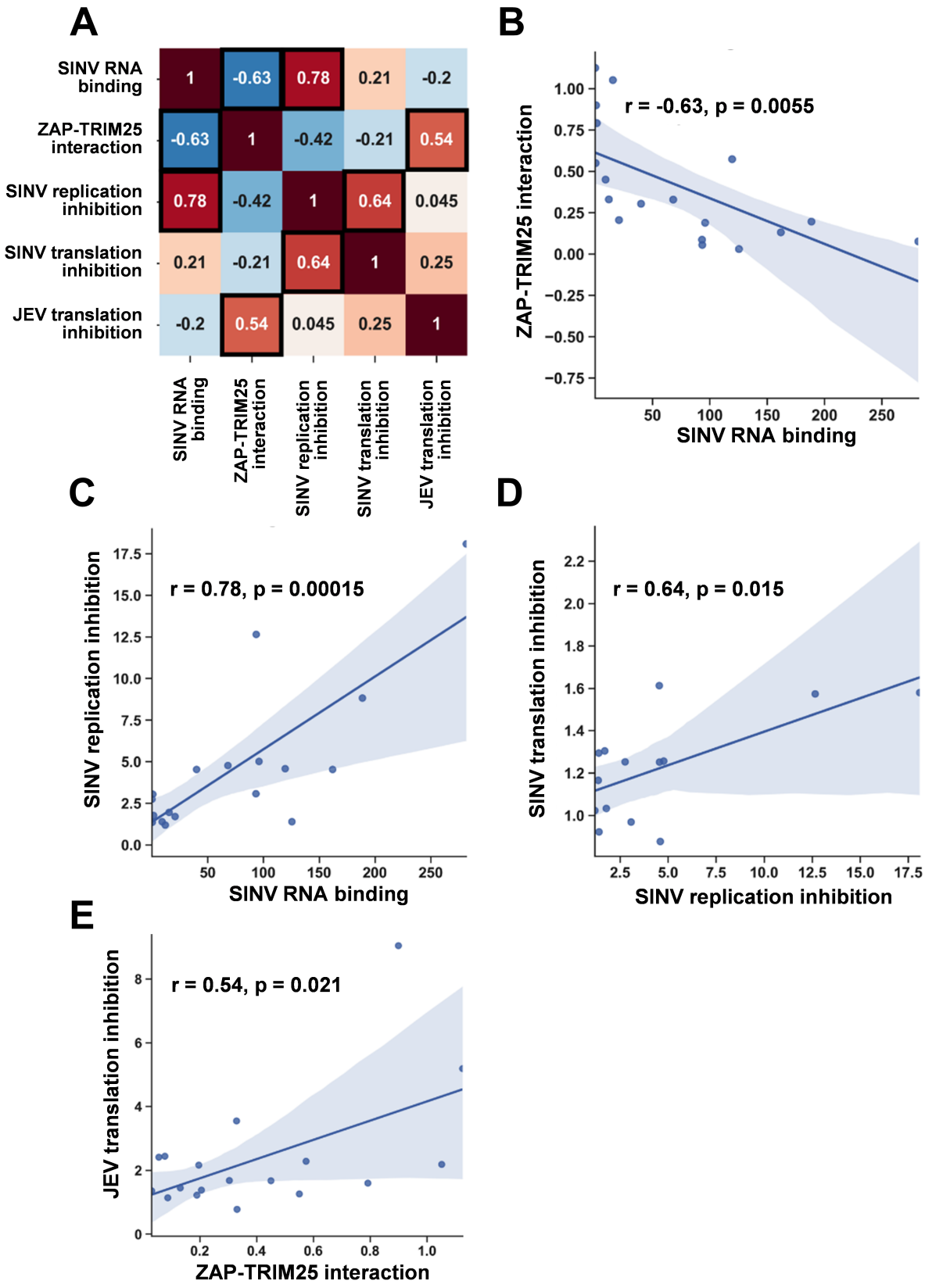
A
SINV RNA binding
ZAP-TRIM25 interaction
SINV replication inhibition
SINV translation inhibition
JEV translation inhibition
1
-0.63
0.78
0.21
-0.2
-0.63
1
-0.42
-0.21
0.54
0.78
-0.42
1
0.64
0.045
0.21
-0.21
0.64
1
0.25
-0.2
0.54
0.045
0.25
1
B
r = -0.63, p = 0.0055
ZAP-TRIM25 interaction
SINV RNA binding
C
r = 0.78, p = 0.00015
SINV replication inhibition
SINV RNA binding
D
r = 0.64, p = 0.015
SINV translation inhibition
SINV replication inhibition
E
r = 0.54, p = 0.021
JEV translation inhibition
ZAP-TRIM25 interaction

Figure 22. Correlation analysis of ZAP RNA binding mutant phenotypes.

Pearson correlation coefficients (r) and p-values (p) were calculated using the SciPy package in Python and plotted using the Matplotlib and Seaborn packages. **(A)** Pearson correlation coefficients are summarized in a heat map. Boxed coefficients have statistically significant p-values ($p<0.05$). Pairwise correlations with significant p-values from **(A)** are shown in **(B-E)**.

Table 5. Quantified values for ZAP RNA binding mutant phenotypes.

Immunoblots for ZAP SINV RNA binding assays and ZAP-TRIM25 co-IPs were quantified in ImageJ, with higher values indicating increased RNA or TRIM25 interaction. Fold inhibition values for viral inhibition assays were calculated relative to empty plasmid transfection, with higher values indicating greater viral replication or translation inhibition. N/A: SINV translation inhibition data on ZAP H191R and EKR mutants were not collected for analysis. Data are combined from two independent experiments.

Isoform	Mutant	SINV RNA binding	ZAP-TRIM25 interaction	SINV replication inhibition	SINV translation inhibition	JEV translation inhibition
ZAPS	WT for ZnF mutants	161.914	0.131	4.545	1.252	1.446
ZAPS	C88R	9.083	0.450	1.395	1.295	1.676
ZAPS	H191R	15.452	1.052	1.951	N/A	2.184
ZAPS	WT for cavity mutants	40.011	0.304	4.542	1.613	1.684
ZAPS	V72A/Y108A/F144A	1.444	0.792	1.777	1.033	1.598
ZAPS	H176A/Y184A/R189A	20.797	0.205	1.706	1.305	1.381
ZAPS	C96A/Y98A	0.408	0.550	1.361	1.166	1.260
ZAPS	K107A/Y108A	11.959	0.330	1.190	1.023	0.780
ZAPS	E148A/K151A/R170A	95.909	0.189	5.015	N/A	1.226
ZAPL	WT for ZnF mutants	93.414	0.055	12.652	1.574	2.416
ZAPL	C88R	0.034	1.126	2.756	1.253	5.191
ZAPL	H191R	0.761	0.899	3.043	N/A	9.046
ZAPL	WT for cavity mutants	281.812	0.076	18.090	1.580	2.444
ZAPL	V72A/Y108A/F144A	119.441	0.574	4.590	0.878	2.281
ZAPL	H176A/F184A/R189A	125.392	0.030	1.396	0.922	1.357
ZAPL	C96A/Y98A	68.060	0.329	4.774	1.257	3.551
ZAPL	K107A/Y108A	93.185	0.086	3.071	0.969	1.138
ZAPL	E148A/K151A/R170A	188.614	0.196	8.828	N/A	2.165

to inhibit JEV translation. Because we had a limited number of mutants for TRIM25, we were unable to find significant correlations between any pair of TRIM25 phenotypes (data not shown).

DISCUSSION

While the RNA binding functions of ZAP and TRIM25 have been previously dissected, in this study, we placed these functions in a wider context of viral translation inhibition. We found that ZAP and TRIM25 RNA binding domains contribute in varying degrees to their ability to bind SINV genomic RNA. We also observed that reduction of RNA binding by ZAP and TRIM25 generally increases their ability to interact with each other while reducing both of their abilities to inhibit SINV replication. When looking at viral translation inhibition more specifically, we found that the function of the ZAP CpG RNA binding cavities is most important for SINV and JEV translation inhibition, while general ZAP RNA binding and TRIM25 RNA binding is less critical. Some of our findings diverge from those observed previously, demonstrating the importance of studying ZAP and TRIM25 functions in a more biologically relevant context with the presence of full-length viral RNA.

Our SINV genomic RNA binding assays mostly recapitulate the results of prior studies, which investigated binding to synthetic viral RNA fragments or RNA constructs. Notably, we showed that all four ZnFs are individually required for efficient ZAP binding to SINV RNA (Figure 17A), while previously, only ZnF 2 has been demonstrated to be required for binding to SINV RNA fragments (Guo *et al*, 2004; Wang *et al*, 2010). Our findings also diverge from previous studies for the ZAP EKR CpG binding cavity mutant, which has reduced binding to a 6-nt single-stranded RNA probe (Luo *et al*, 2020); we showed that the ZAPS and ZAPL EKR mutants bind SINV RNA to a greater degree than their WT counterparts (Figure 17B). These contrasting findings may be a result of the different

assays used in our studies and suggest that the function of the CpG-specific binding residues within ZnF 3 varies based on its specific RNA target. We also found that impairing ZAP RNA binding results in increased association with TRIM25 (Figure 18A-B and Figure 22B), consistent with previous findings (Gonçalves-Carneiro *et al*, 2021). Given that ZAP has also been shown to interact with TRIM25 through its N-terminal ZnFs, we hypothesize that RNA binding may compete with ZAP-TRIM25 interaction, though further experiments are required to test this hypothesis.

As expected, we found that the ZAP RNA binding mutants show deficiencies in their ability to inhibit SINV viral replication and translation (Figures 19 and 20) recapitulating previous findings on their inhibition of SINV viral production and luciferase expression from reporters containing ZAP-sensitive fragments (Guo *et al*, 2004; Chen *et al*, 2012; Luo *et al*, 2020). When looking at SINV translation inhibition specifically, certain residues appear to be more critical for inhibition, particularly the CpG RNA binding mutants with the mutation Y108A (Figure 20A-B). Taken with our finding of a significant positive correlation between ZAP SINV RNA binding and SINV replication inhibition (Figure 22B), but no correlation between SINV RNA binding and SINV translation inhibition (Table 5), our data suggest that general ZAP RNA binding is less important than binding by particular residues for the specific step of translation inhibition. We observed a similar rescue of JEV translation inhibition with certain CpG RNA binding cavity mutants (Figure 21A-B), pointing to the importance of the ZAP CpG RNA binding cavity in facilitating translation inhibition of diverse viruses.

Deletion of all four ZnFs eliminates ZAP's ability to restrict JEV (Chiu *et al*, 2018), but our data suggests that mutation of ZnF 2 (C88R) and 4 (H191R) individually increases antiviral activity

(Figure 21A-B), potentially due to these mutants' increased ability to interact with TRIM25 (Figure 18A-B). Consistent with this, we found a significant positive correlation between ZAP's ability to interact with TRIM25 and its inhibition of JEV translation (Figure 22E). We speculate that ZAP-TRIM25 interaction might potentiate TRIM25 recruitment and ubiquitination of cellular substrates important for mediating JEV translation inhibition and/or RNA degradation, since ZAP can also mediate degradation of JEV RNA (Chiu *et al*, 2018). One possible such substrate is KHNYN, which functions in viral RNA degradation by ZAP and requires TRIM25 for its antiviral activity (Ficarelli *et al*, 2019). Additional studies are needed to evaluate these hypotheses.

By studying ZAP RNA binding mutations in both full-length ZAPS and ZAPL, we uncovered isoform differences in their effects on viral inhibition. The HFR CpG RNA binding cavity mutant shows an impaired ability to inhibit replication of SINV and translation of SINV and JEV in ZAPL, but not in ZAPS (Figures 19-21). ZAPL contains a catalytically inactive C-terminal PARP-like domain (Kerns *et al*, 2008) and a prenylation motif within this domain that targets it to endosomal membranes (Schwerk *et al*, 2019; Kmiec *et al*, 2021), which together may alter the ability of ZAPL to bind RNA, interact with other cellular or viral proteins, and inhibit viral translation in different viral contexts. Additional mutagenesis studies targeting the PARP-like domain are needed to tease out its role in mediating RNA binding. Because we introduced our mutants into ZAP KO cells, further work is also needed to address the possibility that the function of ZAP RNA binding mutants could be modulated by interactions between ZAPS and ZAPL, as well as with the additional isoforms ZAPM and ZAPXL (Li *et al*, 2019).

For TRIM25, we found that the TRIM25 ΔRBD mutant has lost the ability to bind SINV and JEV replicon RNA (Figures 17C and 21D). On the other hand, the TRIM25 7KA mutant shows increased binding to SINV and JEV replicon RNA, as well as the Fluc control RNA that is not bound by TRIM25 WT (Figures 17C and 21D). Previously, the TRIM25 7KA mutant was shown to be deficient in binding to a short double-stranded RNA probe (Sanchez *et al*, 2018). Similar to the ZAPS EKR mutant, we speculate that our divergent findings on the TRIM25 7KA mutant may result from differences in assays, and that the binding function of the 7K motif may depend on the specific RNA target. In our hands, the TRIM25 ΔRBD mutant is less stable than the other TRIM25 constructs, and so its expression is likely too low to be detected in the ZAP co-IP (Figure 18C). We did observe that the TRIM25 7KA mutant shows a more robust interaction with ZAPS and ZAPL than TRIM25 WT (Figure 18C). Taken together with the increased binding of this mutant to SINV RNA, our results suggest that RNA and ZAP binding are not inversely related for TRIM25, unlike for ZAP. While the TRIM25 ΔRBD mutant has lost its ability to restrict SINV replication (Figure 19C), it is still able to inhibit SINV translation similarly to TRIM25 WT despite some variability across replicates (Figure 20C). We hypothesize that these divergent phenotypes for SINV replication and translation result from variations in the TRIM25 ΔRBD mutant expression, rather than a defect in activity. While the 7K motif has been shown to be required for TRIM25 inhibition of dengue virus (Sanchez *et al*, 2018), which is not sensitive to ZAP inhibition (Chiu *et al*, 2018), our observations suggest that it is dispensable in the context of ZAP-mediated viral translation inhibition. In fact, given that the TRIM25 7KA mutant loses the ability to inhibit JEV translation (Figure 21C) and binds JEV replicon RNA more robustly than TRIM25 WT (Figure 21D), excess binding of TRIM25 to its target RNA

may even impede viral translation inhibition in certain contexts. It is possible that an increased presence of TRIM25 may hinder RNA or TRIM25 interactions with co-factors that function in JEV translation inhibition, but not SINV translation inhibition; further work is required to test this hypothesis. Taken together, our results indicate that while RNA binding is important for TRIM25's general ability to inhibit SINV replication, it is likely not required for translation inhibition specifically.

Overall, our findings suggest while ZAP RNA binding is required for its antiviral activity, its ability to specifically recognize CpG dinucleotides in viral RNA is more critical in the process of viral translation inhibition. Additionally, ZAP RNA binding and interaction with TRIM25 may represent two distinct determinants for ZAP antiviral activity in varying viral contexts. Altogether, our study has shed more light on the roles of viral RNA binding and co-factor dependency in the mechanism of ZAP translation inhibition and raise interesting questions on the requirement of specific residues for ZAP and TRIM25 RNA binding, protein-protein interaction, and antiviral activity.

ACKNOWLEDGMENTS

We thank Dr. Keriann Backus, Dr. Jian Cao, and Ashley Julio at the University of California, Los Angeles, for technical help with the streptavidin dot blot.

MATERIALS AND METHODS

Cell culture, viruses, and infections

Dr. Akinori Takaoka at Hokkaido University generously provided ZAP KO 293T cells (clone 89) and its parental 293T lines (Hayakawa *et al*, 2011). TRIM25 KO 293T cells were generated using CRISPR-Cas9 as previously described (Li *et al*, 2017; unpublished data). Cells were cultured in Dulbecco's Modified Eagle Medium (DMEM; Thermo Fisher Scientific, Waltham, MA) with 10% fetal bovine serum (FBS) added.

Infections with SINV expressing firefly luciferase (Toto1101/Luc) and temperature-sensitive SINV (Toto1101/Luc:ts6) have been previously described (Rice *et al*, 1987; Bick *et al*, 2003). Each independent experiment included triplicate wells of biological replicates per condition.BHK-21 cells were used to generate viral stocks and titers for multiplicity of infection calculations (Bick *et al*, 2003).

Plasmids and transfections

The replication-defective JEV replicon plasmid was generously provided by Dr. Bo Zhang at the Wuhan Institute of Virology (Li *et al*, 2016). The plasmid pcDNA3.1-3XFLAG was kindly gifted to us by Dr. Oliver Fregoso at UCLA. To generate pcDNA3.1-myc, a myc tag was swapped in for the 3XFLAG tag using *BamHI* and *HindIII* restriction sites. ZAPS and ZAPL were cloned into pcDNA3.1-3XFLAG from pTRIP-TagRFP-hZAPS and pTRIP-TagRFP-hZAPL, respectively, using *NotI* and *XbaI* restriction sites (Li *et al*, 2017). Dr. Jae U. Jung at the University of Southern California generously provided full-length TRIM25 (Gack *et al*, 2007). TRIM25 was cloned into both pcDNA3.1-3XFLAG and pcDNA3.1-myc using *XhoI* and *XbaI* restriction sites. All ZAP and TRIM25 constructs are myc- or 3XFLAG-tagged on the N-terminal end.

Point mutations in ZAPS and ZAPL were generated using the Q5 Site-Directed Mutagenesis Kit (New England Biolabs, Ipswich, MA) and all plasmids were verified by sequencing (Genewiz, South Plainfield, NJ). Primers for mutations were synthesized by Integrated DNA Technologies (IDT; Coralville, IA; Supplementary Table 3.1). The TRIM25 ΔRBD mutant (Choudhury *et al*, 2017) was generated by overlapping PCR (Supplementary Table 3.1). The TRIM25 7KA mutant was generated by ordering a gBlocks Gene Fragment from IDT with all lysines in $_{381}$KKVSKEEKKSKK$_{392}$ mutated to alanines (Sanchez *et al*, 2018), and utilizing innate restriction sites in TRIM25, *BsrGI* and *BamHI* (underlined), to replace WT sequence in TRIM25. The 7KA mutated sequence is bolded and underlined in the below gene block, and nonessential nucleotides on the 5' and 3' ends are written in lowercase.

5'-gttt<u>TGTACA</u>GTCAGATCAACGGGGCGTCGAGAGCACTGGATGATGTGAGAAACAGG
CAGCAGGATGTGCGGATGACTGCAAACAGAAAGGTGGAGCAGCTACAACAAGAATAC
ACGGAAATGAAGGCTCTCTTGGACGCCTCAGAGACCACCTCGACAAGGAAGATAAAG
GAAGAGGAGAAGAGGGTCAACAGCAAGTTTGACACCATTTATCAGATTCTCCTCAAG
AAGAAGAGTGAGATCCAGACCTTGAAGGAGGAGATTGAACAGAGCCTGACCAAGAGG
GATGAGTTCGAGTTTCTGGAGAAAGCATCAAAACTGCGAGGAATCTCAACAAAGCCA
GTCTACATCCCCGAGGTGGAACTGAACCACAAGCTGATAAAAGGCATCCACCAGAGC
ACCATAGACCTCAAAAACGAGCTGAAGCAGTGCATCGGGCGGCTCCAGGAGCCCACC
CCCAGTTCAGGTGACCCTGGAGAGCATGACCCAGCGTCCACACACAAATCCACACGC
CCTGTG**<u>GCAGCAGTCTCCGCAGAGGAAGCAGCATCCGCAGCA</u>**CCTCCCCCTGTCCC
TGCCTTACCCAGCAAGCTTCCCACGTTTGGAGCCCCGGAACAGTTAGTGGATTTAAA
ACAAGCTGGCTTGGAGGCTGCAGCCAAAGCCACCAGCTCACATCCGAACTCAACATC
TCTCAAGGCCAAGGTGCTGGAGACCTTCCTGGCCAAGTCCAGACCTGAGCTCCTGG
AGTATTACATTAAAGTCATCCTGGACTACAACACCGCCCACAACAAAGTGGCTCTGTC
AGAGTGCTATACAGTAGCTTCTGTGGCTGAGATGCCTCAGAACTACCGGCCGCATC
CCCAGAGGTTCACATACTGCTCTCAGGTGCTGGGCCTGCACTGCTACAAGAAG<u>GGG
ATCC</u>gttt(3')

X-tremeGENE9 DNA Transfection Reagent (Roche Life Science, Basel, Switzerland) was used to transfect cells at a ratio of 3 µL to 1 µg DNA according to the manufacturer's instructions. To

keep the total plasmid amount in co-transfections constant, empty vectors pcDNA3.1-myc or 3XFLAG were transfected as necessary (6 well plate, 2 µg total input; 24 well plate, 250 ng total input).

In vitro *transcription*

SINV DNA templates for transcription were generated by *XhoI* linearization of pToto1101 (Rice *et al*, 1987). SINV RNA was transcribed *in vitro* by Sp6 RNA polymerase (New England Biolabs) in the presence of the cap analog [m7G(5')ppp(5')G] (New England Biolabs). Fluc DNA templates for transcription were amplified from the pGL3-Control plasmid (Promega, Madison, WI). Fluc RNA was transcribed *in vitro* using the mMESSAGE mMACHINE T7 Transcription Kit (Invitrogen, Waltham, MA). Biotin-labeled RNAs were generated by adding 10mM biotin-16-UTP (Roche Life Science) to *in vitro* transcription reactions. JEV replicon DNA templates for transcription were generated by *XhoI* linearization and transcribed *in vitro* using the mMESSAGE mMACHINE T7 Transcription Kit (Invitrogen). Transcribed RNAs were purified using the *Quick*-RNA Miniprep Kit (Zymo Research, Irvine, CA) and biotinylation was confirmed by streptavidin dot blot (Chan *et al*, 2020).

In vitro *RNA pull-down assay*

0.4 pmol of biotin-labeled SINV or Fluc RNA probes were heated for 2 min at 90°C, chilled on ice for 2 min, and incubated with 50 µL 2x RNA structure buffer for 30 min at room temperature to ensure proper secondary RNA structure formation, as previously described (Bai *et al*, 2016). *In vitro* RNA pull-down was then performed as previously described (Chiu *et al*, 2018). In brief, RNA probes were incubated with 100 µg of lysates from ZAP or TRIM25 KO 293T cells transfected with ZAP or TRIM25 constructs for 48 hours. Cell extracts were lysed by CHAPS lysis buffer (10 mM Tris-HCl

[pH 7.4], 1 mM $MgCl_2$, 1 mM EGTA, 0.5% CHAPS, 10% glycerol, and 5 mM 2-mercaptoethanol) with complete protease inhibitor cocktail (Roche Life Science) and incubated with RNA probes in a final volume of 100 µL RNA binding buffer supplemented with 1 unit/µL RNAseOUT (Thermo Fisher Scientific), 1 µg/µL heparin (Sigma-Aldrich, St. Louis, MO), and 100 ng/µL yeast tRNA (Thermo Fisher Scientific) for 30 min at 30°C. Lysate-RNA mixtures were then incubated with 300 µL of Dynabeads M-280 Streptavidin (Invitrogen) for 30 min at room temperature on a shaker. Protein-RNA complexes were washed three times by RNA binding buffer, and proteins were eluted by incubation with 30 µL of 4x Laemmli Sample Buffer (Bio-Rad, Hercules, CA) for 5 min at 95°C. The proteins were further analyzed by immunoblot and quantified by ImageJ as previously described (Davarinejad, 2015). Briefly, to calculate the quantity of ZAP or TRIM25 bound to RNA relative to input ZAP or TRIM25 protein, the net value of the FLAG (ZAP or TRIM25) band in the whole cell lysate was divided by the net value of the β-actin loading control band in the whole cell lysate, giving a normalized input value. The net value of the FLAG band in the RNA IP band was then divided by the normalized input value.

Immunoblot analysis

Proteins were resolved through SDS-PAGE using NuPAGE MOPS SDS running buffer (Thermo Fisher Scientific) and 4-15% precast Mini-PROTEAN TGX Gels (Bio-Rad) before transferring to a PVDF membrane (Bio-Rad). Immunodetection was achieved with 1:2,500 anti-myc (Cell Signaling Technology, Danvers, MA), 1:20,000 anti-FLAG (Sigma-Aldrich), and 1:20,000 anti-actin-HRP (Sigma-Aldrich). Primary antibodies were detected with 1:20,000 goat anti-mouse HRP (Jackson ImmunoResearch, West Grove, PA) or 1:20,000 goat anti-rabbit HRP (Thermo Fisher

Scientific). Proteins were visualized on a ChemiDoc (Bio-Rad) using ProSignal Pico ECL Reagent (Genesee Scientific, San Diego, CA). ImageJ was used to quantify western blots as previously described (Davarinejad, 2015). Briefly, protein band intensities for each blot were measured by taking the net grey mean value of each band. The net grey mean value is defined as the inverted pixel density (255 – grey mean value) of a band with the inverted pixel density of the background (defined as an equivalent area of the blot above or below the band) subtracted.

Co-immunoprecipitation assay

To assess ZAP or TRIM25 co-immunoprecipitation (co-IP) with RNA binding mutants of TRIM25 or ZAP, respectively, cells were transfected in 6-well plates, collected, and then lysed by rotating in FLAG IP buffer (100 mM Tris-HCl 8.0, 150 mM NaCl, 5 mM EDTA, 1 mM DTT, 5% glycerol, 0.1% NP-40) supplemented with a complete protease inhibitor cocktail (Roche Life Science) at 4˚C for 30 min, before spinning down at 14,000 rpm at 4˚C for 15 min. To equilibrate beads prior to use, anti-FLAG beads (EZview™ Red ANTI-FLAG M2 Affinity Gel, Sigma-Aldrich) or anti-myc beads (EZview™ Red Anti-c-Myc Affinity Gel, Sigma-Aldrich) were washed 3 times in FLAG IP buffer. Three hundred µL of whole cell lysate (WCL) were incubated with 30 µL of anti-FLAG or -myc beads rotating at 4˚C for 45 minutes. FLAG IP buffer was used to wash immunoprecipitates 3 times before eluting bound proteins with SDS loading buffer, and boiling for 5 minutes for immunoblot analysis. Western blot ImageJ analysis was performed as previously described (Davarinejad, 2015). Briefly, to calculate the relative quantity of ZAP RNA binding mutants in the myc (TRIM25) co-IP, the net value of the FLAG (ZAP) IP band, defined as the net grey mean value of ZAP alone subtracted from each mutant band, was divided by the net value of the myc IP for each mutant. To calculate the relative

quantity of TRIM25 RNA binding mutants in the FLAG (ZAP) co-IP, the net value of the myc (TRIM25) IP band, defined as the net grey mean value of TRIM25 alone subtracted from each mutant band, was divided by the net value of the FLAG IP for each mutant. To account for the different expression levels of TRIM25 mutants, the myc IP band was first divided by the net grey mean value of the myc WCL band for each mutant, normalized to the value of the band for TRIM25 alone.

JEV replicon reporter assay

Following transfection of ZAP or TRIM25 constructs into ZAP or TRIM25 KO 293T for 48 hours, JEV replicon RNA was transfected by *Trans*IT-mRNA Transfection Kit (Mirus Bio, Madison, WI). Cells were lysed 4 hours post-transfection of replicon RNA and luciferase activity was measured by Dual-Luciferase Reporter Assay (Promega). Each independent experiment included triplicate wells of biological replicates per condition.

Statistical analysis

Statistical analyses in Figures 19-21 were performed on biological replicates from triplicate wells using GraphPad Prism. Statistical analyses in Figure 22 were performed using the SciPy package in Python and visualized using the Matplotlib and Seaborn packages (Hunter, 2007; Virtanen *et al*, 2020; Waskom, 2021).

SUPPLEMENTARY MATERIAL

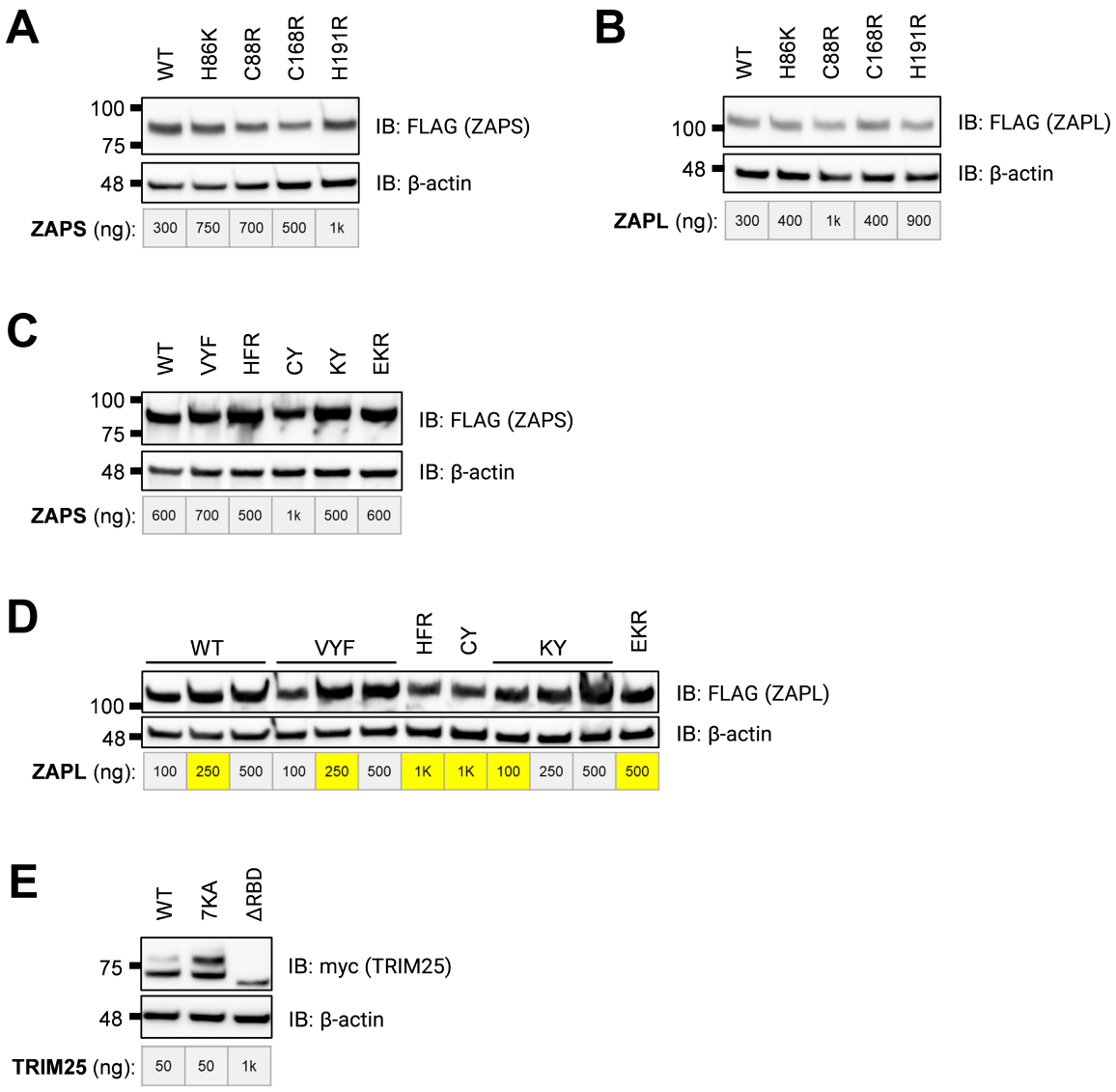

Supplemental Figure 3.1. Expression of ZAP and TRIM25 mutants.

(A-E) Final transfected DNA amounts for each mutant written below, where 1k = 1 µg of DNA. **(A)** Western blot of ZAPS zinc finger (ZnF) mutants. **(B)** Western blot of ZAPL ZnF mutants. **(C)** Western blot of ZAPS CpG RNA binding cavity mutants. **(D)** Western blot of ZAPL CpG RNA binding cavity mutants. Yellow highlighted cells indicate the selected amount to transfect for subsequent experiments. **(E)** Western blot of TRIM25 RNA binding mutants.

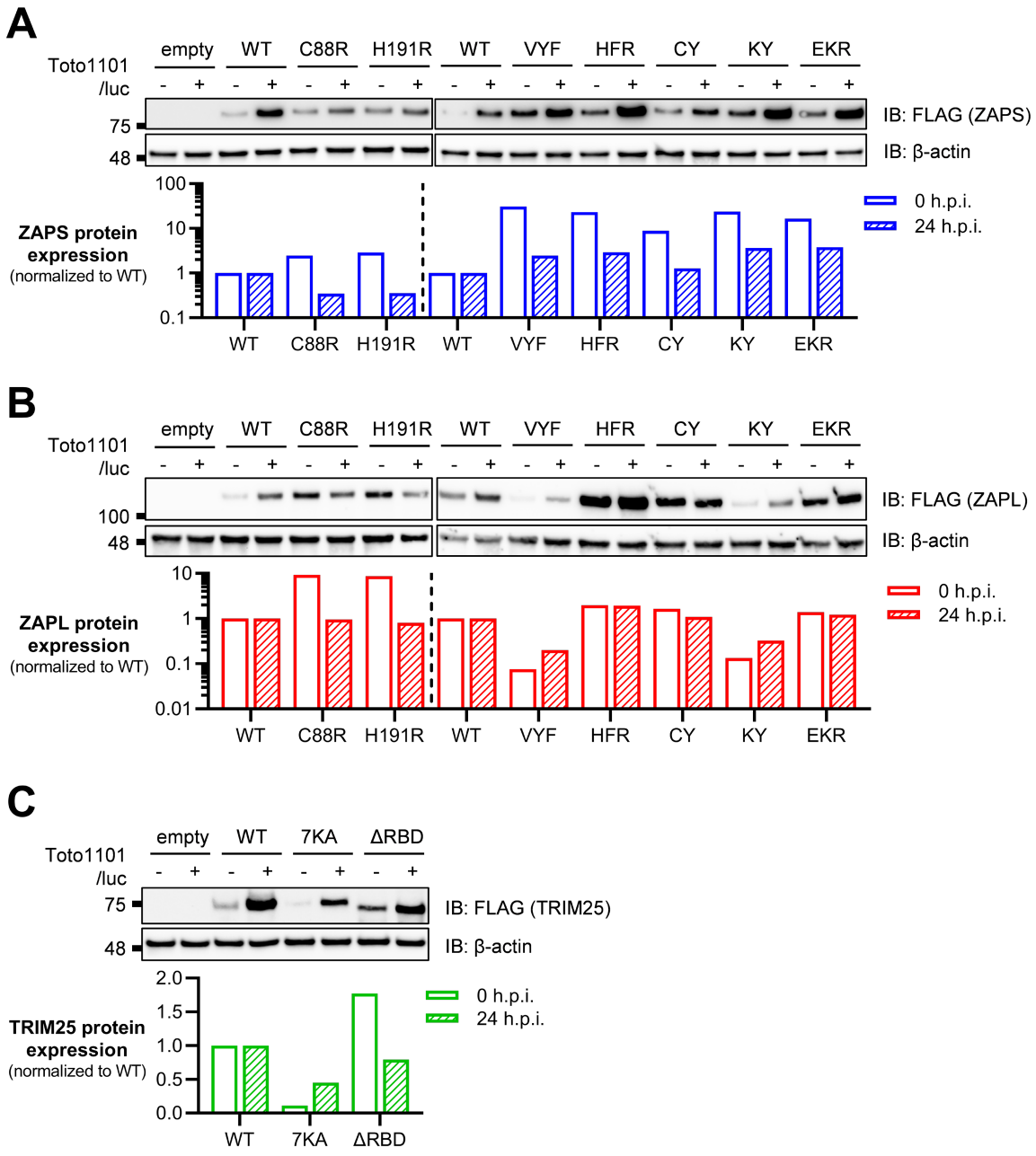

Supplemental Figure 3.2. Effect of SINV infection on ZAP and TRIM25 protein expression.

(A-B) ZAP KO 293T cells or (C) TRIM25 KO 293T cells were transfected with (A) ZAPS RNA binding mutants, (B) ZAPL RNA binding mutants, or (C) TRIM25 RNA binding mutants. Lysates were harvested at 0 and 24 h.p.i. with SINV Toto1101/Luc infection at an MOI of 0.01 PFU/cell. Data from triplicate wells are representative of two independent experiments

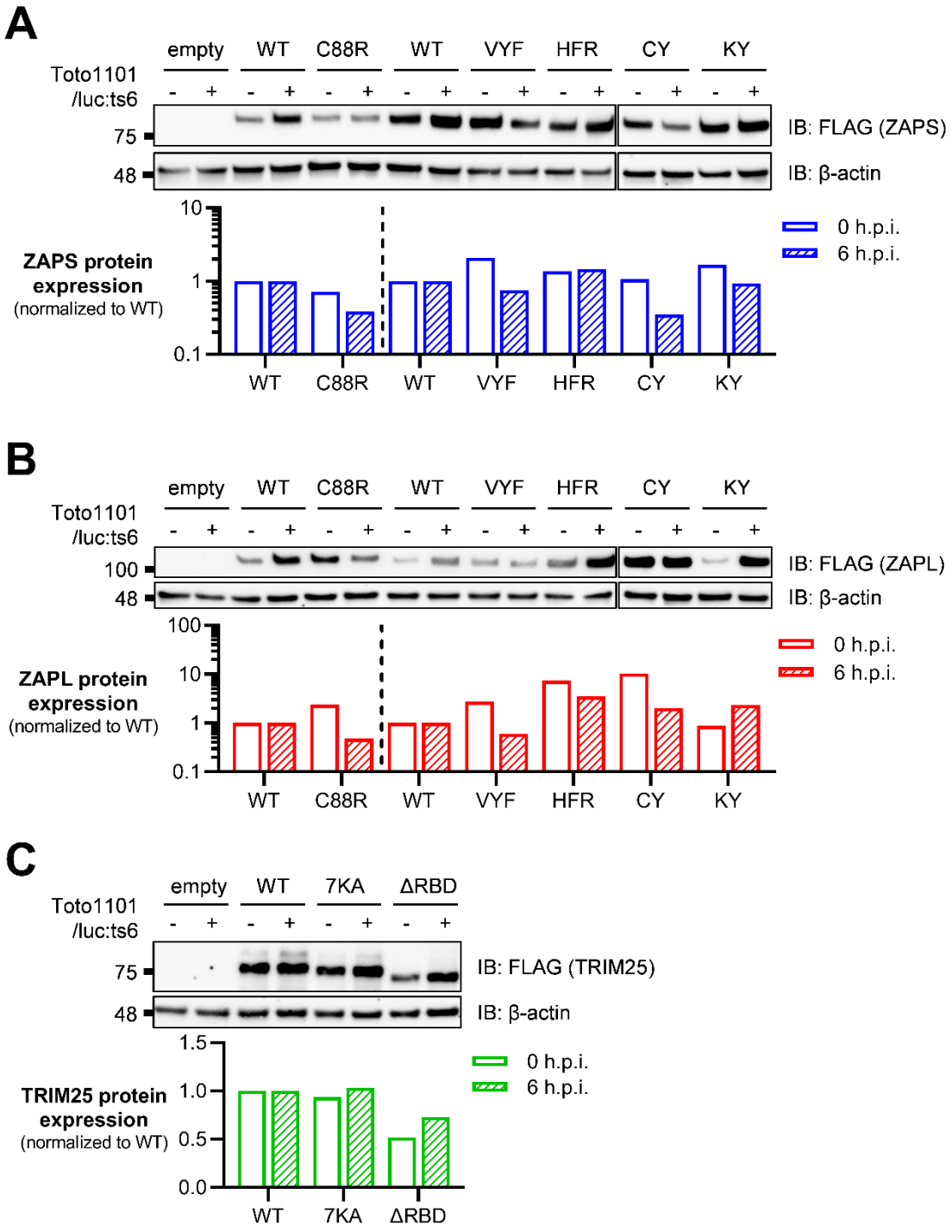

Supplemental Figure 3.3. Effect of replication-deficient SINV infection on ZAP and TRIM25 protein expression.

(**A-B**) ZAP KO 293T cells or (**C**) TRIM25 KO 293T cells were transfected with (**A**) ZAPS RNA binding mutants, (**B**) ZAPL RNA binding mutants, or (**C**) TRIM25 RNA binding mutants. Lysates were harvested at 0 and 6 h.p.i. with SINV Toto1101/Luc:ts6 infection at an MOI of 1 PFU/cell. Data from triplicate wells are representative of two independent experiments.

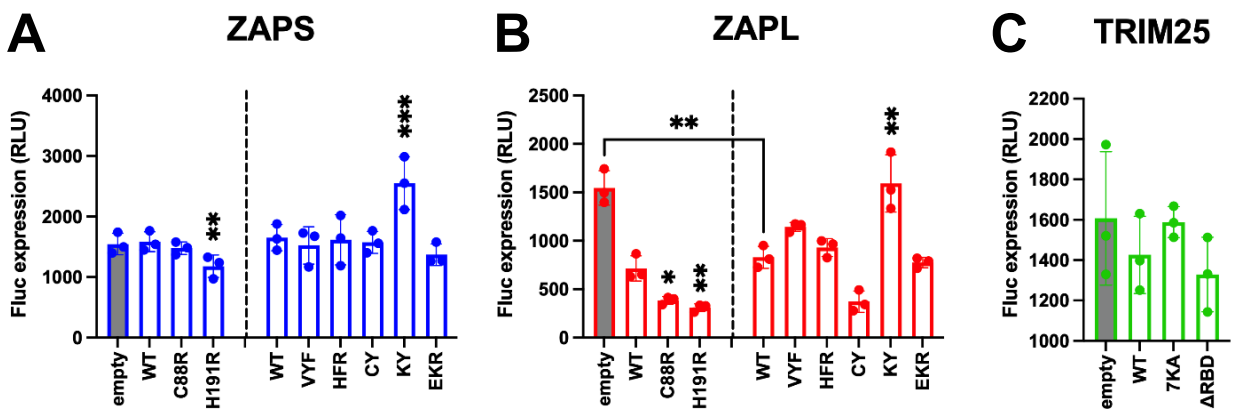

Supplemental Figure 3.4. Sensitivity of the firefly luciferase control RNA to ZAP.

(**A-B**) ZAP KO 293T cells or (**C**) TRIM25 KO 293T cells were transfected with (**A**) ZAPS RNA binding mutants, (**B**) ZAPL RNA binding mutants, or (**C**) TRIM25 RNA binding mutants, transfected with firefly luciferase (Fluc) RNA, and lysed 4 hours post-RNA transfection for measurement of luciferase activity. Data from triplicate wells are representative of two independent experiments. Asterisks indicate statistically significant differences as compared to (**A-B**) ZAP WT or (**C**) TRIM25 WT within each subset of RNA binding mutants (by one-way ANOVA and Dunnett's multiple comparisons test: *, $p<0.05$; **, $p<0.01$; ***, $p<0.001$). Unlabeled comparisons are not significant.

Supplementary Table 3.1. Primers used to generate ZAP and TRIM25 RNA binding mutants.

Additional features pertinent to primer design, such as additional mutations, are noted as necessary. Nonessential sequences written in lowercase.

RNA binding mutant	Mutation	Sequence (5'-3')	Forward (F) /Reverse (R)	Included features
ZAP-ZnF1	H86K	GAGACCCTGCGATAACCTGAAGCTCTGCAAACTCAACTTGC	F	
		GCAAGTTGAGTTTGCAGAGCTTCAGGTTATCGCAGGGTCTC	R	
ZAP-ZnF2	C88R	GCGATAACCTGCATCTCCGCAAACTCAACTTGCTG	F	
		CAGCAAGTTGAGTTTGCGGAGATGCAGGTTATCGC	R	
ZAP-ZnF3	C168R	ACCAGCAGCCACCGCGTTCAAGACTCCAC	F	
		GTGGAGTCTTGAACGCGGTGGCTGCTGGT	R	
ZAP-ZnF4	H191R	CTGCCTCCGGTCCCGTAACCTGATGGACA	F	
		TGTCCATCAGGTTACGGGACCGGAGGCAG	R	
ZAP-VYF	V72A	TTGCGACGGCAGGCCCGGGCTCTAG	F	
		CTAGAGCCCGGGCCTGCCGTCGCAA	R	
	Y108A	GTCCGAGCGGAATTTATGCAAAGCTTCTCATGAGGTTCTCTCAG	F	
		CTGAGAGAACCTCATGAGAAGCTTTGCATAAATTCCGCTCGGAC	R	
	F144A	CCTCCTCCAAAGTGATGCTTTTATGCCCGAGATATGC	F	
		GCATATCTCGGGCATAAAAGCAGGATCACTTTGGAGGAGG	R	
ZAP-HFR	H176A	CATCTGTGACGCCTTCACCCGAGG	F	
		TGGAGTCTTGAACACGGT	R	
	F184A	ACCCGAGGGAACTGTCGTGCTCCCAACTGCCTC	F	
		GAGGCAGTTGGGAGCACGACAGTTCCCTCGGGT	R	
	R189A	CCATCAGGTTATGGGACGCGAGGCAGTTGGGAAAAC	F	
		GTTTTCCCAACTGCCTCGCGTCCCATAACCTGATGG	R	
ZAP-CY	C96A	GCTGGGCCGGGCCAACTATTCGC	F	
		AAGTTGAGTTTGCAGAGATGC	R	
	Y98A	CCGGGCCAACGCATCGCAGTCCG	F	Includes C96A mutation
		CCCAGCAAGTTGAGTTTG	R	
ZAP-KY	K107A	GAATTTATGCGCATATTCTCATGAGGTTCTCTCAG	F	
		CGCTCGGACTGCGAATAG	R	

	Y108A	TTTATGCGCAGCCTCTCATGAGGTTCTCTCAGAAGAG	F	Includes K107A mutation
		TTCCGCTCGGACTGCGAA	R	
ZAP-EKR	E148A	TTTATGCCCGCGATATGCAAAAG	F	
		AAAAGGATCACTTTGGAG	R	
	K151A	CGCGATATGCGCAAGTTATAAGG	F	Includes E148A mutation
		GGCATAAAAAAAGGATCAC	R	
	R170A	ACCGTGTTCAGCACTCCACATCTG	F	
		GGCTGCTGGTTACAAATC	R	
TRIM25Δ RBD	TRIM25 aa 1-469	gttt*CTCGAGGTATCG*ATATGGCAGAGCTGTGCCCC	F	Includes XhoI and ClaI sites (italicized);
		TTTGTTGTGGGCGGTGTTGTAGTC	R	Deletion upstream sequence (underlined, nt 1384-1407)
	TRIM25 aa 464-469, 509-630	CAACACCGCCCACAACAAA**AAGGGGATCCACTACTGGGA**	F	Includes TRIM25 sequence upstream (underlined, nt 1384-1407) and downstream of the deletion (bolded, nt 1525-1544)
		gttt*TCTAGAGCGGCCGCC*TA	R	Includes XbaI and NotI sites (italicized)

Chapter 4

—

A novel class of positive Gaussian curvature-inducing peptides remodels membranes and inhibits alphavirus replication

BACKGROUND

Over the past two decades, the global community has faced multiple significant outbreaks of emerging and re-emerging viruses that cause severe disease. Emerging novel viruses pose an enormous threat to global public health due their unpredictable pathogenicity and transmissibility in combination with our lack of natural immunity. Though modern technology and medical advances have afforded us reduced morbidity and mortality from infectious diseases, at the same time, increasing globalization, urbanization, and climate change create opportune conditions for viral pathogen emergence and spread (Baker *et al*, 2022). The COVID-19 pandemic has not only shown us the painful reality of this threat but also underscored the vital need for greater preparedness against future outbreaks.

Vaccines and antiviral agents are the most effective countermeasures to prevent and treat viral disease. However, the majority of these currently target a specific virus or virus family, and thus, are insufficient for responding to the increasing number of emerging and re-emerging viruses. Given the inherent unpredictable identity and nature of a new pathogen and the time required to develop a vaccine, there is a pressing need for broad-spectrum prophylactic and therapeutic antivirals that can offer prompt control of outbreaks. Notably, the vast majority of viruses that are responsible for recent outbreaks and/or emerging infectious diseases are enveloped viruses (NIAID Emerging Infectious Diseases/Pathogens). Enveloped viruses, which are characterized by an outer lipid membrane, enter cells via fusion of viral and host-cell membranes (Harrison, 2008), and at the final stage of their replication cycle, progeny virions exit the cell by budding and release via membrane fission (Welsch *et al*, 2007; Rossman and Lamb, 2013).

Enveloped viruses employ three different classes of viral fusion proteins (Rey and Lok, 2018). Much attention has already been given to developing inhibitors against Class I fusion proteins, which are utilized by influenzavirus, human immunodeficiency virus (HIV)-1, and coronaviruses (Düzgüneş *et al*, 2021; Wang and Wang, 2022). Class II viral fusion proteins are utilized by the arthropod-transmitted alphaviruses and flavivurses, which include several important human pathogenic viruses, such as chikungunya virus, dengue virus, and Zika virus (Rey and Lok, 2018). These viruses possess increasing pandemic potential, owing to climate change-induced enlarging distribution of their mosquito vectors (Kraemer *et al*, 2019; Messina *et al*, 2019). The primary strategy in developing broad-spectrum antivirals is to target common conserved viral features and pathways. With this in mind, antivirals that interfere with the membrane fusion and fission processes of the viral life cycle have the potential to be broadly active against enveloped viruses.

Membrane fusion and fission are two opposing membrane-remodeling processes that proceed through analogous deformational steps in opposite order; both form a common hourglass-shaped intermediate structure referred to as the "fusion pore" or "fission neck" that connects two aqueous compartments (Chernomordik and Kozlov, 2003; Kozlov *et al*, 2010). Membrane restructuring and conformational changes that underlie biological membrane remodeling events involve the induction and stabilization of membrane curvature (McMahon and Gallop, 2005; Zimmerberg and Kozlov, 2006; Lipowsky, 2022). Membrane bending and shape are commonly described in terms of curvature. To briefly review, the local shape at a given point on a surface is characterized by its two principal curvatures, c_1 and c_2, which are the maximum and minimum normal curvatures and are orthogonal to one another. Curvature is by definition $c = 1/r$, the reciprocal of the radius, r, of the circle that best

fits the curve at the point. Furthermore, curvature can be positive or negative. By convention, a membrane monolayer that bends to form a convex hydrophilic surface has positive curvature, while a monolayer that bends in the opposite direction to form a concave hydrophilic surface has negative curvature (Figure 23).

Gaussian curvature, $K = c_1c_2$, is the product of the principal curvatures and commonly used to describe the shape of surfaces. For a flat surface, both principal curvatures are zero, and so $K = 0$. For a dome-shaped surface, both principal curvatures are positive, which results in $K > 0$ (Figure 23A). A saddle-shaped surface, which is convex in one direction and concave in the other, has principal curvatures that are opposite in sign, thus resulting in $K < 0$ (Figure 23B). More specifically, saddle-shaped negative Gaussian curvature (NGC) is the distinct type of membrane curvature that is topologically required to produce the deformations involved in membrane-remodeling processes, including fusion and fission intermediates, transmembrane (TM) pores, blebs, tubules, and invaginations (Siegel, 2008; Schmidt *et al*, 2011; Frolov *et al*, 2015; Chabanon and Rangamani, 2018). Notably, a TM pore is most often described as a torus-shaped channel that is formed when the normally planar and separate inner and outer monolayers bend and merge to create a single, highly curved continuous surface (Brogden, 2005) (Figure 23B). In contrast, the formation of membrane fusion and fission intermediates requires NGC of a lipid bilayer, which is distinct from the monolayer NGC of TM pores (Figure 23B).

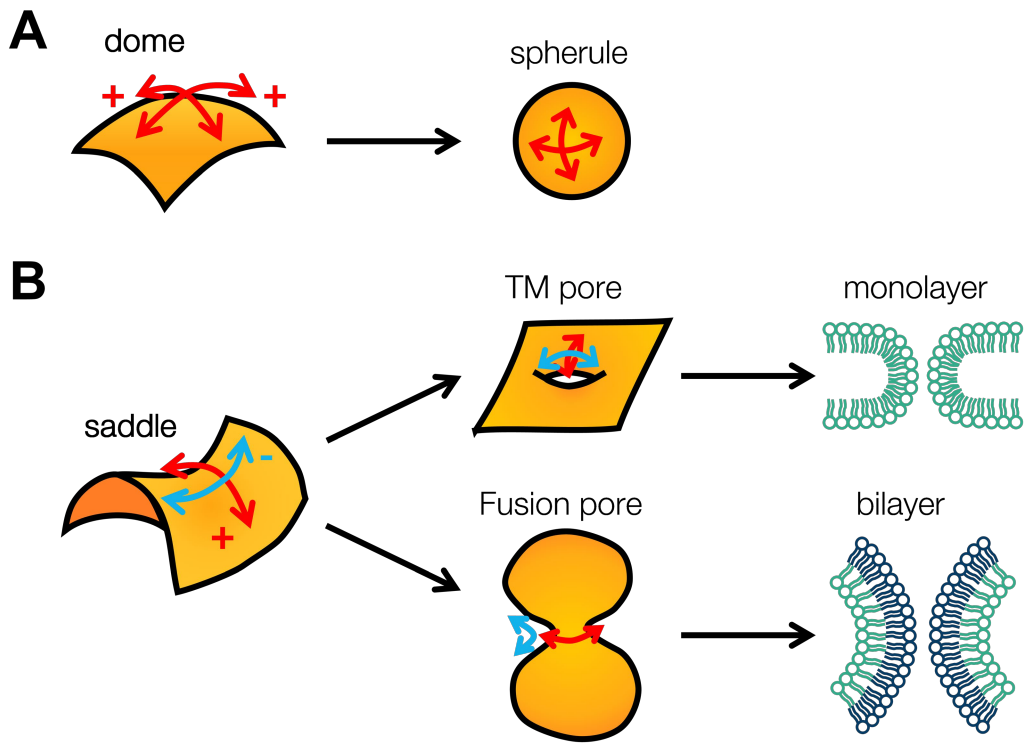

Figure 23. Schematic of positive and negative Gaussian curvatures.

(A) Positive Gaussian curvature (PGC) generates dome-shaped surfaces present in spherule formation. **(B)** Both negative Gaussian curvature (NGC) and PGC are necessary to generate saddle-shaped curves, which appear during formation of transmembrane (TM) and fusion pores. While TM pores employ a membrane monolayer, fusion pores utilize a membrane bilayer to achieve the same effect. Red arrows, PGC; blue arrows, NGC.

A diverse range of proteins and peptides have been shown to induce or promote membrane curvature, including NGC and positive Gaussian curvature (PGC). For example, the generation of NGC by pore-forming antimicrobial peptides (Keller *et al*, 1996; Prenner *et al*, 1997; Hickel *et al*, 2008; Schmidt *et al*, 2011), cell-penetrating peptides (Schmidt *et al*, 2010; Mishra *et al*, 2011), and fusion and fission machinery proteins (Schmidt *et al*, 2013; Yao *et al*, 2015; Lee *et al*, 2017; Thorsen *et al*, 2021) is well-recognized. Accumulating evidence suggests the induction or stabilization of PGC by apolipoprotein A-I (apoA-I) (Forte *et al*, 1971; Jonas *et al*, 1990; Lee *et al*, 2021; Melchior *et al*, 2021) and the endophilin N-BAR domain (Gallop *et al*, 2006).

While all of these curvature-inducing proteins and peptides bind to lipid membranes, the two groups generate contrasting membrane curvatures due to differences in their amino acid compositions and physicochemical properties, such as hydrophobicity and net charge. Interestingly, recent work has demonstrated that PGC antagonizes NGC. An apoA-I mimetic peptide was shown to induce PGC and to suppress NGC generated by histone H4, thereby preventing lytic TM pore formation and mitigating tissue damage and uncontrolled inflammation (Lee *et al*, 2021).

Because the capacity of a protein or peptide to induce membrane curvature relates to its physicochemical characteristics and non-specific membrane interactions, the ability to induce PGC to interfere with NGC generation is not expected to be unique to apoA-I and its mimetics. For this reason, we propose that PGC can be applied as a general mechanism to inhibit membrane-remodeling events that require NGC. We hypothesize that is it is possible to design PGC-inducing peptides that suppress bilayer NGC to inhibit membrane fusion and fission, thereby impairing the replication cycle of enveloped viruses. We speculate that peptides that optimally turn off bilayer NGC and those that turn off monolayer NGC (e.g. TM pores) are related but not necessarily the same. In this work, we use a combination of machine learning, *in vitro* cell studies, synchrotron small-angle X-ray scattering (SAXS), and molecular dynamics (MD) simulations to show that a class of peptides induces PGC and displays robust antiviral activity against enveloped viruses. We employ the alphavirus genus of enveloped RNA viruses as our model system due to its representation of this increasingly important class of arthropod-borne human pathogens and its suite of molecular tools. Here, we report on the antiviral activities of a novel class of peptides against the prototypical alphavirus, Sindbis virus (SINV), and three additional species.

RESULTS

Design of PGC-generating peptides

Based on properties observed in proteins and peptides known to induce membrane curvature, we designed a class of 13 "AP" peptides (19–21 residues in length) with the objective of generating PGC to suppress bilayer NGC (Table 6). We previously established that an apoA-I mimetic peptide is capable of generating PGC (Lee *et al*, 2021). For this reason, we used a machine learning classifier to examine how the physicochemical properties of our peptide designs compare with subsequences of apolipoproteins and TM proteins. The classifier assigned each AP sequence with a numerical σ score based on its similarity to apolipoprotein sequences with respect to their characteristics, not sequence homology (data not shown). From these σ scores, we learned that the AP sequences are more similar to apolipoprotein sequences than to TM protein sequences.

Table 6. Properties of positive Gaussian curvature (PGC)-inducing peptides utilized in this study.

Charge and hydrophobicity scores are provided. The machine-learning σ score > 0 and P(+1) value > 0.5 signify that the peptide is predicted to induce PGC.

Name	Sequence	Charge	Hydrophobicity	σ score	P(+1)
AP1	GDAVREWFEKAWQRVREFF	-0.2	0.33	0.8132	0.9862
AP2	FFERVRQWAKEFWERVADG	-0.2	0.33	0.8046	0.9855
AP3	GDAVREVIEKAVQRVREIV	-0.2	0.188	0.5027	0.9191
AP4	GDAVKEWFEKAWQKVKEFF	-0.2	0.337	0.8210	0.9868
AP5	GERAKEWVEAFWEKAREYF	-1.2	0.222	0.5647	0.9426
AP6	GERVKEFFEAFFEKAREYW	-1.2	0.278	0.7189	0.9762
AP7	GEKAKEWVQAFWQKAKEYF	0.8	0.271	0.6304	0.9604
AP8	GEKVKEFFQAFFQKAKEYW	0.8	0.327	0.7088	0.9747
AP9	GDAVKEWFEKAWQKVKEFL	-0.2	0.332	0.6992	0.9733
AP10	GEQLKQKFQEFWDKLKEWY	-0.2	0.285	1.1749	1.0000
AP11	GEKLKQKAQEFFDAVKEWF	-0.2	0.226	0.9936	0.9952
AP12	GKEKAEEFFQALKEWFDKFKN	-0.2	0.234	0.8148	0.9864
AP13	GEQFKQAFQEWWDKLKEKY	-0.2	0.208	1.0073	0.9956

APs inhibit SINV replication

We examined the peptides for inhibitory activity against alphavirus replication in HEK293T cells using a SINV luciferase reporter virus (Toto1101/Luc) in which the expression of luciferase correlates with viral replication (Bick *et al*, 2003). A dose response analysis of the peptides that displayed effective inhibition of SINV replication was performed to calculate the half maximal effective concentration (EC50), which is the concentration required to achieve 50% inhibition (Figure 24).

However, EC50 values could not be determined for peptides AP3, AP5, AP6, AP12, and AP13 because no significant inhibition was observed at concentrations up to 125 μM (Supplemental Figure 4.1). For the remaining APs, we observed EC50 values ranging from the very potent AP4 at 0.98 μM (Figure 24C; 95% CI, 0.47–1.84) to the less inhibitory AP10 with an EC50 of 26.23 μM (Figure 24G; 95% CI, 22.47–30.52). AP1, 8, and 9 also strongly inhibit SINV replication with EC50s of 3.59, 5.86, and 5.90 μM, respectively (Figure 24A, E-F), while AP2 and 7 exhibit a more moderate phenotype with EC50s of 9.07 and 10.48 μM, respectively (Figure 24B, D). We also measured cytotoxicity of each peptide concentration using an MTT proliferation assay. Here, we found that most of the APs were minimally cytotoxic with <20% cytotoxicity across the concentration range tested (Figure 24A-C, G-H), with the exception being AP7, 8, and 9, which can cause up to 50% cytotoxicity at higher concentrations (Figure 24D-F).

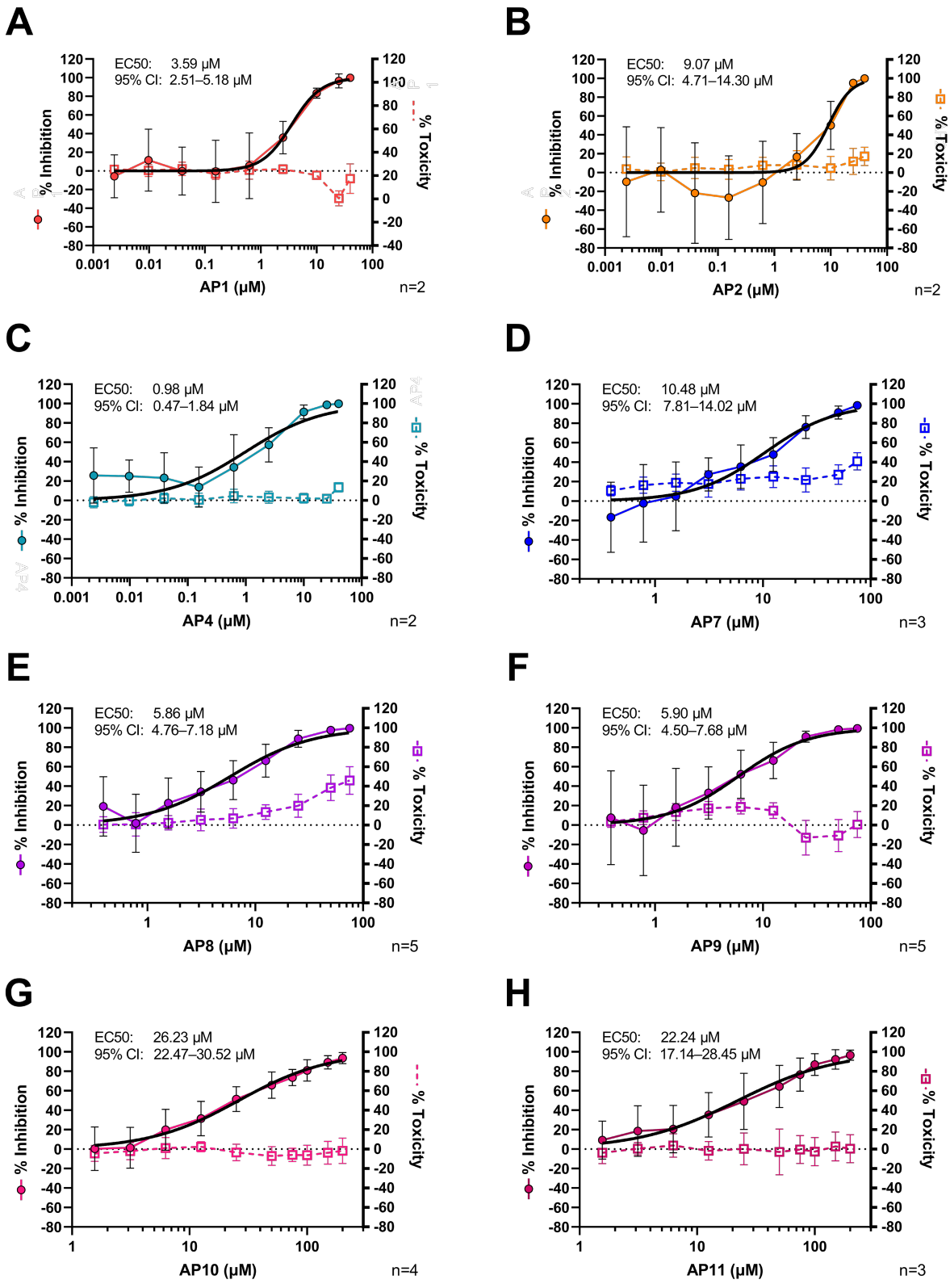
A
EC50: 3.59 μM
95% CI: 2.51–5.18 μM
% Inhibition
% Toxicity
AP1 (μM)
n=2
B
EC50: 9.07 μM
95% CI: 4.71–14.30 μM
% Inhibition
% Toxicity
AP2 (μM)
n=2
C
EC50: 0.98 μM
95% CI: 0.47–1.84 μM
% Inhibition
% Toxicity
AP4 (μM)
n=2
D
EC50: 10.48 μM
95% CI: 7.81–14.02 μM
% Inhibition
% Toxicity
AP7 (μM)
n=3
E
EC50: 5.86 μM
95% CI: 4.76–7.18 μM
% Inhibition
% Toxicity
AP8 (μM)
n=5
F
EC50: 5.90 μM
95% CI: 4.50–7.68 μM
% Inhibition
% Toxicity
AP9 (μM)
n=5
G
EC50: 26.23 μM
95% CI: 22.47–30.52 μM
% Inhibition
% Toxicity
AP10 (μM)
n=4
H
EC50: 22.24 μM
95% CI: 17.14–28.45 μM
% Inhibition
% Toxicity
AP11 (μM)
n=3

Figure 24. SINV replication is variably inhibited by APs.

HEK293T cells were infected by Toto1101/Luc for at a multiplicity of infection (MOI) of 0.01 plaque forming units (PFU)/cell in the presence of varying concentrations of **(A)** AP1, **(B)** AP2, **(C)** AP4, **(D)** AP7, **(E)** AP8, **(F)** AP9, **(G)** AP10, or **(H)** AP11. Lysates were harvested at 24 hours post infection (h.p.i.) and measured for luciferase activity. Cytotoxicity at 24 hours for varying peptide concentrations was measured using a MTT proliferation assay. The [Agonist] vs. normalized response – Variable slope equation on GraphPad Prism was used to calculate EC50 and a nonlinear fitted curve (black line). Data are combined from independent experiments as indicated in each panel.

APs reduce production of infectious SINV virions

Next, we examined the impact of the two peptides with the greatest SINV replication inhibition, AP1 and AP4, on the production of infectious SINV virions. We infected 293T cells with wild-type SINV (Toto1101 strain) in the presence of 25 μM AP1 or AP4, after which we replaced with fresh media without AP1 or AP4 added. After 24 hours of infection, we harvested the supernatant and titered SINV on BHK-21 cells. Treatments of 25 μM of either AP1 and AP4 reduced viral titers by about 1-log, with AP1 displaying marginally better inhibition of SINV virion production as compared to AP4, demonstrating their inhibitory effect on SINV infectivity (Figure 25).

APs suppress membrane remodeling

Because the ability to achieve membrane fusion and fission can affect viral replication and virion production, we investigated whether the inhibition of SINV replication by APs could stem from

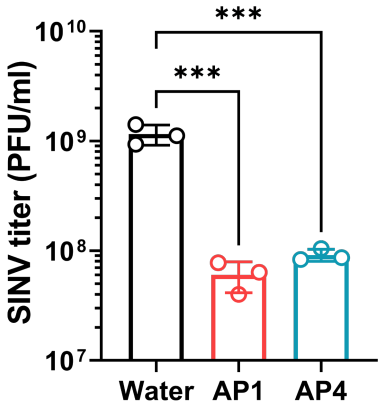

Figure 25. AP1 and AP4 inhibit SINV virion production.

HEK293T cells were infected by SINV Toto1101 for at an MOI of 1 PFU/cell in the presence of 25 μM AP1 or AP4. Fresh media, without AP added, was used to wash cells after infection. Supernatant was harvested at 24 h.p.i. and subsequently used to infect BHK-21 cells to titer production of infectious SINV virions. Asterisks indicate statistically significant differences, calculated using one-way ANOVA and Dunnett's multiple comparison test: ***, $p<0.001$. Data are representative of two independent experiments.

an ability to suppress NGC and, accordingly, membrane remodeling. For seven peptides that displayed efficient SINV replication inhibition (Figure 24; AP1, AP2, AP4, AP7, AP8, AP9, and AP10), we used synchrotron SAXS to evaluate their effects on NGC generation by a well-established membrane pore-forming peptide, HIV TAT (Mishra *et al*, 2008, 2011).

First, we performed control experiments to confirm the individual effects of each AP and HIV TAT on membranes. Small unilamellar vesicles (SUVs) were incubated with an AP or HIV TAT at a peptide/lipid (P/L) molar ratio of 1/50 or 1/20, respectively, and the resulting membrane structures and phase behavior were characterized using SAXS. More specifically, we assayed for the existence of cubic phases, which are rich in NGC, the type of curvature required for membrane remodeling. We found that APs alone do not restructure membranes; their scattering curves show a broad feature consistent with the form factor expected of unilamellar vesicles and closely resemble the scattering profile of control SUVs (Supplemental Figure 4.2). By contrast, the SAXS profile of SUVs exposed to HIV TAT exhibit two sets of correlation peaks, which index to a coexistence of a lamellar phase (L_α) (peak position ratio of 1:2) with a periodicity of 5.80 nm and a *Pn3m* cubic phase (peak position ratio of $\sqrt{2}$: $\sqrt{3}$) with a lattice parameter of 15.70 nm (Supplemental Figure 4.2). An inverse bicontinuous inverted cubic phase (Q_{II}), such as the *Pn3m* "double diamond" and *Im3m* "plumber's nightmare" space groups, consists of two non-intersecting aqueous volumes that are separated by a lipid bilayer with NGC at every point on its surface. Therefore, in context, the generation of NGC corresponds to the stabilization of cubic phases.

After establishing that HIV TAT induces NGC and that the APs do not, we incubated SUVs with HIV TAT in the presence of an AP and measured the induced membrane curvature deformations.

In these samples, the quantity of HIV TAT was held constant at P/L = 1/20, while for each AP, the P/L was as varied as 1/100, 1/50, and 1/25. We found that coadministration of AP with HIV TAT leads to dose-dependent suppression of cubic phase generation, with complete inhibition by P/L = 1/25 for all tested APs (Figure 26). As NGC is an intrinsic characteristic of cubic phases, these results reveal that the tested APs display comparable NGC inhibitory activity. In fact, at both P/L = 1/100 and 1/50, the magnitude of NGC for each identified cubic phase is similar across all seven APs (Supplementary Table 4.1). More importantly, these findings indicate that the APs have the capacity to modulate effects associated with NGC generation.

It should be noted that HIV TAT penetrates cells by creating TM pores, which as discussed earlier, possess monolayer NGC. Thus, from these SAXS experiments, one might reasonably conclude that the inhibitory effect of the APs against NGC induction would be limited to instances of monolayer NGC. However, given that the APs impede the formation of cubic phases (Figure 26), which are characterized by bilayer NGC, it can be inferred that the APs have the capacity to suppress both monolayer NGC and bilayer NGC.

Previous studies have shown viral fusion peptide activity to be associated with cubic phase stabilization (Tenchov *et al*, 2013). Conversely, here we observed a correlation between the ability of the seven APs to inhibit SINV replication and their ability to destabilize or suppress cubic phases (Figures 24 and 26). Taken together, these results strongly suggest that the AP inhibition of viral replication is likely attributed to, at least in part, a non-specific membrane curvature-mediated mechanism that obstructs membrane remodeling. Moreover, the ability of AP1 and AP4 to reduce virion production would be consistent with impaired membrane fusion and fission.

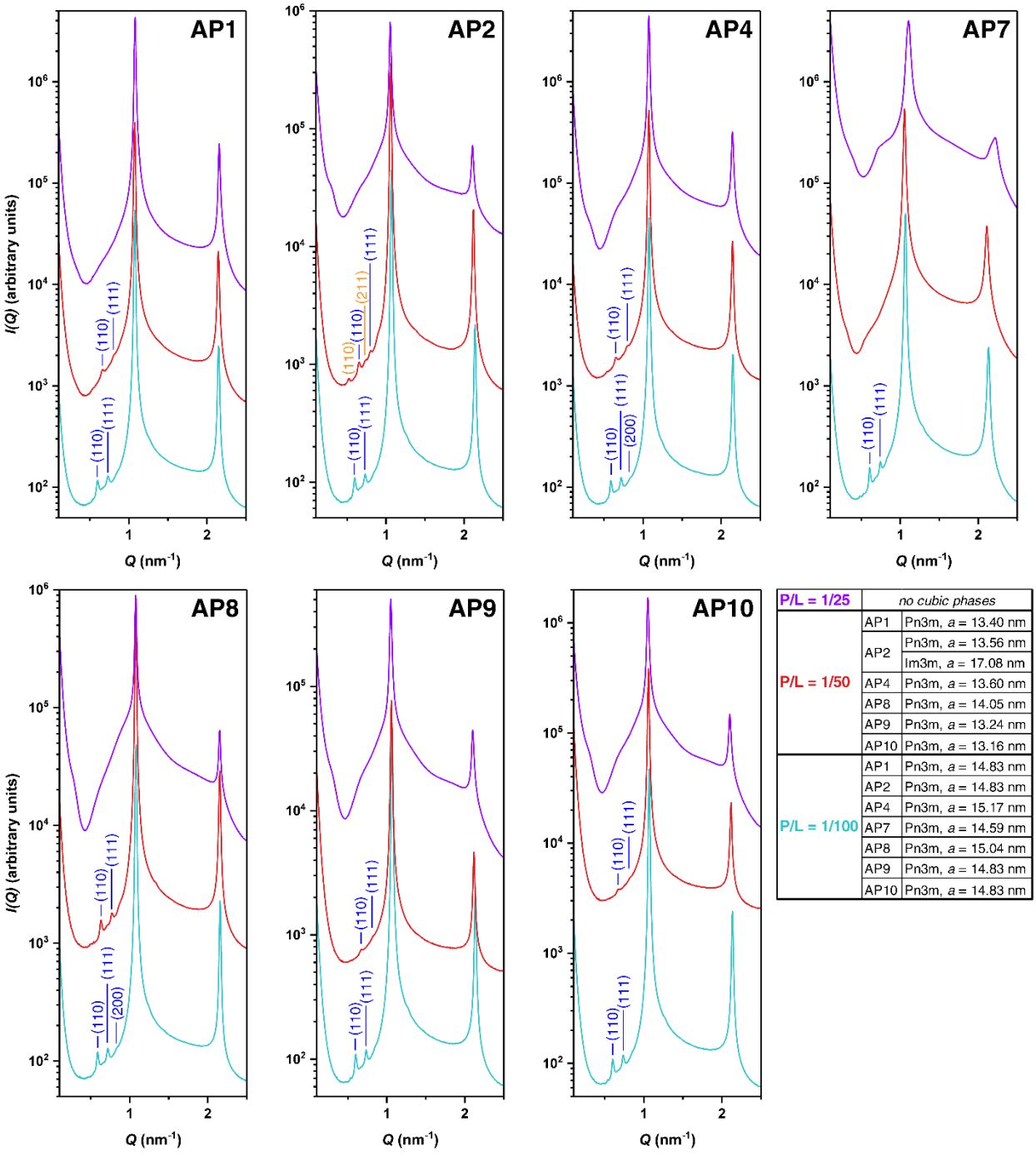

Figure 26. APs suppress HIV TAT-induced NGC.

For AP1, AP2, AP4, AP7, AP8, AP9, and AP10, SAXS scattering curves of SUVs (DOPS/DOPE 20/80) incubated with HIV TAT in the presence of AP. The P/L molar ratio of HIV TAT was held constant at 1/20, while the P/L molar ratio of AP was varied (1/100 (cyan), 1/50 (red), and 1/25 (violet)). The peaks corresponding to the cubic phases induced by HIV TAT were suppressed at high concentrations of AP to leave behind zero-curvature lamellar phases. Assigned reflections for *Pn3m* (blue) and *Im3m* (orange) cubic phases are labeled above the corresponding peaks. To facilitate visualization, spectra have been offset along the y-axis by scaling each curve by a multiplicative factor. The lattice parameters of the indexed cubic phases are provided in the inset (lower right).

APs generate positive Gaussian curvature

With the understanding that APs can inhibit NGC generation in membranes, we further studied their membrane interactions in greater detail to gain insight into the mechanism underlying their activity. We hypothesized that their ability to suppress NGC results from the generation of the opposite curvature, PGC, which has been shown to antagonize NGC (Lee *et al*, 2021). To evaluate this hypothesis and the capacity of APs to induce membrane curvature, we examined AP1.

We performed MD simulations to investigate the membrane bending capability of AP1. Eight AP1 peptides were placed on top of a flat mixed lipid bilayer. Upon equilibration, the peptides spontaneously adsorbed on the bilayer surface, and the central part of the membrane gradually adopted a dome-like shape (Figure 27A) to counter the pressure imbalance caused by the shallow insertion of the peptides. To quantify the membrane curvature generated by the peptides, we divided the membrane patch into 1 nm × 1 nm grids, and then the center of mass positions of the phosphorus (P) atoms of both leaflets in each grid were time averaged for 50 ns. We calculated the variation of the bilayer center as a function of the X and Y coordinates (Figure 27B); evidently, the AP1 peptides generate significant PGC at the central region of the membrane, in line with experimental results.

We performed additional simulations to investigate whether AP1 is capable of destabilizing a membrane pore. We chose histone H4 as an example membrane pore former. Histone H4 is a protein component of neutrophil extracellular traps that can porate membranes to induce lytic cell death, consequently triggering tissue injury and inflammation (Silvestre-Roig *et al*, 2019). The membrane pore-forming activity of histone H4 has been primarily attributed to its N-terminal tail. First, we prepared a membrane pore stabilized by six copies of the H4 N-terminal tail (Supplemental Figure

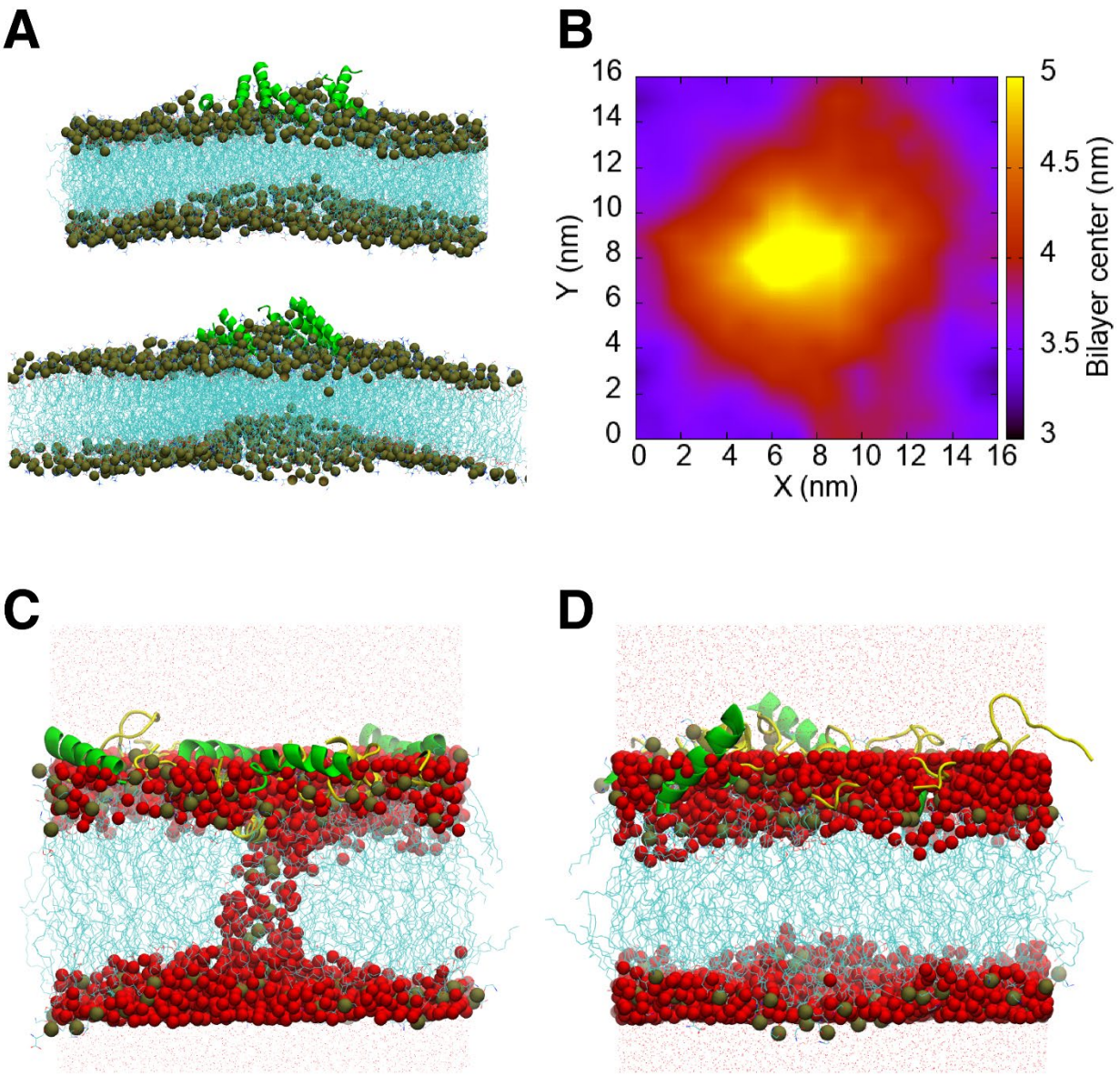

Figure 27. AP1 generates PGC and destabilizes histone H4-induced membrane pore.

(A) Side (top) and 45-degree (bottom) rotated views of a snapshot of the membrane-peptide complex sampled in our MD simulations illustrate the positive membrane curvature generated by the AP1 peptides, where the central part of the lipid membrane is bent upward. DOPC and DOPS lipids are represented by cyan lines and olive spheres represent the phosphate atoms of the lipids. The AP1 peptides are shown in the green cartoon form. **(B)** 2D color plot of the membrane center as a function of the lateral dimensions (*X* and *Y*), which illustrates the positive membrane curvature generated at the location of absorbed peptides and in the surrounding area. **(C)** Five copies of the AP1 peptides (green cartoon) placed near the mouth of a membrane pore generated by the H4 N-terminal tails (yellow cartoon). Water inside the membrane pore and at the membrane surface are highlighted by red spheres. Cyan lines represent the DOPE and DOPS lipid tails and the phosphate atoms of the lipid headgroups are represented by olive spheres. **(D)** The membrane pore is destabilized as indicated by the disappearance of the water channel after less than 100 ns during the simulation.

4.3A). These H4 peptides were observed to strongly adsorb on the membrane surface, creating negatively curved valleys in the bilayer (Supplemental Figure 4.3B). To assess the stability of the membrane pore, we calculated the number of water molecules in a cylindrical region of 1 nm width near the center of the membrane pore, finding that the membrane pore remained stable for the duration of the simulation (Supplemental Figure 4.3C, 415 ns). One of the H4 peptides inserted deep into the membrane and aligned with the water channel; several lipids near the water channel changed their orientation such that the polar heads remained in contact with the water channel (Supplemental Figure 4.3D) and the hydrophobic tails were oriented perpendicular to the membrane normal, as is often observed in a disordered toroidal membrane pore.

To investigate if AP1 can destabilize the membrane pore by opposing the NGC generated by the H4 peptides, we placed five copies of the AP1 peptide near the mouth of a membrane pore. We observed that the number of water molecules present in the pore decreases to zero at around 85 ns, indicating destabilization of the H4 generated membrane pore in the presence of AP1 (Supplemental Figure 4.3C). AP1 peptides induce PGC upon adsorption and pulled up the lipid heads near the pore mouth, countering the NGC induced by the H4 peptides. As a result, the phosphate groups that were in contact with the water channel of the stable membrane pore gradually move back to the membrane surface (Supplemental Figure 4.3E). This lipid rearrangement reduced the width of the membrane pore and the water channel completely disappears when no phosphate group was left near the bilayer counter. Once the membrane pore was destabilized, it did not reopen (Figure 27D).

APs are inhibitory against multiple alphaviruses

Because these peptide designs operate via a membrane-based mechanism on general biophysical processes common to enveloped viruses, their inhibitory effects should not be exclusive to one virus species. To evaluate the broader application of this peptide class, we examined the efficacy of lead peptides AP1 and AP4 to inhibit replication of three additional alphavirus species, namely Venezuelan equine encephalitis virus (VEEV), o'nyong'nyong virus (ONNV), and Ross River virus (RRV). We infected HEK293T cells with SINV, VEEV, ONNV, and RRV GFP-reporter viruses with varying MOIs to maximize percentage of infected cells, fixed cells 18 hours post infection. We then

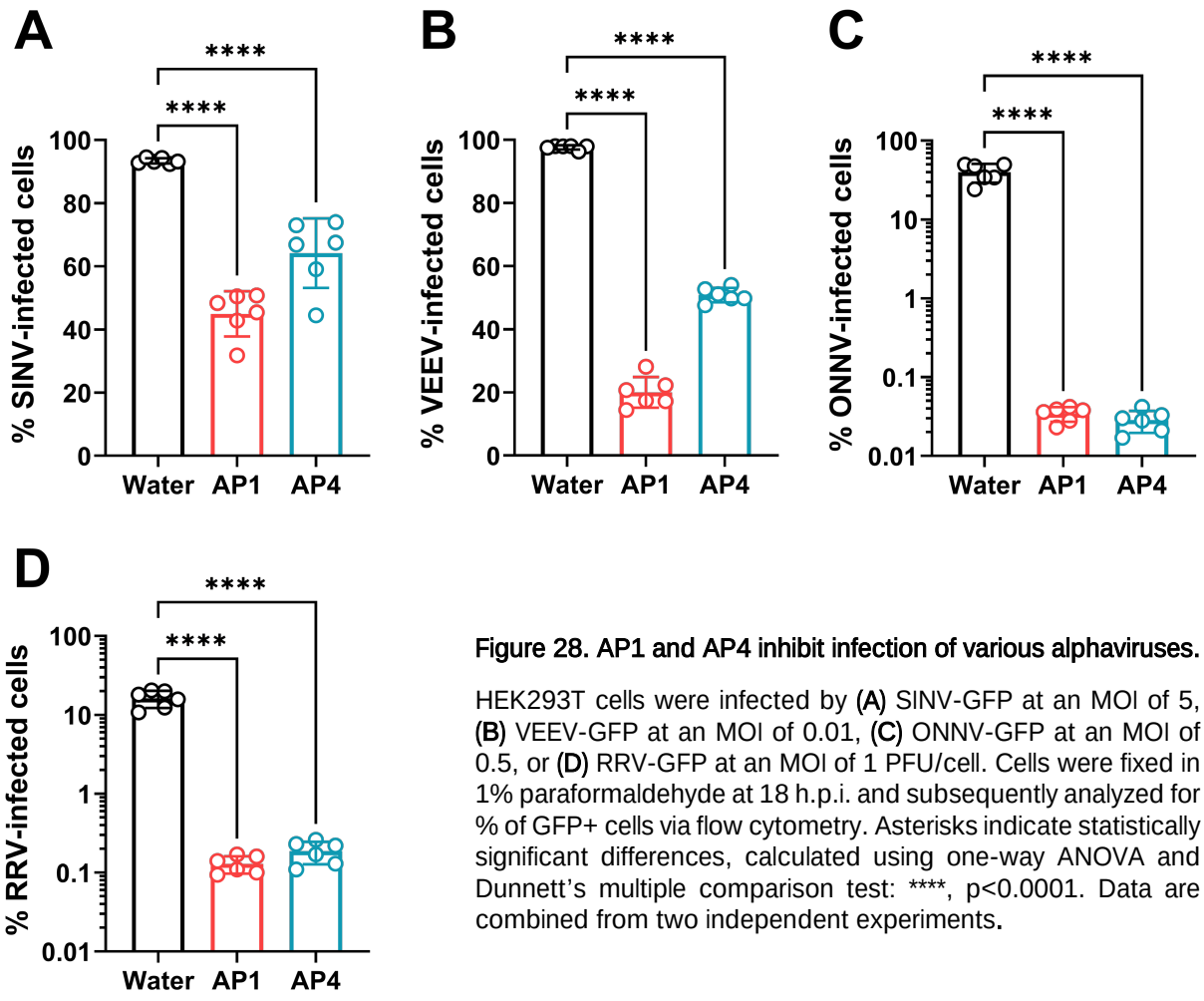

Figure 28. AP1 and AP4 inhibit infection of various alphaviruses.

HEK293T cells were infected by **(A)** SINV-GFP at an MOI of 5, **(B)** VEEV-GFP at an MOI of 0.01, **(C)** ONNV-GFP at an MOI of 0.5, or **(D)** RRV-GFP at an MOI of 1 PFU/cell. Cells were fixed in 1% paraformaldehyde at 18 h.p.i. and subsequently analyzed for % of GFP+ cells via flow cytometry. Asterisks indicate statistically significant differences, calculated using one-way ANOVA and Dunnett's multiple comparison test: ****, $p<0.0001$. Data are combined from two independent experiments.

analyzed %GFP+ cells via flow cytometry as a measure of the % infected cells. Similar to the effects seen for inhibition of SINV virion production (Figure 25), while both AP1 and AP4 significantly inhibit percentage of infected cells for all four viruses (Figure 28), AP1 inhibits alphavirus infection demonstrably better than AP4 for SINV and VEEV infections (Figure 28A, 28C). These data capture the effectiveness of this mechanism of action against multiple species in the alphavirus genus.

DISCUSSION

In this study, we present a class of peptides that apply a non-specific membrane curvature-mediated mechanism to suppress membrane-remodeling processes such as those vital to the viral life cycle. More specifically, this mechanism directly interferes with the lipid dynamics that drive membrane fusion and fission, and consequently, can impair the ability to achieve viral entry and virion release. While different proteins facilitate the conformational changes involved in membrane fusion and fission, there exist essential underlying biophysical features of these processes that are shared by enveloped viruses (Martens and McMahon, 2008; Markvoort and Marrink, 2011; Rossman and Lamb, 2013). Most current inhibitor designs focus on blocking specific ligand-receptor interactions, limiting their application as broad antiviral therapeutics (Düzgüneş *et al*, 2021). Therefore, by targeting these key commonalities, our membrane curvature-mediated mechanism has the potential to be an effective broad-spectrum antiviral strategy against enveloped viruses. Moreover, the ability to inhibit both viral entry and egress holds promise for preventing infection and transmission, and reducing disease progression. In addition, a membrane-based mechanism of action is further likely to offer a high barrier to the development of viral resistance (Vigant *et al*, 2015).

Here, we characterized the antiviral properties of a novel class of antifusion peptides against alphaviruses. Collectively, the peptides demonstrated a range of cytotoxicity and inhibition against SINV replication (Figure 24 and Supplemental Figure 4.1). We further characterized the two most potent APs, AP1 and AP4, and found that they were both able to potently inhibit production of infectious SINV virions (Figure 25) and inhibit replication of three other alphaviruses (Figure 28). SAXS experiments on seven APs with high levels of inhibition against SINV replication demonstrate that they all suppress NGC generation (Figure 26). MD simulations further demonstrate that the AP membrane-stabilizing activity is driven by their ability to generate PGC (Figure 27), which is the type of curvature antagonistic to NGC, thereby inhibiting membrane remodeling. Further work is required to examine how different physical properties of these peptides affect their ability to induce PGC and thereby inhibit viral fusion.

It is important to note that there are currently no vaccines or treatments available for alphaviruses (Azar *et al*, 2020; Stromberg *et al*, 2020; Read *et al*, 2021), and thus, the identification of new strategies toward the development of antiviral prophylactics and therapeutics has significant implications for the prevention and control of human disease caused by alphaviruses. As the membrane curvature-mediated mechanism presented here acts on essential, conserved biophysical processes and features shared by enveloped viruses, it is non-specific by nature. Further work is required to investigate whether the antifusion peptides tested here are also inhibitory against class I and class III viral fusion proteins.

ACKNOWLEDGMENTS

We thank the Stanford Synchrotron Radiation Lightsource (Menlo Park, CA) for access to beamline 4-2. Use of the SSRL, SLAC National Accelerator Laboratory, is supported by the U.S. Department of Energy, Office of Science, Office of Basic Energy Sciences under contract no. DE-AC02-76SF00515. The SSRL Structural Molecular Biology Program is supported by the U.S. Department of Energy, Office of Biological and Environmental Research, and by the National Institutes of Health, National Institute of General Medical Sciences (P30GM133894).

MATERIALS AND METHODS

Peptides

Lyophilized AP peptides synthesized using solid-phase synthesis were purchased at high purity (>95% HPLC) from LifeTein (Somerset, NJ). Lyophilized HIV TAT peptide was purchased from Anaspec (Fremont, CA). Peptides were dissolved in ultrapure water before use.

Viruses

Wild-type SINV (Toto1101), SINV expressing firefly luciferase (Toto1101/Luc), SINV expressing EGFP (TE/5'2J/GFP), ONNV expressing EGFP (gifted by Dr. Steve Higgs, Kansas State University), RRV expressing EGFP (gifted by Dr. Mark Heise, University of North Carolina), and VEEV vaccine strain TC-83 (gifted by Dr. Ilya Frolov, University of Alabama at Birmingham) have been previously described (Frolova *et al*, 2002; Bick *et al*, 2003; Gorchakov *et al*, 2012; Brault *et al*, 2004; Morrison *et al*, 2006). BHK-21 cells were used to generate viral stocks and titers for multiplicity of infection (MOI) calculations as previously described (Bick *et al*, 2003). HEK 293T cells (gifted by Dr. Oliver Fregoso, University of California at Los Angeles) were cultured in Dulbecco's modified eagle medium (DMEM; Gibco, Waltham, MA) supplemented with 10% FBS, while BHK-21 cells were cultured in MEM (Gibco) supplemented with 7.5% FBS.

SINV replication inhibition assays

Viral infections were performed essentially as previously described (Bick *et al*, 2003). Infections were carried out in either 24-well or 96-well culture plates, with 150 µL or 50 µL inoculum per well, respectively. Plates were coated with poly-L-lysine prior to seeding with HEK 293T cells. Briefly, virus was diluted in Dulbecco's phosphate-buffered saline (DPBS; Gibco) supplemented with 1% FBS and

antifusion peptide (AP) prior to infection. One day after seeding, media was aspirated and replaced with either 150 mL of viral inoculum for 24 well plates or 50 mL for 96 well plates. After 1 hour of adsorption at 37C, fresh media supplemented with the corresponding concentration of AP was added to each well for a final volume of 500 µL for 24 well plates and 150 µl for 96 well plates. Lysates were harvested in 1X passive lysis buffer at 24 hours post infection (h.p.i.) and luciferase activity was determined with the luciferase assay system (Promega, Madison, WI) according to the manufacturer's recommendations. Luciferase activity was measured on a Biotek Synergy H1 plate reader (Agilent, Santa Clara, CA). EC50, and 95% CI, and agonist response curves for each peptide were calculated on GraphPad Prism 9.4 using the nonlinear regression analysis with the [Agonist] vs. normalized response – Variable slope equation.

Cytotoxicity assays

HEK293T cells were seeded in a poly-L-lysine coated 96 well plate. One day post-seeding, media was aspirated, and 100 µL fresh media supplemented with AP was added to each well. A MTT Cell Proliferation Assay (ATCC, Manassas, VA) was used to assess cytotoxicity per manufacturer instructions 24 hours after AP was added.

SINV plaque assays

Plaque assays were performed essentially as previously described (Bick *et al*, 2003). Briefly, HEK293T cells were seeded in poly-L-lysine coated 24-well plates. One day later, cells were infected as previously described with inoculum supplemented with AP treatment at 25 µM. After 1 hour of adsorption at 37˚C, cells were washed once with fresh media before replacing with 500 mL of fresh media to wells, without AP present. Supernatant was harvested at 24 h.p.i. and subsequently used for

plaque assays on BHK-21 cells. BHK-21 cells were seeded in 6-well plates. One day post-seeding, viral supernatant was serially diluted in PBS supplemented with 1% FBS. After aspirating the media. 200 µl of serially diluted inoculum was added to each well, and cells were incubated at 37˚C for 1 hour with occasional rocking. Following adsorption, an MEM overlay supplemented with 4.2% Avicel and penicillin/streptomycin was added to the wells. A 7% paraformaldehyde solution was added to each well 24 h.p.i., and wells were subsequently stained with crystal violet before washing and counting plaques for viral titer calculations.

Preparation of single unilamellar vesicles (SUVs)

Lyophilized phospholipids 1,2-dioleoyl-*sn*-glycero-3-phospho-L-serine (DOPS) and 1,2-dioleoyl-*sn*-glycero-3-phosphoethanolamine (DOPE) purchased from Avanti Polar Lipids (Alabaster, AL) were dissolved in chloroform at 20 mg/mL to yield individual stock solutions. A lipid composition was prepared from lipid stock solutions as a mixture of DOPS/DOPE at a molar ratio of 20/80. The lipid mixture was evaporated under nitrogen and desiccated overnight under vacuum to form lipid films. The lipid film was resuspended in physiological aqueous buffer (140 mM NaCl, 10 mM HEPES, pH 7.4) and incubated overnight at 37 °C. The lipid suspension was sonicated until clear and extruded through a 0.2-µm pore Anotop syringe filter (Whatman) to form SUVs.

SAXS experiments

SUVs were mixed with peptides at specified P/L molar ratios and hermetically sealed into 1.5 mm quartz capillaries (Hilgenberg GmbH, Mark-tubes). SAXS measurements of the peptide–lipid samples were taken at the Stanford Synchrotron Radiation Lightsource (beamline 4-2) using monochromatic X-rays with an energy of 9 keV. Samples were incubated at 37°C and centrifuged

before measurement. Scattered radiation was collected using a DECTRIS PILATUS3 X 1M detector with a 172-μm pixel size. The 2D powder diffraction patterns were azimuthally integrated into 1D patterns using the Nika 1.76 package (Ilavsky, 2012) for Igor Pro 7.04 (Wavemetrics).

The integrated scattering intensity $I(q)$ vs. q was plotted using OriginPro (OriginLab). To identify the phases present in each sample, ratios of the q-values of observed peaks were compared to the permitted reflections for different liquid-crystalline lipid phases (e.g. lamellar, cubic). Lamellar phases index to integer ratios of 1:2:3:4. For cubic phases, the *Pn3m* space group permits reflections at ratios of √2:√3:√4:√6:√8 and the *Im3m* space group permits reflections at ratios of √2:√4:√6:√8:√10. For each cubic phase, the measured q positions for the Bragg peak reflections were fitted to the equation $q_{measured} = 2\pi\sqrt{(h^2+k^2+l^2)}/a$, where hkl are the Miller indices and a is the lattice parameter. For each of the measured cubic phases, the quantity of induced NGC was calculated as the average NGC per unit cell volume using the equation $\langle K\rangle = 2\pi\chi/A_0a^2$, where χ is the Euler characteristic and A_0 is the surface area per cubic unit cell. Parameter values are $\chi = -2$ and $A_0 = 1.919$ for *Pn3m* cubic phases. Parameter values are $\chi = -4$ and $A_0 = 2.345$ for *Im3m* cubic phases. For each lamellar phase, the measured q positions for the reflections were fitted to $q_{measured} = 2\pi n/d$, where n is the order of the reflection and d is the periodic spacing.

Molecular dynamics (MD) simulations

A model AP1 peptide was built in the helical form using the UCSF Chimera software (Yang *et al*, 2012). Eight copies of the built peptide were placed on top of a mixed lipid bilayer consisting of 640 1,2-dioleoyl-*sn*-glycero-3-phosphocholine (DOPC) and 160 DOPS lipids. The bilayer was built using the CHARMM-GUI software (Jo *et al*, 2008). The built lipid-peptide complex structure was

then solvated using a TIP3P water (Jorgensen *et al*, 1983) box of size ~16.6 × 16.6 × 8.4 nm^3. Appropriate number of Na^+ ions were added to maintain charge neutrality. The CHARMM36 forcefield (Klauda *et al*, 2010; Best *et al*, 2012; Huang and MacKerell Jr, 2013) was used to describe the peptides, lipids, and ions. The solvated peptide-lipid complex structure was first energy minimized using the steepest descent and conjugate gradient methods to remove any bad contacts. This step was followed by a 75 ns long equilibration at constant pressure (1 bar) and at constant temperature (303 K). The pressure and temperature of the system were controlled using a Parrinello–Rahman (Parrinello and Rahman, 1981) barostat with a time constant of 5 ps and a Nosé–Hoover (Nosé, 1984; Hoover, 1985) thermostat with a time constant of 1 ps, respectively. The LINCS algorithm (Hess *et al*, 1997) was used to constrain the hydrogen atoms that allowed a time step of 2 fs for the integrations.

We considered a membrane pore formed by the N-terminal tail (aa1–24) of histone H4 to investigate the capability of membrane pore destabilization by the AP1 peptides. Coordinates of the H4 N-terminal tail were taken from the protein data bank (PDB: 1KX5). Six copies of the H4 tail were placed on top of a DOPE/DOPS (160:40) mixed lipid bilayer. Simulations of membrane pore formation were performed in the following steps. In the first step, lipids tails were modelled using the Highly Mobile Membrane Mimetic (HMMM) model (Ohkubo *et al*, 2012) to achieve rapid equilibration of local lipid distributions around the peptides. The HMMM equilibrated membrane-peptide complex structure was then converted to the full lipid model using the CHARMM-GUI tool. We then simulated the full lipid membrane-peptide complex using constant pressure – constant area (NPAT) ensemble in which the area per lipid was taken to be 50% higher than its equilibrium value, which facilitates water channel formation across the membrane by the H4 peptides. A configuration

from the NPAT simulation trajectory was then simulated in a restraint-free constant pressure (1 bar), constant temperature (303 K) ensemble for 415 ns during which the simulation box lengths readjusted spontaneously to achieve the correct lipid density and a stable water channel was formed across the membrane. Once formed, the water channel remained stable throughout the entire 415 ns long simulation (Supplemental Figure 4.3C); stability of the membrane pore was assessed by monitoring the number of water molecules near the center of the membrane pore.

To investigate the interactions of the AP1 peptides with the membrane pore, we removed the bulk water from a stable membrane pore, but the water inside the membrane pore and the water at the membrane surface were kept intact. Five copies of the AP1 peptide were then placed on the membrane surface (Figure 27C). The membrane/H4 peptide/AP1 peptide complex system was then solvated and an appropriate number of ions were added to maintain charge neutrality. The solvated system was then energy minimized using the steepest descent and conjugate gradient method to remove any bad contacts. The energy minimized structure was then equilibrated at constant pressure (1 bar) and constant temperature (303 K). The pressure and temperature of the system were controlled using a Parrinello–Rahman barostat with a time constant of 5 ps and a Nosè–Hoover thermostat with a time constant of 1 ps, respectively. A time step of 1.5 fs was used for the integration of equations of motion. Upon equilibration, the AP1 peptides gradually adsorbed on the membrane surface and destabilized the membrane pore. All simulations were performed using GROMACS package (Abraham *et al*, 2015).

Flow cytometry analysis

Flow cytometry was performed essentially as previously described (Bick *et al*, 2003). Briefly, HEK293T cells were seeded in poly-L-lysine coated 24-well plates. One day later, cells were infected with EGFP expressing viruses at an MOI of 0.01-5 PFU/cell (ONNV-GFP, MOI 0.5; RRV-GFP, MOI 1; SINV-GFP, MOI 5; VEEV-GFP, MOI 0.01) in the presence of 25 μM of AP1 or AP4. After 1 hour of adsorption at 37°C, media supplemented with 25 μM of AP1 or AP4 was added back to the appropriate wells. Cells were harvested at 18 h.p.i. and fixed in 1% paraformaldehyde for flow cytometry analysis. A MACSQuant Analyzer 10 (Miltenyi Biotec, Auburn, CA) was used to acquire data, which was subsequently analyzed using FlowJo (BD Biosciences, Franklin Lakes, NJ) to calculate percent infected (GFP+) cells.

SUPPLEMENTARY MATERIAL

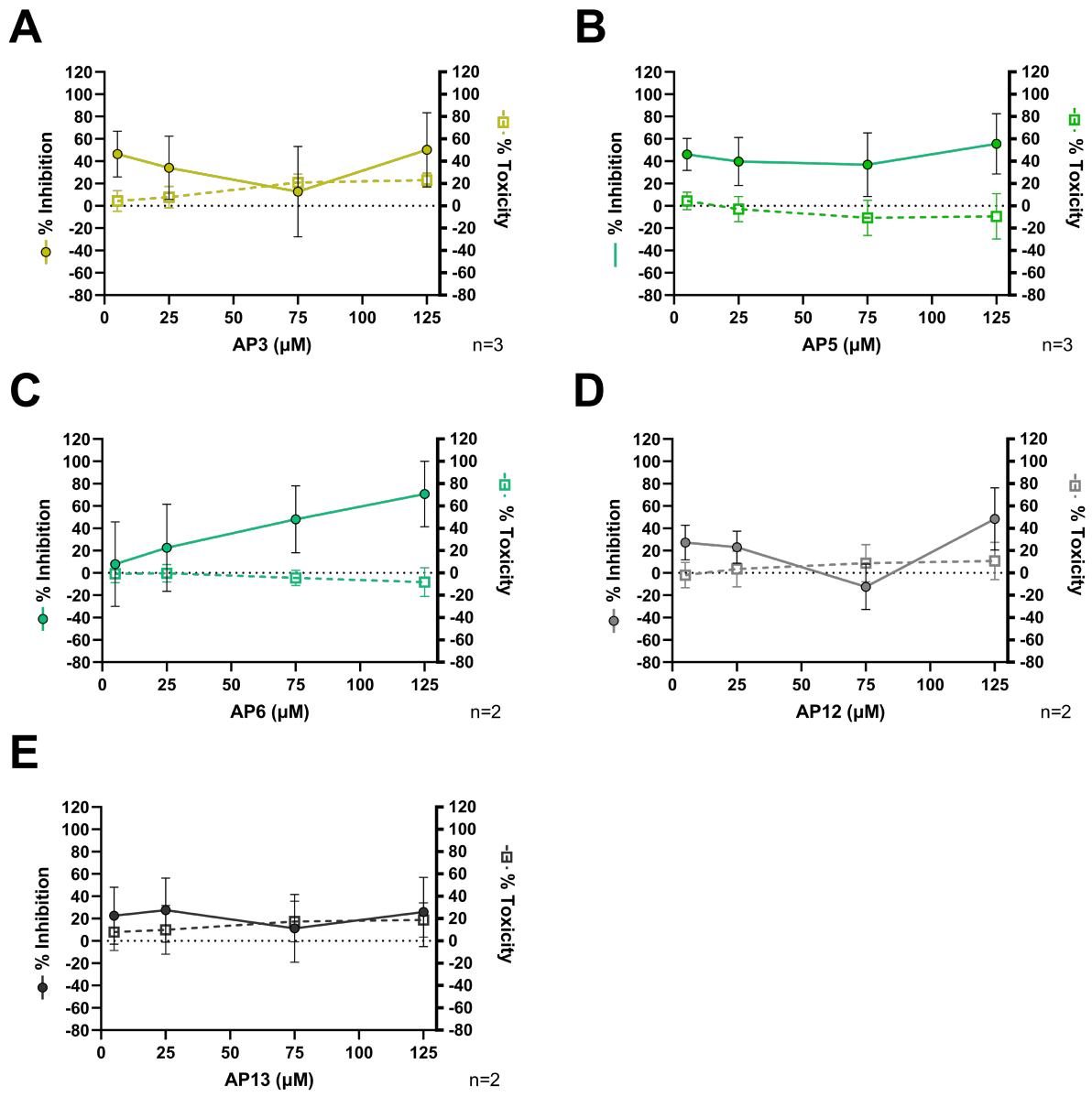

Supplemental Figure 4.1. AP3, 5, 6, 12, and 13 do not inhibit SINV replication.

HEK293T cells were infected by Toto1101/Luc at an MOI of 0.01 PFU/cell in the presence of varying concentrations of **(A)** AP3, **(B)** AP5, **(C)** AP6, **(D)** AP12, or **(E)** AP13. Lysates were harvested at 24 h.p.i. and measured for luciferase activity. Cytotoxicity at 24 hours for varying peptide concentrations was measured using a MTT proliferation assay. Data are combined from 2-3 independent experiments as indicated in each panel.

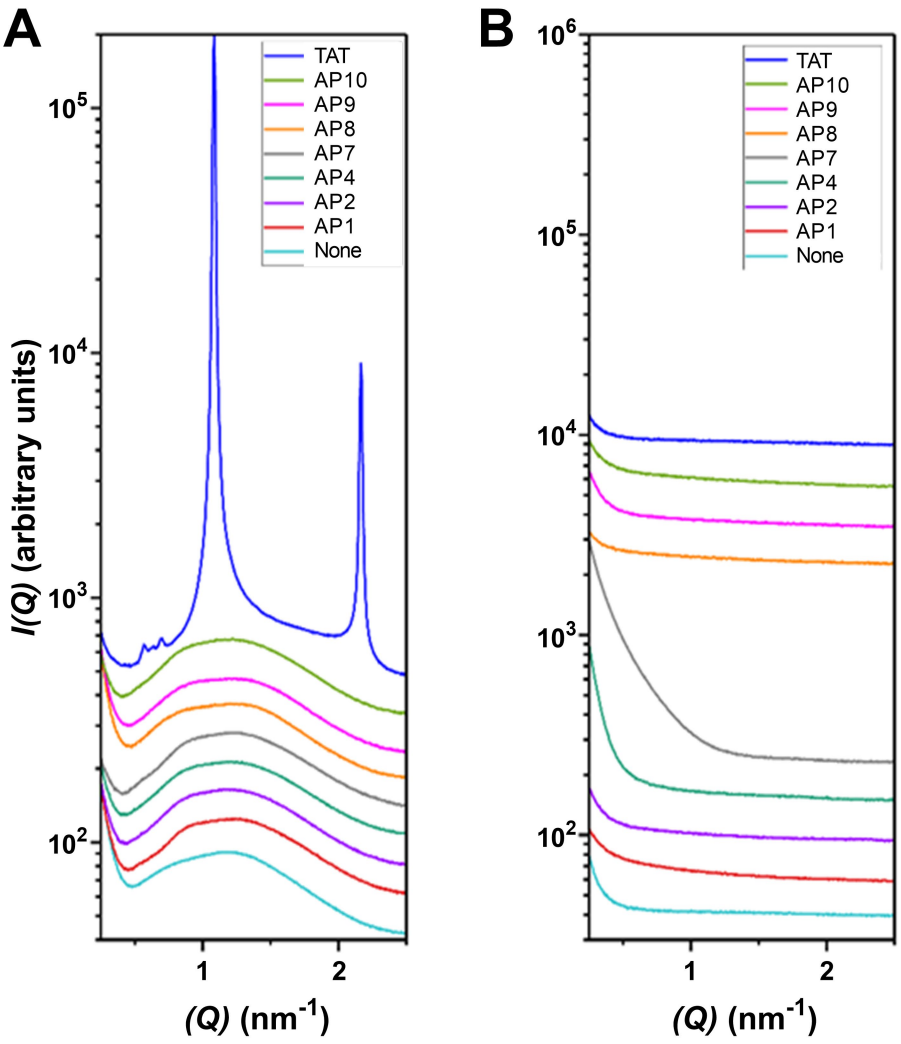

Supplemental Figure 4.2. SAXS scattering curves of control samples.

Control samples containing **(A)** SUVs incubated with individual peptides, and **(B)** individual peptides in aqueous buffer. To facilitate visualization, spectra have been offset along the y-axis by scaling each curve by a multiplicative factor.

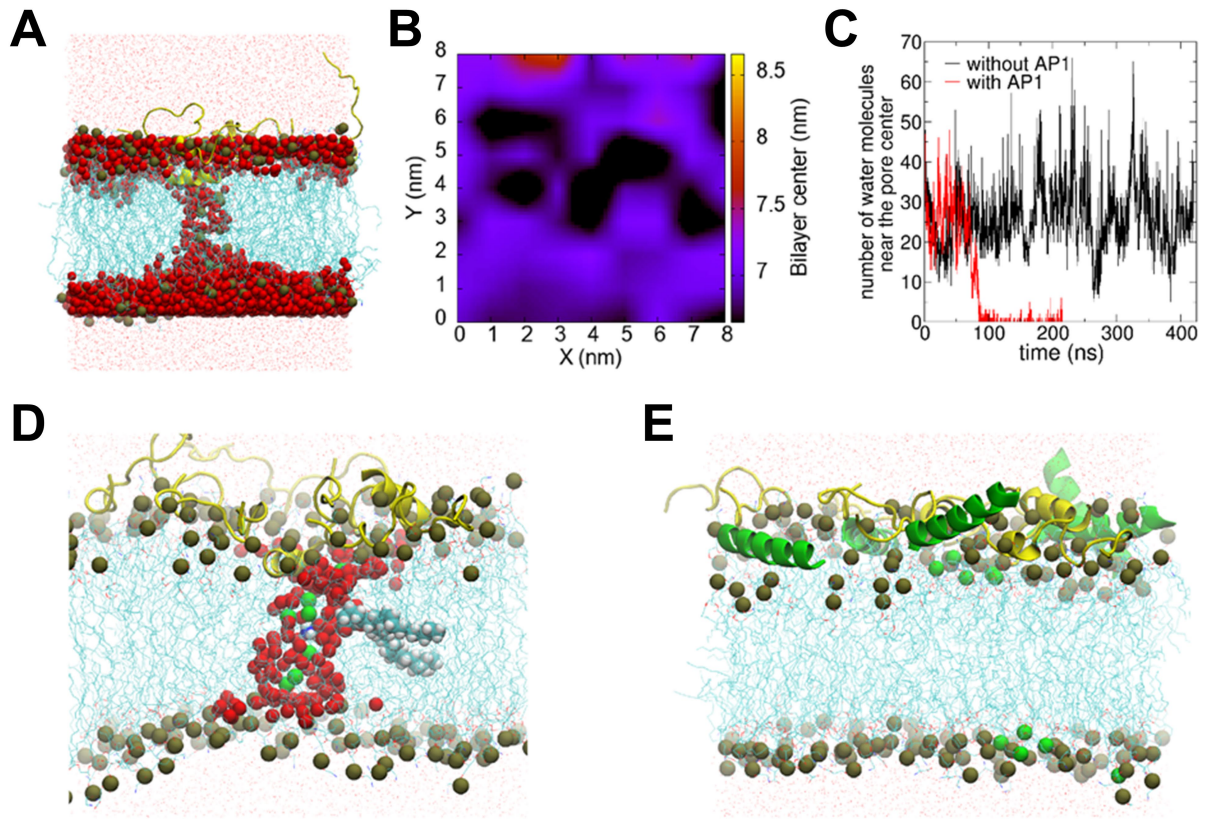

Supplemental Figure 4.3. Membrane pore formed by the N-terminal tail of histone H4 is destabilized by AP1.

(A) Equilibrated structure of a membrane pore formed by the H4 N-terminal tails, which are shown in the yellow cartoon form. Water molecules inside the membrane pore and near the membrane surface are shown as red spheres. Cyan lines represent the DOPE and DOPS lipid tails and the olive spheres represent the phosphate atoms of the lipid headgroups. (B) 2D color plot of the membrane center as a function of lateral dimensions (*X* and *Y*). Black spots represent the negative membrane curvature induced by the H4 peptides. (C) Number of water molecules in a region of 1 nm width near the pore center as a function of simulation time. The number of water molecules decreased to zero at around 85 ns in the presence of AP1 peptides, which indicates the destabilization of the membrane pore by the AP1 peptides. (D) A zoomed-in view of the membrane pore showing that phosphate groups (represented by green spheres) of several lipids remain in contact with the water channel (red spheres); the tails of these lipids are almost perpendicularly oriented with respect to the membrane surface. (E) AP1 peptides (represented by green cartoon) destabilize the membrane pore by opposing the negative curvature induced by the H4 peptides. The phosphate groups that stabilize the water inside the membrane core move back to the membrane surface.

Supplementary Table 4.1. Identified phases in membranes co-treated with HIV TAT and APs.

Lattice parameter (nm) and corresponding magnitude of NGC, |<K>|, if present, is listed for all identified phases.

HIV TAT P/L	AP P/L	AP	Phase	Lattice Parameter (nm)	|<K>| (nm^{-2})
1/20	1/25	AP1	Lα	5.83	
		AP2	Lα	5.96	
		AP4	Lα	5.86	
		AP7	Lα	5.65	
		AP8	Lα	5.84	
		AP9	Lα	5.99	
		AP10	Lα	5.99	
	1/50	AP1	QII *Pn3m*	13.40	3.65E-02
			Lα	5.86	
		AP2	QII *Pn3m*	13.56	3.56E-02
			QII *Im3m*	17.08	3.67E-02
			Lα	5.93	
		AP4	QII *Pn3m*	13.60	3.54E-02
			Lα	5.86	
		AP7	Lα	5.95	
		AP8	QII *Pn3m*	14.05	3.32E-02
			Lα	5.84	
		AP9	QII *Pn3m*	13.24	3.74E-02
			Lα	5.94	
		AP10	QII *Pn3m*	13.16	3.78E-02
			Lα	5.94	
	1/100	AP1	QII *Pn3m*	14.83	2.98E-02
			Lα	5.84	
		AP2	QII *Pn3m*	14.83	2.98E-02
			Lα	5.87	
		AP4	QII *Pn3m*	15.17	2.85E-02
			Lα	5.85	
		AP7	QII *Pn3m*	14.59	3.08E-02
			Lα	5.89	
		AP8	QII *Pn3m*	15.04	2.89E-02
			Lα	5.83	
		AP9	QII *Pn3m*	14.83	2.98E-02
			Lα	5.89	
		AP10	QII *Pn3m*	14.83	2.98E-02
			Lα	5.89	
	0		QII *Pn3m*	15.70	2.66E-02
			Lα	5.80	

Chapter 5

—

Concluding remarks

SUMMARY

The work I presented in this doctoral dissertation explores the role of ubiquitination and RNA binding in antiviral mechanisms utilized by TRIM25 and ZAP.

First, we utilized a "substrate trapping" approach to identify and characterize TRIM25 ubiquitination substrates involved in varied biological processes, representing a significant advance in the ubiquitination field. This approach relies on a point mutation in the TRIM25 RING catalytic domain, abolishing ligase activity (Figure 9) and trapping substrates (Figure 10). By doing so, we are able to identify TRIM25 interactors in a more physiological setting as opposed to generating artificial E3-Ub binding domain fusions. We demonstrate that TRIM25 ubiquitinates proteins implicated in stress granule formation (Figure 11, G3BP1/2), nonsense-mediated mRNA decay (Figure 12, UPF1), nucleoside synthesis (Figure 13, NME1), and mRNA translation and stability (Figure 14, PABPC4). Additionally, we show that the R54P mutation nullifies TRIM25 inhibition of alphaviruses independent of the host IFN response (Figure 15), and that TRIM25 antiviral activity is diminished upon knockdown of NME1 and PABPC4 (Figure 16). Our study is the first presenting a comprehensive ubiquitinome analysis of this important cellular factor, given TRIM25's involvement in both antiviral innate immunity and cancer cell biology.

We then characterized the effects of ZAP and TRIM25 RNA binding on inhibiting SINV and JEV, given their susceptibility to ZAP-mediated translation inhibition. Our work is the first to generate a comprehensive panel of ZAP and TRIM25 RNA binding mutants and dissect the impact of RNA binding (Figure 17) on not only their ability to interact with one another (Figure 18), but also to restrict viral replication and translation (Figures 19-21). Moreover, we utilized full-length ZAP

and TRIM25 in addition to full-length SINV gRNA in order to examine the impact of RNA binding in a more physiologically relevant setting. We showed that mutations impacting ZAP CpG-specific RNA binding significantly affect its ability to restrict SINV replication, SINV translation, and JEV translation (Figure 22). We also demonstrate that ZAP RNA binding is significantly negatively correlated with the rigor of its TRIM25 interaction (Figure 22). Altogether, we identify two distinct, viral context-specific determinants for ZAP antiviral mechanisms, namely ZAP RNA binding and association with TRIM25.

Finally, our collaborative work characterizing the ability of novel antifusion peptides to remodel membranes and restrict alphavirus replication (Figures 24-28) represents the development of a promising far-reaching antiviral therapeutic, potentially capable of inhibiting all enveloped viruses. These antifusion peptides are predicted to generate a positive Gaussian curvature contrary to the negative Gaussian curvature created by viral fusion peptides during their entry, thus blocking their ability to fuse with host membranes and invade cells.

Altogether, my doctoral dissertation represents a significant advancement in understanding TRIM25 and ZAP inhibition of viral replication, with a specific focus on illuminating the roles of ubiquitination and RNA binding in their restriction of alphavirus translation. My work adds to the growing body of knowledge examining how ISGs work together to stymy viral replication and helps paint a picture of how cellular co-factors are nature's "antiviral cocktail," a multipronged defense against the perpetual viral onslaught. After all, the best defense is a good offense.

FUTURE DIRECTIONS

Validation of additional TRIM25 substrates

Perhaps the most obvious, low-hanging fruit (albeit possibly difficult to pluck) would be to continue validating and characterizing TRIM25 interactors identified in our co-IP/MS (Tables 1-4) as bona fide TRIM25 substrates. There are several proteins of interest, including the IGF2BP family of m^{6}A readers, the stress granule proteins FXR1 and FMR1, and the RNA binding proteins DDX21, DDX50, ZCCHC3.

A family of m^{6}A readers: IGF2BP2 and IGF2BP3

Insulin like growth factor 2 mRNA binding (IGF2BP) proteins 2 and 3 enriched strongly with TRIM25 in our co-IP/MS in the absence of infection (Tables 1-2; IGF2BP2, log2FC 1.73–3.23; IGF2BP3, log2FC 2.67 – 3.56). The IGF2BP family of proteins was identified as N^6-methyladenosine (m^{6}A) readers, which is the most common reversible post-transcriptional modification on cellular RNAs (Zaccara *et al*, 2019). Three primary types of proteins are involved in m^{6}A modification: writers, erasers, and readers, which add, remove, and bind m^{6}A, respectively. Viral RNA containing m^{6}A has been shown to evade detection by cellular PRRs (Tong *et al*, 2022).

Though only possessing a weak binding affinity for m^{6}A, the IGF2BP family is thought to promote m^{6}A mRNA stability and storage (Huang *et al*, 2018). Interestingly, all IGF2BP members bind to the oncogenic gene *c-myc* mRNA and promote its stability, thus driving oncogenesis (Huang *et al*, 2018). IGF2BPs utilize RNA recognition motifs (RRM) and KH domains as their RNA binding domains, wherein the KH3-4 di-domain is thought to be the primary determinant for m^{6}A recognition (Huang *et al*, 2018). Both IGF2BP2 and IGF2BP3 possess predicted ubiquitination sites within their

KH domains (Hornbeck *et al*, 2015). Moreover, ubiquitination of IGF2BP3 by MKRN2 or HECTD4 likely targets it for degradation (Jia *et al*, 2020; Pan *et al*, 2022). Importantly, TRIM25 was recently identified to ubiquitinate IGF2BP1-3 and target them for degradation, utilizing m^6A-containing *circNDUFB2* RNA as a scaffold (Li *et al*, 2021a).

Taken together, TRIM25-mediated ubiquitination of IGF2BP2 and 3 may function in antiviral innate immunity through several distinct scenarios. I hypothesize that IGF2BP may bind to m^6A-containing viral RNA and serve to 1) mask them from detection by PRRs and/or 2) enhance their stability and translation. In the first scenario, TRIM25 ubiquitination of IGF2BP proteins would unmask viral RNA and boost the host innate immune response, likely driving production of type I IFN. In the second scenario, TRIM25 ubiquitination of IGFBP proteins would lower stability of viral RNA and subsequent translation, appearing as TRIM25 restriction of viral translation. Further experiments are required to assess which viral RNA species IGF2BP bind, and whether IGF2BP ubiquitination by TRIM25 results in inhibition of viral replication.

Components of stress granules or alphavirus replication complexes: FXR1 and FMR1

In addition to the core SG proteins G3BP, we also identified the SG proteins fragile-X mental retardation autosomal 1 (FXR1) and fragile X messenger ribonucleoprotein 1 (FMR1) as robust TRIM25-WT interactors in the absence of infection (Table 2; FXR1, log2FC 1.52–4.86; FMR1, log2FC 2.14–2.16). FXR1 and FMR1, named after their role in Fragile X syndrome, are RNA binding proteins that localize to SGs (Youn *et al*, 2018). As previously discussed in Chapter 2, the Old World alphaviruses SINV and CHIKV utilize the SG proteins G3BP to cluster their viral replication

complexes and recruit translation initiation machinery (Cristea *et al*, 2010; Scholte *et al*, 2015; Kim *et al*, 2016; Götte *et al*, 2019, 2020).

In contrast, the New World alphavirus VEEV interacts not with G3BP, but with all members of the Fragile X family, FXR1, FXR2, and FMR1, requiring the presence of at least one family member to facilitate formation of viral replication complexes (Kim *et al*, 2016). While we did not identify a sufficient role for G3BP in mediating TRIM25 inhibition of SINV or CHIKV replication (Supplemental Figure 3.2), it is still possible that TRIM25-mediated ubiquitination of FXR1 and/or FMR1 may inhibit replication of New World alphaviruses, given that TRIM25 is able to inhibit VEEV infection (Figure 15D).

RNA binding and unwinding: DDX21, DDX50, and ZCCHC3

One final group of putative TRIM25 substrates of interest consists of RNA binding proteins: the DExD-box (DDX) helicases 21 (DDX21) and 50 (DDX50) and the zinc finger CCHC domain-containing protein 3 (ZCCHC3). We found that DDX21 consistently interacts with TRIM25 only in the absence of infection (Tables 1 and 2, log2FC 1.60–3.52) while both DDX50 and ZCCHC3 robustly interact with TRIM25 in all conditions tested (Tables 1-4; DDX50, log2FC 2.44–5.52; ZCCHC3, 2.47–5.21).

The DDX RNA helicase family consists of ATPase dependent RNA helicases that regulate all aspects of RNA metabolism, and includes the classic dsRNA sensor RIG-I, also known as DDX58 (Cordin *et al*, 2006). In particular, DDX21 is thought to coordinate transcription and ribosomal RNA processing in addition to safeguarding genome integrity (Calo *et al*, 2015; Song *et al*, 2017). While

DDX21 has been shown to occupy both pro-viral and antiviral roles during infection (for a comprehensive review, see Ullah *et al*, 2022), of special consideration is DDX21 inhibition of IAV RNA synthesis by binding to the PB1 subunit of the viral RdRp (Chen *et al*, 2014) – the same step at which TRIM25 has been shown to inhibit IAV RNA synthesis (Meyerson *et al*, 2017). Moreover, the viral NS1 protein has been demonstrated to bind both DDX21 and TRIM25 (Gack *et al*, 2009; Chen *et al*, 2014). It is interesting to speculate that DDX21 and TRIM25 work in concert to inhibit IAV RNA synthesis, though this hypothesis has yet to be tested.

Though DDX50 shares over half of its sequence identity with DDX21, it is not as well characterized. However, DDX50 has been shown to enhance IRF3 activation and upregulate subsequent IFN-β and NF-κB signaling, thereby inhibiting replication of both RNA and DNA viruses (Han *et al*, 2017; Pallett *et al*, 2022). It is possible that TRIM25 acts at multiple steps to regulate IFN signaling, and could ubiquitinate DDX50 to drive an even more robust type I IFN response.

In contrast to the DDX family of RNA helicases, ZCCHC3 binds not only to RNA but also to DNA, interacting only with the double-stranded (ds) versions of both (Lian *et al*, 2018a, 2018b). In line with its ability to bind both dsDNA and dsRNA, ZCCHC3 functions as a co-sensor for the dsDNA sensor cGAS (Lian *et al*, 2018a) and the RLR dsRNA sensors RIG-I and MDA5 (Lian *et al*, 2018b). For the latter, ZCCHC3 recruits TRIM25 to RIG-I and MDA5 complexes to facilitate their K63-linked polyubiquitination and activation (Lian *et al*, 2018b). However, it remains unknown whether ZCCHC3 itself is a TRIM25 substrate, though it does possess several predicted ubiquitination sites (Hornbeck *et al*, 2015). It would be interesting to test whether TRIM25 interacts

with and/or ubiquitinates ZCCHC3 in its role as a cGAS co-sensor, potentially functioning as an additional ZAP co-factor and explaining ZAP inhibition of DNA viruses (Ficarelli *et al*, 2021).

ZAP modulation of TRIM25 substrates

My work identified TRIM25 ubiquitination targets that may be involved in TRIM25 inhibition of viral translation (Figure 10, Tables 1-4). However, it remains unclear whether ZAP modulates TRIM25 substrates to function in its restriction of viral translation. To address this question, we stably knocked down ZAP expression in our TRIM25 inducible cell lines using lentiviral delivery of *ZC3HAV1* shRNA (Appendix 2). We then performed one co-IP/MS experiment with these cell lines, using the same experimental set up as Figure 10A.

We hypothesized that comparing differences in TRIM25 interactors in the presence and absence of ZAP would identify ZAP-dependent TRIM25 substrates. Because we only ran this experiment once, we are unable to draw any definitive conclusions. However, we were able to observe some interesting trends. In the absence of viral infection, TRIM25-WT interacted with many more proteins when ZAP was present in contrast to TRIM25-R54P, which interacted with more proteins when ZAP was absent (Figure 29). TRIM25-R54P had more interactions in general than TRIM25-WT in the absence of infection; during infection, the number of interactors was comparable between TRIM25-WT and -R54P (Figure 29). This experiment bears repeating in order to draw more concrete conclusions about which identified interactors display consistent, ZAP-dependent association with TRIM25.

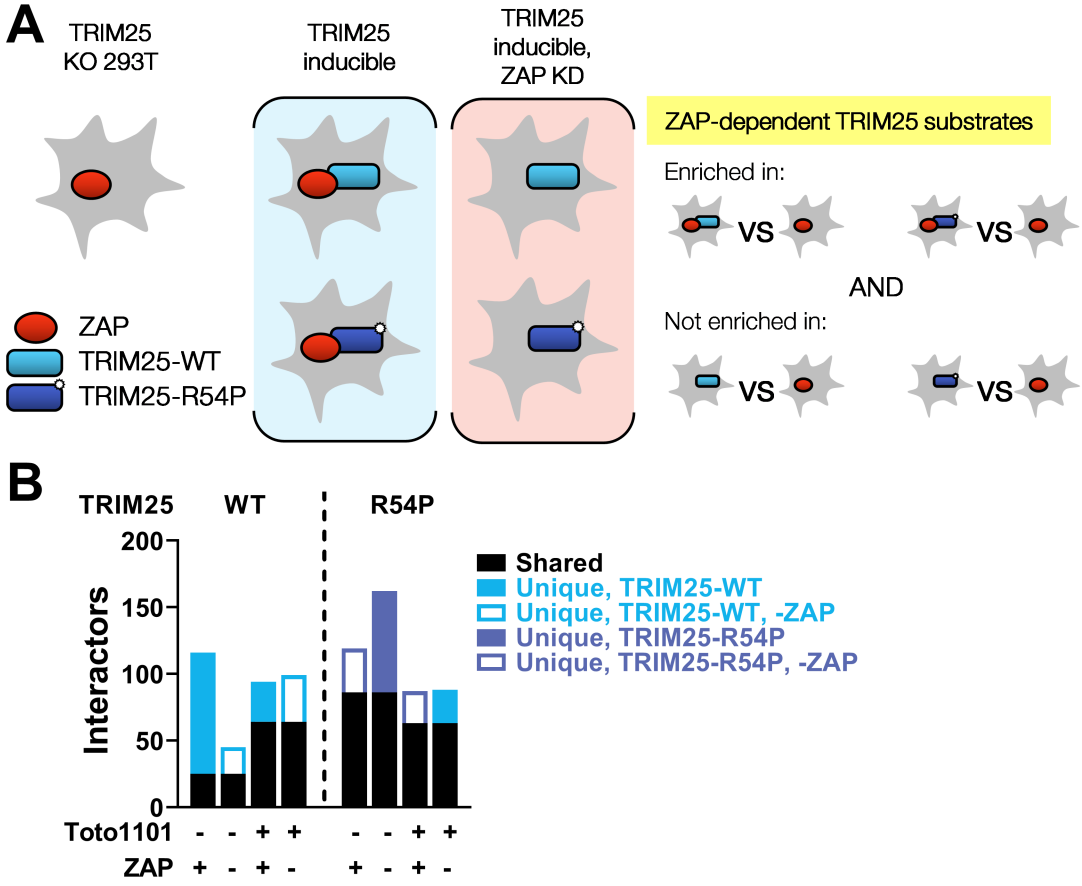

Figure 29. Elucidation of ZAP-dependent TRIM25 substrates.

(A) Schematic of TRIM25 inducible +/- ZAP KD cell lines and comparisons. "vs" indicates comparison of enriched substrates in the lefthand group as compared to the right. **(B)** Number of TRIM25 interactors enriched in co-IP/MS analysis of each cell line as compared to TRIM25 KO 293T. Interactors are classified as Log2FC>2 and Pvalue<0.05, or iLog2FC>2 and iPvalue<0.05, where the "i" stands for imputed. If both the imputed and real values exist for a protein, the real values were used. The black bars indicated shared interactors for each cell line / virus condition in the presence or absence of ZAP. n = 1

Assaying requirement for TRIM25 substrates in ZAP antiviral activity in varied contexts

How ZAP is able to inhibit a broad range of viruses via diverse mechanisms despite lacking catalytic activity has been a long-standing question (Yang and Li, 2020; Ficarelli *et al*, 2021). We hypothesize that TRIM25-mediated ubiquitination of varied substrates may enable ZAP antiviral activity in differing contexts, functioning as "co-co-factors" so to speak. The partial species-specificity

of TRIM25 and ZAP with regards to their cooperative antiviral activity (Gonçalves-Carneiro *et al*, 2021) may be due to species-specific TRIM25 substrates that function in ZAP antiviral activity. While we did not find G3BP and UPF1 to be sufficient to mediate TRIM25 inhibition of alphaviruses in human cells (Supplemental Figure 2.2), this does not preclude their involvement in TRIM25 inhibition of alphaviruses in other species, given that alphaviruses are able to replicate in arthropods, birds, reptiles, fish, and mammals (Griffin, 2013).

Though we identified TRIM25 interactors in the context of alphavirus replication (Tables 1-4), some of these may function in TRIM25-ZAP inhibition of other viruses. For example, TRIM25, ZAPL, and DDX21 may all work together to inhibit IAV replication. Not only do they each individually interact with IAV proteins (DDX21 with PB1, TRIM25 with NP, and ZAPL with PB2 and PA), but they also interact with each other. Collectively, these protein-protein interactions may allosterically enhance their inhibition of IAV RNA synthesis. It is also interesting to speculate that ZAPL antagonism of IAV involves TRIM25-mediated ubiquitination, given that ZAPL interaction with the viral polymerase subunits PB2 and PA results in their ubiquitination and subsequent proteasomal degradation (Liu *et al*, 2015).

A delicate binding balance: TRIM25, ZAP, and RNA

We are the first to show that ZAP mutants with reduced ability to bind SINV RNA (Figure 17) associate more strongly with TRIM25 (Figure 18); in other words, that ZAP RNA binding is significantly negatively correlated with its interaction with TRIM25 (Figure 22). This is in line with data that show that the N-terminal ZAP ZnFs are required both for its interaction with TRIM25 (Gonçalves-Carneiro *et al*, 2021) and for binding to RNA (Guo *et al*, 2004). Therefore, we hypothesize

that SINV RNA and TRIM25 competitively bind to ZAP, which may serve to maintain a delicate balance of multiple necessary molecular interactions for ZAP antiviral activity. It is possible that stronger association of ZAP RNA binding mutants with TRIM25 could prevent TRIM25 from interacting with its substrates necessary for inhibition of SINV translation.

CLOSING STATEMENT

In producing the first comprehensive TRIM25 ubiquitinome analysis and thoroughly characterizing the role of RNA binding in TRIM25 and ZAP restriction of viral translation, my dissertation work has helped lay the foundation to an in-depth understanding of both TRIM25 diverse biological processes and ZAP antiviral mechanisms. In the future, elucidating the antiviral function of TRIM25 substrates may enable the development of pan-antivirals that rely on harnessing natural host defenses, such as by engineering post-translational modifications. Such therapeutic advancements would potentially assist in alleviating any future pandemic viral spillover events.

Appendices

—

Appendix 1

—

All about the RNA: Interferon-stimulated genes that interfere with viral RNA processes

frontiers in Immunology

REVIEW
published: 09 December 2020
doi: 10.3389/fimmu.2020.605024

All About the RNA: Interferon-Stimulated Genes That Interfere With Viral RNA Processes

Emily Yang[1,2] *and Melody M. H. Li*[1,2*]

[1] Molecular Biology Institute, University of California, Los Angeles, Los Angeles, CA, United States, [2] Department of Microbiology, Immunology, and Molecular Genetics, University of California, Los Angeles, Los Angeles, CA, United States

Interferon (IFN) signaling induces the expression of a wide array of genes, collectively referred to as IFN-stimulated genes (ISGs) that generally function to inhibit viral replication. RNA viruses are frequently targeted by ISGs through recognition of viral replicative intermediates and molecular features associated with viral genomes, or the lack of molecular features associated with host mRNAs. The ISGs reviewed here primarily inhibit viral replication in an RNA-centric manner, working to sense, degrade, or repress expression of viral RNA. This review focuses on dissecting how these ISGs exhibit multiple antiviral mechanisms, often through use of varied co-factors, highlighting the complexity of the type I IFN response. Specifically, these ISGs can mediate antiviral effects through viral RNA degradation, viral translation inhibition, or both. While the OAS/RNase L pathway globally degrades RNA and arrests translation, ISG20 and ZAP employ targeted RNA degradation and translation inhibition to block viral replication. Meanwhile, SHFL targets translation by inhibiting -1 ribosomal frameshifting, which is required by many RNA viruses. Finally, a number of E3 ligases inhibit viral transcription, an attractive antiviral target during the lifecycle of negative-sense RNA viruses which must transcribe their genome prior to translation. Through this review, we aim to provide an updated perspective on how these ISGs work together to form a complex network of antiviral arsenals targeting viral RNA processes.

Keywords: interferon-stimulated genes, co-factors, viral RNA degradation, translation inhibition, RNA sensing

OPEN ACCESS

Edited by:
Mark R. Walter,
University of Alabama at Birmingham, United States

Reviewed by:
Preeti Bharaj,
University of Texas Medical Branch at Galveston, United States
Ronald L. Rabin,
United States Food and Drug Administration, United States

***Correspondence:**
Melody M. H. Li
manhingli@mednet.ucla.edu

Specialty section:
This article was submitted to Cytokines and Soluble Mediators in Immunity, a section of the journal Frontiers in Immunology

Received: *11 September 2020*
Accepted: *09 November 2020*
Published: *09 December 2020*

Citation:
Yang E and Li MMH (2020) All About the RNA: Interferon-Stimulated Genes That Interfere With Viral RNA Processes. Front. Immunol. 11:605024. doi: 10.3389/fimmu.2020.605024

INTRODUCTION

Organisms must constantly defend themselves against viral pathogens. In order to stem viral spread, cells must both signal the presence of viral infection and hinder their replication. One key first line of cellular defense in vertebrates is the type I interferon (IFN) response. Hosts possess sensors which recognize pathogen-associated molecular patterns (PAMPs) of invading viruses such as the viral replicative intermediate double-stranded RNA (dsRNA) and activate transcription factors such as IFN-regulatory factors 3 or 7 (IRF3/7) and nuclear factor kappa-light-chain-enhancer of activated B cells (NFκB). As a result, these transcription factors translocate to the nucleus to activate expression of type I IFN and other proinflammatory cytokines.

The type I IFN receptor is expressed ubiquitously on almost all cell types, allowing for IFN signaling in both infected and neighboring cells that are uninfected. Janus kinase-signal transducer and activator of transcription (JAK-STAT) is the predominant, canonical pathway that regulates ISG transcription. IFN binding to its cell surface receptor, comprised of IFN-α receptor 1 (IFNAR1) and IFN-α receptor 2 (IFNAR2), leads to phosphorylation of pre-associated JAK1. Phosphorylated JAK1 and tyrosine kinase 2 (TYK2) then phosphorylate the IFN receptor, which recruits STAT1/2 to be phosphorylated themselves. Phosphorylated STAT1/2 recruit IRF9 to form the transcription factor complex IFN-stimulated gene factor 3 (ISGF3). ISGF3 translocates to the nucleus where STAT1 is further phosphorylated for full activation. Within the nucleus, ISGF3 binds to IFN-stimulated response elements present in the promoters of IFN-stimulated genes (ISGs), which then effect an antiviral cellular environment [for a comprehensive review on IFN signaling, see (1)].

Interestingly, a growing body of evidence in recent years suggests a plethora of non-canonical mechanisms [for a comprehensive review on canonical and non-canonical regulation of ISG transcription, see (2)]. Non-canonical ISGF3 complexes containing unphosphorylated STAT2, unphosphorylated STAT1 and STAT2, or STAT2 and IRF9 only have been found to mediate expression of specific ISGs (3–6). Other transcription complexes such as STAT5-CrkL (7, 8) or transcription factors such as IRF1 (9) can induce ISG expression. Additionally, cytokines such as TNF-α can moderately induce a subset of ISGs through the NFκB protein complex and further synergize with type I or II IFN to jointly upregulate antiviral ISG expression (10–13). Surprisingly, cellular pathways that have no apparent connection to the innate immune response have been linked to ISG induction. For example, inhibitors of nucleotide synthesis have been shown to effectively upregulate ISG expression in a JAK-STAT-independent manner (14–17). Differences in the extent and timing of ISG upregulation likely depend on the complex interplay between these various mechanisms.

Broadly speaking, an ISG is any gene whose expression is induced by IFN signaling. Advances in RNA-sequencing (RNA-seq) technology have enabled the identification of ISGs across varied cell lines by measuring changes in the transcriptome in response to IFN stimulation. The online database INTERFEROME continues to catalog the results of such gene profiling studies (18). However, ISG expression is more nuanced in reality. A subset of ISGs are direct targets of IRF3/7 and can be induced with or without downstream IFN signaling (**Figure 1**) (1). Other ISGs are both basally expressed and IFN-inducible, while still others are cell-type specific (19, 20). Moreover, there are three types of IFN, wherein type I and III are the classic antiviral IFNs. Though type I and III IFNs bind to different receptors, they signal through the same JAK-STAT pathway, thus inducing a shared array of ISGs. Still, type I and III IFN signaling pathways are differentiated by expression kinetics and cell-type specific receptor expression [for a recent review, see (21)]. Tight regulation of ISG expression is necessary because dysregulation of the type I IFN response results in interferonopathies or systemic inflammation deleterious to the organism (22).

In addition to regulating their own expression, ISGs are well known for their inhibition of viral replication. They employ diverse mechanisms to block virtually every step of viral replication, though ISGs have been shown to target different viral life cycle stages for different viruses [for recent reviews on a broad range of antiviral ISGs, see (20, 23)]. For example, the IFITM family blocks viral entry of diverse viruses (24) while the Mx GTPases recognize diverse nucleocapsids and block their

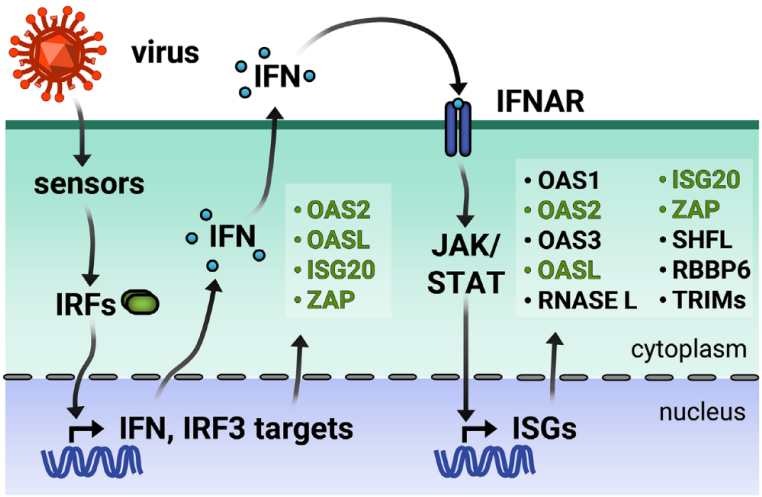

FIGURE 1 | Viral infection triggers the type I interferon (IFN) response. Virus entry triggers cellular pathogen sensors, which induce production of IFN and IFN regulatory factor 3 (IRF)-dependent genes. Type I IFN is secreted and binds to IFN-α receptor on the same and neighboring cells, activating production of a wider array of IFN-stimulated genes (ISGs). IRF3-dependent ISGs are colored in green. TRIMs is not inclusive of the entire TRIM family, but only those inducible by IFN.

nuclear import (25). TRIM5α disrupts retrovirus uncoating and targets several viral proteins for proteasomal degradation (26). However, these only represent a tip of the iceberg. Recent advances in systematic approaches have allowed us to unbiasedly uncover ISGs with previously uncharacterized antiviral activity. Compiled ISG libraries have facilitated focused loss-of-function or gain-of-function screens of hundreds of ISGs, illuminating the contribution of individual ISGs in varied viral contexts (27–30). Furthermore, as advances in omics approaches allow examination of cellular changes on a systemic level, attention is shifting to how ISGs interact and even synergize with one another (27, 31, 32). Moreover, detailed mechanistic studies are still needed in order to unravel their mode of action. As ISGs may employ different antiviral mechanisms against different viruses, studies in varied viral systems will illuminate how ISGs might recruit different cellular pathways or factors.

Rather than provide a comprehensive, surface-level view of myriad ISGs with their arrayed antiviral functions, we have chosen to focus on a subset of ISGs that interfere with viral RNA processes. Recent studies have provided an emerging view on the diversity and complexity of RNA-based mechanisms by which different ISGs inhibit viruses with an RNA genome. With the exception of retroviruses which replicate through a DNA intermediate, single-stranded RNA (ssRNA) viruses can generally be categorized as positive-sense and negative-sense. Positive-sense (+) ssRNA viruses possess genomes that generally resemble mRNA, in that it can be translated directly by host translation machinery. However, negative-sense (-) ssRNA viruses code their proteins in the reverse orientation. Therefore, they must package their own RNA-dependent RNA polymerases and transcribe their genomes before viral protein synthesis can occur. While there are many more ISGs that inhibit viral RNA processes (**Tables 1** and **2**), this review will highlight recent exciting work on a subset of ISGs that act in an RNA-centric manner to sense, degrade, or inhibit transcription or translation of both (+) and (-) ssRNA viral genomes (**Figure 2**). We have chosen the ISGs here because at the time of writing of this review, they have not been comprehensively reviewed in the antiviral innate immunity field, and exciting developments have either illuminated nuances of well-characterized mechanisms or uncovered entirely new mechanisms by which these ISGs inhibit viral replication. We synthesized diverse antiviral mechanisms of individual ISGs and provided hypotheses for how cellular co-factors mediate the distinct antiviral activities of these ISGs, which not many previously published reviews have done. We will begin our discussion with the 2'-5' oligoadenylate synthetase (OAS)/RNase L pathway, which both senses and degrades RNA, making it a potent early inhibitor of viral replication. We will then segue into ISGs that both degrade RNA and inhibit translation, such as ISG20 and zinc finger antiviral protein (ZAP), before focusing on a novel means of translation inhibition by Shiftless (SHFL). We will end with a discussion of E3 ligases that inhibit viral transcription. Though there are many additional ISGs that block these RNA-centric steps of viral replication, this review focuses on ISGs that possess multiple or seemingly contradictory antiviral mechanisms. Protein-protein interactions or cellular co-factors could explain diverse antiviral mechanisms of individual ISGs.

TABLE 1 | ISGs that must bind RNA to inhibit viral RNA processes.

Gene	Mode of inhibition	RNA motif	References
ADAR1	A-to-I sequence conversion	dsRNA	(33)
IFIT1, -2, -3, -5	Translation inhibition	Type 0 cap structure lacking 2'-*O*-methylation at the 5' end of ssRNA	(34, 35)
ISG20	RNA degradation, translation inhibition	Largely unknown; recognizes m^6A on HBV RNA	(36–38)
MDA5	RNA sensor	Long cytosolic dsRNA (> 1,000-2,000 bp)	(39–41)
OAS1, -2, -3	RNA sensor, synthesize 2-5A to activate RNase L	dsRNA	(40, 42)
OASL	RNA sensor, promotes RIG-I signaling and inhibits cGAS signaling	dsRNA	(43)
PARP12	Translation inhibition	Unknown	(44–46)
PKR	RNA sensor, translation inhibition	dsRNA	(40)
RIG-I	RNA sensor	short cytosolic dsRNA or ssRNA (10-300 bp) with 5'-triphosphate ends, enriched in poly-U/UC or AU sequences	(39–41)
RNase L	RNA degradation	ssRNA, cleaves at ^ in U^N, where N is any nucleotide	(47)
TRIM25	Translation inhibition	Unknown	(48–50),
ZAP	RNA degradation, translation inhibition, ISG synergy	ssRNA, CG dinucleotide	(23)
ZCCHC3	RNA sensor	dsRNA	(51)
ZNFX1	RNA sensor	dsRNA	(52)

Mode of inhibition, RNA motif or substrate preference, and references for the most recent reviews are listed for ISGs that bind RNA to inhibit viral RNA processes.

TABLE 2 | ISGs that inhibit viral RNA processes with no known dependence on RNA binding.

Gene	Inhibited process	Known mechanism(s)	References
RBBP6	Transcription	Competitively binds to viral RNA polymerase	(53)
SHFL	Translation	Inhibits -1 ribosomal frameshifting	(54)
TRIM22	Transcription	Prevents transcription factor binding to HIV-1 promoter	(55)
TRIM25	Transcription	Blocks IAV RNA elongation	(56)
TRIM32	Transcription	Targets IAV polymerase for degradation	(57)
TRIM69	Transcription	Sequesters VSV_{IND} P	(58, 59)
Viperin	Viral RNA synthesis	Synthesizes chain terminator from cytidine triphosphate	(60)

Viral RNA process inhibited (viral RNA synthesis, transcription, or translation) known mechanism(s), and references for the most recent reviews are listed for ISGs that inhibit viral RNA processes without a strict requirement for RNA binding.

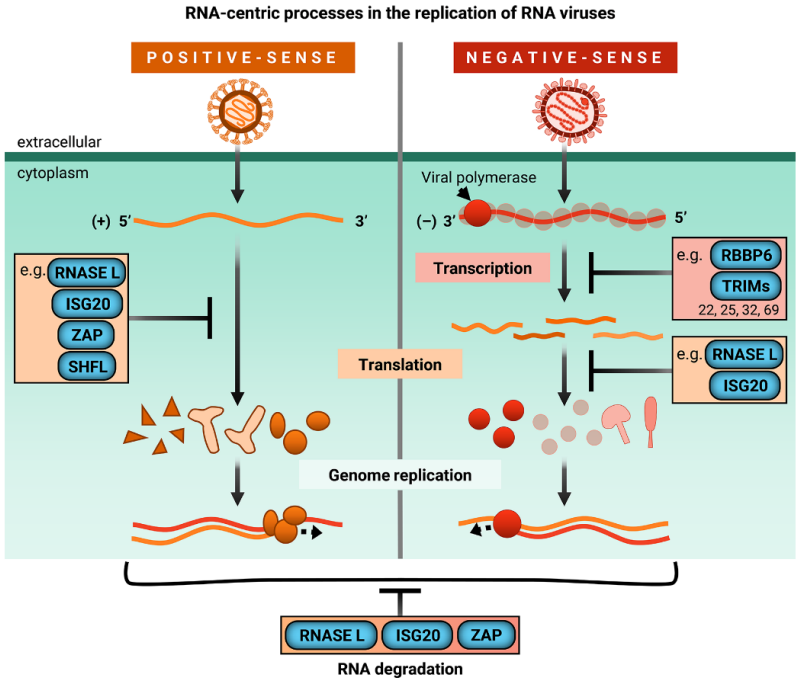

FIGURE 2 | ISGs inhibit RNA-centric processes in replication of RNA viruses. Upon infection, positive-sense single-stranded RNA genomes are directly translated by host machinery. Following expression of viral replicase proteins, genome replication occurs. However, negative-sense single-stranded RNA viruses bring their own RNA-dependent RNA polymerase and viral co-factors to transcribe their genomes before the viral mRNAs can be translated by host machinery for genome replication. ISGs covered in this review are shown to block global or viral translation (RNaseL, ISG20, ZAP, SHFL) and viral transcription (RBBP6, TRIMs). They can also inhibit viral replication by degrading cellular and/or viral RNA (RNase L, ISG20, ZAP). TRIMs that inhibit transcription are limited to those mentioned in this review, specifically TRIM22, TRIM25, TRIM32, and TRIM69.

OAS/RNASE L: SENSING VIRAL PAMP TRIGGERS GLOBAL RNA DEGRADATION AND TRANSLATIONAL ARREST

Degrading viral genomes presents one potent method of antiviral activity; digesting viral genetic material ensures that no further steps in replication can occur. However, the challenge lies within being able to control RNA degradation to ensure cellular survival or limit destruction within the host. The OAS/RNase L pathway is activated upon sensing the PAMP of dsRNA, serving two functions: sensing viral intruders and inhibiting viral replication by degrading RNA almost indiscriminately, inducing global translational arrest.

The OAS/RNase L pathway was one of the first ISG antiviral mechanisms to be identified and elucidated in the 1970s [reviewed in (61–64)]. Binding to dsRNA activates OAS, which then synthesizes 2'-5' oligoadenylates (commonly abbreviated as 2-5A) that in turn activate RNase L to cleave cytoplasmic RNA, thereby inhibiting viral replication (**Figure 3A**). Humans possess three catalytically active OAS genes (OAS1-3) and one inactive gene (OASL). Each OAS is composed of 1 (OAS1 and OASL), 2 (OAS2), or 3 (OAS3) basal OAS units (**Figure 3A**). While only the C-terminal OAS unit in each protein is catalytically active and responsible for synthesizing 2-5A, both active and inactive OAS units can still bind dsRNA. RNase L, present in cellular cytoplasm as an inactive monomer, forms a catalytically active dimer upon binding to 2-5A and cleaves RNA in a seemingly indiscriminate manner. Though OAS1-3 all carry signatures of positive selection, which is indicative of rapid evolution resulting from host-pathogen interactions, OASL does not. Furthermore, OAS1 displays much stronger signatures than OAS2 or OAS3 (65, 66). RNase L also carries signatures of positive selection and some of the positively selected residues are located within the RNA-binding domain (66).

In the past 10 years, great strides have been made in clarifying dsRNA substrate specificity and 2-5A synthesis activity of individual OAS isoforms due to the advent of CRISPR-Cas9 gene-editing techniques and generation of OAS knockout cell lines and mouse models. Moreover, sweeping improvements in genome-wide RNA-seq and in-depth proteomics have illuminated new intricacies of OAS/RNase L-mediated inhibition of viral replication, which we will review here.

OAS1-3: 2-5A Messenger Synthesis

Recent years have not only seen a flurry of biochemical and structural studies on individual OAS paralogs, which have advanced understanding of their RNA substrate specificity and

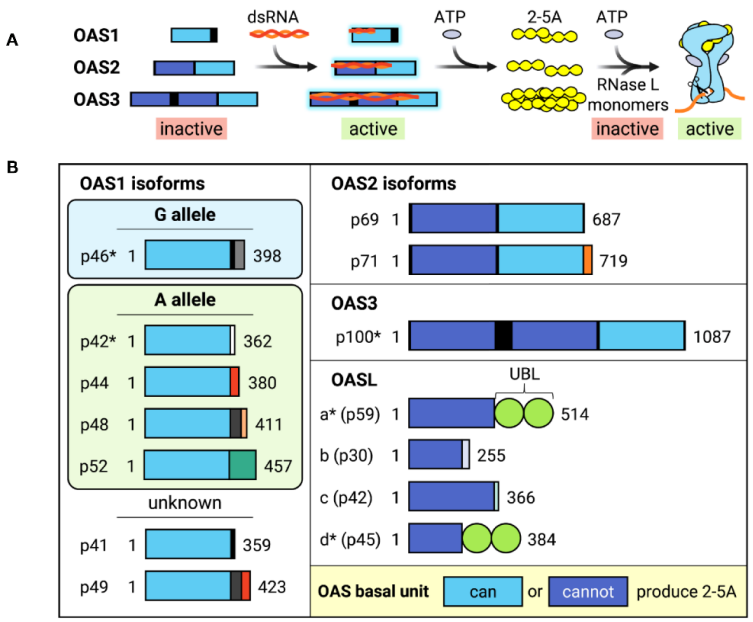

FIGURE 3 | Activation and dsRNA binding of OAS isoforms. **(A)** Diagram of how OAS is activated by viral dsRNA and synthesizes 2-5A to activate RNase L. Longer OAS isoforms are activated by longer dsRNA. Though all are able to synthesize 2-5A, OAS3 2-5A synthesis is necessary and sufficient for RNase L activation. RNase L exists as inactive free monomers, but dimerizes and activates upon binding to 2-5A and ATP, thereby cleaving RNA. Interestingly, IFN and some ISG transcripts are resistant to RNase L cleavage, resulting in preservation of antiviral signaling. **(B)** Schematic of known human OAS isoforms encoded by OAS genes OAS1, OAS2, OAS3, and OASL. Isoforms marked with * have demonstrated direct antiviral activity. Length of boxes approximates gene length, with different colored C-terminal boxes representing different coding sequences. Light blue OAS basal units are able to synthesize 2-5A, while dark blue OAS basal units are catalytically inactive. Most OAS1 isoforms are expressed by either G or A alleles, which differ by the inclusion of a G or A nucleotide at a splice acceptor site. However, OAS1 p41 and p49 have not been attributed to either G or A and are therefore labelled as "unknown." UBL, Ubiquitin-like domain.

activation, but also of their individual splice variants. Surprisingly, OAS3 has been identified as the main contributor to the OAS/RNase L pathway, as OAS3-mediated 2-5A synthesis has been demonstrated as necessary and sufficient for RNase L pathway (67).

Though there are four OAS genes in humans, alternative splicing of additional 3' exons generates 10 different catalytically active and 4 inactive isoforms (**Figure 3B**) (62, 68, 69). OAS isoforms can vary greatly in size and degree of catalytic activity within the same gene (69). Though OAS1 isoforms differ from each other in their C-terminal regions, all are able to synthesize 2-5A *in vitro* after incubation with poly(I:C), a dsRNA mimetic, with isoforms p42 and p46 expressed more highly in HEK293 cells (69). A yeast two-hybrid screen for p42 and p44, predicted to be expressed by all humans (70), revealed different binding partners, suggesting that OAS1 unique C-terminal regions may alter protein-protein interactions mediating isoform-specific functions (69). In support of this hypothesis, p46 possesses a CaaX prenylation motif that causes it to localize to mitochondria, whereas p42 lacks the CaaX motif and is cytoplasmic (71, 72). This difference in cellular localization is thought to contribute to their divergent impact on cellular respiration upon overexpression (72), and could contribute to their differential antiviral activity.

Genome-wide association studies of 2-5A synthesis activity revealed the presence of two OAS1 alleles which differ by the presence of a G or A at a splice acceptor site (70). Individuals with the G allele have high 2-5A activity and express the OAS1 p46 isoform, whereas individuals with 1-2 copies of the A allele have significantly lower OAS activity and express the OAS1 p42, p44, p48, and p52 isoforms (**Figure 3B**) (70, 73). This G/A single nucleotide polymorphism is associated with a variety of infectious diseases, such as the (+) ssRNA viruses West Nile virus (WNV) and hepatitis C virus (HCV), in addition to a hepatitis B virus (HBV)-associated autoimmune disease; wherein the G allele confers resistance and the A allele is associated with higher risk (74–78). A comprehensive study of OAS isoform-specific antiviral activity against dengue virus (DENV) found that out of all catalytically active isoforms, only OAS1 p42 and p46 and OAS3 p100 were able to block DENV replication through an RNase L-dependent mechanism (79). Furthermore, degree of antiviral activity was positively correlated with amount of RNase L activity, as measured by 28S and 18S rRNA cleavage, wherein OAS3 inhibited DENV replication more robustly than either OAS1 isoform.

This finding of RNase L-dependent antiviral activity of OAS3 was surprising at the time. OAS3 was thought to primarily

synthesize the minimal dimeric 2-5A molecule, composed solely of two adenylate groups, which poorly activates RNase L (80, 81). More recently, it was shown that not only does OAS3 require 3-4 logs lower concentration of dsRNA than OAS1 for 2-5A synthesis, but it also readily synthesizes 2-5As of 3 or more linked ATPs both *in vivo* and *in vitro* (82). Increased OAS3 sensitivity to dsRNA can be explained by its additional, catalytically inactive OAS units, which retain ability to bind dsRNA (83). Though catalytically inactive itself, deletion of the most N-terminal OAS unit in OAS3 (OAS3.DI) nearly abolished OAS3 catalytic activity and dsRNA binding (83). Given that OAS3 is thought to adopt an elongated conformation (82), dsRNA binding by OAS3.DI may determine OAS3 preference for longer dsRNA substrates, and may explain its greater dependency on dsRNA length for activation as compared to OAS1 (83, 84). This could help OAS3 discriminate self from non-self dsRNA, as long dsRNA is absent from uninfected cells (85). These studies culminated with the novel finding that OAS3 is the primary driver of RNase L antiviral activity (67). The replication of both DNA (vaccinia virus (VV)) and RNA viruses ((+) ssRNA: WNV, Sindbis virus (SINV); (-) ssRNA: influenza A virus (IAV)) was tested in OAS1-3 single KO cells. While wild-type WNV and SINV trigger the OAS/RNase L pathway, wild-type VV and IAV do not due to their active antagonism of the pathway. Therefore, mutant VV and IAV strains that lacked viral antagonists were used. OAS3 KO cells have negligible rRNA degradation and 2-5A production during both poly(I:C) treatment and viral infection, in stark contrast to OAS1 and OAS2 KO cells which had high rRNA degradation and 2-5A production (67). This generally correlated with inhibition of virion production, as OAS3 and RNase L single KO cells had significantly higher viral titers than parental and single OAS1 and OAS2 KO cells for all viruses tested. These data suggest that OAS3 is both necessary and sufficient to drive RNase L-dependent antiviral activity against diverse viruses.

Though OAS3 possesses a dominant role in RNase L-dependent antiviral activity, more antiviral and cellular roles of OAS1 and OAS2 are beginning to be elucidated. In fact, OAS1 and OAS2 are responsible for some antiviral activity against WNV and SINV, albeit to a lesser extent than OAS3/RNase L (67). OAS2 was found to inhibit the (+) ssRNA virus Zika virus (ZIKV) replication through positive regulation of IFN signaling (86). OAS2 may also play a role in lactation, as it was identified in a screen for genes with roles in mammary development (87). Moreover, a novel role for OAS1 and 2-5A synthesis was recently identified in the context of poly-ADP-ribosylation (PAR) and DNA damage-induced cell death (88). As part of the DNA damage response, poly-ADP-ribose polymerase 1 (PARP1) synthesizes PAR polymers to recruit and modify DNA repair proteins (89). Upon resolution of the response, PAR products are hydrolyzed and can trigger apoptosis. ADP-ribose is a known substrate of OAS (90) and addition of 2-5A linkage onto ADP-ribose effectively functions as a chain terminator of PARylation (88). As a result, OAS1 p42 protects cells from DNA damage-induced death by reducing PARP1-mediated PARylation. The absence of OAS1 dramatically increased PAR accumulation within cells upon H_2O_2 treatment, which was not rescued by a catalytically inactive OAS1 mutant (88). These data agree with the observation that cancer cells resistant to DNA-damaging therapies frequently highly express OAS1 (91, 92), as it is hypothesized OAS1 confers resistance to DNA damage-induced cell death.

RNase L: RNA Degradation and Global Translational Arrest

Upon activation by 2-5A, ubiquitous RNA degradation by RNase L simultaneously inhibits many facets of viral replication. Not only does RNase L activity directly degrade single-stranded cellular and viral RNAs, but it also promotes apoptosis, stimulates immune signaling, and induces rapid translational arrest (61).

Activation of RNase L quickly arrests global translation. This rapid translational arrest is traditionally attributed to degradation of transcripts involved in host translation machinery, as evidenced by degradation of 28S and 18S rRNA upon RNase L activation. However, closer examination revealed that at least 50% of 28S rRNA remains and overall tRNA levels are unchanged at the onset of global translation shut-off, challenging this prevailing hypothesis (93). Thus, degradation of translational machinery transcripts cannot explain early translational arrest (93). Another group presents the compelling hypothesis that translational arrest results from almost indiscriminate degradation of cellular RNA by RNase L, crippling gene expression by depriving ribosomes of substrates (94). Comparison of mRNA abundance in parental and RNase L KO A549s revealed reduction in almost all abundant mRNAs in parental, but not in RNase L KO cells after poly(I:C) stimulation. However, some mRNAs are resistant to RNase L cleavage, such as *IFN-β*. Furthermore, mRNAs that substantially increase in both parental and RNase L KO cells in response to poly(I:C) are highly enriched for ISGs such as *IFIT2*, *OAS2*, *MDA5*, and *RIG-I*, suggesting that antiviral mRNAs are resistant to RNase L turnover (94). Determinants of RNase L resistance have yet to be identified. These data are compatible with the independent observation that both type I and III IFN are still produced from seemingly translationally arrested cells (95). Together, these data support a model in which the rapid translational arrest by the OAS-RNase L pathway is doubly beneficial to the organism by both inhibiting viral replication and by permitting antiviral signaling to inhibit viral spread within the host.

RNase L structural studies have uncovered nuances of RNase L substrate selectivity. The first near full-length human RNase L crystal structure allowed for detailed analysis of RNase L dimerization, substrate recognition, and ribonuclease activity (96). In agreement with previous studies that found RNase L cleavage after UU and UA dinucleotides (97), recent structural analysis suggests that RNase L recognizes and cleaves the pattern UN^N (N: any nucleotide, ^: cleavage site) (96). Two different RNA-seq approaches have been utilized to identify RNase L substrates. One approach sequenced RNAs enriched for poly-A-tails after incubating lysates with either 2-5A or pre-activated RNase L. Their results suggest that RNase L selectively degrades

transcripts similar to those regulated by miRNAs, achieving a redundant outcome of suppression of mammalian cell adhesion and proliferation (98, 99). In contrast, another approach capitalized on the characteristic 2',3'-cyclic phosphate termini of RNase L cleavage products. They used a 2',3'-cyclic phosphate RNA-seq analysis in order to identify small RNA cleavage products (93). Here, it was found that most highly-upregulated reads map to tRNAs and Y-RNAs. Analysis of these RNAs revealed site-specific cleavage in both tRNAs and Y-RNAs, which may be shaped by post-transcriptional modifications. Interestingly, though cleavage sites of the tRNAs and other Y-RNAs followed UN^N specificity, the Y-RNA RNY4 was cleaved at CA^G. This unusual cleavage was not recapitulated in the absence of cellular proteins, suggesting that RNase L may acquire site-specificity by recognizing protein/Y-RNA complexes. In this way, RNase L could require co-factors to determine cleavage specificity. It is interesting to speculate that putative co-factors bound to ISG transcripts could also shield cleavage sites to enable their escape from RNase L recognition.

OASL

Though OASL lacks the ability to synthesize 2-5A and thus to participate in RNase L-dependent antiviral activity, it is still potently induced upon IFN stimulation and is also a direct target of IRF3 (100). OASL is composed of an N-terminal, catalytically inactive basal OAS unit followed by a tandem ubiquitin-like domain (UBL) (**Figure 3B**) (43) and possesses antiviral activity against several RNA viruses (27, 68, 101, 102). However, OASL promotes replication of the DNA virus, Kaposi sarcoma herpesvirus (KSHV) (103). These conflicting data can be reconciled by the recently uncovered divergent roles of OASL in both enhancing signaling of the dsRNA sensor RIG-I, thus inhibiting replication of RNA viruses (104), and inhibiting signaling of the cytoplasmic dsDNA sensor cGAS, hence promoting replication of DNA viruses (105, 106). Activation of RIG-I requires its simultaneous binding to dsRNA and poly-ubiquitin chains (107). OASL was shown to interact and colocalize with RIG-I, enhancing RIG-I signaling *via* its C-terminal UBL domain which acts as a poly-ubiquitin mimic to activate RIG-I (104). Furthermore, OASL antiviral activity is suggested to be completely RIG-I dependent, as its viral inhibition is abolished in the absence of RIG-I (104).

Meanwhile, two independent groups simultaneously identified the role of OASL in suppressing cGAS activity (105, 106). One group took a proteomics-based approach to uncover cGAS interactors in the context of herpesvirus infection, identifying OASL as a cGAS interactor and inhibitor (105). Another group utilized a targeted approach to assess the role of OASL during infection with varied DNA viruses, and verified the importance of OASL in promoting DNA viral replication *in vivo* by using a murine model for OASL KO (106). They observed that OASL deficiency results in increased IFN induction and reduced viral titers (106). Both groups found that the OAS-like domain is responsible for interacting with cGAS and that OASL-cGAS interaction is independent of cGAS DNA binding (105, 106). Enzyme inhibition kinetics experiments with OASL, cGAS, and the cGAS substrates ATP and GTP showed that OASL non-competitively inhibits cGAS production of its signaling molecule, cGAMP (106).

The OAS/RNase L pathway effectively inhibits viral replication by linking viral sensing to global inhibition of cellular processes. Widespread RNA degradation by activated RNase L globally not only arrests translation, preventing viruses from synthesizing new proteins, but also still allows for IFNs and several ISGs to be translated, promoting the establishment of an antiviral environment. Furthermore, the catalytically inactive OASL functions as a double-edged sword in its modulation of innate immune signaling, simultaneously inhibiting replication of RNA viruses while enhancing replication of DNA viruses.

MULTIFACETED RNA-DEPENDENT ANTIVIRAL MECHANISMS: FROM TARGETED VIRAL RNA DEGRADATION TO TRANSLATION INHIBITION

The following three ISGs are like the OAS/RNase L pathway in inhibiting viral translation, but dissimilar in their mechanism of inhibition. While the OAS/RNase L pathway employs global translation inhibition, ISG20, ZAP, and SHFL target specific RNA substrates. Furthermore, both ISG20 and ZAP have been shown to directly or indirectly degrade viral RNA, but their RNA degradation differs from OAS/RNase L in two major ways. They target specific viral RNA substrates for degradation, and this activity is independent of their inhibition of viral translation. The multiple, diverse, independent antiviral mechanisms of ISG20, ZAP, and SHFL can be explained through their recruitment of different co-factors, which this section will explore in depth.

ISG20

Antiviral activity of ISG20 has been attributed to two distinct mechanisms so far: degradation of viral RNA and translation inhibition, which can be direct or indirect. ISG20 was first identified as upregulated in response to IFN over 20 years ago (108). ISG20 is expressed in both the cell nucleus and cytoplasm, and is part of the DEDDh subgroup of the larger 3' to 5' DEDD exonuclease superfamily, which possesses a large exonuclease domain (EXO III domain) of about 150 amino acids that can confer DNase and/or RNase activity. The EXO III domain is characterized by three distinct exonuclease motifs defined by four invariant amino acids which lend this superfamily its name: three aspartate (D) and one glutamate (E) residue (109). The DEDDh subgroup also includes a conserved histidine residue. DEDDh exonucleases share a conserved fold and active site but have divergent substrate-binding sites, allowing them to recognize and thus degrade different substrates. Biochemical studies have shown that ISG20 degrades both ssRNA and DNA, with higher nuclease activity against RNA substrates (110).

Because ISG20 is a 3' to 5' RNA exonuclease, it has long been thought that ISG20 antiviral activity results primarily from degradation of viral RNA. In line with this hypothesis, ISG20 has been shown to exhibit antiviral activity primarily against RNA viruses (111). Overexpression and knockdown experiments

show that ISG20 widely suppresses viral replication of diverse (+) ssRNA viruses from *Togaviridae* (SINV), *Flaviviridae* (yellow fever virus (YFV), WNV, HCV), *Picornaviridae* (encephalomyocarditis virus, hepatitis A virus), and (-) ssRNA viruses from *Rhabdoviridae* (vesicular stomatitis virus (VSV)), *Orthomyxoviridae* (IAV), and *Bunyaviridae* (111, 112). ISG20 also inhibits human immunodeficiency virus-1 (HIV-1) and HBV, a DNA virus with an RNA replicative intermediate (36, 37, 113–115). However, ISG20 does not display pan-antiviral activity, as it fails to inhibit severe acute respiratory syndrome coronavirus (SARS-CoV), a member of the (+) ssRNA virus family *Coronaviridae* (38), and adenovirus, a DNA virus (111). The hypothesis that ISG20 degrades viral RNA is supported by reduced expression of various viral mRNAs and replicons in the presence of catalytically active, but not catalytically inactive ISG20 (36, 111, 112, 116).

One long-standing question has been how ISG20 selectively degrades RNA, given that ISG20 does not have any apparent regulatory domains and that its overexpression does not decimate cellular RNA. It is thought that ISG20 may interact with cellular co-factors, supported by its cell-type specific inhibition of YFV (38). The cellular N^6-methyladenosine (m^6A) pathway has been linked to ISG20 antiviral activity in the context of HBV infection. Briefly, m^6A is the most common reversible post-transcriptional modification that occurs on cellular RNAs. The m^6A pathway involves three primary types of proteins—writers, erasers, and readers—which respectively add, remove, and bind m^6A (117). Readers affect stability, translation, and localization of m^6A mRNA (117). One main group of m^6A readers is the YT521-B homology (YTH) domain-containing proteins. The cytoplasmic YTH members (YTHDF1-3) were recently found to play redundant roles in mediating degradation of m^6A-mRNAs (118). HBV transcripts are methylated within the epsilon stem-loop structure (ϵ), which is present at the 3' end of all HBV RNAs and repeated twice in the pregenomic RNA (pgRNA) (37). The HBV polymerase binds the 5' ϵ in pgRNA to initiate packaging and reverse transcription. ISG20 was shown to inhibit HBV replication by binding to ϵ (115). Furthermore, ϵ contains a conserved m^6A consensus sequence that negatively regulates HBV RNA stability in a YTHDF2-dependent manner (119). It was then demonstrated that YTHDF2 and ISG20 interact in an HBV-independent manner and that depletion of YTHDF2 abolishes IFN-dependent HBV RNA degradation (37). They propose that m^6A modification of ϵ is recognized by YTHDF2, which then recruits ISG20 to target HBV pgRNA for RNA degradation (**Figure 4A**). Based on these data, YTHDF2 was identified as an essential ISG20 co-factor, marking the first time any group has identified a regulator of ISG20 substrate specificity.

Still, the role of RNA degradation in ISG20 antiviral activity remains open for debate. Multiple studies have shown that ISG20 overexpression inhibits viral replication in an exonuclease-dependent manner, and several have observed a corresponding decrease in viral RNA (38, 111–113, 120). Moreover, most studies on ISG20 have utilized the catalytically inactive mutant D94G (110) to support the hypothesis that ISG20 exonuclease

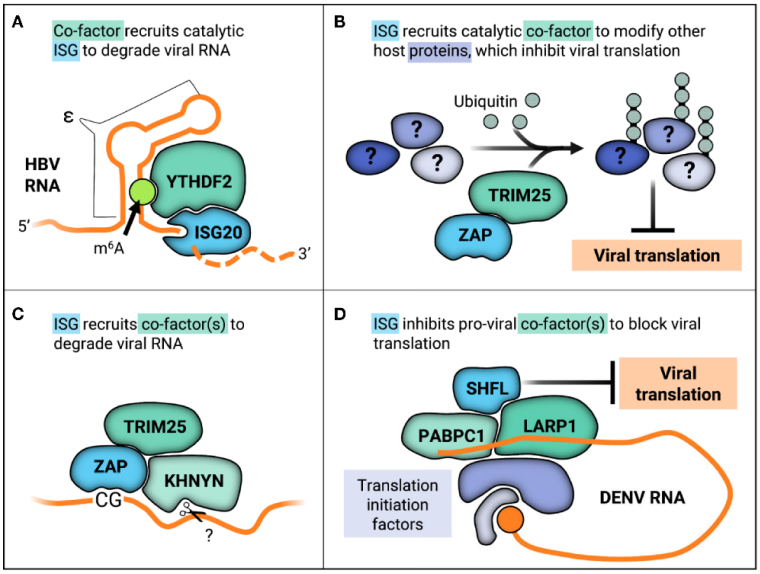

FIGURE 4 | ISGs work with co-factors in varied ways to inhibit viral replication through diverse mechanisms. **(A)** YTHDF2 recognizes m^6A methylation on the ϵ in HBV RNA transcripts, recruiting catalytic ISG20 to degrade HBV RNA. **(B)** ZAP recruits TRIM25 to ubiquitinate other host proteins, which may alter their native cellular or viral-associated activities in order to inhibit viral translation. **(C)** ZAP recognizes CG motifs in viral RNA and forms a complex with TRIM25 and the endonuclease KHNYN, which then putatively cleaves ZAP-bound RNA. **(D)** SHFL inhibits DENV replication by interacting with the viral RNA 3'UTR binding proteins PABPC1 and LARP1 and potentially inhibiting recruitment of further translation machinery.

activity is required for antiviral activity (38, 111–113, 116, 120, 121). This invariant residue is crucial to ISG20 structure as it helps coordinate an Mn^{2+} ion in the active site (122). It is unknown what other deleterious effects D94G may have on the overall structure of ISG20. One group mutated all Asp residues in the DEDDh catalytic motif to Gly (D11G, D94G, and D154G) and found that while all three mutations abolished exonuclease activity, only D11G and D94G also lost antiviral activity against HBV. Surprisingly, the exonuclease-deficient ISG20-D154G was still able to inhibit HBV replication (36). This suggests that ISG20 possesses both exonuclease-dependent and -independent antiviral activities.

Recently, two groups have independently found that ISG20 mediates antiviral activity through translation inhibition and not RNA degradation, but propose two divergent mechanisms (121, 123). One group proposes that ISG20-mediated translation inhibition is indirect, mediated through ISG20-dependent upregulation of other ISGs (123). They found that overexpression of ISG20 upregulates expression of many IRF3-dependent genes in mouse embryonic fibroblasts, such as IFIT1, an ISG that inhibits translation of viral RNA with non-2'O-methylated 5' caps (124). Furthermore, they showed that mutant alphavirus normally recognized and attenuated by IFIT1 is equally virulent as the wild-type virus in the absence of ISG20 *in vivo*, suggesting that ISG20 inhibits translation by promoting IFIT1 expression (123). On the contrary, the second group proposes that ISG20 is critical for discrimination of non-self nucleic acids from self to inhibit viral translation (121). By examining luciferase reporter activity, they found that ISG20 inhibited translation for all exogenous DNA of both viral and host origins. However, when a CMV-GFP cassette was integrated into the host genome, ISG20 failed to inhibit GFP produced from this context as it did when the identical cassette was transfected into the same cells. They also generated a series of mutants outside of the invariant DEDD residues to explore how non-exonuclease regions impact ISG20 antiviral activity. Notably, mutations predicted to affect phosphorylation and cellular trafficking but not exonuclease activity still lose antiviral activity against VSV. This loss of antiviral activity correlates with inability to inhibit translation of non-self nucleic acids. Contrary to previous findings, the second group did not find that ISG20 induces IFIT1 expression in HEK293T or U937 cells. They propose instead that ISG20 recruits foreign RNA to P bodies, sites of RNA storage, where translation is repressed in the absence of RNA degradation (121).

All in all, ISG20 effectively inhibits viral replication by degrading or inhibiting translation of specific RNAs. ISG20 co-opts the cellular m^6A pathway component, YTHDF2, to recognize and target modified HBV RNA (37). ISG co-factors such as IFIT1 may also be required in ISG20 translation inhibition, as ISG20 does not globally arrest translation like the OAS/RNase L pathway, but rather specifically targets non-self transcripts.

ZAP

ZAP, encoded by the gene *ZC3HAV1*, is a potent antiviral factor which broadly inhibits replication of HIV-1 (*Retroviridae*), HBV (*Hepadnaviridae*), the (-) ssRNA viruses Ebola virus (EBOV, *Filoviridae*) and IAV (*Orthomyxoviridae*), and (+) ssRNA viruses such as alphaviruses (*Togaviridae*), coxsackievirus B3 (CVB3, *Picornaviridae*), and Japanese encephalitis virus (JEV, *Flaviviridae*) (125–132). ZAP antiviral activity can be selective within viral families and genera, as not all flaviviruses and picornaviruses tested are sensitive to ZAP (126, 131). It also post-transcriptionally regulates expression of cellular mRNA (133) and restricts retrotransposition of human retrotransposons (134, 135). ZAP possesses four N-terminal zinc fingers (136) that directly bind to viral RNA, are required for antiviral activity, and dictate its mostly cytoplasmic and stress granule localization (134, 137–139). Phosphorylation of this minimal antiviral N-terminal region by glycogen synthase kinase 3β enhances ZAP antiviral activity, though its mechanistic contribution remains unclear (140). Alternative splicing results in multiple splice variants which differ from one another in expression, localization, and antiviral activity. ZAP is also known as PARP13, due to poly-ADP-polymerase 13 (PARP13), due to the inclusion of a catalytically inactive C-terminal PARP-like domain in its long splice variant (ZAPL). In addition to a short splice variant that lacks this C-terminal domain (ZAPS), alternative splicing of a 121 aa extension of exon 4 results in two additional splice variants ZAPM and ZAPXL, whose antiviral activities are similar to ZAPS and ZAPL, respectively (141).

ZAP targets viruses primarily by two distinct antiviral mechanisms, namely viral translation inhibition (for the (+) ssRNA viruses SINV and JEV) and viral RNA degradation (for HIV-1, HBV, the (-) ssRNA virus EBOV, and the (+) ssRNA viruses CVB3 and JEV). These disparate mechanisms can be explained in part by recruitment of co-factors and differing viral contexts. ZAP inhibition of SINV translation has been linked to its disruption of the interaction between translation initiation factors eIF4A and eIF4G (142). This disruption does not affect global translation seeing as polysome profiles were unchanged when ZAP was overexpressed (142). ZAP is also able to repress translation of a luciferase reporter containing the minimal ZAP responsive fragment in the SINV genome without promoting degradation of the reporter (142). More recently, the E3 ligase tripartite motif-containing protein 25 (TRIM25) was uncovered as a novel ZAP co-factor in the context of alphavirus infection (47, 143). TRIM25 is absolutely required for inhibition of viral translation by ZAP, as ZAP is unable to inhibit translation of a replication-deficient reporter virus in TRIM25-deficient cells (47). Not only is TRIM25 putatively required for ZAP recognition of its RNA substrates, as TRIM25 knockdown decreases ZAP association with luciferase reporter RNA, but also TRIM25 ubiquitin ligase activity is essential for ZAP antiviral activity (47, 143). Curiously, though TRIM25 ubiquitinates ZAP, TRIM25 still contributes to ZAP antiviral activity in the presence of a ubiquitination-deficient ZAP mutant (47), suggesting that TRIM25-mediated ubiquitination of host factors other than ZAP is critical for the inhibitory effects (**Figure 4B**). Moreover, it is likely that K63-linked ubiquitination is required for ZAP antiviral activity, as overexpression of a ubiquitin K63R mutant unable to form K63 linkages reduces ZAP inhibition of SINV replication (143). The identity of these TRIM25 substrates that function in ZAP antiviral

activity remains to be discovered, as does how they contribute to viral translation suppression.

Apart from inhibiting viral translation, ZAP also induces viral RNA degradation by recruiting an array of RNA helicases, the endonuclease KHNYN, and exosome components (144–147). ZAP selectively affects cellular transcripts, as it destabilizes the TRAILR4 mRNA and inhibits retrotransposition of endogenous retroelements such as Long INterspersed Element-1 (LINE-1) and Alu (133, 134). ZAP substrate specificity determinants largely remained a mystery until it was demonstrated to inhibit HIV-1 with synonymous, elevated CG dinucleotide mutations (HIV^{CG}) but not wild-type HIV-1 (148). Interestingly, only elevation of CG dinucleotides in the 5' third of the HIV-1 envelope gene caused ZAP susceptibility (149). Solving the crystal structure of ZAP in complex with CG-rich RNA revealed that ZAP has a CG-dinucleotide specific binding pocket and binds to ss nucleic acids (150, 151). ZAP preference for CG-rich substrates could explain in part why many RNA viruses infecting mammals and other vertebrates, such as IAV and SARS-CoV-2, exhibit CG suppression (152–155). ZAP can even sense CG dinucleotides within individual RNA transcripts of DNA viruses, as in the case of human cytomegalovirus (156). Here, CG suppression within the major immediate early transcript 1 confers ZAP resistance (156). However, CG suppression does not always confer resistance to ZAP as in the case of SARS-CoV-2 (154). Though initially identified in the context of translation inhibition, ZAP was also shown to form a complex with TRIM25 and the endonuclease KHNYN to inhibit HIV^{CG} (**Figure 4C**) and knockdown of KHNYN abolished HIV^{CG} sensitivity to ZAP (147).

All three ZAP antiviral activities of CG dinucleotide sensing, RNA degradation, and translation inhibition were linked in the context of JEV infection, wherein ZAP bound CG-rich regions of JEV RNA and inhibited translation at early time points without RNA degradation, and degraded RNA in an exosome-dependent manner at later time points of a JEV replicon (131). Therefore, ZAP can block viral translation in the context of alphavirus infection, target viral RNA for degradation in the context of retrovirus infection, and do both in the context of JEV infection.

To complicate matters further, ZAP splice variants also display differences in antiviral activity. ZAPL is more antiviral than ZAPS (141, 157). This boost to antiviral activity is attributed to its PARP-like domain. Not only does the PARP-like domain carry signatures of positive selection (157), but it also has a prenylation motif that targets ZAPL to endolysosomes (158, 159). Addition of this prenylation motif to ZAPS increases its antiviral activity, though not to the same extent as ZAPL (159). Curiously enough, ZAPL's catalytically dead PARP triad motif is required for its antiviral activity; its replacement with the canonical active PARP motif abolishes ZAPL antiviral activity, though it remains unclear how this inactive motif is required (160). Furthermore, ZAPL is constitutively expressed in cells, while ZAPS expression is induced by innate immune signaling (141, 159). Studies conflict as to how ZAPS contributes to innate immune signaling. Though one group showed that ZAPS stimulates RIG-I dependent IFN response upon stimulation with a RIG-I RNA agonist (161), others found that ZAP mediates a RIG-I-independent antiviral response to retroviruses and HBV (128, 162, 163). More recently, ZAPS was shown to negatively regulate the type I IFN response by binding to and stimulating the degradation of *IFN* mRNAs; ZAP-deficient Huh7 cells had a higher and more prolonged IFN response upon treatment with a RIG-I agonist (159). On the other hand, ZAPS was found to synergize with other ISGs, wherein 31 ISGs have a statistically significant increase in antiviral activity in the presence of ZAP (32). In addition to its role as a co-factor in ZAP translation inhibition and CG sensing, TRIM25 may also modulate expression of ZAP isoforms by regulating alternative splicing, wherein TRIM25 is required for efficient expression of ZAPS (156).

All in all, ZAP inhibition of viral replication layers in complexity through its diverse mechanisms of translation inhibition and RNA degradation, recruitment of varied co-factors, and further differences between splice variants. The differing C-termini, expression kinetics, and cellular localization between splice variants could facilitate recruitment of divergent co-factors to enable different antiviral roles. As the PARP-like domain of ZAPL lacks any catalytic activity, it likely acts as an interaction domain to recruit specific co-factors that might be ADP-ribosylated to effect the RNA-centric antiviral mechanisms of ZAP.

SHFL

SHFL, variously referred to as C19orf66, RyDEN, IRAV, or FLJ11286, is a 291 amino acid protein that is predicted to consist of eight α-helices and seven β-strands and possess both a nuclear export and localization signal, a zinc-ribbon domain, and a coiled-coil motif (164). SHFL binds nucleic acids and shows greater preference for ss nucleic acids and for RNA over DNA *via* fluorescence polarization assays (165). No catalytic activity is currently attributed to SHFL.

In uninfected cells, SHFL resides primarily in the cytoplasm in punctate structures, associating with both stress granule and P body proteins in HEK293 and Huh7.5 cells (165, 166), but was also more recently identified as an antiviral effector counteracting replication of RNA viruses (27, 28, 164, 167). For example, SHFL broadly inhibits replication of members of the (+) ssRNA virus family *Flaviviridae*, including all four DENV serotypes, WNV, ZIKV, and HCV (164–166, 168). SHFL also inhibits the virion production of chikungunya virus and SINV, members of the (+) ssRNA virus family *Togaviridae*. However, SHFL selectively inhibits members of another (+) ssRNA family, *Picornaviridae*, inhibiting replication of encephalomyocarditis virus but not poliovirus or enterovirus 71 (164, 165). SHFL selective inhibition also extends to DNA viruses, as its overexpression inhibits virion production of *Adenoviridae* member human adenovirus type 3, and *Herpesviridae* members KSHV and herpes simplex virus-1 (HSV-1), but not HSV-2 (164, 169).

A recently proposed mechanism for SHFL antiviral activity is suppression of viral translation. In line with this hypothesis, SHFL associates specifically with DENV RNA (164) and co-immunoprecipitates with other RNA-binding proteins that bind to mRNA 3' UTRs such as PABPC1, LARP1, MOV10, and UPF1 (164, 165). Given that PABPC1 is critical for translation, overexpression of SHFL suppresses translation of a DENV replication-deficient

luciferase reporter (164). Co-immunoprecipitation and immunofluorescence techniques were used to show that SHFL interacts with MOV10 and UPF1 even in the presence of RNase A, though the interaction was diminished (165). It is likely that SHFL mediates viral translation inhibition by interacting with the viral RNA 3'UTR binding proteins such as PABPC1 and LARP1 to block recruitment of further translation machinery (**Figure 4D**).

A separate, better characterized mechanism that SHFL utilizes to block viral translation is its broad inhibition of -1 programmed ribosomal frameshifting (-1PRF) which is crucial for many viruses to control protein expression levels (54). SHFL inhibits HIV-1 replication by altering the Gag to Gag-Pol protein ratio *via* inhibition of -1PRF, wherein knockdown of SHFL results in increased Gag-Pol expression without obviously altering either Gag or capsid expression (54). Noticeably, these data are in agreement with previous findings of unchanged p24 levels upon SHFL overexpression, which were originally interpreted as evidence that HIV-1 is not inhibited by SHFL (164). SHFL was also demonstrated to inhibit both viral and cellular mRNAs -1PRF signals in the context of a dual luciferase reporter construct (54). It is important to note that overall cellular translation and protein expression and ISG expression are unchanged in the presence of SHFL overexpression or knockdown in Huh7.5 cells (166), supporting the notion that SHFL antiviral activity is not due to modulating ISG expression or alteration of global translation (166).

However, SHFL may also act on some viruses independent of its direct effects on viral translation. For example, SHFL associates with the flavivirus replication complex in both DENV and ZIKV infections and interacts specifically with nonstructural protein 3 (NS3) in an RNA-independent manner (165, 168). By doing so, SHFL induces lysosomal-mediated degradation of NS3 in ZIKV-infected cells. SHFL is thought to inhibit HCV replication by interfering with the HCV-induced remodeling of the ER, which generates a membranous web that scaffolds assembly of viral replication complexes (166).

Taken together, SHFL inhibits viral replication by regulating translation through -1PRF-dependent and independent mechanisms and by specific antagonism of viral proteins and structures. SHFL displays both RNA-independent and -dependent interactions with other proteins, relying on RNA for its interaction with cellular RNA helicases MOV10 and UPF1 while interacting with flavivirus NS3 in the absence of RNA. These varied requirements for protein-protein interactions may reflect SHFL's diverse antiviral mechanisms.

RING IN VIRAL TRANSCRIPTION: UBIQUITIN LIGASE-DEPENDENT AND -INDEPENDENT INHIBITION

The really interesting new gene (RING) proteins are the most abundant family of E3 ligases, characterized by their N-terminal catalytic RING domain. E3 ligases occupy the final step in cellular ubiquitination. Ubiquitination of a protein can alter its cellular fate depending on the type of linkage, ranging from proteasomal degradation to scaffold formation for assembly of cellular signaling complexes (170). In order for ubiquitin to be ligated to an acceptor lysine, it must be sequentially activated by the E1 enzyme, carried by the E2 conjugating enzyme, and finally ligated to an acceptor lysine by one of over 600 human E3 ligases. Though many of the antiviral effectors mentioned in this section have other known cellular and antiviral roles, this section will focus on how IFN-inducible RING ligases inhibit viral transcription by both ligase-dependent and -independent mechanisms.

RBBP6: Ligase-Independent Viral Mimicry

Retinoblastoma binding protein 6 (RBBP6) is a RING E3 ligase that inhibits transcription of the (-) ssRNA virus EBOV (*Filoviridae)* (53). RBBP6 was identified in an affinity-purification mass spectrometry screen to map host-EBOV protein-protein interactions as the most robust host interactor with the EBOV transcription regulator viral protein 30 (VP30) (53). RBBP6 competes with the EBOV nucleoprotein for binding to VP30 in an RNA-independent manner; the minimal RBBP6 interaction motif is sufficient to inhibit viral transcription, demonstrating a ligase-independent antiviral mechanism for RBBP6 (53). However, full-length RBBP6 causes dose-dependent decrease of VP30 protein in a manner dependent on the RBBP6-VP30 interaction, potentially suggesting a ligase-dependent antiviral mechanism (53). Curiously, RBBP6 also causes a dose-dependent decrease of VP30 mRNA independent of RBBP6-VP30 interaction. This suggests that RBBP6 either degrades VP30 mRNA through an uncharacterized exonuclease domain or recruits co-factor(s) that possess exonuclease activity (53). Knockdown of RBBP6 enhances EBOV RNA synthesis and replication. Taken together, these results suggest that RBBP6 inhibits EBOV replication through a three-pronged approach, and that both ligase-dependent and -independent antiviral mechanisms and exonuclease-dependent mechanism may be waiting to be further characterized.

TRIMming Viral Transcription

The tripartite motif containing proteins (TRIM) are the largest group of RING E3 ligases and constitute an important family of proteins in the type I IFN response (171, 172). There are over 70 human TRIM proteins, many of which are induced by type I IFN (171, 173). Interestingly, the rapid expansion of the TRIM family coincides with the development of adaptive immunity, suggesting that TRIMs may have evolved to play a role in immune regulation (171). These proteins typically possess three conserved domains at the N-terminus—a catalytic RING domain, one to two B-box domains that are thought to function in higher order oligomerization, and a coiled-coil domain that allows TRIMs to dimerize and potentially oligomerize (174). Most TRIMs directly inhibit viral replication by targeting viral components for degradation, or indirectly inhibit by modulating innate immune signaling (175, 176).

Multiple TRIM members have been found to inhibit viral transcription *via* both ligase-dependent and -independent mechanisms. TRIM22 does both, though its ligase activity is required to inhibit HBV transcription, it inhibits HIV-1

transcription independent of its ligase activity (177–179). TRIM22 inhibits HBV core promoter activity, which is critical for HBV pgRNA synthesis and hence viral transcription and reverse transcription (177, 180). A single point mutation in its RING domain abolishes its inhibition of viral replication, strongly implicating ligase activity in anti-HBV effects of TRIM22 (177). Meanwhile, TRIM22 inhibits HIV-1 basal transcription independent of its ligase activity by indirectly preventing the transcription factor specific protein 1 (Sp1) from binding to the HIV-1 promoter, thus facilitating HIV-1 latency (181, 182). As TRIM22 neither directly interacts with Sp1 nor binds to the HIV-1 promoter, it is possible that TRIM22 recruits another co-factor to alter chromatin state or stimulate Sp1 post-translational modification (181). Two independent TRIMs inhibit IAV transcription, a (-) ssRNA virus. TRIM32 depends on its ligase activity, ubiquitinating the core component of the IAV RNA polymerase complex and targeting it for degradation, subsequently reducing polymerase activity (57). On the other hand, TRIM25 restricts IAV RNA synthesis in a ligase-independent manner by binding to viral ribonucleoproteins and blocking RNA chain elongation (56).

TRIM69 is a more recently identified ISG and antiviral effector that shares high homology with TRIM25. Recently, two independent groups found that TRIM69 inhibits replication of the Indiana strain of VSV (VSV_{IND}), a (-) ssRNA virus, in ligase-independent manner (58, 59). Both groups identified TRIM69 through targeted screens using complementary approaches, either overexpressing an array of known ISGs or knocking down VSV-induced host genes (58). In addition, both groups found that TRIM69 inhibition of VSV is highly specific, as overexpression of TRIM69 fails to inhibit the New Jersey strain of VSV (VSV_{NJ}) or other negative-strand RNA viruses such as SeV, rabies virus, or IAV (58, 59). VSV_{IND} sensitivity to TRIM69 was mapped to a short peptide sequence within the viral phosphoprotein P by serial passaging VSV_{IND} in the presence of TRIM69 overexpression and sequencing escape mutants (58, 59). VSV_{NJ} differs from VSV_{IND} at five out of six amino acids within this TRIM69 P sensitivity determinant, potentially explaining differential resistance between VSV strains. TRIM69 physically associates with VSV_{IND} P but does not require its ligase activity or target it for degradation. Instead, TRIM69-inhibition of VSV_{IND} requires its multimerization in order to sequester VSV_{IND} P into filamentous structures, thus disrupting viral replication machinery.

To summarize, RING E3 ligases combat viral transcription in myriad ways. Many do not rely on their ligase activity to inhibit transcription by directly binding to components of viral transcription machinery to inhibit protein-protein interactions, such as RBBP6, TRIM25, and TRIM69. Others ubiquitinate viral components to target them for degradation, such as TRIM22 and TRIM32.

DISCUSSION

Inhibition of viral replication by ISGs grows more nuanced as every new study promises to uncover new facets of antiviral or pro-viral activity. Even well-characterized ISGs such as OAS/RNase L, ISG20, and ZAP have had new aspects of their antiviral mechanisms come to light in recent years. RNA viruses present a plethora of unique viral RNA processes that host cells can identify and inhibit. They rely on their own viral RNA-dependent RNA polymerases to transcribe and replicate genomic RNA, generating dsRNA intermediates that host cells recognize as foreign. Each RNA-centric antiviral mechanism mentioned in this review affords specific advantages and disadvantages. Blocking viral translation is especially effective against positive-stranded RNA viruses, which must translate their incoming genomes before any further steps in viral replication can occur. Likewise, inhibiting viral transcription is especially effective against negative-stranded RNA viruses, which prioritize transcribing their genomes upon entry. While degrading genomes outright appears to be the most straightforward and universal way to inhibit replication of RNA viruses, RNA degradation presents its own set of challenges of distinguishing foreign from self RNA. In the case of OAS/RNase L, dsRNA sensing by OAS leads to virtually indiscriminate degradation of viral and host RNAs, curtailing viral replication but also killing the infected cell. Some especially pathogenic viruses such as Middle East respiratory syndrome coronavirus (MERS-CoV) circumvent RNA degradation by enzymatically degrading 2-5A, thus preventing RNase L activation (183). Meanwhile, other ISGs, such as ZAP, recognize specific motifs in the viral genome distinct from host genomes so only viral RNA is selectively targeted. However, ZAP specificity for CG dinucleotides may have driven selection against high CG content in RNA viral genomes, thus potentially rendering ZAP ineffective (152, 153).

The perpetual arms race between antiviral effectors and viruses has likely driven the development of multilayered mechanisms of viral inhibition. Some individual ISGs have acquired multiple antiviral mechanisms, enabling them to circumvent viral evasion. For example, ZAP is still able to inhibit replication of SARS-CoV-2, a positive-sense ssRNA virus with highly suppressed CG content (154). This suggests that ZAP inhibits SARS-CoV-2 not by CG sensing alone and that there are likely additional sequence or structural motifs that are recognized and targeted by ZAP. Another way ISGs may prevent viral evasion is through the use of co-factors, which could function as a natural "antiviral cocktail" (**Figure 4**). By using co-factors, host cells employ a multipronged attack on viral replication that could help minimize evasion by RNA viruses. ISGs that work in concert to recognize specific viral RNA motifs could make it difficult for viruses to simultaneously mutate all recognizable motifs in their genomes. Though it is known that TRIM25 functions as a ZAP co-factor (47, 143), that both TRIM25 and ZAP bind RNA (48, 139, 184, 185), and that RNA binding is crucial for their antiviral activity (136, 185), it remains unexplored whether TRIM25 and ZAP work together to recognize viral RNA substrates or motifs or both. TRIM25 and ZAP putative cooperation in viral recognition could help explain why many alphaviruses have not acquired ZAP resistance and remain acutely sensitive to its inhibition (126, 141).

In-depth characterization of ISG antiviral mechanisms and methods of viral evasion has been facilitated by rapid expansion of CRISPR-Cas technologies. For example, identification of OAS3 as necessary and sufficient for RNase L activation was enabled by generation of single OAS KO cell lines (67). CRISPR-Cas technologies have also enabled the discovery and interrogation of functions of novel ISGs and their splice variants or polymorphisms (186). Genome-wide CRISPR-Cas9 KO and targeted ISG overexpression screens have been used to great effect, identifying novel host factors and highlighting important antiviral ISGs to characterize [reviewed in (20)]. One exciting new avenue for RNA-centric ISG identification lies at the intersection of chemical biology. Generation of nucleotide analogs that can be incorporated into RNA, cross-linked to proximally bound proteins, and immunoprecipitated for subsequent proteomic analysis enables the identification of novel RNA-binding proteins (187). Variations on this approach have been used several times in the context of positive-sense RNA virus infections by *Togaviridae* and *Flaviviridae* family members to elucidate new host-virus interactions (49, 188–190). It is not always feasible to target host factors required for viral replication, since these host factors may also be essential for cell survival. Furthermore, overexpression of any given protein may yield false phenotypes that are not biologically relevant. In contrast, *in situ* labeling and identification of endogenous RNA-binding proteins offers a more specific and minimally disruptive approach with fewer effects on cell viability. Cross-referencing ISGs with novel viral RNA-binding proteins could yield promising candidates to characterize and open up new horizons for antiviral exploration.

AUTHOR CONTRIBUTIONS

EY and ML determined the scope and focus of the review. EY drafted the manuscript and generated all figures. ML provided critical feedback on the manuscript. All authors contributed to the article and approved the submitted version.

FUNDING

This work was supported in part by the UC Cancer Research Coordinating Committee Faculty Seed Grant (CRN-20-637544; M.M.L.), UCLA AIDS Institute and Charity Treks 2019 Seed Grant (ML), and Ruth L. Kirschstein Multidisciplinary Training Grant in Microbial Pathogenesis (NRSA AI007323; EY).

ACKNOWLEDGMENTS

We thank Michael Emerman and Quan (Dylan) Zhou for critically reading the manuscript.

REFERENCES

1. Au-Yeung N, Horvath CM. Transcriptional and chromatin regulation in interferon and innate antiviral gene expression. *Cytokine Growth Factor Rev* (2018) 44:11–7. doi: 10.1016/j.cytogfr.2018.10.003
2. Wang W, Xu L, Su J, Peppelenbosch MP, Pan Q. Transcriptional Regulation of Antiviral Interferon-Stimulated Genes. *Trends Microbiol* (2017) 25:573–84. doi: 10.1016/j.tim.2017.01.001
3. Morrow AN, Schmeisser H, Tsuno T. Zoon KC. A Novel Role for IFN-Stimulated Gene Factor 3II in IFN-γ Signaling and Induction of Antiviral Activity in Human Cells. *J Immunol* (2011) 186:1685–93. doi: 10.4049/jimmunol.1001359
4. Fink K, Grandvaux N. STAT2 and IRF9. *JAK-STAT* (2013) 2:e27521. doi: 10.4161/jkst.27521
5. Cheon H, Holvey-Bates EG, Schoggins JW, Forster S, Hertzog P, Imanaka N, et al. IFNβ-dependent increases in STAT1, STAT2, and IRF9 mediate resistance to viruses and DNA damage. *EMBO J* (2013) 32:2751–63. doi: 10.1038/emboj.2013.203
6. Sung PS, Cheon H, Cho CH, Hong S-H, Park DY, Seo H-I, et al. Roles of unphosphorylated ISGF3 in HCV infection and interferon responsiveness. *PNAS* (2015) 112:10443–8. doi: 10.1073/pnas.1513341112
7. Platanias LC. Mechanisms of type-I- and type-II-interferon-mediated signalling. *Nat Rev Immunol* (2005) 5:375–86. doi: 10.1038/nri1604
8. Fish EN, Uddin S, Korkmaz M, Majchrzak B, Druker BJ, Platanias LC. Activation of a CrkL-Stat5 Signaling Complex by Type I Interferons. *J Biol Chem* (1999) 274:571–3. doi: 10.1074/jbc.274.2.571
9. Escalante CR, Yie J, Thanos D, Aggarwal AK. Structure of IRF-1 with bound DNA reveals determinants of interferon regulation. *Nature* (1998) 391:103–6. doi: 10.1038/34224
10. Bartee E, Mohamed MR, Lopez MC, Baker HV, McFadden G. The Addition of Tumor Necrosis Factor plus Beta Interferon Induces a Novel Synergistic Antiviral State against Poxviruses in Primary Human Fibroblasts. *J Virol* (2009) 83:498–511. doi: 10.1128/JVI.01376-08
11. Wang W, Xu L, Brandsma JH, Wang Y, Hakim MS, Zhou X, et al. Convergent Transcription of Interferon-stimulated Genes by TNF-α and IFN-α Augments Antiviral Activity against HCV and HEV. *Sci Rep* (2016) 6:25482. doi: 10.1038/srep25482
12. Mestan J, Brockhaus M, Kirchner H, Jacobsen H. Antiviral Activity of Tumour Necrosis Factor. Synergism with Interferons and Induction of Oligo-2′,5′-adenylate Synthetase. *J Gen Virol* (1988) 69:3113–20. doi: 10.1099/0022-1317-69-12-3113
13. Lee J, Tian Y, Chan ST, Kim JY, Cho C, Ou JJ. TNF-α Induced by Hepatitis C Virus via TLR7 and TLR8 in Hepatocytes Supports Interferon Signaling via an Autocrine Mechanism. *PloS Pathog* (2015) 11:e1004937. doi: 10.1371/journal.ppat.1004937
14. Lucas-Hourani M, Dauzonne D, Jorda P, Cousin G, Lupan A, Helynck O, et al. Inhibition of Pyrimidine Biosynthesis Pathway Suppresses Viral Growth through Innate Immunity. *PloS Pathog* (2013) 9:e1003678. doi: 10.1371/journal.ppat.1003678
15. Pan Q, de Ruiter PE, Metselaar HJ, Kwekkeboom J, de Jonge J, Tilanus HW, et al. Mycophenolic acid augments interferon-stimulated gene expression and inhibits hepatitis C Virus infection in vitro and in vivo. *Hepatology* (2012) 55:1673–83. doi: 10.1002/hep.25562
16. Chung D-H, Golden JE, Adcock RS, Schroeder CE, Chu Y-K, Sotsky JB, et al. Discovery of a Broad-Spectrum Antiviral Compound That Inhibits Pyrimidine Biosynthesis and Establishes a Type 1 Interferon-Independent Antiviral State. *Antimicrobial Agents Chemother* (2016) 60:4552–62. doi: 10.1128/AAC.00282-16
17. Wang Y, Wang W, Xu L, Zhou X, Shokrollahi E, Felczak K, et al. Cross Talk between Nucleotide Synthesis Pathways with Cellular Immunity in Constraining Hepatitis E Virus Replication. *Antimicrob Agents Chemother* (2016) 60:2834–48. doi: 10.1128/AAC.02700-15
18. Rusinova I, Forster S, Yu S, Kannan A, Masse M, Cumming H, et al. INTERFEROME v2.0: an updated database of annotated interferon-regulated genes. *Nucleic Acids Res* (2013) 41:D1040–6. doi: 10.1093/nar/gks1215

19. Schneider WM, Chevillotte MD, Rice CM. Interferon-Stimulated Genes: A Complex Web of Host Defenses. *Annu Rev Immunol* (2014) 32:513–45. doi: 10.1146/annurev-immunol-032713-120231
20. Schoggins JW. Interferon-Stimulated Genes: What Do They All Do? *Annu Rev Virol* (2019) 6:567–84. doi: 10.1146/annurev-virology-092818-015756
21. Lazear HM, Schoggins JW, Diamond MS. Shared and Distinct Functions of Type I and Type III Interferons. *Immunity* (2019) 50:907–23. doi: 10.1016/j.immuni.2019.03.025
22. Melki I, Frémond M-L. Type I Interferonopathies: from a Novel Concept to Targeted Therapeutics. *Curr Rheumatol Rep* (2020) 22:32. doi: 10.1007/s11926-020-00909-4
23. Chemudupati M, Kenney AD, Bonifati S, Zani A, McMichael TM, Wu L, et al. From APOBEC to ZAP: Diverse mechanisms used by cellular restriction factors to inhibit virus infections. *Biochim Biophys Acta (BBA) Mol Cell Res* (2019) 1866:382–94. doi: 10.1016/j.bbamcr.2018.09.012
24. Liao Y, Goraya MU, Yuan X, Zhang B, Chiu S-H, Chen J-L. Functional Involvement of Interferon-Inducible Transmembrane Proteins in Antiviral Immunity. *Front Microbiol* (2019) 10:1097. doi: 10.3389/fmicb.2019.01097
25. Haller O, Staeheli P, Schwemmle M, Kochs G. Mx GTPases: dynamin-like antiviral machines of innate immunity. *Trends Microbiol* (2015) 23:154–63. doi: 10.1016/j.tim.2014.12.003
26. Ganser-Pornillos BK, Pornillos O. Restriction of HIV-1 and other retroviruses by TRIM5. *Nat Rev Microbiol* (2019) 17:546–56. doi: 10.1038/s41579-019-0225-2
27. Schoggins JW, Wilson SJ, Panis M, Murphy MY, Jones CT, Bieniasz P, et al. A diverse range of gene products are effectors of the type I interferon antiviral response. *Nature* (2011) 472:481–5. doi: 10.1038/nature09907
28. Li J, Ding SC, Cho H, Chung BC, Gale M, Chanda SK, et al. A Short Hairpin RNA Screen of Interferon-Stimulated Genes Identifies a Novel Negative Regulator of the Cellular Antiviral Response. *mBio* (2013) 4(3):e00385–13. doi: 10.1128/mBio.00385-13
29. Subramanian G, Kuzmanovic T, Zhang Y, Peter CB, Veleeparambil M, Chakravarti R, et al. A new mechanism of interferon's antiviral action: Induction of autophagy, essential for paramyxovirus replication, is inhibited by the interferon stimulated gene, TDRD7. *PloS Pathog* (2018) 14:e1006877. doi: 10.1371/journal.ppat.1006877
30. OhAinle M, Helms L, Vermeire J, Roesch F, Humes D, Basom R, et al. A virus-packageable CRISPR screen identifies host factors mediating interferon inhibition of HIV. *eLife* (2018) 7:e39823. doi: 10.7554/eLife.39823
31. Hubel P, Urban C, Bergant V, Schneider WM, Knauer B, Stukalov A, et al. A protein-interaction network of interferon-stimulated genes extends the innate immune system landscape. *Nat Immunol* (2019) 20:493–502. doi: 10.1038/s41590-019-0323-3
32. Karki S, Li MMH, Schoggins JW, Tian S, Rice CM, MacDonald MR. Multiple Interferon Stimulated Genes Synergize with the Zinc Finger Antiviral Protein to Mediate Anti-Alphavirus Activity. *PloS One* (2012) 7:e37398. doi: 10.1371/journal.pone.0037398
33. Samuel CE. Adenosine deaminase acting on RNA (ADAR1), a suppressor of double-stranded RNA–triggered innate immune responses. *J Biol Chem* (2019) 294:1710–20. doi: 10.1074/jbc.TM118.004166
34. Leung DW, Amarasinghe GK. When your cap matters: structural insights into self vs non-self recognition of 5′ RNA by immunomodulatory host proteins. *Curr Opin Struct Biol* (2016) 36:133–41. doi: 10.1016/j.sbi.2016.02.001
35. Vladimer GI, Górna MW, Superti-Furga G. IFITs: Emerging Roles as Key Anti-Viral Proteins. *Front Immunol* (2014) 5:94. doi: 10.3389/fimmu.2014.00094
36. Leong CR, Funami K, Oshiumi H, Mengao D, Takaki H, Matsumoto M, et al. Interferon-stimulated gene of 20 kDa protein (ISG20) degrades RNA of hepatitis B virus to impede the replication of HBV in vitro and in vivo. *Oncotarget* (2016) 7:68179–93. doi: 10.18632/oncotarget.11907
37. Imam H, Kim G-W, Mir SA, Khan M, Siddiqui A. Interferon-stimulated gene 20 (ISG20) selectively degrades N6-methyladenosine modified Hepatitis B Virus transcripts. *PloS Pathog* (2020) 16:e1008338. doi: 10.1371/journal.ppat.1008338
38. Zhou Z, Wang N, Woodson SE, Dong Q, Wang J, Liang Y, et al. Antiviral activities of ISG20 in positive-strand RNA virus infections. *Virology* (2011) 409:175–88. doi: 10.1016/j.virol.2010.10.008
39. Chow KT, Gale M, Loo Y-M. RIG-I and Other RNA Sensors in Antiviral Immunity. *Annu Rev Immunol* (2018) 36:667–94. doi: 10.1146/annurev-immunol-042617-053309
40. Hur S. Double-Stranded RNA Sensors and Modulators in Innate Immunity. *Annu Rev Immunol* (2019) 37:349–75. doi: 10.1146/annurev-immunol-042718-041356
41. Liu G, Gack MU. Distinct and Orchestrated Functions of RNA Sensors in Innate Immunity. *Immunity* (2020) 53:26–42. doi: 10.1016/j.immuni.2020.03.017
42. Schwartz SL, Conn GL. RNA regulation of the antiviral protein 2′-5′-oligoadenylate synthetase. *WIREs RNA* (2019) 10:e1534. doi: 10.1002/wrna.1534
43. Zhu J, Ghosh A, Sarkar SN. OASL—a new player in controlling antiviral innate immunity. *Curr Opin Virol* (2015) 12:15–9. doi: 10.1016/j.coviro.2015.01.010
44. Welsby I, Hutin D, Gueydan C, Kruys V, Rongvaux A, Leo O. PARP12, an Interferon-stimulated Gene Involved in the Control of Protein Translation and Inflammation. *J Biol Chem* (2014) 289:26642–57. doi: 10.1074/jbc.M114.589515
45. Atasheva S, Frolova EI, Frolov I. Interferon-Stimulated Poly(ADP-Ribose) Polymerases Are Potent Inhibitors of Cellular Translation and Virus Replication. *J Virol* (2014) 88:2116–30. doi: 10.1128/JVI.03443-13
46. Atasheva S, Akhrymuk M, Frolova EI, Frolov I. New PARP Gene with an Anti-Alphavirus Function. *J Virol* (2012) 86:8147–60. doi: 10.1128/JVI.00733-12
47. Gusho E, Baskar D, Banerjee S. New advances in our understanding of the "unique" RNase L in host pathogen interaction and immune signaling. *Cytokine* (2020) 133:153847. doi: 10.1016/j.cyto.2016.08.009
48. Li MMH, Lau Z, Cheung P, Aguilar EG, Schneider WM, Bozzacco L, et al. TRIM25 Enhances the Antiviral Action of Zinc-Finger Antiviral Protein (ZAP). *PloS Pathog* (2017) 13:e1006145. doi: 10.1371/journal.ppat.1006145
49. Sanchez JG, Sparrer KMJ, Chiang C, Reis RA, Chiang JJ, Zurenski MA, et al. TRIM25 Binds RNA to Modulate Cellular Anti-viral Defense. *J Mol Biol* (2018) 430:5280–93. doi: 10.1016/j.jmb.2018.10.003
50. Garcia-Moreno M, Noerenberg M, Ni S, Järvelin AI, González-Almela E, Lenz CE, et al. System-wide Profiling of RNA-Binding Proteins Uncovers Key Regulators of Virus Infection. *Mol Cell* (2019) 74:196–211.e11. doi: 10.1016/j.molcel.2019.01.017
51. Lian H, Zang R, Wei J, Ye W, Hu M-M, Chen Y-D, et al. The Zinc-Finger Protein ZCCHC3 Binds RNA and Facilitates Viral RNA Sensing and Activation of the RIG-I-like Receptors. *Immunity* (2018) 49:438–448.e5. doi: 10.1016/j.immuni.2018.08.014
52. Wang Y, Yuan S, Jia X, Ge Y, Ling T, Nie M, et al. Mitochondria-localised ZNFX1 functions as a dsRNA sensor to initiate antiviral responses through MAVS. *Nat Cell Biol* (2019) 21:1346–56. doi: 10.1038/s41556-019-0416-0
53. Batra J, Hultquist JF, Liu D, Shtanko O, Von Dollen J, Satkamp L, et al. Protein Interaction Mapping Identifies RBBP6 as a Negative Regulator of Ebola Virus Replication. *Cell* (2018) 175:1917–1930.e13. doi: 10.1016/j.cell.2018.08.044
54. Wang X, Xuan Y, Han Y, Ding X, Ye K, Yang F, et al. Regulation of HIV-1 Gag-Pol Expression by Shiftless, an Inhibitor of Programmed -1 Ribosomal Frameshifting. *Cell* (2019) 176:625–635.e14. doi: 10.1016/j.cell.2018.12.030
55. Hattlmann CJ, Kelly JN, Barr SD. TRIM22: A Diverse and Dynamic Antiviral Protein. *Mol Biol Int* (2012) 2012:e153415. doi: 10.1155/2012/153415
56. Meyerson NR, Zhou L, Guo YR, Zhao C, Tao YJ, Krug RM, et al. Nuclear TRIM25 Specifically Targets Influenza Virus Ribonucleoproteins to Block the Onset of RNA Chain Elongation. *Cell Host Microbe* (2017) 22:627–638.e7. doi: 10.1016/j.chom.2017.10.003
57. Fu B, Wang L, Ding H, Schwamborn JC, Li S, Dorf ME. TRIM32 Senses and Restricts Influenza A Virus by Ubiquitination of PB1 Polymerase. *PloS Pathog* (2015) 11:e1004960. doi: 10.1371/journal.ppat.1004960
58. Kueck T, Bloyet L-M, Cassella E, Zang T, Schmidt F, Brusic V, et al. Vesicular Stomatitis Virus Transcription Is Inhibited by TRIM69 in the Interferon-Induced Antiviral State. *J Virol* (2019) 93:23. doi: 10.1128/JVI.01372-19
59. Rihn SJ, Aziz MA, Stewart DG, Hughes J, Turnbull ML, Varela M, et al. TRIM69 Inhibits Vesicular Stomatitis Indiana Virus. *J Virol* (2019) 93:e00951–19. doi: 10.1128/JVI.00951-19
60. Ghosh S, Marsh ENG. Viperin: An ancient radical SAM enzyme finds its place in modern cellular metabolism and innate immunity. *J Biol Chem* (2020) 295:11513–28. doi: 10.1074/jbc.REV120.012784

61. Silverman RH. Viral Encounters with 2′,5′-Oligoadenylate Synthetase and RNase L during the Interferon Antiviral Response. *J Virol* (2007) 81:12720–9. doi: 10.1128/JVI.01471-07
62. Kristiansen H, Gad HH, Eskildsen-Larsen S, Despres P, Hartmann R. The Oligoadenylate Synthetase Family: An Ancient Protein Family with Multiple Antiviral Activities. *J Interferon Cytokine Res* (2010) 31:41–7. doi: 10.1089/jir.2010.0107
63. Chakrabarti A, Ghosh PK, Banerjee S, Gaughan C, Silverman RH. RNase L Triggers Autophagy in Response to Viral Infections. *J Virol* (2012) 86:11311–21. doi: 10.1128/JVI.00270-12
64. Hornung V, Hartmann R, Ablasser A, Hopfner K-P. OAS proteins and cGAS: unifying concepts in sensing and responding to cytosolic nucleic acids. *Nat Rev Immunol* (2014) 14:521–8. doi: 10.1038/nri3719
65. Hancks DC, Hartley MK, Hagan C, Clark NL, Elde NC. Overlapping Patterns of Rapid Evolution in the Nucleic Acid Sensors cGAS and OAS1 Suggest a Common Mechanism of Pathogen Antagonism and Escape. *PloS Genet* (2015) 11:e1005203. doi: 10.1371/journal.pgen.1005203
66. Mozzi A, Pontremoli C, Forni D, Clerici M, Pozzoli U, Bresolin N, et al. OASes and STING: Adaptive Evolution in Concert. *Genome Biol Evol* (2015) 7:1016–32. doi: 10.1093/gbe/evv046
67. Li Y, Banerjee S, Wang Y, Goldstein SA, Dong B, Gaughan C, et al. Activation of RNase L is dependent on OAS3 expression during infection with diverse human viruses. *PNAS* (2016) 113:2241–6. doi: 10.1073/pnas.1519657113
68. Guo X, Li X, Xu Y, Sun T, Yang G, Wu Z, et al. Identification of OASL d, a splice variant of human OASL, with antiviral activity. *Int J Biochem Cell Biol* (2012) 44:1133–8. doi: 10.1016/j.biocel.2012.04.001
69. Di H, Elbahesh H, Brinton MA. Characteristics of Human OAS1 Isoform Proteins. *Viruses* (2020) 12:152. doi: 10.3390/v12020152
70. Bonnevie-Nielsen V, Leigh Field L, Lu S, Zheng D-J, Li M, Martensen PM, et al. Variation in Antiviral 2′,5′-Oligoadenylate Synthetase (2′5′AS) Enzyme Activity Is Controlled by a Single-Nucleotide Polymorphism at a Splice-Acceptor Site in the OAS1 Gene. *Am J Hum Genet* (2005) 76:623–33. doi: 10.1086/429391
71. Kjær KH, Pahus J, Hansen MF, Poulsen JB, Christensen EI, Justesen J, et al. Mitochondrial localization of the OAS1 p46 isoform associated with a common single nucleotide polymorphism. *BMC Cell Biol* (2014) 15:33. doi: 10.1186/1471-2121-15-33
72. Skrivergaard S, Jensen MS, Rolander TB, Nguyen TBN, Bundgaard A, Nejsum LN, et al. The Cellular Localization of the p42 and p46 Oligoadenylate Synthetase 1 Isoforms and Their Impact on Mitochondrial Respiration. *Viruses* (2019) 11:1122. doi: 10.3390/v11121122
73. Carey CM, Govande AA, Cooper JM, Hartley MK, Kranzusch PJ, Elde NC. Recurrent Loss-of-Function Mutations Reveal Costs to OAS1 Antiviral Activity in Primates. *Cell Host Microbe* (2019) 25:336–343.e4. doi: 10.1016/j.chom.2019.01.001
74. Lim JK, Lisco A, McDermott DH, Huynh L, Ward JM, Johnson B, et al. Genetic Variation in OAS1 Is a Risk Factor for Initial Infection with West Nile Virus in Man. *PloS Pathog* (2009) 5:e1000321. doi: 10.1371/journal.ppat.1000321
75. Awady MKE, Anany MA, Esmat G, Zayed N, Tabll AA, Helmy A, et al. Single nucleotide polymorphism at exon 7 splice acceptor site of OAS1 gene determines response of hepatitis C virus patients to interferon therapy. *J Gastroenterol Hepatol* (2011) 26:843–50. doi: 10.1111/j.1440-1746.2010.06605.x
76. Bader El Din NG, Anany MA, Dawood RM, Ibrahim MK, El-Shenawy R, El Abd YS, et al. Impact of OAS1 Exon 7 rs10774671 Genetic Variation on Liver Fibrosis Progression in Egyptian HCV Genotype 4 Patients. *Viral Immunol* (2015) 28:509–16. doi: 10.1089/vim.2015.0041
77. Liu X, Xing H, Gao W, Yu D, Zhao Y, Shi X, et al. A functional variant in the OAS1 gene is associated with Sjögren's syndrome complicated with HBV infection. *Sci Rep* (2017) 7:17571. doi: 10.1038/s41598-017-17931-9
78. Wu S, Wang Y, Chen G, Zhang M, Wang M, He J-Q. 2′-5′-Oligoadenylate synthetase 1 polymorphisms are associated with tuberculosis: a case-control study. *BMC Pulmonary Med* (2018) 18:180. doi: 10.1186/s12890-018-0746-x
79. Lin R-J, Yu H-P, Chang B-L, Tang W-C, Liao C-L, Lin Y-L. Distinct Antiviral Roles for Human 2′,5′-Oligoadenylate Synthetase Family Members against Dengue Virus Infection. *J Immunol* (2009) 183:8035–43. doi: 10.4049/jimmunol.0902728
80. Rebouillat D, Hovnanian A, Marié I, Hovanessian AG. The 100-kDa 2′,5′-Oligoadenylate Synthetase Catalyzing Preferentially the Synthesis of Dimeric pppA2′p5′A Molecules Is Composed of Three Homologous Domains. *J Biol Chem* (1999) 274:1557–65. doi: 10.1074/jbc.274.3.1557
81. Marié I, Blanco J, Rebouillat D, Hovanessian AG. 69-kDa and 100-kDa Isoforms of Interferon-Induced (2′-5′)Oligoadenylate Synthetase Exhibit Differential Catalytic Parameters. *Eur J Biochem* (1997) 248:558–66. doi: 10.1111/j.1432-1033.1997.t01-1-00558.x
82. Ibsen MS, Gad HH, Thavachelvam K, Boesen T, Desprès P, Hartmann R. The 2′-5′-Oligoadenylate Synthetase 3 Enzyme Potently Synthesizes the 2′-5′-Oligoadenylates Required for RNase L Activation. *J Virol* (2014) 88:14222–31. doi: 10.1128/JVI.01763-14
83. Donovan J, Whitney G, Rath S, Korennykh A. Structural mechanism of sensing long dsRNA via a noncatalytic domain in human oligoadenylate synthetase 3. *PNAS* (2015) 112:3949–54. doi: 10.1073/pnas.1419409112
84. Wang Y, Holleufer A, Gad HH, Hartmann R. Length dependent activation of OAS proteins by dsRNA. *Cytokine* (2020) 126:154867. doi: 10.1016/j.cyto.2019.154867
85. Schlee M, Hartmann G. Discriminating self from non-self in nucleic acid sensing. *Nat Rev Immunol* (2016) 16:566–80. doi: 10.1038/nri.2016.78
86. Liao X, Xie H, Li S, Ye H, Li S, Ren K, et al. 2′, 5′-Oligoadenylate Synthetase 2 (OAS2) Inhibits Zika Virus Replication through Activation of Type ι IFN Signaling Pathway. *Viruses* (2020) 12:418. doi: 10.3390/v12040418
87. Oakes SR, Gallego-Ortega D, Stanford PM, Junankar S, Au WWY, Kikhtyak Z, et al. A mutation in the viral sensor 2'-5'-oligoadenylate synthetase 2 causes failure of lactation. *PloS Genet* (2017) 13:e1007072. doi: 10.1371/journal.pgen.1007072
88. Kondratova AA, Cheon H, Dong B, Holvey-Bates EG, Hasipek M, Taran I, et al. Suppressing PARylation by 2′,5′-oligoadenylate synthetase 1 inhibits DNA damage-induced cell death. *EMBO J* (2020) 39:e101573. doi: 10.15252/embj.2019101573
89. Luo X, Kraus WL. On PAR with PARP: cellular stress signaling through poly (ADP-ribose) and PARP-1. *Genes Dev* (2012) 26:417–32. doi: 10.1101/gad.183509.111
90. Cayley PJ, Kerr IM. Synthesis, Characterisation and Biological Significance of (2′-5′)Oiigoadenylate Derivatives of NAD+, ADP-Ribose and Adenosine (5′)Tetraphosph0(5′)Adenosine. *Eur J Biochem* (1982) 122:601–8. doi: 10.1111/j.1432-1033.1982.tb06481.x
91. Khodarev NN, Beckett M, Labay E, Darga T, Roizman B, Weichselbaum RR. STAT1 is overexpressed in tumors selected for radioresistance and confers protection from radiation in transduced sensitive cells. *PNAS* (2004) 101:1714–9. doi: 10.1073/pnas.0308102100
92. Weichselbaum RR, Ishwaran H, Yoon T, Nuyten DSA, Baker SW, Khodarev N, et al. An interferon-related gene signature for DNA damage resistance is a predictive marker for chemotherapy and radiation for breast cancer. *Proc Natl Acad Sci U S A* (2008) 105:18490–5. doi: 10.1073/pnas.0809242105
93. Donovan J, Rath S, Kolet-Mandrikov D, Korennykh A. Rapid RNase L-driven arrest of protein synthesis in the dsRNA response without degradation of translation machinery. *RNA* (2017) 23:1660–71. doi: 10.1261/rna.062000.117
94. Burke JM, Moon SL, Matheny T, Parker R. RNase L Reprograms Translation by Widespread mRNA Turnover Escaped by Antiviral mRNAs. *Mol Cell* (2019) 75:1203–1217.e5. doi: 10.1016/j.molcel.2019.07.029
95. Chitrakar A, Rath S, Donovan J, Demarest K, Li Y, Sridhar RR, et al. Real-time 2-5A kinetics suggest that interferons β and λ evade global arrest of translation by RNase L. *PNAS* (2019) 116:2103–11. doi: 10.1073/pnas.1818363116
96. Han Y, Donovan J, Rath S, Whitney G, Chitrakar A, Korennykh A. Structure of Human RNase L Reveals the Basis for Regulated RNA Decay in the IFN Response. *Science* (2014) 343:1244–8. doi: 10.1126/science.1249845
97. Chakrabarti A, Jha BK, Silverman RH. New Insights into the Role of RNase L in Innate Immunity. *J Interferon Cytokine Res* (2010) 31:49–57. doi: 10.1089/jir.2010.0120
98. Rath S, Donovan J, Whitney G, Chitrakar A, Wang W, Korennykh A. Human RNase L tunes gene expression by selectively destabilizing the microRNA-regulated transcriptome. *PNAS* (2015) 112:15916–21. doi: 10.1073/pnas.1513034112
99. Banerjee S, Li G, Li Y, Gaughan C, Baskar D, Parker Y, et al. RNase L is a negative regulator of cell migration. *Oncotarget* (2015) 6:44360–72. doi: 10.18632/oncotarget.6246

100. Melchjorsen J, Kristiansen H, Christiansen R, Rintahaka J, Matikainen S, Paludan SR, et al. Differential Regulation of the OASL and OAS1 Genes in Response to Viral Infections. *J Interferon Cytokine Res* (2009) 29:199–208. doi: 10.1089/jir.2008.0050
101. Marques J, Anwar J, Eskildsen-Larsen S, Rebouillat D, Paludan SR, Sen G, et al. The p59 oligoadenylate synthetase-like protein possesses antiviral activity that requires the C-terminal ubiquitin-like domain. *J Gen Virol* (2008) 89:2767–72. doi: 10.1099/vir.0.2008/003558-0
102. Ishibashi M, Wakita T, Esumi M. 2′,5′-Oligoadenylate synthetase-like gene highly induced by hepatitis C virus infection in human liver is inhibitory to viral replication in vitro. *Biochem Biophys Res Commun* (2010) 392:397–402. doi: 10.1016/j.bbrc.2010.01.034
103. Bussey KA, Lau U, Schumann S, Gallo A, Osbelt L, Stempel M, et al. The interferon-stimulated gene product oligoadenylate synthetase-like protein enhances replication of Kaposi's sarcoma-associated herpesvirus (KSHV) and interacts with the KSHV ORF20 protein. *PloS Pathog* (2018) 14: e1006937. doi: 10.1371/journal.ppat.1006937
104. Zhu J, Zhang Y, Ghosh A, Cuevas RA, Forero A, Dhar J, et al. Antiviral Activity of Human OASL Protein Is Mediated by Enhancing Signaling of the RIG-I RNA Sensor. *Immunity* (2014) 40:936–48. doi: 10.1016/j.immuni.2014.05.007
105. Lum KK, Song B, Federspiel JD, Diner BA, Howard T, Cristea IM. Interactome and Proteome Dynamics Uncover Immune Modulatory Associations of the Pathogen Sensing Factor cGAS. *Cell Syst* (2018) 7:627–642.e6. doi: 10.1016/j.cels.2018.10.010
106. Ghosh A, Shao L, Sampath P, Zhao B, Patel NV, Zhu J, et al. Oligoadenylate-Synthetase-Family Protein OASL Inhibits Activity of the DNA Sensor cGAS during DNA Virus Infection to Limit Interferon Production. *Immunity* (2019) 50:51–63.e5. doi: 10.1016/j.immuni.2018.12.013
107. Chan YK, Gack MU. Viral evasion of intracellular DNA and RNA sensing. *Nat Rev Microbiol* (2016) 14:360–73. doi: 10.1038/nrmicro.2016.45
108. Gongora C, David G, Pintard L, Tissot C, Hua TD, Dejean A, et al. Molecular Cloning of a New Interferon-induced PML Nuclear Body-associated Protein. *J Biol Chem* (1997) 272:19457–63. doi: 10.1074/jbc.272.31.19457
109. Zuo Y, Deutscher MP. Exoribonuclease superfamilies: structural analysis and phylogenetic distribution. *Nucleic Acids Res* (2001) 29:1017–26. doi: 10.1093/nar/29.5.1017
110. Nguyen LH, Espert L, Mechti N, Wilson DM. The Human Interferon- and Estrogen-Regulated ISG20/HEM45 Gene Product Degrades Single-Stranded RNA and DNA in Vitro. *Biochemistry* (2001) 40:7174–9. doi: 10.1021/bi010141t
111. Espert L, Degols G, Gongora C, Blondel D, Williams BR, Silverman RH, et al. ISG20, a New Interferon-induced RNase Specific for Single-stranded RNA, Defines an Alternative Antiviral Pathway against RNA Genomic Viruses. *J Biol Chem* (2003) 278:16151–8. doi: 10.1074/jbc.M209628200
112. Feng J, Wickenhagen A, Turnbull ML, Rezelj VV, Kreher F, Tilston-Lunel NL, et al. Interferon-Stimulated Gene (ISG)-Expression Screening Reveals the Specific Antibunyaviral Activity of ISG20. *J Virol* (2018) 92:e02140–17. doi: 10.1128/JVI.02140-17
113. Espert L, Degols G, Lin Y-L, Vincent T, Benkirane M, Mechti N. Interferon-induced exonuclease ISG20 exhibits an antiviral activity against human immunodeficiency virus type 1. *J Gen Virol* (2005) 86:2221–9. doi: 10.1099/vir.0.81074-0
114. Wieland S, Thimme R, Purcell RH, Chisari FV. Genomic analysis of the host response to hepatitis B virus infection. *PNAS* (2004) 101:6669–74. doi: 10.1073/pnas.0401771101
115. Liu Y, Nie H, Mao R, Mitra B, Cai D, Yan R, et al. Interferon-inducible ribonuclease ISG20 inhibits hepatitis B virus replication through directly binding to the epsilon stem-loop structure of viral RNA. *PloS Pathog* (2017) 13:e1006296. doi: 10.1371/journal.ppat.1006296
116. Jiang D, Weidner JM, Qing M, Pan X-B, Guo H, Xu C, et al. Identification of Five Interferon-Induced Cellular Proteins That Inhibit West Nile Virus and Dengue Virus Infections. *J Virol* (2010) 84:8332–41. doi: 10.1128/JVI.02199-09
117. Zaccara S, Ries RJ, Jaffrey SR. Reading, writing and erasing mRNA methylation. *Nat Rev Mol Cell Biol* (2019) 20:608–24. doi: 10.1038/s41580-019-0168-5
118. Zaccara S. Jaffrey SR. A Unified Model for the Function of YTHDF Proteins in Regulating m6A-Modified mRNA. *Cell* (2020) 181:1582–1595.e18. doi: 10.1016/j.cell.2020.05.012
119. Imam H, Khan M, Gokhale NS, McIntyre ABR, Kim G-W, Jang JY, et al. N6-methyladenosine modification of hepatitis B virus RNA differentially regulates the viral life cycle. *PNAS* (2018) 115:8829–34. doi: 10.1073/pnas.1808319115
120. Jiang D, Guo H, Xu C, Chang J, Gu B, Wang L, et al. Identification of Three Interferon-Inducible Cellular Enzymes That Inhibit the Replication of Hepatitis C Virus. *J Virol* (2008) 82:1665–78. doi: 10.1128/JVI.02113-07
121. Wu N, Nguyen X-N, Wang L, Appourchaux R, Zhang C, Panthu B, et al. The interferon stimulated gene 20 protein (ISG20) is an innate defense antiviral factor that discriminates self versus non-self translation. *PloS Pathog* (2019) 15:e1008093. doi: 10.1371/journal.ppat.1008093
122. Horio T, Murai M, Inoue T, Hamasaki T, Tanaka T, Ohgi T. Crystal structure of human ISG20, an interferon-induced antiviral ribonuclease. *FEBS Lett* (2004) 577:111–6. doi: 10.1016/j.febslet.2004.09.074
123. Weiss CM, Trobaugh DW, Sun C, Lucas TM, Diamond MS, Ryman KD, et al. The Interferon-Induced Exonuclease ISG20 Exerts Antiviral Activity through Upregulation of Type I Interferon Response Proteins. *mSphere* (2018) 3:e00209–18. doi: 10.1128/mSphere.00209-18
124. Diamond MS. IFIT1: A dual sensor and effector molecule that detects non-2′-O methylated viral RNA and inhibits its translation. *Cytokine Growth Factor Rev* (2014) 25:543–50. doi: 10.1016/j.cytogfr.2014.05.002
125. Gao G, Guo X, Goff SP. Inhibition of Retroviral RNA Production by ZAP, a CCCH-Type Zinc Finger Protein. *Science* (2002) 297:1703–6. doi: 10.1126/science.1074276
126. Bick MJ, Carroll J-WN, Gao G, Goff SP, Rice CM, MacDonald MR. Expression of the Zinc-Finger Antiviral Protein Inhibits Alphavirus Replication. *J Virol* (2003) 77:11555–62. doi: 10.1128/JVI.77.21.11555-11562.2003
127. Müller S, Möller P, Bick MJ, Wurr S, Becker S, Günther S, et al. Inhibition of Filovirus Replication by the Zinc Finger Antiviral Protein. *J Virol* (2007) 81:2391–400. doi: 10.1128/JVI.01601-06
128. Mao R, Nie H, Cai D, Zhang J, Liu H, Yan R, et al. Inhibition of Hepatitis B Virus Replication by the Host Zinc Finger Antiviral Protein. *PloS Pathog* (2013) 9:e1003494. doi: 10.1371/journal.ppat.1003494
129. Zhu Y, Chen G, Lv F, Wang X, Ji X, Xu Y, et al. Zinc-finger antiviral protein inhibits HIV-1 infection by selectively targeting multiply spliced viral mRNAs for degradation. *PNAS* (2011) 108:15834–9. doi: 10.1073/pnas.1101676108
130. Li M, Yan K, Wei L, Yang J, Lu C, Xiong F, et al. Zinc finger antiviral protein inhibits coxsackievirus B3 virus replication and protects against viral myocarditis. *Antiviral Res* (2015) 123:50–61. doi: 10.1016/j.antiviral.2015.09.001
131. Chiu H-P, Chiu H, Yang C-F, Lee Y-L, Chiu F-L, Kuo H-C, et al. Inhibition of Japanese encephalitis virus infection by the host zinc-finger antiviral protein. *PloS Pathog* (2018) 14:e1007166. doi: 10.1371/journal.ppat.1007166
132. Liu C-H, Zhou L, Chen G, Krug RM. Battle between influenza A virus and a newly identified antiviral activity of the PARP-containing ZAPL protein. *PNAS* (2015) 112:14048–53. doi: 10.1073/pnas.1509745112
133. Todorova T, Bock FJ, Chang P. PARP13 regulates cellular mRNA post-transcriptionally and functions as a pro-apoptotic factor by destabilizing TRAILR4 transcript. *Nat Commun* (2014) 5:5362. doi: 10.1038/ncomms6362
134. Goodier JL, Pereira GC, Cheung LE, Rose RJ, Kazazian HH. The Broad-Spectrum Antiviral Protein ZAP Restricts Human Retrotransposition. *PloS Genet* (2015) 11:e1005252. doi: 10.1371/journal.pgen.1005252
135. Moldovan JB, Moran JV. The Zinc-Finger Antiviral Protein ZAP Inhibits LINE and Alu Retrotransposition. *PloS Genet* (2015) 11:e1005121. doi: 10.1371/journal.pgen.1005121
136. Chen S, Xu Y, Zhang K, Wang X, Sun J, Gao G, et al. Structure of N-terminal domain of ZAP indicates how a zinc-finger protein recognizes complex RNA. *Nat Struct Mol Biol* (2012) 19:430–5. doi: 10.1038/nsmb.2243
137. Youn J-Y, Dunham WH, Hong SJ, Knight JDR, Bashkurov M, Chen GI, et al. High-Density Proximity Mapping Reveals the Subcellular Organization of mRNA-Associated Granules and Bodies. *Mol Cell* (2018) 69:517–532.e11. doi: 10.1016/j.molcel.2017.12.020
138. Law LMJ, Razooky BS, Li MMH, You S, Jurado A, Rice CM, et al. ZAP's stress granule localization is correlated with its antiviral activity and induced by virus replication. *PloS Pathog* (2019) 15:e1007798. doi: 10.1371/journal.ppat.1007798

139. Guo X, Carroll J-WN, MacDonald MR, Goff SP, Gao G. The Zinc Finger Antiviral Protein Directly Binds to Specific Viral mRNAs through the CCCH Zinc Finger Motifs. *J Virol* (2004) 78:12781–7. doi: 10.1128/JVI.78.23.12781-12787.2004
140. Sun L, Lv F, Guo X, Gao G. Glycogen Synthase Kinase 3β (GSK3β) Modulates Antiviral Activity of Zinc-finger Antiviral Protein (ZAP). *J Biol Chem* (2012) 287:22882–8. doi: 10.1074/jbc.M111.306373
141. Li MMH, Aguilar EG, Michailidis E, Pabon J, Park P, Wu X, et al. Characterization of Novel Splice Variants of Zinc Finger Antiviral Protein (ZAP). *J Virol* (2019) 93:e00715–19. doi: 10.1128/JVI.00715-19
142. Zhu Y, Wang X, Goff SP, Gao G. Translational repression precedes and is required for ZAP-mediated mRNA decay: ZAP-mediated translational repression versus mRNA decay. *EMBO J* (2012) 31:4236–46. doi: 10.1038/emboj.2012.271
143. Zheng X, Wang X, Tu F, Wang Q, Fan Z, Gao G. TRIM25 Is Required for the Antiviral Activity of Zinc Finger Antiviral Protein. *J Virol* (2017) 91:e00088–17. doi: 10.1128/JVI.00088-17
144. Guo X, Ma J, Sun J, Gao G. The zinc-finger antiviral protein recruits the RNA processing exosome to degrade the target mRNA. *Proc Natl Acad Sci* (2007) 104:151–6. doi: 10.1073/pnas.0607063104
145. Chen G, Guo X, Lv F, Xu Y, Gao G. p72 DEAD box RNA helicase is required for optimal function of the zinc-finger antiviral protein. *Proc Natl Acad Sci* (2008) 105:4352–7. doi: 10.1073/pnas.0712276105
146. Ye P, Liu S, Zhu Y, Chen G, Gao G. DEXH-Box protein DHX30 is required for optimal function of the zinc-finger antiviral protein. *Protein Cell* (2010) 1:956–64. doi: 10.1007/s13238-010-0117-8
147. Ficarelli M, Wilson H, Pedro Galão R, Mazzon M, Antzin-Anduetza I, Marsh M, et al. KHNYN is essential for the zinc finger antiviral protein (ZAP) to restrict HIV-1 containing clustered CpG dinucleotides. *eLife* (2019) 8: e46767. doi: 10.7554/eLife.46767
148. Takata MA, Gonçalves-Carneiro D, Zang TM, Soll SJ, York A, Blanco-Melo D, et al. CG dinucleotide suppression enables antiviral defence targeting non-self RNA. *Nature* (2017) 550:124–7. doi: 10.1038/nature24039
149. Kmiec D, Nchioua R, Sherrill-Mix S, Stürzel CM, Heusinger E, Braun E, et al. CpG Frequency in the 5′ Third of the env Gene Determines Sensitivity of Primary HIV-1 Strains to the Zinc-Finger Antiviral Protein. *mBio* (2020) 11: e02903–19. doi: 10.1128/mBio.02903-19
150. Meagher JL, Takata M, Gonçalves-Carneiro D, Keane SC, Rebendenne A, Ong H, et al. Structure of the zinc-finger antiviral protein in complex with RNA reveals a mechanism for selective targeting of CG-rich viral sequences. *Proc Natl Acad Sci USA* (2019) 116:24303–9. doi: 10.1073/pnas.1913232116
151. Luo X, Wang X, Gao Y, Zhu J, Liu S, Gao G, et al. Molecular Mechanism of RNA Recognition by Zinc-Finger Antiviral Protein. *Cell Rep* (2020) 30:46–52. doi: 10.1016/j.celrep.2019.11.116
152. Greenbaum BD, Levine AJ, Bhanot G, Rabadan R. Patterns of Evolution and Host Gene Mimicry in Influenza and Other RNA Viruses. *PloS Pathog* (2008) 4:e1000079. doi: 10.1371/journal.ppat.1000079
153. Cheng X, Virk N, Chen W, Ji S, Ji S, Sun Y, et al. CpG Usage in RNA Viruses: Data and Hypotheses. *PloS One* (2013) 8:e74109. doi: 10.1371/journal.pone.0074109
154. Nchioua R, Kmiec D, Müller J, Conzelmann C, Groß R, Swanson C, et al. SARS-CoV-2 Is Restricted by Zinc Finger Antiviral Protein despite Preadaptation to the Low-CpG Environment in Humans. *mBio* (2020), 11:e01930–20. doi: 10.1128/mBio.01930-20
155. Gioacchino AD, Šulc P, Komarova AV, Greenbaum BD, Monasson R, Cocco S. The heterogeneous landscape and early evolution of pathogen-associated CpG dinucleotides in SARS-CoV-2. *bioRxiv* (2020), 2020.05.06.074039. doi: 10.1101/2020.05.06.074039
156. Lin Y-T, Chiweshe S, McCormick D, Raper A, Wickenhagen A, DeFillipis V, et al. Human cytomegalovirus evades ZAP detection by suppressing CpG dinucleotides in the major immediate early 1 gene. *PloS Pathog* (2020) 16: e1008844. doi: 10.1371/journal.ppat.1008844
157. Kerns JA, Emerman M, Malik HS. Positive Selection and Increased Antiviral Activity Associated with the PARP-Containing Isoform of Human Zinc-Finger Antiviral Protein. *PloS Genet* (2008) 4:e21. doi: 10.1371/journal.pgen.0040021
158. Charron G, Li MMH, MacDonald MR, Hang HC. Prenylome profiling reveals S-farnesylation is crucial for membrane targeting and antiviral activity of ZAP long-isoform. *Proc Natl Acad Sci* (2013) 110:11085–90. doi: 10.1073/pnas.1302564110
159. Schwerk J, Soveg FW, Ryan AP, Thomas KR, Hatfield LD, Ozarkar S, et al. RNA-binding protein isoforms ZAP-S and ZAP-L have distinct antiviral and immune resolution functions. *Nat Immunol* (2019) 20:1610–20. doi: 10.1038/s41590-019-0527-6
160. Gläsker S, Töller M, Kümmerer BM. The alternate triad motif of the poly (ADP-ribose) polymerase-like domain of the human zinc finger antiviral protein is essential for its antiviral activity. *J Gen Virol* (2014) 95:816–22. doi: 10.1099/vir.0.060988-0
161. Hayakawa S, Shiratori S, Yamato H, Kameyama T, Kitatsuji C, Kashigi F, et al. ZAPS is a potent stimulator of signaling mediated by the RNA helicase RIG-I during antiviral responses. *Nat Immunol* (2011) 12:37–44. doi: 10.1038/ni.1963
162. Lee H, Komano J, Saitoh Y, Yamaoka S, Kozaki T, Misawa T, et al. Zinc-finger antiviral protein mediates retinoic acid inducible gene I-like receptor-independent antiviral response to murine leukemia virus. *Proc Natl Acad Sci* (2013) 110:12379–84. doi: 10.1073/pnas.1310604110
163. Wang X, Tu F, Zhu Y, Gao G. Zinc-Finger Antiviral Protein Inhibits XMRV Infection. *PloS One* (2012) 7:e39159. doi: 10.1371/journal.pone.0039159
164. Suzuki Y, Chin W-X, Han Q, Ichiyama K, Lee CH, Eyo ZW, et al. Characterization of RyDEN (C19orf66) as an Interferon-Stimulated Cellular Inhibitor against Dengue Virus Replication. *PloS Pathog* (2016) 12:e1005357. doi: 10.1371/journal.ppat.1005357
165. Balinsky CA, Schmeisser H, Wells AI, Ganesan S, Jin T, Singh K, et al. IRAV (FLJ11286), an Interferon-Stimulated Gene with Antiviral Activity against Dengue Virus, Interacts with MOV10. *J Virol* (2017) 91:e01606–16. doi: 10.1128/JVI.01606-16
166. Kinast V, Plociennikowska A, Anggakusuma, Bracht T, Todt D, Brown RJP, et al. C19orf66 is an interferon-induced inhibitor of HCV replication that restricts formation of the viral replication organelle. *J Hepatol* (2020) 73 (3):549–558. doi: 10.1016/j.jhep.2020.03.047
167. Schmeisser H, Mejido J, Balinsky CA, Morrow AN, Clark CR, Zhao T, et al. Identification of Alpha Interferon-Induced Genes Associated with Antiviral Activity in Daudi Cells and Characterization of IFIT3 as a Novel Antiviral Gene. *J Virol* (2010) 84:10671–80. doi: 10.1128/JVI.00818-10
168. Wu Y, Yang X, Yao Z, Dong X, Zhang D, Hu Y, et al. C19orf66 interrupts Zika virus replication by inducing lysosomal degradation of viral NS3. *PloS Neglected Trop Dis* (2020) 14:e0008083. doi: 10.1371/journal.pntd.0008083
169. Rodriguez W, Srivastav K, Muller M. C19ORF66 Broadly Escapes Virus-Induced Endonuclease Cleavage and Restricts Kaposi's Sarcoma-Associated Herpesvirus. *J Virol* (2019) 93:e00373–19. doi: 10.1128/JVI.00373-19
170. Komander D, Rape M. The Ubiquitin Code. *Annu Rev Biochem* (2012) 81:203–29. doi: 10.1146/annurev-biochem-060310-170328
171. Rajsbaum R, García-Sastre A, Versteeg GA. TRIMmunity: The Roles of the TRIM E3-Ubiquitin Ligase Family in Innate Antiviral Immunity. *J Mol Biol* (2014) 426:1265–84. doi: 10.1016/j.jmb.2013.12.005
172. Bottermann M, James LC. *Thirteen - Intracellular Antiviral Immunity*. Elsevier (2018) 100:309–54. doi: 10.1016/bs.aivir.2018.01.002
173. Vunjak M, Versteeg GA. TRIM proteins. *Curr Biol* (2019) 29:R42–4. doi: 10.1016/j.cub.2018.11.026
174. Esposito D, Koliopoulos MG, Rittinger K. Structural determinants of TRIM protein function. *Biochem Soc Trans* (2017) 45:183–91. doi: 10.1042/BST20160325
175. van Gent M, Sparrer KMJ, Gack MU. TRIM Proteins and Their Roles in Antiviral Host Defenses. *Annu Rev Virol* (2018) 5:385–405. doi: 10.1146/annurev-virology-092917-043323
176. Hage A, Rajsbaum R. To TRIM or not to TRIM: the balance of host–virus interactions mediated by the ubiquitin system. *J Gen Virol* (2019) 100:1641–62. doi: 10.1099/jgv.0.001341
177. Gao B, Duan Z, Xu W, Xiong S. Tripartite motif-containing 22 inhibits the activity of hepatitis B virus core promoter, which is dependent on nuclear-located RING domain. *Hepatology* (2009) 50:424–33. doi: 10.1002/hep.23011
178. Tissot C, Mechti N. Molecular Cloning of a New Interferon-induced Factor That Represses Human Immunodeficiency Virus Type 1 Long Terminal Repeat Expression. *J Biol Chem* (1995) 270:14891–8. doi: 10.1074/jbc.270.25.14891

179. Kajaste-Rudnitski A, Marelli SS, Pultrone C, Pertel T, Uchil PD, Mechti N, et al. TRIM22 Inhibits HIV-1 Transcription Independently of Its E3 Ubiquitin Ligase Activity, Tat, and NF-κB-Responsive Long Terminal Repeat Elements. *J Virol* (2011) 85:5183–96. doi: 10.1128/JVI.02302-10
180. Yuen M-F, Chen D-S, Dusheiko GM, Janssen HLA, Lau DTY, Locarnini SA, et al. Hepatitis B virus infection. *Nat Rev Dis Primers* (2018) 4:1–20. doi: 10.1038/nrdp.2018.35
181. Turrini F, Marelli S, Kajaste-Rudnitski A, Lusic M, Van Lint C, Das AT, et al. HIV-1 transcriptional silencing caused by TRIM22 inhibition of Sp1 binding to the viral promoter. *Retrovirology* (2015) 12:104. doi: 10.1186/s12977-015-0230-0
182. Turrini F, Saliu F, Forlani G, Das AT, Van Lint C, Accolla RS, et al. Interferon-inducible TRIM22 contributes to maintenance of HIV-1 proviral latency in T cell lines. *Virus Res* (2019) 269:197631. doi: 10.1016/j.virusres.2019.05.009
183. Thornbrough JM, Jha BK, Yount B, Goldstein SA, Li Y, Elliott R, et al. Middle East Respiratory Syndrome Coronavirus NS4b Protein Inhibits Host RNase L Activation. *mBio* (2016) 7(2):e00258–16. doi: 10.1128/mBio.00258-16
184. Choudhury NR, Heikel G, Trubitsyna M, Kubik P, Nowak JS, Webb S, et al. RNA-binding activity of TRIM25 is mediated by its PRY/SPRY domain and is required for ubiquitination. *BMC Biol* (2017) 15:105. doi: 10.1186/s12915-017-0444-9
185. Choudhury NR, Heikel G, Michlewski G. TRIM25 and its emerging RNA-binding roles in antiviral defense. *WIREs RNA* (2020) 11:e1588. doi: 10.1002/wrna.1588
186. Adli M. The CRISPR tool kit for genome editing and beyond. *Nat Commun* (2018) 9:1911. doi: 10.1038/s41467-018-04252-2
187. Hentze MW, Castello A, Schwarzl T, Preiss T. A brave new world of RNA-binding proteins. *Nat Rev Mol Cell Biol* (2018) 19:327–41. doi: 10.1038/nrm.2017.130
188. Flynn RA, Martin L, Spitale RC, Do BT, Sagan SM, Zarnegar B, et al. Dissecting noncoding and pathogen RNA–protein interactomes. *RNA* (2015) 21:135–43. doi: 10.1261/rna.047803.114
189. Ooi YS, Majzoub K, Flynn RA, Mata MA, Diep J, Li JK, et al. An RNA-centric dissection of host complexes controlling flavivirus infection. *Nat Microbiol* (2019) 4:2369–82. doi: 10.1038/s41564-019-0518-2
190. Kim B, Arcos S, Rothamel K, Jian J, Rose KL, McDonald WH, et al. Discovery of Widespread Host Protein Interactions with the Pre-replicated Genome of CHIKV Using VIR-CLASP. *Mol Cell* (2020) 78:624–40.e7. doi: 10.1016/j.molcel.2020.04.013

Conflict of Interest: The authors declare that the research was conducted in the absence of any commercial or financial relationships that could be construed as a potential conflict of interest.

Appendix 2

—

Generation of ZAP shRNA integrated

TRIM25 inducible cell lines

MATERIALS AND METHODS

Generation of ZAP shRNA lentiviruses

ZC3HAV1 lentiviral shRNAs in pGIPZ (Dharmacon; Appendix 2, Table 1) were generously provided by Dr. Robert Damoiseaux at the UCLA Molecular Screening Shared Resource facilities. 293T LentiX (Takara Bio) were seeded at 4 x 10^5 cells/well in a 6 well plate in 10% FBS DMEM. Media was changed 1 day post-seeding to 1 mL/well of pseudoparticle media (DMEM, 3% FBS, 1XNEAA) and transfected with 800 ng HIV gag-Pol, 200 ng VSV-G, and 1 µg *ZC3HAV1* shRNA in pGIPZ using X-tremeGene9 (Roche Life Science). At 6 hours post-transfection, media was changed to 1.5 mL pseudoparticle media. Supernatant was collected 48 hours post-transfection. Polybrene (final concentration 4 µg/mL) and HEPES (final concentration 20 mM) were added to the supernatant before spinning down cell debris at 1500 rpm for 5 min, 4˚C. Pseudoparticle-containing supernatant was aliquoted into 3 tubes at 500 µL per tube and stored at -80 ˚C.

Generation of ZAP shRNA cell lines

TRIM25 KO 293T cells were seeded in a poly-L-lysine coated 6 well plate at 4 x 10^5 cells/well in 1 mL 3% FBS DMEM, 1XNEAA, 20mM HEPES, 4 µg/mL polybrene. One day post-seeding, 1 mL of *ZC3HAV1* shRNA lentivirus was added to each well, and parafilmed plates were "spin-oculated" at 1500 rpm for 1 hour at 37˚C in a pre-heated centrifuge (spun at 3000 rpm for 1 hour at 37˚C). Media was replaced with 10% FBS DMEM 6 hours post transduction. One day post-transduction, each well was re-seeded into a T25 for optimized confluency of 50-60% the following day to allow for efficient puromycin treatment at 1 µg/mL. ZAP shRNA efficiency was assessed via western blot (Appendix 2, Figure 1A). Efficacy of ZAP knockdown (KD) was further assessed via infection with

Toto1101/Luc (Appendix 2, Figure 1B). These combined results led to our selection of ZAP shRNA #7 for transduction of TRIM25 inducible cell lines, given it achieved the most robust knockdown and the highest rescue of viral replication (Appendix 2, Figure 1A-B).

Because the TRIM25 inducible cell lines already included puromycin as a selection marker from the ePB transposon, we were unable to select for pure populations of ZAP shRNA transduced cells with puromycin treatment. Therefore, we utilized GFP sorting through the UCLA Flow Cytometry Core Laboratory at UCLA, generating GFP^{hi} and GFP^{lo} cell lines (Appendix 2, Figure 1C). The resultant cell lines were analyzed via western blot to confirm ZAP KD (Appendix 2, Figure 1D) and further characterized via Toto1101/Luc infection, wherein we saw that the TRIM25 inducible GFP^{hi} cell lines exhibited comparable levels of viral replication to ZAP KO 293T cells, and that the GFP^{lo} cell lines exhibited an intermediate phenotype (Appendix 2, Figure 1E).

Analysis of ZAP-dependent TRIM25 interactors

See Chapter 2: Materials and Methods for detailed methods on mass spectrometry protocol and analyses. TRIM25 interactors were classified as either Log2FC>2 and Pvalue<0.05, or iLog2FC > 2 and iPvalue<0.05. If both Log2FC and iLog2FC values were present, the Log2FC value and Pvalue were used.

Appendix 2, Table 1. *ZC3HAV1* shRNA sequences.

Sense sequence (and its complement) is underlined and bracketed with parentheses in the full hairpin sequence.

ZC3HAV1 shRNA	Target	Full hairpin sequence	Sense sequence
1	Exon 4-5 junction	TGCTGTTGACAGTGAGCGCG(CACTTGTTAACGATTCTTT)ATAGTGAAGCCACAGATGTAT(AAAGAATCGTTAACAAGTG)CTTGCCTACTGCCTCGGA	CACTTGTTAACGATTCTTT
2	Exon 1-2 junction	TGCTGTTGACAGTGAGCGAC(GAGCGGAATTTATGCAAAT)ATAGTGAAGCCACAGATGTAT(ATTTGCATAAATTCCGCTC)GGTGCCTACTGCCTCGGA	GAGCGGAATTTATGCAAAT
3	Exon 2	TGCTGTTGACAGTGAGCGCG(CAAATATTCTCATGAGGTT)CTAGTGAAGCCACAGATGTAG(AACCTCATGAGAATATTTG)CATGCCTACTGCCTCGGA	CAAATATTCTCATGAGGTT
6	Exon 13	TGCTGTTGACAGTGAGCGCC(TGGTTGGAAAGTTTACTGA)ATAGTGAAGCCACAGATGTAT(TCAGTAAACTTTCCAACCA)GATGCCTACTGCCTCGGA	CAAATATTCTCATGAGGTT
7	Exon 2-3 junction	TGCTGTTGACAGTGAGCGAC(CCGAGATATGCAAAAGTTA)TTAGTGAAGCCACAGATGTAA(TAACTTTTGCATATCTCGG)GCTGCCTACTGCCTCGGA	TGGTTGGAAAGTTTACTGA

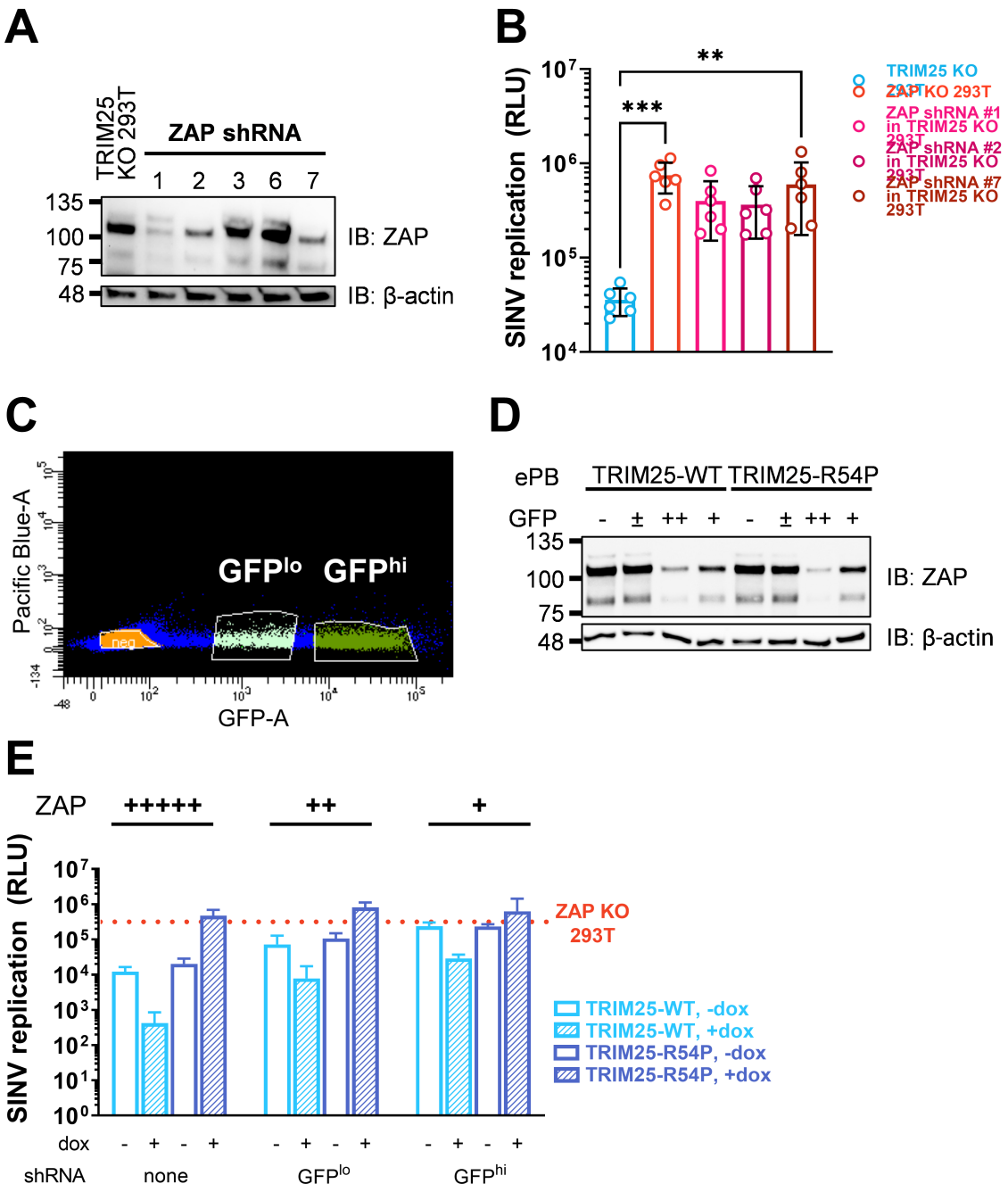

Appendix 2, Figure 1. Establishment and characterization of ZAP shRNA integrated TRIM25 inducible cell lines.

(**A**) Western blot of ZAP shRNA integrated TRIM25 KO 293T cell lines. (**B**) ZAP shRNA TRIM25 KO 293T cells were infected with Toto1101/Luc at an MOI of 0.01 PFU/cell and lysed at 40 hours post infection (h.p.i.) for measurement of luciferase activity. Data combined from two independent experiments. Asterisks indicate statistically significant differences as compared to TRIM25 KO 293T, calculated using one-way ANOVA and Dunnett's multiple comparisons test; **, $p<0.01$, ***, $p<0.001$. (**C**) Gating strategy for sorting TRIM25 inducible cells transduced with ZAP shRNA #7. (**D**) Western blot of TRIM25 inducible cell populations depicted in (**C**), where GFP- is the parental population; ±, total transduced population; ++, GFP^{hi}; and +, GFP^{lo}. (**E**) TRIM25 inducible cells ± ZAP shRNA were induced for TRIM25-WT or -R54P expression at 1 µg/mL dox, infected with Toto1101/Luc at an MOI of 0.01 PFU/cell, and lysed at 40 h.p.i. for measurement of luciferase activity.

Appendix 3

—

Key resources

ANTIBODIES

Description	*Source or reference*	*Identifiers*	*Additional information*
anti-actin-HRP, mouse monoclonal	Sigma-Aldrich	A3854	WB (1:20,000)
anti-EFP/TRIM25, mouse monoclonal	BD Biosciences	610570	WB (1:5,000)
anti-FLAG, mouse monoclonal	Sigma-Aldrich	F1804	WB (1:20,000)
anti-G3BP1, mouse monoclonal	Santa Cruz	sc-365338	WB (1:500)
anti-G3BP2, rabbit polyclonal	Assay Biotech	C18193	WB (1:1,000)
anti-HA, rat monoclonal	Roche Life Science	3F10	WB (1:1,000)
anti-myc, rabbit polyclonal	Cell Signaling Technology	2272S	WB (1:2,500)
anti-NM23A (NME1), rabbit monoclonal	Abcam	ab171935	WB (1:10,000)
anti-PABPC4, rabbit polyclonal	Proteintech	14960-1-AP	WB (1:2,000)
anti-UPF1, rabbit monoclonal	Cell Signaling Technology	12040	WB (1:1,000)
anti-V5, mouse monoclonal	Invitrogen	MA5-1523	WB (1:5,000)
donkey anti-rat HRP	Jackson ImmunoResearch	712-035-153	WB (1:20,000)
goat anti-mouse HRP	Jackson ImmunoResearch	115-035-146	WB (1:20,000)
goat anti-rabbit HRP	Thermo Fisher Scientific	31462	WB (1:20,000)

CHEMICAL COMPOUNDS AND DRUGS

Description	*Source or reference*	*Identifiers*
biotin-16-UTP	Roche Life Science	11388908910
m7G(5')ppp(5')G RNA Cap Structure Analog	New England Biolabs	S1404L
4X Laemmli Sample Buffer	Bio-Rad	1610747
poly(I:C) HMW	InvivoGen	tlrl-pic
poly-L-lysine hydrobromide	Sigma-Aldrich	P2636
RNaseOUT Recombinant Ribonuclease Inhibitor	Invitrogen	10-777-019
cOmplete Mini, EDTA-free Protease Inhibitor Cocktail	Roche Life Science	11836170001
Yeast tRNA	Thermo Fisher Scientific	AM7119

COMMERCIAL ASSAYS OR KITS

Description	*Source or reference*	*Identifiers*
Lenti-X™ 293T Cell Line	Takara Bio	632180
DharmaFECT 1 Transfection Reagent	Horizon Discovery	T-2001-01
Dual-Luciferase Reporter Assay	Promega	E1980
Dynabeads™ Protein A for Immunoprecipitation	Invitrogen	10-002-D
Dynabeads™ M-280 Streptavidin	Invitrogen	11205D
EZview Red ANTI-FLAG M2 Affinity Gel	Sigma-Aldrich	F2426
EZview Red ANTI-MYC M2 Affinity Gel	Sigma-Aldrich	E6654
KOD Hot Start Master Mix	Sigma-Aldrich	71842
Luciferase assay system	Promega	E4550
Luna Universal qPCR Master Mix	New England Biolabs	M3003X
Mini-PROTEAN TGX Gels, 4-15%, 15 well	Bio-Rad	4568086
mMESSAGE mMACHINE T7 Transcription Kit	Invitrogen	AM1344
MTT Cell Proliferation Assay	ATCC	30-1010K
NuPAGE MOPS SDS running buffer	Invitrogen	NP0001
ProSignal Full-Range Prestained Protein Ladder	Genesee Scientific	83-650
ProSignal Pico ECL Reagent	Genesee Scientific	20-300B
Protoscript II First Strand cDNA Synthesis Kit	New England Biolabs	E6560L
Q5 Site-Directed Mutagenesis Kit	New England Biolabs	E0552S
Quick-DNA Miniprep-Plus kit	Zymo Research	D4068
Quick-RNA kit	Zymo Research	R1055
QuikChange II XL Site-Directed Mutagenesis Kit	Agilent	210518
RNeasy mini kit	Qiagen	74104
Trans-Blot Turbo RTA Midi 0.45 µM PVDF Transfer Kit	Bio-Rad	1704273
*Trans*IT-mRNA Trnasfection Kit	Mirus Bio	MIR 2250
X-tremeGENE9 Transfection Reagent	Sigma-Aldrich	6365787001

SOFTWARE AND ALGORITHMS

Description	*Source or reference*	*URL*
CHOPCHOP	Labun *et al*, 2016	https://chopchop.cbu.uib.no
Database for Annotation, Visualization and Integrated Discovery v6.8	Frederick National Laboratory for Cancer Research, Frederick, MD	https://david.ncifcrf.gov/home.jsp
EnhancedVolcano	Clinical Bioinformatics Research LTD, United Kingdom	https://github.com/kevinblighe/EnhancedVolcano
FlowJo	BD Biosciences, Franklin, NJ	https://flowjo.com
Geneious Prime (2021.2)	Biomatters, San Diego, CA	https://geneious.com
GraphPad Prism 9 (v.9.2.0)	GraphPad Software, San Diego, CA	https://graphpad.com
ImageJ	National Institutes of Health, Bethesda, MD	https://imagej.net/
Matplotlib	Hunter, 2007	https://matplotlib.org
MIT Optimized CRISPR Design portal	Massachusetts Institute of Technology, Boston, MA	https://crispr.mit.edu
RStudio software (v.1.4.1106)	RStudio, Boston, MA	https://rstudio.com
SciPy	Virtanen *et al*, 2020	https://scipy.org
Seaborn	Waskom, 2021	https://seaborn.pydata.org
UCSF Chimera	University of California, San Francisco, San Francisco, CA	https://www.rbvi.ucsf.edu/chimera/

VIRUSES AND TRANSFECTED CONSTRUCTS

Reagent type (species) or resource	***Description***	***Source or reference***	***Identifiers / Additional information***
strain (*Chikungunya virus*)	CHIKV strain 7142.181/25	Gorchakov et al., 2012	
strain (*O'nyongnyong virus*)	ONNV-GFP	Brault et al., 2004	SG650 genome (GenBank AF079456)
strain (*Ross river virus*)	RR64-GFP	Morrison et al., 2006	
strain (*Sindbis virus)*	Toto1101	Rice et al., 1987	
strain (*Sindbis virus*)	Toto1101/Luc	Bick et al., 2003	
strain (*Sindbis virus*)	Toto1101/Luc:ts6	Bick et al., 2003	
strain (*Sindbis virus*)	TE-5'2J/GFP	Frolova et al., 2002	
strain (*Venezuelan equine encephalitis virus*)	VEEV-GFP	Atasheva et al., 2010	vaccine strain TC-83
transfected construct (*Homo sapiens*)	pGL3-Control Vector	Promega	E1741
transfected construct (*Japanese encephalitis virus*)	JEV-Rluc-Rep	Li et al., 2016	

References

—

Abraham, M. J., Murtola, T., Schulz, R., Páll, S., Smith, J. C., Hess, B., and Lindahl, E. (2015). GROMACS: High performance molecular simulations through multi-level parallelism from laptops to supercomputers. *SoftwareX* 1–2, 19–25. doi: 10.1016/j.softx.2015.06.001.

Atasheva, S., Krendelchtchikova, V., Liopo, A., Frolova, E., and Frolov, I. (2010). Interplay of Acute and Persistent Infections Caused by Venezuelan Equine Encephalitis Virus Encoding Mutated Capsid Protein. *Journal of Virology* 84, 10004–10015. doi: 10.1128/JVI.01151-10.

Au-Yeung, N., and Horvath, C. M. (2018). Transcriptional and chromatin regulation in interferon and innate antiviral gene expression. *Cytokine & Growth Factor Reviews* 44, 11–17. doi: 10.1016/j.cytogfr.2018.10.003.

Azar, S. R., Campos, R. K., Bergren, N. A., Camargos, V. N., and Rossi, S. L. (2020). Epidemic Alphaviruses: Ecology, Emergence and Outbreaks. *Microorganisms* 8, E1167. doi: 10.3390/microorganisms8081167.

Bai, Q., Bai, Z., Xu, S., and Sun, L. (2016). Detection of RNA-binding Proteins by In Vitro RNA Pull-down in Adipocyte Culture. *Journal of Visualized Experiments* e54207. doi: 10.3791/54207.

Baker, R. E., Mahmud, A. S., Miller, I. F., Rajeev, M., Rasambainarivo, F., Rice, B. L., Takahashi, S., Tatem, A. J., Wagner, C. E., Wang, L.-F., Wesolowski, A., and Metcalf, C. J. E. (2022). Infectious disease in an era of global change. *Nature Reviews Microbioliology* 20, 193–205. doi: 10.1038/s41579-021-00639-z.

Balistreri, G., Horvath, P., Schweingruber, C., Zünd, D., McInerney, G., Merits, A., Mühlemann, O., Azzalin, C., and Helenius, A. (2014). The Host Nonsense-Mediated mRNA Decay Pathway Restricts Mammalian RNA Virus Replication. *Cell Host & Microbe* 16, 403–411. doi: 10.1016/j.chom.2014.08.007.

Best, R. B., Zhu, X., Shim, J., Lopes, P. E. M., Mittal, J., Feig, M., and MacKerell, A. D. (2012). Optimization of the Additive CHARMM All-Atom Protein Force Field Targeting Improved Sampling of the Backbone ϕ, ψ and Side-Chain χ1 and χ2 Dihedral Angles. *Journal of Chemical Theory and Computation* 8, 3257–3273. doi: 10.1021/ct300400x.

Bick, M. J., Carroll, J.-W. N., Gao, G., Goff, S. P., Rice, C. M., and MacDonald, M. R. (2003). Expression of the Zinc-Finger Antiviral Protein Inhibits Alphavirus Replication. *Journal of Virology* 77, 11555–11562. doi: 10.1128/JVI.77.21.11555-11562.2003.

●● **This was the first study to show ZAP inhibition of alphavirus replication. This work also developed the SINV luciferase reporter viruses heavily utilized in this dissertation.**

Blighe, K., Rana, S., and Lewis, M. (2021). *EnhancedVolcano: Publication-ready volcano plots with enhanced colouring and labeling*. Available at: https://github.com/kevinblighe/EnhancedVolcano.

Bottermann, M., and James, L. C. (2018). Intracellular Antiviral Immunity. *Advances in Virus Research* 309–354. doi: 10.1016/bs.aivir.2018.01.002.

Brault, A. C., Foy, B. D., Myles, K. M., Kelly, C. L. H., Higgs, S., Weaver, S. C., Olson, K. E., Miller, B. R., and Powers, A. M. (2004). Infection patterns of o'nyong nyong virus in the malaria-transmitting mosquito, Anopheles gambiae. *Insect Molecular Biology* 13, 625–635. doi: 10.1111/j.0962-1075.2004.00521.x.

Brogden, K. A. (2005). Antimicrobial peptides: pore formers or metabolic inhibitors in bacteria? *Nature Reviews Microbiology* 3, 238–250. doi: 10.1038/nrmicro1098.

Burgess, H. M., Richardson, W. A., Anderson, R. C., Salaun, C., Graham, S. V., and Gray, N. K. (2011). Nuclear relocalisation of cytoplasmic poly(A)-binding proteins PABP1 and PABP4 in response to UV irradiation reveals mRNA-dependent export of metazoan PABPs. *Journal of Cell Science* 124, 3344–3355. doi: 10.1242/jcs.087692.

Cadena, C., Ahmad, S., Xavier, A., Willemsen, J., Park, S., Park, J. W., Oh, S.-W., Fujita, T., Hou, F., Binder, M., and Hur, S. (2019). Ubiquitin-Dependent and -Independent Roles of E3 Ligase RIPLET in Innate Immunity. *Cell* 177, 1187-1200.e16. doi: 10.1016/j.cell.2019.03.017.

Calo, E., Flynn, R. A., Martin, L., Spitale, R. C., Chang, H. Y., and Wysocka, J. (2015). RNA helicase DDX21 coordinates transcription and ribosomal RNA processing. *Nature* 518, 249–253. doi: 10.1038/nature13923.

Carpentier, K. S., and Morrison, T. E. (2018). Innate immune control of alphavirus infection. *Current Opinion in Virology* 28, 53–60. doi: 10.1016/j.coviro.2017.11.006.

Castanier, C., Zemirli, N., Portier, A., Garcin, D., Bidère, N., Vazquez, A., and Arnoult, D. (2012). MAVS ubiquitination by the E3 ligase TRIM25 and degradation by the proteasome is involved in type I interferon production after activation of the antiviral RIG-I-like receptors. *BMC Biology* 10, 44. doi: 10.1186/1741-7007-10-44.

Castello, A., Fischer, B., Eichelbaum, K., Horos, R., Beckmann, B. M., Strein, C., Davey, N. E., Humphreys, D. T., Preiss, T., Steinmetz, L. M., Krijgsveld, J., and Hentze, M. W. (2012). Insights into RNA Biology from an Atlas of Mammalian mRNA-Binding Proteins. *Cell* 149, 1393–1406. doi: 10.1016/j.cell.2012.04.031.

Castello, A., Fischer, B., Frese, C. K., Horos, R., Alleaume, A.-M., Foehr, S., Curk, T., Krijgsveld, J., and Hentze, M. W. (2016). Comprehensive Identification of RNA-Binding Domains in Human Cells. *Molecular Cell* 63, 696–710. doi: 10.1016/j.molcel.2016.06.029.

Chabanon, M., and Rangamani, P. (2018). Gaussian curvature directs the distribution of spontaneous curvature on bilayer membrane necks. *Soft Matter* 14, 2281–2294. doi: 10.1039/c8sm00035b.

Chan, D., Feng, C., England, W., Wyman, D., Flynn, R. A., Wang, X., Shi, Y., Mortazavi, A., and Spitale, R. C. (2020). Transcriptome-Wide Combinatorial RNA Structure Probing in Living Cells. *bioRxiv* 2020.03.24.006866. doi: 10.1101/2020.03.24.006866.

Charron, G., Li, M. M. H., MacDonald, M. R., and Hang, H. C. (2013). Prenylome profiling reveals S-farnesylation is crucial for membrane targeting and antiviral activity of ZAP long-isoform. *PNAS* 110, 11085–11090. doi: 10.1073/pnas.1302564110.

Chemudupati, M., Kenney, A. D., Bonifati, S., Zani, A., McMichael, T. M., Wu, L., and Yount, J. S. (2019). From APOBEC to ZAP: Diverse mechanisms used by cellular restriction factors to inhibit virus infections. *Biochimica et Biophysica Acta - Molecular Cell Research* 1866, 382–394. doi: 10.1016/j.bbamcr.2018.09.012.

Chen, G., Guo, X., Lv, F., Xu, Y., and Gao, G. (2008). p72 DEAD box RNA helicase is required for optimal function of the zinc-finger antiviral protein. *PNAS* 105, 4352–4357. doi: 10.1073/pnas.0712276105.

Chen, G., Liu, C.-H., Zhou, L., and Krug, R. M. (2014). Cellular DDX21 RNA Helicase Inhibits Influenza A Virus Replication but Is Counteracted by the Viral NS1 Protein. *Cell Host & Microbe* 15, 484–493. doi: 10.1016/j.chom.2014.03.002.

Chen, S., Xu, Y., Zhang, K., Wang, X., Sun, J., Gao, G., and Liu, Y. (2012). Structure of N-terminal domain of ZAP indicates how a zinc-finger protein recognizes complex RNA. *Nature Structural & Molecular Biology* 19, 430–435. doi: 10.1038/nsmb.2243.

- **This was the first crystal structure of NZAP.**

Chen, W., Xiong, S., Li, J., Li, X., Liu, Y., Zou, C., and Mallampalli, R. K. (2015). The Ubiquitin E3 Ligase SCF-FBXO24 Recognizes Deacetylated Nucleoside Diphosphate Kinase A To Enhance Its Degradation. *Molecular and Cellular Biology* 35, 1001–1013. doi: 10.1128/MCB.01185-14.

Cheng, X., Virk, N., Chen, W., Ji, S., Ji, S., Sun, Y., and Wu, X. (2013). CpG Usage in RNA Viruses: Data and Hypotheses. *PLoS ONE* 8, e74109. doi: 10.1371/journal.pone.0074109.

Chernomordik, L. V., and Kozlov, M. M. (2003). Protein-lipid interplay in fusion and fission of biological membranes. *Annual Review of Biochemistry* 72, 175–207. doi: 10.1146/annurev.biochem.72.121801 .161504.

Chiu, H.-P., Chiu, H., Yang, C.-F., Lee, Y.-L., Chiu, F.-L., Kuo, H.-C., Lin, R.-J., and Lin, Y.-L. (2018). Inhibition of Japanese encephalitis virus infection by the host zinc-finger antiviral protein. *PLoS Pathogens* 14, e1007166. doi: 10.1371/journal.ppat.1007166.

Choudhury, N. R., Heikel, G., and Michlewski, G. (2020). TRIM25 and its emerging RNA-binding roles in antiviral defense. *WIREs RNA* 11, e1588. doi: 10.1002/wrna.1588.

Choudhury, N. R., Heikel, G., Trubitsyna, M., Kubik, P., Nowak, J. S., Webb, S., Granneman, S., Spanos, C., Rappsilber, J., Castello, A., and Michlewski, G. (2017). RNA-binding activity of TRIM25 is mediated by its PRY/SPRY domain and is required for ubiquitination. *BMC Biology* 15, 105. doi: 10.1186/s12915-017-0444-9.

●● This was the first study to tie TRIM25 RNA binding activity to its ligase activity.

Clark, L. E., Clark, S. A., Lin, C., Liu, J., Coscia, A., Nabel, K. G., Yang, P., Neel, D. V., Lee, H., Brusic, V., Stryapunina, I., Plante, K. S., Ahmed, A. A., Catteruccia, F., Young-Pearse, T. L., Chiu, I. M., Llopis, P. M., Weaver, S. C., and Abraham, J. (2022). VLDLR and ApoER2 are receptors for multiple alphaviruses. *Nature* 602, 475–480. doi: 10.1038/s41586-021-04326-0.

Cordin, O., Banroques, J., Tanner, N. K., and Linder, P. (2006). The DEAD-box protein family of RNA helicases. *Gene* 367, 17–37. doi: 10.1016/j.gene.2005.10.019.

Cox, J., and Mann, M. (2008). MaxQuant enables high peptide identification rates, individualized p.p.b.-range mass accuracies and proteome-wide protein quantification. *Nature Biotechnology* 26, 1367–1372. doi: 10.1038/nbt.1511.

Cristea, I. M., Carroll, J.-W. N., Rout, M. P., Rice, C. M., Chait, B. T., and MacDonald, M. R. (2006). Tracking and Elucidating Alphavirus-Host Protein Interactions. *Journal of Biological Chemistry* 281, 30269–30278. doi: 10.1074/jbc.M603980200.

Cristea, I. M., Rozjabek, H., Molloy, K. R., Karki, S., White, L. L., Rice, C. M., Rout, M. P., Chait, B. T., and MacDonald, M. R. (2010). Host Factors Associated with the Sindbis Virus RNA-Dependent RNA Polymerase: Role for G3BP1 and G3BP2 in Virus Replication. *Journal of Virology* 84, 6720–6732. doi: 10.1128/JVI.01983-09.

Daugherty, M. D., and Malik, H. S. (2012). Rules of Engagement: Molecular Insights from Host-Virus Arms Races. *Annual Review of Genetics* 46, 677–700. doi: 10.1146/annurev-genet-110711-155522.

Davarinejad, H. (2015). Quantifications of western blots with ImageJ. *University of York*.

Decorsière, A., Mueller, H., van Breugel, P. C., Abdul, F., Gerossier, L., Beran, R. K., Livingston, C. M., Niu, C., Fletcher, S. P., Hantz, O., and Strubin, M. (2016). Hepatitis B virus X protein identifies the Smc5/6 complex as a host restriction factor. *Nature* 531, 386–380. doi: 10.1038/nature17170.

●● This work inspired the design of the "substrate trapping" approach utilized in Chapter 2.

Deutschmann, J., and Gramberg, T. (2021). SAMHD1 … and Viral Ways around It. *Viruses* 13, 395. doi: 10.3390/v13030395.

Domingo, E., García-Crespo, C., Lobo-Vega, R., and Perales, C. (2021). Mutation Rates, Mutation Frequencies, and Proofreading-Repair Activities in RNA Virus Genetics. *Viruses* 13, 1882. doi: 10.3390/v13091882.

Dong, X.-Y., Fu, X., Fan, S., Guo, P., Su, D., and Dong, J.-T. (2012). Oestrogen causes ATBF1 protein degradation through the oestrogen-responsive E3 ubiquitin ligase EFP. *Biochemical Journal* 444, 581–590. doi: 10.1042/BJ20111890.

Duffy, S. (2018). Why are RNA virus mutation rates so damn high? *PLoS Biology* 16, e3000003. doi: 10.1371/journal.pbio.3000003.

Düzgüneş, N., Fernandez-Fuentes, N., and Konopka, K. (2021). Inhibition of Viral Membrane Fusion by Peptides and Approaches to Peptide Design. *Pathogens* 10, 1599. doi: 10.3390/pathogens10121599.

Esposito, D., Koliopoulos, M. G., and Rittinger, K. (2017). Structural determinants of TRIM protein function. *Biochemical Society Transactions* 45, 183–191. doi: 10.1042/BST20160325.

Feng, Q., Jagannathan, S., and Bradley, R. K. (2017). The RNA Surveillance Factor UPF1 Represses Myogenesis via Its E3 Ubiquitin Ligase Activity. *Molecular Cell* 67, 239-251.e6. doi: 10.1016/j.molcel.2017.05.034.

Ficarelli, M., Antzin-Anduetza, I., Hugh-White, R., Firth, A. E., Sertkaya, H., Wilson, H., Neil, S. J. D., Schulz, R., and Swanson, C. M. (2020). CpG Dinucleotides Inhibit HIV-1 Replication through Zinc Finger Antiviral Protein (ZAP)-Dependent and -Independent Mechanisms. *Journal of Virology* 94, e01337–19. doi: 10.1128/JVI.01337-19.

Ficarelli, M., Neil, S. J. D., and Swanson, C. M. (2021). Targeted Restriction of Viral Gene Expression and Replication by the ZAP Antiviral System. *Annual Review of Virology.* 8, 265–283. doi: 10.1146/annurev-virology-091919-104213.

Ficarelli, M., Wilson, H., Pedro Galão, R., Mazzon, M., Antzin-Anduetza, I., Marsh, M., Neil, S. J., and Swanson, C. M. (2019). KHNYN is essential for the zinc finger antiviral protein (ZAP) to restrict HIV-1 containing clustered CpG dinucleotides. *eLife* 8, e46767. doi: 10.7554/eLife.46767.

●● **This study identified KHNYN, a putative endoribonuclease, as the ZAP co-factor likely responsible for degrading HIV-1 RNA in the context of ZAP viral inhibition.**

Fischer, J. W., Busa, V. F., Shao, Y., and Leung, A. K. L. (2020). Structure-Mediated RNA Decay by UPF1 and G3BP1. *Molecular Cell* 78, 70-84. doi: 10.1016/j.molcel.2020.01.021.

Flint, J., Racaniello, V. R., Rall, G. F., Skalka, A. M., and Enquist, L. W. (2015). *Principles of Virology*. 4th ed. Washington, D.C.: ASM Press.

Forte, T. M., Nichols, A. V., Gong, E. L., Levy, R. I., and Lux, S. (1971). Electron microscopic study on reassembly of plasma high density apoprotein with various lipids. *Biochimica et Biophysica Acta* 248, 381–386. doi: 10.1016/0005-2760(71)90026-9.

Frolov, V. A., Escalada, A., Akimov, S. A., and Shnyrova, A. V. (2015). Geometry of membrane fission. *Chemistry and Physics of Lipids* 185, 129–140. doi: 10.1016/j.chemphyslip.2014.07.006.

Frolova, E. I., Fayzulin, R. Z., Cook, S. H., Griffin, D. E., Rice, C. M., and Frolov, I. (2002). Roles of Nonstructural Protein nsP2 and Alpha/Beta Interferons in Determining the Outcome of Sindbis Virus Infection. *Journal of Virology* 76, 11254–11264. doi: 10.1128/JVI.76.22.11254-11264.2002.

Gack, M. U., Albrecht, R. A., Urano, T., Inn, K.-S., Huang, I.-C., Carnero, E., Farzan, M., Inoue, S., Jung, J. U., and García-Sastre, A. (2009). Influenza A Virus NS1 Targets the Ubiquitin Ligase TRIM25 to Evade Recognition by the Host Viral RNA Sensor RIG-I. *Cell Host & Microbe* 5, 439–449. doi: 10.1016/j.chom.2009.04.006.

Gack, M. U., Kirchhofer, A., Shin, Y. C., Inn, K.-S., Liang, C., Cui, S., Myong, S., Ha, T., Hopfner, K.-P., and Jung, J. U. (2008). Roles of RIG-I N-terminal tandem CARD and splice variant in TRIM25-mediated antiviral signal transduction. *PNAS* 105, 16743–16748. doi: 10.1073/pnas.0804947105.

Gack, M. U., Shin, Y. C., Joo, C.-H., Urano, T., Liang, C., Sun, L., Takeuchi, O., Akira, S., Chen, Z., Inoue, S., and Jung, J. U. (2007). TRIM25 RING-finger E3 ubiquitin ligase is essential for RIG-I-mediated antiviral activity. *Nature* 446, 916–920. doi: 10.1038/nature05732.

●● **This was the first study to identify TRIM25 as ubiquitinating and activating RIG-I (dsRNA sensor).**

Galão, R. P., Wilson, H., Schierhorn, K. L., Debeljak, F., Bodmer, B. S., Goldhill, D., Hoenen, T., Wilson, S. J., Swanson, C. M., and Neil, S. J. D. (2022). TRIM25 and ZAP target the Ebola virus ribonucleoprotein complex to mediate interferon-induced restriction. *PLoS Pathogens* 18, e1010530. doi: 10.1371/journal.ppat.1010530.

● **This study demonstrates TRIM25 and ZAP cooperative inhibition of an EBOV replicon.**

Gallop, J. L., Jao, C. C., Kent, H. M., Butler, P. J. G., Evans, P. R., Langen, R., and McMahon, H. T. (2006). Mechanism of endophilin N-BAR domain-mediated membrane curvature. *EMBO Journal* 25, 2898–2910. doi: 10.1038/sj.emboj.7601174.

Ganser-Pornillos, B. K., and Pornillos, O. (2019). Restriction of HIV-1 and other retroviruses by TRIM5. *Nature Reviews Microbiology* 17, 546–556. doi: 10.1038/s41579-019-0225-2.

Gao, G., Guo, X., and Goff, S. P. (2002). Inhibition of Retroviral RNA Production by ZAP, a CCCH-Type Zinc Finger Protein. *Science* 297, 1703–1706. doi: 10.1126/science.1074276.

●● **This was the first study to identify ZAP.**

Gao, J., Tang, Y.-D., Hu, W., and Zheng, C. (2022). When Poly(A) Binding Proteins Meet Viral Infections, Including SARS-CoV-2. *Journal of Virology* 96, e00136-22. doi: 10.1128/jvi.00136-22.

Garcia-Moreno, M., Noerenberg, M., Ni, S., Järvelin, A. I., González-Almela, E., Lenz, C. E., Bach-Pages, M., Cox, V., Avolio, R., Davis, T., Hester, S., Sohier, T. J. M., Li, B., Heikel, G., Michlewski, G., Sanz, M. A., Carrasco, L., Ricci, E. P., Pelechano, V., Davis, I., Fischer, B., Mohammed, S., and Castello, A. (2019). System-wide Profiling of RNA-Binding Proteins Uncovers Key Regulators of Virus Infection. *Molecular Cell* 74, 196-211.e11. doi: 10.1016/j.molcel.2019.01.017.

●● **This study utilized RNA interactome capture to demonstrate that TRIM25 and ZAP bind to SINV gRNA during infection, and that their RNA binding activity increases during infection.**

Gioacchino, A. D., Šulc, P., Komarova, A. V., Greenbaum, B. D., Monasson, R., and Cocco, S. (2020). The heterogeneous landscape and early evolution of pathogen-associated CpG dinucleotides in SARS-CoV-2. *bioRxiv* 2020.05.06.074039. doi: 10.1101/2020.05.06.074039.

Gläsker, S., Töller, M., and Kümmerer, B. M. (2014). The alternate triad motif of the poly(ADP-ribose) polymerase-like domain of the human zinc finger antiviral protein is essential for its antiviral activity. *Journal of General Virology* 95, 816–822. doi: 10.1099/vir.0.060988-0.

- **Interestingly, this study showed that replacing the inactive catalytic triad in the ZAP PARP-like domain with an active triad diminishes ZAPL antiviral activity.**

Gonçalves-Carneiro, D., Takata, M. A., Ong, H., Shilton, A., and Bieniasz, P. D. (2021). Origin and evolution of the zinc finger antiviral protein. *PLoS Pathogens* 17, e1009545. doi: 10.1371/journal.ppat.1009545.

- ● **This study demonstrated some species-specific preferences for ZAP-TRIM25 pairing to inhibit HIV-1^{CG} replication.**

Gonzalez-Perez, A. C., Stempel, M., Wyler, E., Urban, C., Piras, A., Hennig, T., Ganskih, S., Wei, Y., Heim, A., Landthaler, M., Pichlmair, A., Dölken, L., Munschauer, M., Erhard, F., and Brinkmann, M. M. (2021). The Zinc Finger Antiviral Protein ZAP Restricts Human Cytomegalovirus and Selectively Binds and Destabilizes Viral UL4/UL5 Transcripts. *mBio* 12, e02683-20. doi: 10.1128/mBio.02683-20.

Goodier, J. L., Pereira, G. C., Cheung, L. E., Rose, R. J., and Kazazian, H. H. (2015). The Broad-Spectrum Antiviral Protein ZAP Restricts Human Retrotransposition. *PLoS Genetics* 11, e1005252. doi: 10.1371/journal.pgen.1005252.

- **This study identified ZAPL interactors via co-IP/MS and used IF to verify interactions with GFP-ZAPS, demonstrating that ZAP and its interactors localize to SGs.**

Gorchakov, R., Wang, E., Leal, G., Forrester, N. L., Plante, K., Rossi, S. L., Partidos, C. D., Adams, A. P., Seymour, R. L., Weger, J., Borland, E. M., Sherman, M. B., Powers, A. M., Osorio, J. E., and Weaver, S. C. (2012). Attenuation of Chikungunya Virus Vaccine Strain 181/Clone 25 Is Determined by Two Amino Acid Substitutions in the E2 Envelope Glycoprotein. *Journal of Virology* 86, 6084–6096. doi: 10.1128/JVI.06449-11.

Götte, B., Liu, L., and McInerney, G. (2018). The Enigmatic Alphavirus Non-Structural Protein 3 (nsP3) Revealing Its Secrets at Last. *Viruses* 10, 105. doi: 10.3390/v10030105.

Götte, B., Panas, M. D., Hellström, K., Liu, L., Samreen, B., Larsson, O., Ahola, T., and McInerney, G. M. (2019). Separate domains of G3BP promote efficient clustering of alphavirus replication complexes and recruitment of the translation initiation machinery. *PLoS Pathogens* 15, e1007842. doi: 10.1371/journal.ppat.1007842.

Götte, B., Utt, A., Fragkoudis, R., Merits, A., and McInerney, G. M. (2020). Sensitivity of Alphaviruses to G3BP Deletion Correlates with Efficiency of Replicase Polyprotein Processing. *Journal of Virology* 94, e01681-19. doi: 10.1128/JVI.01681-19.

Greenbaum, B. D., Levine, A. J., Bhanot, G., and Rabadan, R. (2008). Patterns of Evolution and Host Gene Mimicry in Influenza and Other RNA Viruses. *PLoS Pathogens* 4, e1000079. doi: 10.1371/journal.ppat.1000079.

Griffin, D. E. (2013). "Chapter 23. Alphaviruses," in *Fields Virology* (Lippincott Williams & Wilkins), 629–650.

Guo, X., Carroll, J.-W. N., MacDonald, M. R., Goff, S. P., and Gao, G. (2004). The Zinc Finger Antiviral Protein Directly Binds to Specific Viral mRNAs through the CCCH Zinc Finger Motifs. *Journal of Virology* 78, 12781–12787. doi: 10.1128/JVI.78.23.12781-12787.2004.

●● **This was the first study to show ZAP binding to viral RNAs via its N-terminal ZnFs. It demonstrated that ZnF 2 and 4 were critical for ZAP antiviral activity, but only demonstrated direct involvement of ZnF 2 in RNA binding.**

Guo, X., Ma, J., Sun, J., and Gao, G. (2007). The zinc-finger antiviral protein recruits the RNA processing exosome to degrade the target mRNA. *PNAS* 104, 151–156. doi: 10.1073/pnas.0607063104.

Hage, A., and Rajsbaum, R. (2019). To TRIM or not to TRIM: the balance of host–virus interactions mediated by the ubiquitin system. *Journal of General Virology* 100, 1641–1662. doi: 10.1099/jgv.0.001341.

Haller, O., Staeheli, P., Schwemmle, M., and Kochs, G. (2015). Mx GTPases: dynamin-like antiviral machines of innate immunity. *Trends in Microbiology* 23, 154–163. doi: 10.1016/j.tim.2014.12.003.

Han, P., Ye, W., Lv, X., Ma, H., Weng, D., Dong, Y., Cheng, L., Chen, H., Zhang, L., Xu, Z., Lei, Y., and Zhang, F. (2017). DDX50 inhibits the replication of dengue virus 2 by upregulating IFN-β production. *Archives of Virology* 162, 1487–1494. doi: 10.1007/s00705-017-3250-3.

Harrison, S. C. (2008). Viral membrane fusion. *Nature Structural & Molecular Biology* 15, 690–698. doi: 10.1038/nsmb.1456.

Hatakeyama, S. (2017). TRIM Family Proteins: Roles in Autophagy, Immunity, and Carcinogenesis. *Trends in Biochemical Sciences* 42, 297–311. doi: 10.1016/j.tibs.2017.01.002.

Hayakawa, S., Shiratori, S., Yamato, H., Kameyama, T., Kitatsuji, C., Kashigi, F., Goto, S., Kameoka, S., Fujikura, D., Yamada, T., Mizutani, T., Kazumata, M., Sato, M., Tanaka, J., Asaka, M., Ohba, Y., Miyazaki, T., Imamura, M., and Takaoka, A. (2011). ZAPS is a potent stimulator of signaling mediated by the RNA helicase RIG-I during antiviral responses. *Nature Immunology* 12, 37–44. doi: 10.1038/ni.1963.

Hayman, T. J., Hsu, A. C., Kolesnik, T. B., Dagley, L. F., Willemsen, J., Tate, M. D., Baker, P. J., Kershaw, N. J., Kedzierski, L., Webb, A. I., Wark, P. A., Kedzierska, K., Masters, S. L., Belz, G. T., Binder, M., Hansbro, P. M., Nicola, N. A., and Nicholson, S. E. (2019). RIPLET, and not TRIM25, is required for endogenous RIG-I-dependent antiviral responses. *Immunology & Cell Biology* 97, 840–852. doi: 10.1111/imcb.12284.

Heikel, G., Choudhury, N. R., and Michlewski, G. (2016). The role of Trim25 in development, disease and RNA metabolism. *Biochemical Society Transactions* 44, 1045–1050. doi: 10.1042/BST20160077.

Hess, B., Bekker, H., Berendsen, H. J. C., and Fraaije, J. G. E. M. (1997). LINCS: A linear constraint solver for molecular simulations. *Journal of Computational Chemistry* 18, 1463–1472. doi: 10.1002/(SICI)1096-987X(199709)18:12<1463::AID-JCC4>3.0.CO;2-H.

Hickel, A., Danner-Pongratz, S., Amenitsch, H., Degovics, G., Rappolt, M., Lohner, K., and Pabst, G. (2008). Influence of antimicrobial peptides on the formation of nonlamellar lipid mesophases. *Biochimica et Biophysica Acta - Biomembranes* 1778, 2325–2333. doi: 10.1016/j.bbamem.2008.05.014.

Hoover, W. G. (1985). Canonical dynamics: Equilibrium phase-space distributions. *Physical Review A* 31, 1695–1697. doi: 10.1103/PhysRevA.31.1695.

Hornbeck, P. V., Zhang, B., Murray, B., Kornhauser, J. M., Latham, V., and Skrzypek, E. (2015). PhosphoSitePlus, 2014: mutations, PTMs and recalibrations. *Nucleic Acids Research* 43, D512–D520. doi: 10.1093/nar/gku1267.

Hou, F., Sun, L., Zheng, H., Skaug, B., Jiang, Q.-X., and Chen, Z. J. (2011). MAVS Forms Functional Prion-like Aggregates to Activate and Propagate Antiviral Innate Immune Response. *Cell* 146, 448–461. doi: 10.1016/j.cell.2011.06.041.

Huang, D. W., Sherman, B. T., and Lempicki, R. A. (2009). Systematic and integrative analysis of large gene lists using DAVID bioinformatics resources. *Nature Protocols* 4, 44–57. doi: 10.1038/nprot.2008.211.

Huang, H., Weng, H., Sun, W., Qin, X., Shi, H., Wu, H., Zhao, B. S., Mesquita, A., Liu, C., Yuan, C. L., Hu, Y.-C., Hüttelmaier, S., Skibbe, J. R., Su, R., Deng, X., Dong, L., Sun, M., Li, C., Nachtergaele, S., Wang, Y., Hu, C., Ferchen, K., Greis, K. D., Jiang, X., Wei, M., Qu, L., Guan, J.-L., He, C., Yang, J., and Chen, J. (2018). Recognition of RNA N6-methyladenosine by IGF2BP proteins enhances mRNA stability and translation. *Nature Cell Biology* 20, 285–295. doi: 10.1038/s41556-018-0045-z.

Huang, J., and MacKerell Jr, A. D. (2013). CHARMM36 all-atom additive protein force field: Validation based on comparison to NMR data. *Journal of Computational Chemistry* 34, 2135–2145. doi: 10.1002/jcc.23354.

Huang, Y.-J. S., Higgs, S., and Vanlandingham, D. L. (2019). Emergence and re-emergence of mosquito-borne arboviruses. *Current Opinion in Virology* 34, 104–109. doi: 10.1016/j.coviro.2019.01.001.

Hubel, P., Urban, C., Bergant, V., Schneider, W. M., Knauer, B., Stukalov, A., Scaturro, P., Mann, A., Brunotte, L., Hoffmann, H. H., Schoggins, J. W., Schwemmle, M., Mann, M., Rice, C. M., and Pichlmair, A. (2019). A protein-interaction network of interferon-stimulated genes extends the innate immune system landscape. *Nature Immunology* 20, 493–502. doi: 10.1038/s41590-019-0323-3.

Hunter, J. D. (2007). Matplotlib: A 2D Graphics Environment. *Computing in Science Engineering* 9, 90–95. doi: 10.1109/MCSE.2007.55.

Ikeda, K., Orimo, A., Higashi, Y., Muramatsu, M., and Inoue, S. (2000). Efp as a primary estrogen-responsive gene in human breast cancer. *FEBS Letters* 472, 9–13. doi: 10.1016/S0014-5793(00)01421-6.

Ilavsky, J. (2012). Nika: software for two-dimensional data reduction. *Journal of Applied Crystallography* 45, 324–328. doi: 10.1107/S0021889812004037.

Inoue, S., Orimo, A., Hosoi, T., Kondo, S., Toyoshima, H., Kondo, T., Ikegami, A., Ouchi, Y., Orimo, H., and Muramatsu, M. (1993). Genomic Binding-Site Cloning Reveals an Estrogen-Responsive Gene that Encodes a RING Finger Protein. *PNAS* 90, 11117–11121.
●● This was the first study to identify TRIM25 (initially named EFP).

Inoue, S., Orimo, A., Matsuda, Y., Inazawa, J., Emi, M., Nakamura, Y., Hori, T., and Muramatsu, M. (1995). Chromosome mapping of human (ZNF147) and mouse genes for estrogen-responsive finger protein (efp), a member of the RING finger family. *Genomics* 25, 581–583. doi: 10.1016/0888-7543(95)80064-S.

Jami-Alahmadi, Y., Pandey, V., Mayank, A. K., and Wohlschlegel, J. A. (2021). A Robust Method for Packing High Resolution C18 RP-nano-HPLC Columns. *Journal of Visualized Experiments* e62380. doi: 10.3791/62380.

Jia, C., Tang, H., Yang, Y., Yuan, S., Han, T., Fang, M., Huang, S., Hu, R., Li, C., and Geng, W. (2020). Ubiquitination of IGF2BP3 by E3 ligase MKRN2 regulates the proliferation and migration of human neuroblastoma SHSY5Y cells. *Biochemical and Biophysical Research Communications* 529, 43–50. doi: 10.1016/j.bbrc.2020.05.112.

Jiang, X., Kinch, L. N., Brautigam, C. A., Chen, X., Du, F., Grishin, N. V., and Chen, Z. J. (2012). Ubiquitin-Induced Oligomerization of the RNA Sensors RIG-I and MDA5 Activates Antiviral Innate Immune Response. *Immunity* 36, 959–973. doi: 10.1016/j.immuni.2012.03.022.

Jiao, Y., Kong, N., Wang, H., Sun, D., Dong, S., Chen, X., Zheng, H., Tong, W., Yu, H., Yu, L., Huang, Y., Wang, H., Sui, B., Zhao, L., Liao, Y., Zhang, W., Tong, G., and Shan, T. (2021). PABPC4 Broadly Inhibits Coronavirus Replication by Degrading Nucleocapsid Protein through Selective Autophagy. *Microbiology Spectrum* 9, e00908-21. doi: 10.1128/Spectrum.00908-21.

Jimenez-Morales, D., Rosa Campos, A., and Von Dollen, J. (2019). artMS: Analytical R tools for Mass Spectrometry. R package version 1.4.2.

Jo, S., Kim, T., Iyer, V. G., and Im, W. (2008). CHARMM-GUI: A web-based graphical user interface for CHARMM. *Journal of Computational Chemistry* 29, 1859–1865. doi: 10.1002/jcc.20945.

Jonas, A., Wald, J. H., Toohill, K. L., Krul, E. S., and Kézdy, K. E. (1990). Apolipoprotein A-I structure and lipid properties in homogeneous, reconstituted spherical and discoidal high density lipoproteins. *Journal of Biological Chemistry* 265, 22123–22129. doi: 10.1016/S0021-9258(18)45679-7.

Jorgensen, W. L., Chandrasekhar, J., Madura, J. D., Impey, R. W., and Klein, M. L. (1983). Comparison of simple potential functions for simulating liquid water. *Journal of Chemical Physics* 79, 926–935. doi: 10.1063/1.445869.

Judd, E. N., Gilchrist, A. R., Meyerson, N. R., and Sawyer, S. L. (2021). Positive natural selection in primate genes of the type I interferon response. *BMC Ecology and Evolution* 21, 65. doi: 10.1186/s12862-021-01783-z.

Kang, W., Wang, Y., Yang, W., Zhang, J., Zheng, H., and Li, D. (2021). Research Progress on the Structure and Function of G3BP. *Frontiers in Immunology* 12:718548. doi: 10.3389/fimmu.2021.718548.

Karki, S., Li, M. M. H., Schoggins, J. W., Tian, S., Rice, C. M., and MacDonald, M. R. (2012). Multiple Interferon Stimulated Genes Synergize with the Zinc Finger Antiviral Protein to Mediate Anti-Alphavirus Activity. *PLoS ONE* 7, e37398. doi: 10.1371/journal.pone.0037398.

Keller, S. L., Gruner, S. M., and Gawrisch, K. (1996). Small concentrations of alamethicin induce a cubic phase in bulk phosphatidylethanolamine mixtures. *Biochimica et Biophysica Acta - Biomembranes* 1278, 241–246. doi: 10.1016/0005-2736(95)00229-4.

Kerns, J. A., Emerman, M., and Malik, H. S. (2008). Positive Selection and Increased Antiviral Activity Associated with the PARP-Containing Isoform of Human Zinc-Finger Antiviral Protein. *PLoS Genetics* 4, e21. doi: 10.1371/journal.pgen.0040021.

Kim, D. Y., Reynaud, J. M., Rasalouskaya, A., Akhrymuk, I., Mobley, J. A., Frolov, I., and Frolova, E. I. (2016). New World and Old World Alphaviruses Have Evolved to Exploit Different Components of Stress Granules, FXR and G3BP Proteins, for Assembly of Viral Replication Complexes. *PLoS Pathogens* 12, e1005810. doi: 10.1371/journal.ppat.1005810.

Kim, W., Bennett, E. J., Huttlin, E. L., Guo, A., Li, J., Possemato, A., Sowa, M. E., Rad, R., Rush, J., Comb, M. J., Harper, J. W., and Gygi, S. P. (2011). Systematic and Quantitative Assessment of the Ubiquitin-Modified Proteome. *Molecular Cell* 44, 325–340. doi: 10.1016/j.molcel.2011.08.025.

Kim, Y. K., and Maquat, L. E. (2019). UPFront and center in RNA decay: UPF1 in nonsense-mediated mRNA decay and beyond. *RNA* 25, 407–422. doi: 10.1261/rna.070136.118.

Klauda, J. B., Venable, R. M., Freites, J. A., O'Connor, J. W., Tobias, D. J., Mondragon-Ramirez, C., Vorobyov, I., MacKerell, A. D., and Pastor, R. W. (2010). Update of the CHARMM All-Atom Additive Force Field for Lipids: Validation on Six Lipid Types. *Journal of Physical Chemistry B* 114, 7830–7843. doi: 10.1021/jp101759q.

Kmiec, D., Lista, M. J., Ficarelli, M., Swanson, C. M., and Neil, S. J. D. (2021). S-farnesylation is essential for antiviral activity of the long ZAP isoform against RNA viruses with diverse replication strategies. *PLoS Pathogens* 17, e1009726. doi: 10.1371/journal.ppat.1009726.

Kmiec, D., Nchioua, R., Sherrill-Mix, S., Stürzel, C. M., Heusinger, E., Braun, E., Gondim, M. V. P., Hotter, D., Sparrer, K. M. J., Hahn, B. H., Sauter, D., and Kirchhoff, F. (2020). CpG Frequency in the 5′ Third of the env Gene Determines Sensitivity of Primary HIV-1 Strains to the Zinc-Finger Antiviral Protein. *mBio* 11, e02903–19. doi: 10.1128/mBio.02903-19.

Koepke, L., Gack, M. U., and Sparrer, K. M. (2021). The antiviral activities of TRIM proteins. *Current Opinion in Microbiology* 59, 50–57. doi: 10.1016/j.mib.2020.07.005.

Koliopoulos, M. G., Esposito, D., Christodoulou, E., Taylor, I. A., and Rittinger, K. (2016). Functional role of TRIM E3 ligase oligomerization and regulation of catalytic activity. *EMBO Journal* 35, 1204–1218. doi: 10.15252/embj.201593741.

Komander, D., and Rape, M. (2012). The Ubiquitin Code. *Annual Review of Biochemistry* 81, 203–229. doi: 10.1146/annurev-biochem-060310-170328.

Kozlov, M. M., McMahon, H. T., and Chernomordik, L. V. (2010). Protein-driven membrane stresses in fusion and fission. *Trends in Biochemical Sciences* 35, 699–706. doi: 10.1016/j.tibs.2010.06.003.

Kraemer, M. U. G., Reiner, R. C., Brady, O. J., Messina, J. P., Gilbert, M., Pigott, D. M., Yi, D., Johnson, K., Earl, L., Marczak, L. B., Shirude, S., Davis Weaver, N., Bisanzio, D., Perkins, T. A., Lai, S., Lu, X., Jones, P., Coelho, G. E., Carvalho, R. G., Van Bortel, W., Marsboom, C., Hendrickx, G., Schaffner, F., Moore, C. G., Nax, H. H., Bengtsson, L., Wetter, E., Tatem, A. J., Brownstein, J. S., Smith, D. L., Lambrechts, L., Cauchemez, S., Linard, C., Faria, N. R., Pybus, O. G., Scott, T. W., Liu, Q., Yu, H., Wint, G. R. W., Hay, S. I., and Golding, N. (2019). Past and future spread of the arbovirus vectors Aedes aegypti and Aedes albopictus. *Nature Microbiology* 4, 854–863. doi: 10.1038/s41564-019-0376-y.

Kruse, T., Benz, C., Garvanska, D. H., Lindqvist, R., Mihalic, F., Coscia, F., Inturi, R., Sayadi, A., Simonetti, L., Nilsson, E., Ali, M., Kliche, J., Moliner Morro, A., Mund, A., Andersson, E., McInerney, G., Mann, M., Jemth, P., Davey, N. E., Överby, A. K., Nilsson, J., and Ivarsson, Y. (2021). Large scale discovery of coronavirus-host factor protein interaction motifs reveals SARS-CoV-2 specific mechanisms and vulnerabilities. *Nature Communications* 12, 6761. doi: 10.1038/s41467-021-26498-z.

Kuhn, R. J. (2013). "Chapter 22. Togaviridae," in *Fields Virology* (Lippincott Williams & Wilkins), 629–650.

Kwon, S. C., Yi, H., Eichelbaum, K., Föhr, S., Fischer, B., You, K. T., Castello, A., Krijgsveld, J., Hentze, M. W., and Kim, V. N. (2013). The RNA-binding protein repertoire of embryonic stem cells. *Nature Structural & Molecular Biology* 20, 1122–1130. doi: 10.1038/nsmb.2638.

Labun, K., Montague, T. G., Gagnon, J. A., Thyme, S. B., and Valen, E. (2016). CHOPCHOP v2: a web tool for the next generation of CRISPR genome engineering. *Nucleic Acids Research* 44, W272–W276. doi: 10.1093/nar/gkw398.

Lacoste, A., Berenshteyn, F., and Brivanlou, A. H. (2009). An Efficient and Reversible Transposable System for Gene Delivery and Lineage-Specific Differentiation in Human Embryonic Stem Cells. *Cell Stem Cell* 5, 332–342. doi: 10.1016/j.stem.2009.07.011.

Landthaler, M., Gaidatzis, D., Rothballer, A., Chen, P. Y., Soll, S. J., Dinic, L., Ojo, T., Hafner, M., Zavolan, M., and Tuschl, T. (2008). Molecular characterization of human Argonaute-containing ribonucleoprotein complexes and their bound target mRNAs. *RNA* 14, 2580–2596. doi: 10.1261/rna.1351608.

Lau, C., Aubry, M., Musso, D., Teissier, A., Paulous, S., Desprès, P., de-Lamballerie, X., Pastorino, B., Cao-Lormeau, V.-M., and Weinstein, P. (2017). New evidence for endemic circulation of Ross River virus in the Pacific Islands and the potential for emergence. *International Journal of Infectious Diseases* 57, 73–76. doi: 10.1016/j.ijid.2017.01.041.

Law, L. M. J., Razooky, B. S., Li, M. M. H., You, S., Jurado, A., Rice, C. M., and MacDonald, M. R. (2019). ZAP's stress granule localization is correlated with its antiviral activity and induced by virus replication. *PLoS Pathogens* 15, e1007798. doi: 10.1371/journal.ppat.1007798.

Lazear, H. M., Schoggins, J. W., and Diamond, M. S. (2019). Shared and Distinct Functions of Type I and Type III Interferons. *Immunity* 50, 907–923. doi: 10.1016/j.immuni.2019.03.025.

Lee, H., Komano, J., Saitoh, Y., Yamaoka, S., Kozaki, T., Misawa, T., Takahama, M., Satoh, T., Takeuchi, O., Yamamoto, N., Matsuura, Y., Saitoh, T., and Akira, S. (2013). Zinc-finger antiviral protein mediates retinoic acid inducible gene I-like receptor-independent antiviral response to murine leukemia virus. *PNAS* 110, 12379–12384. doi: 10.1073/pnas.1310604110.

Lee, M. W., Lee, E. Y., Lai, G. H., Kennedy, N. W., Posey, A. E., Xian, W., Ferguson, A. L., Hill, R. B., and Wong, G. C. L. (2017). Molecular Motor Dnm1 Synergistically Induces Membrane Curvature To Facilitate Mitochondrial Fission. *ACS Central Science* 3, 1156–1167. doi: 10.1021/acscentsci.7b00338.

Lee, M. W., Luo, E. W.-C., Silvestre-Roig, C., Srinivasan, Y., Akabori, K., Lemnitzer, P., Schmidt, N. W., Lai, G. H., Santangelo, C. D., Soehnlein, O., and Wong, G. C. L. (2021). Apolipoprotein Mimetic Peptide Inhibits Neutrophil-Driven Inflammatory Damage via Membrane Remodeling and Suppression of Cell Lysis. *ACS Nano* 15, 15930–15939. doi: 10.1021/acsnano.1c03978.

Lee, N.-R., Kim, H.-I., Choi, M.-S., Yi, C.-M., and Inn, and K.-S. (2015a). Regulation of MDA5-MAVS Antiviral Signaling Axis by TRIM25 through TRAF6-Mediated NF-κB Activation. *Molecules and Cells* 38, 759–764. doi: 10.14348/molcells.2015.0047.

Lee, S. R., Pratt, G. A., Martinez, F. J., Yeo, G. W., and Lykke-Andersen, J. (2015b). Target Discrimination in Nonsense-Mediated mRNA Decay Requires Upf1 ATPase Activity. *Molecular Cell* 59, 413–425. doi: 10.1016/j.molcel.2015.06.036.

Li, B., Zhu, L., Lu, C., Wang, C., Wang, H., Jin, H., Ma, X., Cheng, Z., Yu, C., Wang, S., Zuo, Q., Zhou, Y., Wang, J., Yang, C., Lv, Y., Jiang, L., and Qin, W. (2021a). circNDUFB2 inhibits non-small cell lung cancer progression via destabilizing IGF2BPs and activating anti-tumor immunity. *Nature Communications* 12, 295. doi: 10.1038/s41467-020-20527-z.

Li, C., Han, T., Li, Q., Zhang, M., Guo, R., Yang, Y., Lu, W., Li, Z., Peng, C., Wu, P., Tian, X., Wang, Q., Wang, Y., Zhou, V., Han, Z., Li, H., Wang, F., and Hu, R. (2021b). MKRN3-mediated ubiquitination of Poly(A)-binding proteins modulates the stability and translation of GNRH1 mRNA in mammalian puberty. *Nucleic Acids Research* 49, 3796–3813. doi: 10.1093/nar/gkab155.

Li, J., Ding, S. C., Cho, H., Chung, B. C., Gale, M., Chanda, S. K., and Diamond, M. S. (2013). A Short Hairpin RNA Screen of Interferon-Stimulated Genes Identifies a Novel Negative Regulator of the Cellular Antiviral Response. *mBio* 4, e00385–13. doi: 10.1128/mBio.00385-13.

Li, M. M. H., Aguilar, E. G., Michailidis, E., Pabon, J., Park, P., Wu, X., de Jong, Y. P., Schneider, W. M., Molina, H., Rice, C. M., and MacDonald, M. R. (2019). Characterization of Novel Splice Variants of Zinc Finger Antiviral Protein (ZAP). *Journal of Virology* 93, e00715-19, /jvi/93/18/JVI.00715-19.atom. doi: 10.1128/JVI.00715-19.

Li, M. M. H., Lau, Z., Cheung, P., Aguilar, E. G., Schneider, W. M., Bozzacco, L., Molina, H., Buehler, E., Takaoka, A., Rice, C. M., Felsenfeld, D. P., and MacDonald, M. R. (2017). TRIM25 Enhances the Antiviral Action of Zinc-Finger Antiviral Protein (ZAP). *PLoS Pathogens* 13, e1006145. doi: 10.1371/journal.ppat.1006145.

●● **This study utilized a genome-wide siRNA screen in the presence of overexpressed ZAP and was the first to identify TRIM25 as a critical ZAP co-factor**

Li, M., Yan, K., Wei, L., Yang, J., Lu, C., Xiong, F., Zheng, C., and Xu, W. (2015). Zinc finger antiviral protein inhibits coxsackievirus B3 virus replication and protects against viral myocarditis. *Antiviral Research* 123, 50–61. doi: 10.1016/j.antiviral.2015.09.001.

Li, W., Bengtson, M. H., Ulbrich, A., Matsuda, A., Reddy, V. A., Orth, A., Chanda, S. K., Batalov, S., and Joazeiro, C. A. P. (2008). Genome-Wide and Functional Annotation of Human E3 Ubiquitin Ligases Identifies MULAN, a Mitochondrial E3 that Regulates the Organelle's Dynamics and Signaling. *PLoS ONE* 3, e1487. doi: 10.1371/journal.pone.0001487.

Li, X.-D., Deng, C.-L., Ye, H.-Q., Zhang, H.-L., Zhang, Q.-Y., Chen, D.-D., Zhang, P.-T., Shi, P.-Y., Yuan, Z.-M., and Zhang, B. (2016). Transmembrane Domains of NS2B Contribute to both Viral RNA Replication and Particle Formation in Japanese Encephalitis Virus. *Journal of Virology* 90, 5735–5749. doi: 10.1128/JVI.00340-16.

Lian, H., Wei, J., Zang, R., Ye, W., Yang, Q., Zhang, X.-N., Chen, Y.-D., Fu, Y.-Z., Hu, M.-M., Lei, C.-Q., Luo, W.-W., Li, S., and Shu, H.-B. (2018a). ZCCHC3 is a co-sensor of cGAS for dsDNA recognition in innate immune response. *Nature Communications* 9, 3349. doi: 10.1038/s41467-018-05559-w.

Lian, H., Zang, R., Wei, J., Ye, W., Hu, M.-M., Chen, Y.-D., Zhang, X.-N., Guo, Y., Lei, C.-Q., Yang, Q., Luo, W.-W., Li, S., and Shu, H.-B. (2018b). The Zinc-Finger Protein ZCCHC3 Binds RNA and Facilitates Viral RNA Sensing and Activation of the RIG-I-like Receptors. *Immunity* 49, 438-448.e5. doi: 10.1016/j.immuni.2018.08.014.

Liang, Y., Nandakumar, K. S., and Cheng, K. (2020). Design and pharmaceutical applications of proteolysis-targeting chimeric molecules. *Biochemical Pharmacology* 182, 114211. doi: 10.1016/j.bcp.2020.114211.

Liao, Y., Goraya, M. U., Yuan, X., Zhang, B., Chiu, S.-H., and Chen, J.-L. (2019). Functional Involvement of Interferon-Inducible Transmembrane Proteins in Antiviral Immunity. *Frontiers in Microbiology* 10, 1097. doi: 10.3389/fmicb.2019.01097.

Lim, K. L., Chew, K. C. M., Tan, J. M. M., Wang, C., Chung, K. K. K., Zhang, Y., Tanaka, Y., Smith, W., Engelender, S., Ross, C. A., Dawson, V. L., and Dawson, T. M. (2005). Parkin Mediates Nonclassical, Proteasomal-Independent Ubiquitination of Synphilin-1: Implications for Lewy Body Formation. *Journal of Neuroscience* 25, 2002–2009. doi: 10.1523/JNEUROSCI.4474-04.2005.

Lin, Y.-T., Chiweshe, S., McCormick, D., Raper, A., Wickenhagen, A., DeFillipis, V., Gaunt, E., Simmonds, P., Wilson, S. J., and Grey, F. (2020). Human cytomegalovirus evades ZAP detection by suppressing CpG

dinucleotides in the major immediate early 1 gene. *PLoS Pathogens* 16, e1008844. doi: 10.1371/journal.ppat.1008844.

●● **This study showed that TRIM25 regulates ZAP alternative splicing, inducing higher expression of ZAPS during HCMV infection.**

Lipowsky, R. (2022). Remodeling of Membrane Shape and Topology by Curvature Elasticity and Membrane Tension. *Advanced Biology (Weinh)* 6, e2101020. doi: 10.1002/adbi.202101020.

Liu, C.-H., Zhou, L., Chen, G., and Krug, R. M. (2015). Battle between influenza A virus and a newly identified antiviral activity of the PARP-containing ZAPL protein. *PNAS* 112, 14048–14053. doi: 10.1073/pnas.1509745112.

Liu, Y., Liu, K., Huang, Y., Sun, M., Tian, Q., Zhang, S., and Qin, Y. (2020a). TRIM25 Promotes TNF-α–Induced NF-κB Activation through Potentiating the K63-Linked Ubiquitination of TRAF2. *Journal of Immunology* 204, 1499–1507. doi: 10.4049/jimmunol.1900482.

Liu, Y., Tao, S., Liao, L., Li, Y., Li, H., Li, Z., Lin, L., Wan, X., Yang, X., and Chen, L. (2020b). TRIM25 promotes the cell survival and growth of hepatocellular carcinoma through targeting Keap1-Nrf2 pathway. *Nature Communications* 11, 348. doi: 10.1038/s41467-019-14190-2.

Luo, X., Wang, X., Gao, Y., Zhu, J., Liu, S., Gao, G., and Gao, P. (2020). Molecular Mechanism of RNA Recognition by Zinc-Finger Antiviral Protein. *Cell Reports* 30, 46-52. doi: 10.1016/j.celrep.2019.11.116.

●● **This was one of two studies to show NZAP complexed with CpG-rich RNA, identifying key residues involved in CpG recognition.**

Luu, A. P., Yao, Z., Ramachandran, S., Azzopardi, S. A., Miles, L. A., Schneider, W. M., Hoffmann, H.-H., Bozzacco, L., Garcia, G., Gong, D., Damoiseaux, R., Tang, H., Morizono, K., Rudin, C. M., Sun, R., Arumugaswami, V., Poirier, J. T., MacDonald, M. R., Rice, C. M., and Li, M. M. H. (2021). A CRISPR Activation Screen Identifies an Atypical Rho GTPase That Enhances Zika Viral Entry. *Viruses* 13, 2113. doi: 10.3390/v13112113.

Ma, H., Kim, A. S., Kafai, N. M., Earnest, J. T., Shah, A. P., Case, J. B., Basore, K., Gilliland, T. C., Sun, C., Nelson, C. A., Thackray, L. B., Klimstra, W. B., Fremont, D. H., and Diamond, M. S. (2020). LDLRAD3 is a receptor for Venezuelan equine encephalitis virus. *Nature* 588, 308–314. doi: 10.1038/s41586-020-2915-3.

Malfavon-Borja, R., Sawyer, S. L., Wu, L. I., Emerman, M., and Malik, H. S. (2013). An Evolutionary Screen Highlights Canonical and Noncanonical Candidate Antiviral Genes within the Primate TRIM Gene Family. *Genome Biology and Evolution* 5, 2141–2154. doi: 10.1093/gbe/evt163.

Mao, R., Nie, H., Cai, D., Zhang, J., Liu, H., Yan, R., Cuconati, A., Block, T. M., Guo, J.-T., and Guo, H. (2013). Inhibition of Hepatitis B Virus Replication by the Host Zinc Finger Antiviral Protein. *PLoS Pathogens* 9, e1003494. doi: 10.1371/journal.ppat.1003494.

Mark, K. G., Loveless, T. B., and Toczyski, D. P. (2016). Isolation of ubiquitinated substrates by tandem affinity purification of E3 ligase–polyubiquitin-binding domain fusions (ligase traps). *Nature Protocols* 11, 291–301. doi: 10.1038/nprot.2016.008.

Markvoort, A. J., and Marrink, S. J. (2011). Lipid acrobatics in the membrane fusion arena. *Current Topics in Membranes* 68, 259–294. doi: 10.1016/B978-0-12-385891-7.00011-8.

Martens, S., and McMahon, H. T. (2008). Mechanisms of membrane fusion: disparate players and common principles. *Nature Reviews Molecular Cell Biology* 9, 543–556. doi: 10.1038/nrm2417.

Martín-Vicente, M., Medrano, L. M., Resino, S., García-Sastre, A., and Martínez, I. (2017). TRIM25 in the Regulation of the Antiviral Innate Immunity. *Frontiers in Immunology* 8, 1187. doi: 10.3389/ fimmu.2017.01187.

Mátyási, B., Farkas, Z., Kopper, L., Sebestyén, A., Boissan, M., Mehta, A., and Takács-Vellai, K. (2020). The Function of NM23-H1/NME1 and Its Homologs in Major Processes Linked to Metastasis. *Pathology & Oncology Research* 26, 49–61. doi: 10.1007/s12253-020-00797-0.

Mayank, A. K., Pandey, V., Vashisht, A. A., Barshop, W. D., Rayatpisheh, S., Sharma, T., Haque, T., Powers, D. N., and Wohlschlegel, J. A. (2019). An Oxygen-Dependent Interaction between FBXL5 and the CIA-Targeting Complex Regulates Iron Homeostasis. *Molecular Cell* 75, 382-393.e5. doi: 10.1016/j.molcel.2019.05.020.

McMahon, H. T., and Gallop, J. L. (2005). Membrane curvature and mechanisms of dynamic cell membrane remodelling. *Nature* 438, 590–596. doi: 10.1038/nature04396.

Meagher, J. L., Takata, M., Gonçalves-Carneiro, D., Keane, S. C., Rebendenne, A., Ong, H., Orr, V. K., MacDonald, M. R., Stuckey, J. A., Bieniasz, P. D., and Smith, J. L. (2019). Structure of the zinc-finger antiviral protein in complex with RNA reveals a mechanism for selective targeting of CG-rich viral sequences. *PNAS* 116, 24303–24309. doi: 10.1073/ pnas.1913232116.
●● This was the other of two studies to show NZAP complexed with CpG-rich RNA.

Melchior, J. T., Street, S. E., Vaisar, T., Hart, R., Jerome, J., Kuklenyik, Z., Clouet-Foraison, N., Thornock, C., Bedi, S., Shah, A. S., Segrest, J. P., Heinecke, J. W., and Davidson, W. S. (2021). Apolipoprotein A-I modulates HDL particle size in the absence of apolipoprotein A-II. *Journal of Lipid Research* 62, 100099. doi: 10.1016/j.jlr.2021.100099.

Melki, I., and Frémond, M.-L. (2020). Type I Interferonopathies: from a Novel Concept to Targeted Therapeutics. *Current Rheumatology Reports* 22, 32. doi: 10.1007/s11926-020-00909-4.

Meroni, G. (2020). TRIM E3 Ubiquitin Ligases in Rare Genetic Disorders. *Proteostasis and Disease* 1233, 311–325. doi: 10.1007/978-3-030-38266-7_14.

Meroni, G., and Desagher, S. (2022). Cellular Function of TRIM E3 Ubiquitin Ligases in Health and Disease. *Cells* 11, 250. doi: 10.3390/cells11020250.

Messina, J. P., Brady, O. J., Golding, N., Kraemer, M. U. G., Wint, G. R. W., Ray, S. E., Pigott, D. M., Shearer, F. M., Johnson, K., Earl, L., Marczak, L. B., Shirude, S., Davis Weaver, N., Gilbert, M., Velayudhan, R., Jones, P., Jaenisch, T., Scott, T. W., Reiner, R. C., and Hay, S. I. (2019). The current and future global distribution and population at risk of dengue. *Nature Microbiology* 4, 1508–1515. doi: 10.1038/s41564-019-0476-8.

Metzger, M. B., Hristova, V. A., and Weissman, A. M. (2012). HECT and RING finger families of E3 ubiquitin ligases at a glance. *Journal of Cell Science* 125, 531–537. doi: 10.1242/jcs.091777.

Meyerson, N. R., Zhou, L., Guo, Y. R., Zhao, C., Tao, Y. J., Krug, R. M., and Sawyer, S. L. (2017). Nuclear TRIM25 Specifically Targets Influenza Virus Ribonucleoproteins to Block the Onset of RNA Chain Elongation. *Cell Host & Microbe* 22, 627-638. doi: 10.1016/j.chom.2017.10.003.

Mishra, A., Gordon, V. D., Yang, L., Coridan, R., and Wong, G. C. L. (2008). HIV TAT Forms Pores in Membranes by Inducing Saddle-Splay Curvature: Potential Role of Bidentate Hydrogen Bonding. *Angewandte Chemie International Edition* 47, 2986–2989. doi: 10.1002/anie.200704444.

Mishra, A., Lai, G. H., Schmidt, N. W., Sun, V. Z., Rodriguez, A. R., Tong, R., Tang, L., Cheng, J., Deming, T. J., Kamei, D. T., and Wong, G. C. L. (2011). Translocation of HIV TAT peptide and analogues induced by multiplexed membrane and cytoskeletal interactions. *PNAS* 108, 16883–16888. doi: 10.1073/pnas.1108795108.

Moldovan, J. B., and Moran, J. V. (2015). The Zinc-Finger Antiviral Protein ZAP Inhibits LINE and Alu Retrotransposition. *PLoS Genetics* 11, e1005121. doi: 10.1371/journal.pgen.1005121.

Morrison, T. E., Whitmore, A. C., Shabman, R. S., Lidbury, B. A., Mahalingam, S., and Heise, M. T. (2006). Characterization of Ross River Virus Tropism and Virus-Induced Inflammation in a Mouse Model of Viral Arthritis and Myositis. *Journal of Virology* 80, 737–749. doi: 10.1128/JVI.80.2.737-749.2006.

Muller, S., Moller, P., Bick, M. J., Wurr, S., Becker, S., Gunther, S., and Kummerer, B. M. (2007). Inhibition of Filovirus Replication by the Zinc Finger Antiviral Protein. *Journal of Virology* 81, 2391–2400. doi: 10.1128/JVI.01601-06.

Nakasato, N., Ikeda, K., Urano, T., Horie-Inoue, K., Takeda, S., and Inoue, S. (2006). A ubiquitin E3 ligase Efp is up-regulated by interferons and conjugated with ISG15. *Biochemical and Biophysical Research Communications* 351, 540–546. doi: 10.1016/j.bbrc.2006.10.061.

Nchioua, R., Kmiec, D., Müller, J., Conzelmann, C., Groß, R., Swanson, C., Neil, S., Stenger, S., Sauter, D., Münch, J., Sparrer, K. M. J., and Kirchhoff, F. (2020). The Zinc Finger Antiviral Protein restricts SARS-CoV-2. *bioRxiv*, 2020.06.04.134379. doi: 10.1101/2020.06.04.134379.

NIAID Emerging Infectious Diseases/ Pathogens | NIH: National Institute of Allergy and Infectious Diseases Available at: https://www.niaid.nih.gov/research/emerging-infectious-diseases-pathogens [Accessed June 13, 2022].

Nomura, K., Klejnot, M., Kowalczyk, D., Hock, A. K., Sibbet, G. J., Vousden, K. H., and Huang, D. T. (2017). Structural analysis of MDM2 RING separates degradation from regulation of p53 transcription activity. *Nature Structural & Molecular Biology* 24, 578–587. doi: 10.1038/nsmb.3414.
●● This study served as the basis for identifying the TRIM25 R54P mutation.

Nosé, S. (1984). A unified formulation of the constant temperature molecular dynamics methods. *Journal of Chemical Physics* 81, 511–519. doi: 10.1063/1.447334.

OhAinle, M., Helms, L., Vermeire, J., Roesch, F., Humes, D., Basom, R., Delrow, J. J., Overbaugh, J., and Emerman, M. (2018). A virus-packageable CRISPR screen identifies host factors mediating interferon inhibition of HIV. *eLife* 7, e39823. doi: 10.7554/eLife.39823.

Ohkubo, Y. Z., Pogorelov, T. V., Arcario, M. J., Christensen, G. A., and Tajkhorshid, E. (2012). Accelerating Membrane Insertion of Peripheral Proteins with a Novel Membrane Mimetic Model. *Biophysical Journal* 102, 2130–2139. doi: 10.1016/j.bpj.2012.03.015.

Okamoto, M., Kouwaki, T., Fukushima, Y., and Oshiumi, H. (2018). Regulation of RIG-I Activation by K63-Linked Polyubiquitination. *Frontiers in Immunology* 8, 1942. doi: 10.3389/fimmu.2017/01942.

Oshiumi, H. (2020). Recent Advances and Contradictions in the Study of the Individual Roles of Ubiquitin Ligases That Regulate RIG-I-Like Receptor-Mediated Antiviral Innate Immune Responses. *Frontiers in Immunology* 11, 1296. doi: 10.3389/fimmu.2020.01296.

Oshiumi, H., Miyashita, M., Matsumoto, M., and Seya, T. (2013). A Distinct Role of Riplet-Mediated K63-Linked Polyubiquitination of the RIG-I Repressor Domain in Human Antiviral Innate Immune Responses. *PLoS Pathogens* 9, e1003533. doi: 10.1371/journal.ppat.1003533.

Ozato, K., Shin, D.-M., Chang, T.-H., and Morse, H. C. (2008). TRIM family proteins and their emerging roles in innate immunity. *Nature Reviews Immunology* 8, 849–860. doi: 10.1038/nri2413.

Pallett, M. A., Lu, Y., and Smith, G. L. (2022). DDX50 Is a Viral Restriction Factor That Enhances IRF3 Activation. *Viruses* 14, 316. doi: 10.3390/v14020316.

Pan, Z., Zhao, R., Li, B., Qi, Y., Qiu, W., Guo, Q., Zhang, S., Zhao, S., Xu, H., Li, M., Gao, Z., Fan, Y., Xu, J., Wang, H., Wang, S., Qiu, J., Wang, Q., Guo, X., Deng, L., Zhang, P., Xue, H., and Li, G. (2022). EWSR1-induced circNEIL3 promotes glioma progression and exosome-mediated macrophage immunosuppressive polarization via stabilizing IGF2BP3. *Molecular Cancer* 21, 16. doi: 10.1186/s12943-021-01485-6.

Panas, M. D., Schulte, T., Thaa, B., Sandalova, T., Kedersha, N., Achour, A., and McInerney, G. M. (2015). Viral and Cellular Proteins Containing FGDF Motifs Bind G3BP to Block Stress Granule Formation. *PLoS Pathogens* 11, e1004659. doi: 10.1371/journal.ppat.1004659.

Parrinello, M., and Rahman, A. (1981). Polymorphic transitions in single crystals: A new molecular dynamics method. *Journal of Applied Physics* 52, 7182–7190. doi: 10.1063/1.328693.

Pazo, A., Pérez-González, A., Oliveros, J. C., Huarte, M., Chavez, J. P., and Nieto, A. (2019). hCLE/RTRAF-HSPC117-DDX1-FAM98B: A New Cap-Binding Complex That Activates mRNA Translation. *Frontiers in Physiology* 10, 92. doi: 10.3389/fphys.2019.00092.

Peisley, A., Wu, B., Xu, H., Chen, Z. J., and Hur, S. (2014). Structural basis for ubiquitin-mediated antiviral signal activation by RIG-I. *Nature* 509, 110–114. doi: 10.1038/nature13140.

Pérez-González, A., Pazo, A., Navajas, R., Ciordia, S., Rodriguez-Frandsen, A., and Nieto, A. (2014). hCLE/C14orf166 Associates with DDX1-HSPC117-FAM98B in a Novel Transcription-Dependent Shuttling RNA-Transporting Complex. *PLoS ONE* 9, e90957. doi: 10.1371/journal.pone.0090957.

Perez-Riverol, Y., Bai, J., Bandla, C., García-Seisdedos, D., Hewapathirana, S., Kamatchinathan, S., Kundu, D. J., Prakash, A., Frericks-Zipper, A., Eisenacher, M., Walzer, M., Wang, S., Brazma, A., and Vizcaíno, J. A. (2022). The PRIDE database resources in 2022: a hub for mass spectrometry-based proteomics evidences. *Nucleic Acids Research* 50, D543–D552. doi: 10.1093/nar/gkab1038.

Pettersen, E. F., Goddard, T. D., Huang, C. C., Couch, G. S., Greenblatt, D. M., Meng, E. C., and Ferrin, T. E. (2004). UCSF Chimera—A visualization system for exploratory research and analysis. *Journal of Computational Chemistry* 25, 1605–1612. doi: 10.1002/jcc.20084.

Pierson, T. C., and Diamond, M. S. (2020). The continued threat of emerging flaviviruses. *Nature Microbiology* 5, 796–812. doi: 10.1038/s41564-020-0714-0.

Prenner, E. J., Lewis, R. N. A. H., Neuman, K. C., Gruner, S. M., Kondejewski, L. H., Hodges, R. S., and McElhaney, R. N. (1997). Nonlamellar Phases Induced by the Interaction of Gramicidin S with Lipid Bilayers. A Possible Relationship to Membrane-Disrupting Activity. *Biochemistry* 36, 7906–7916. doi: 10.1021/bi962785k.

Radivojac, P., Vacic, V., Haynes, C., Cocklin, R. R., Mohan, A., Heyen, J. W., Goebl, M. G., and Iakoucheva, L. M. (2010). Identification, analysis, and prediction of protein ubiquitination sites. *Proteins: Structure, Function, and Bioinformatics* 78, 365–380. doi: 10.1002/prot.22555.

Rajsbaum, R., García-Sastre, A., and Versteeg, G. A. (2014). TRIMmunity: The Roles of the TRIM E3-Ubiquitin Ligase Family in Innate Antiviral Immunity. *Journal of Molecular Biology* 426, 1265–1284. doi: 10.1016/j.jmb.2013.12.005.

Ran, F. A., Hsu, P. D., Wright, J., Agarwala, V., Scott, D. A., and Zhang, F. (2013). Genome engineering using the CRISPR-Cas9 system. *Nature Protocols* 8, 2281–2308. doi: 10.1038/nprot.2013.143.

Read, C. M., Plante, K., Rafael, G., Rossi, S. L., Braun, W., Weaver, S. C., and Schein, C. H. (2021). Designing multivalent immunogens for alphavirus vaccine optimization. *Virology* 561, 117–124. doi: 10.1016/j.virol.2020.11.010.

Rey, F. A., and Lok, S.-M. (2018). Common Features of Enveloped Viruses and Implications for Immunogen Design for Next-Generation Vaccines. *Cell* 172, 1319–1334. doi: 10.1016/j.cell.2018.02.054.

Rice, C. M., Levis, R., Strauss, J. H., and Huang, H. V. (1987). Production of infectious RNA transcripts from Sindbis virus cDNA clones: mapping of lethal mutations, rescue of a temperature-sensitive marker, and in vitro mutagenesis to generate defined mutants. *Journal of Virology* 61, 3809–3819.

Rodriguez, A., Pérez-González, A., and Nieto, A. (2011). Cellular Human CLE/C14orf166 Protein Interacts with Influenza Virus Polymerase and Is Required for Viral Replication. *Journal of Virology* 85, 12062. doi: 10.1128/JVI.00684-11.

Rose, P. P., Hanna, S. L., Spiridigliozzi, A., Wannissorn, N., Beiting, D. P., Ross, S. R., Hardy, R. W., Bambina, S. A., Heise, M. T., and Cherry, S. (2011). Natural Resistance-Associated Macrophage Protein Is a Cellular Receptor for Sindbis Virus in Both Insect and Mammalian Hosts. *Cell Host & Microbe* 10, 97–104. doi: 10.1016/j.chom.2011.06.009.

Rossman, J. S., and Lamb, R. A. (2013). Viral membrane scission. *Annual Review of Cell and Developmental Biology* 29, 551–569. doi: 10.1146/annurev-cellbio-101011-155838.

Rusinova, I., Forster, S., Yu, S., Kannan, A., Masse, M., Cumming, H., Chapman, R., and Hertzog, P. J. (2013). INTERFEROME v2.0: an updated database of annotated interferon-regulated genes. *Nucleic Acids Research* 41, D1040–D1046. doi: 10.1093/nar/gks1215.

Ryman, K. D., and Klimstra, W. B. (2008). Host responses to alphavirus infection. *Immunological Reviews* 225, 27–45. doi: 10.1111/j.1600-065X.2008.00670.x.

Ryman, K. D., Klimstra, W. B., Nguyen, K. B., Biron, C. A., and Johnston, R. E. (2000). Alpha/Beta Interferon Protects Adult Mice from Fatal Sindbis Virus Infection and Is an Important Determinant of Cell and Tissue Tropism. *Journal of Virology* 74, 3366–3378. doi: 10.1128/JVI.74.7.3366-3378.2000.

●● **This study demonstrated the importance of the type I IFN response in restricting the acute phase of alphavirus infection.**

Sanchez, J. G., Sparrer, K. M. J., Chiang, C., Reis, R. A., Chiang, J. J., Zurenski, M. A., Wan, Y., Gack, M. U., and Pornillos, O. (2018). TRIM25 Binds RNA to Modulate Cellular Anti-viral Defense. *Journal of Molecular Biology* 430, 5280–5293. doi: 10.1016/j.jmb.2018.10.003.

●● **This was the second study to identify an RNA binding motif within TRIM25, and the first to explicitly connect RNA binding to TRIM25 antiviral activity.**

Sato, W., Ikeda, K., Urano, T., Abe, Y., Nakasato, N., Horie-Inoue, K., Takeda, S., and Inoue, S. (2018). Efp promotes in vitro and in vivo growth of endometrial cancer cells along with the activation of nuclear factor-κB signaling. *PLoS ONE* 13, e0208351. doi: 10.1371/journal.pone.0208351.

Schlee, M., and Hartmann, G. (2016). Discriminating self from non-self in nucleic acid sensing. *Nature Reviews Immunology* 16, 566–580. doi: 10.1038/nri.2016.78.

Schmidt, N., Mishra, A., Lai, G. H., and Wong, G. C. L. (2010). Arginine-rich cell-penetrating peptides. *FEBS Letters* 584, 1806–1813. doi: 10.1016/j.febslet.2009.11.046.

Schmidt, N. W., Mishra, A., Lai, G. H., Davis, M., Sanders, L. K., Tran, D., Garcia, A., Tai, K. P., McCray, P. B., Ouellette, A. J., Selsted, M. E., and Wong, G. C. L. (2011). Criterion for amino acid composition of defensins and antimicrobial peptides based on geometry of membrane destabilization. *Journal of the American Chemical Society* 133, 6720–6727. doi: 10.1021/ja200079a.

Schmidt, N. W., Mishra, A., Wang, J., DeGrado, W. F., and Wong, G. C. L. (2013). Influenza Virus A M2 Protein Generates Negative Gaussian Membrane Curvature Necessary for Budding and Scission. *Journal of the American Chemical Society* 135, 13710–13719. doi: 10.1021/ja400146z.

Schneider, W. M., Chevillotte, M. D., and Rice, C. M. (2014). Interferon-Stimulated Genes: A Complex Web of Host Defenses. *Annual Review of Immunology* 32, 513–545. doi: 10.1146/annurev-immunol-032713-120231.

Schoggins, J. W. (2019). Interferon-Stimulated Genes: What Do They All Do? *Annual Review of Virology* 6, 567–584. doi: 10.1146/annurev-virology-092818-015756.

Schoggins, J. W., Wilson, S. J., Panis, M., Murphy, M. Y., Jones, C. T., Bieniasz, P., and Rice, C. M. (2011). A diverse range of gene products are effectors of the type I interferon antiviral response. *Nature* 472, 481–485. doi: 10.1038/nature09907.

Scholte, F. E. M., Tas, A., Albulescu, I. C., Žusinaite, E., Merits, A., Snijder, E. J., and van Hemert, M. J. (2015). Stress Granule Components G3BP1 and G3BP2 Play a Proviral Role Early in Chikungunya Virus Replication. *Journal of Virology* 89, 4457–4469. doi: 10.1128/JVI.03612-14.

Schulte, T., Liu, L., Panas, M. D., Thaa, B., Dickson, N., Götte, B., Achour, A., and McInerney, G. M. (2016). Combined structural, biochemical and cellular evidence demonstrates that both FGDF motifs in alphavirus nsP3 are required for efficient replication. *Open Biology* 6, 160078. doi: 10.1098/rsob.160078.

Schwerk, J., Soveg, F. W., Ryan, A. P., Thomas, K. R., Hatfield, L. D., Ozarkar, S., Forero, A., Kell, A. M., Roby, J. A., So, L., Hyde, J. L., Gale, M., Daugherty, M. D., and Savan, R. (2019). RNA-binding protein isoforms ZAP-S and ZAP-L have distinct antiviral and immune resolution functions. *Nature Immunology* 20, 1610–1620. doi: 10.1038/s41590-019-0527-6.

Serdar, L. D., Whiteside, D. L., and Baker, K. E. (2016). ATP hydrolysis by UPF1 is required for efficient translation termination at premature stop codons. *Nature Communications* 7, 14021. doi: 10.1038/ncomms14021.

Shaw, A. E., Hughes, J., Gu, Q., Behdenna, A., Singer, J. B., Dennis, T., Orton, R. J., Varela, M., Gifford, R. J., Wilson, S. J., and Palmarini, M. (2017). Fundamental properties of the mammalian innate immune system revealed by multispecies comparison of type I interferon responses. *PLoS Biology* 15, e2004086. doi: 10.1371/journal.pbio.2004086.

●● **This study undertook a comparative analysis of the interferomes of chicken and nine mammalian species to identified conserved ISGs among all 10 vertebrate species, identifying 62 'core' vertebrate ISGs which include TRIM25 and ZAP.**

Shi, Y., Yuan, B., Zhu, W., Zhang, R., Li, L., Hao, X., Chen, S., and Hou, F. (2017). Ube2D3 and Ube2N are essential for RIG-I-mediated MAVS aggregation in antiviral innate immunity. *Nature Communications* 8, 15138. doi: 10.1038/ncomms15138.

Siegel, D. P. (2008). The Gaussian curvature elastic energy of intermediates in membrane fusion. *Biophysical Journal* 95, 5200–5215. doi: 10.1529/biophysj.108.140152.

Silvestre-Roig, C., Braster, Q., Wichapong, K., Lee, E. Y., Teulon, J. M., Berrebeh, N., Winter, J., Adrover, J. M., Santos, G. S., Froese, A., Lemnitzer, P., Ortega-Gómez, A., Chevre, R., Marschner, J., Schumski, A., Winter, C., Perez-Olivares, L., Pan, C., Paulin, N., Schoufour, T., Hartwig, H., González-Ramos, S., Kamp, F., Megens, R. T. A., Mowen, K. A., Gunzer, M., Maegdefessel, L., Hackeng, T., Lutgens, E., Daemen, M., von Blume, J., Anders, H.-J., Nikolaev, V. O., Pellequer, J.-L., Weber, C., Hidalgo, A., Nicolaes, G. A. F., Wong, G. C. L., and Soehnlein, O. (2019). Externalized histone H4 orchestrates chronic inflammation by inducing lytic cell death. *Nature* 569, 236–240. doi: 10.1038/s41586-019-1167-6.

Song, C., Hotz-Wagenblatt, A., Voit, R., and Grummt, I. (2017). SIRT7 and the DEAD-box helicase DDX21 cooperate to resolve genomic R loops and safeguard genome stability. *Genes & Development* 31, 1370–1381. doi: 10.1101/gad.300624.117.

Stromberg, Z. R., Fischer, W., Bradfute, S. B., Kubicek-Sutherland, J. Z., and Hraber, P. (2020). Vaccine Advances against Venezuelan, Eastern, and Western Equine Encephalitis Viruses. *Vaccines (Basel)* 8, E273. doi: 10.3390/vaccines8020273.

Subramanian, G., Kuzmanovic, T., Zhang, Y., Peter, C. B., Veleeparambil, M., Chakravarti, R., Sen, G. C., and Chattopadhyay, S. (2018). A new mechanism of interferon's antiviral action: Induction of autophagy, essential for paramyxovirus replication, is inhibited by the interferon stimulated gene, TDRD7. *PLoS Pathogens* 14, e1006877. doi: 10.1371/journal.ppat.1006877.

Suzuki, T., Urano, T., Tsukui, T., Horie-Inoue, K., Moriya, T., Ishida, T., Muramatsu, M., Ouchi, Y., Sasano, H., and Inoue, S. (2005). Estrogen-Responsive Finger Protein as a New Potential Biomarker for Breast Cancer. *Clinical Cancer Research* 11, 6148–6154. doi: 10.1158/1078-0432.CCR-05-0040.

Takata, M. A., Gonçalves-Carneiro, D., Zang, T. M., Soll, S. J., York, A., Blanco-Melo, D., and Bieniasz, P. D. (2017). CG dinucleotide suppression enables antiviral defence targeting non-self RNA. *Nature* 550, 124–127. doi: 10.1038/nature24039.

●● **This was the first study to demonstrate ZAP preference for CpG-rich RNA. The authors engineered a CpG-high HIV-1 strain and demonstrated stronger ZAP inhibition of this strain.**

Takayama, K., Suzuki, T., Tanaka, T., Fujimura, T., Takahashi, S., Urano, T., Ikeda, K., and Inoue, S. (2018). TRIM25 enhances cell growth and cell survival by modulating p53 signals via interaction with G3BP2 in prostate cancer. *Oncogene* 37, 2165–2180. doi: 10.1038/s41388-017-0095-x.

Tenchov, B. G., MacDonald, R. C., and Lentz, B. R. (2013). Fusion Peptides Promote Formation of Bilayer Cubic Phases in Lipid Dispersions. An X-Ray Diffraction Study. *Biophysical Journal* 104, 1029–1037. doi: 10.1016/j.bpj.2012.12.034.

Thorsen, M. K., Lai, A., Lee, M. W., Hoogerheide, D. P., Wong, G. C. L., Freed, J. H., and Heldwein, E. E. (2021). Highly Basic Clusters in the Herpes Simplex Virus 1 Nuclear Egress Complex Drive Membrane Budding by Inducing Lipid Ordering. *mBio* 12, e01548-21. doi: 10.1128/mBio.01548-21.

Todorova, T., Bock, F. J., and Chang, P. (2014). PARP13 regulates cellular mRNA post-transcriptionally and functions as a pro-apoptotic factor by destabilizing TRAILR4 transcript. *Nature Communications* 5, 5362. doi: 10.1038/ncomms6362.

Tong, J., Zhang, W., Chen, Y., Yuan, Q., Qin, N.-N., and Qu, G. (2022). The Emerging Role of RNA Modifications in the Regulation of Antiviral Innate Immunity. *Frontiers in Microbiology* 13, 845625. doi: 10.3389/fmicb.2022.845625.

Tourrière, H., Chebli, K., Zekri, L., Courselaud, B., Blanchard, J. M., Bertrand, E., and Tazi, J. (2003). The RasGAP-associated endoribonuclease G3BP assembles stress granules. *Journal of Cell Biology* 160, 823–831. doi: 10.1083/jcb.200212128.

Ullah, R., Li, J., Fang, P., Xiao, S., and Fang, L. (2022). DEAD/H-box helicases: Anti-viral and pro-viral roles during infections. *Virus Research* 309, 198658. doi: 10.1016/j.virusres.2021.198658.

Urano, T., Saito, T., Tsukui, T., Fujita, M., Hosoi, T., Muramatsu, M., Ouchi, Y., and Inoue, S. (2002). Efp targets 14-3-3j for proteolysis and promotes breast tumour growth. *Nature* 417, 871–875. doi: 10.1038/nature00826.

van Gent, M., Sparrer, K. M. J., and Gack, M. U. (2018). TRIM Proteins and Their Roles in Antiviral Host Defenses. *Annual Review of Virology* 5, 385–405. doi: 10.1146/annurev-virology-092917-043323.

Vigant, F., Santos, N. C., and Lee, B. (2015). Broad-spectrum antivirals against viral fusion. *Nature Reviews Microbiology* 13, 426–437. doi: 10.1038/nrmicro3475.

Virtanen, P., Gommers, R., Oliphant, T. E., Haberland, M., Reddy, T., Cournapeau, D., Burovski, E., Peterson, P., Weckesser, W., Bright, J., van der Walt, S. J., Brett, M., Wilson, J., Millman, K. J., Mayorov, N., Nelson, A. R. J., Jones, E., Kern, R., Larson, E., Carey, C. J., Polat, İ., Feng, Y., Moore, E. W., VanderPlas, J., Laxalde, D., Perktold, J., Cimrman, R., Henriksen, I., Quintero, E. A., Harris, C. R., Archibald, A. M., Ribeiro, A. H., Pedregosa, F., and van Mulbregt, P. (2020). SciPy 1.0: fundamental algorithms for scientific computing in Python. *Nature Methods* 17, 261–272. doi: 10.1038/s41592-019-0686-2.

Vunjak, M., and Versteeg, G. A. (2019). TRIM proteins. *Current Biology* 29, R42–R44. doi: 10.1016/j.cub.2018.11.026.

Wang, H., and Wang, C. (2022). Peptide-Based Dual HIV and Coronavirus Entry Inhibitors. *Virus Entry Inhibitors* 1366, 87–100. doi: 10.1007/978-981-16-8702-0_6.

Wang, L.-F., and Anderson, D. E. (2019). Viruses in bats and potential spillover to animals and humans. *Current Opinion in Virology* 34, 79–89. doi: 10.1016/j.coviro.2018.12.007.

Wang, S., Yu, M., Liu, A., Bao, Y., Qi, X., Gao, L., Chen, Y., Liu, P., Wang, Y., Xing, L., Meng, L., Zhang, Y., Fan, L., Li, X., Pan, Q., Zhang, Y., Cui, H., Li, K., Liu, C., He, X., Gao, Y., and Wang, X. (2021). TRIM25 inhibits infectious bursal disease virus replication by targeting VP3 for ubiquitination and degradation. *PLoS Pathogens* 17, e1009900. doi: 10.1371/journal.ppat.1009900.

Wang, X., Lv, F., and Gao, G. (2010). Mutagenesis analysis of the zinc-finger antiviral protein. *Retrovirology* 7, 19. doi: 10.1186/1742-4690-7-19.

Wang, X., Tu, F., Zhu, Y., and Gao, G. (2012). Zinc-Finger Antiviral Protein Inhibits XMRV Infection. *PLoS ONE* 7, e39159. doi: 10.1371/journal.pone.0039159.

Waskom, M. L. (2021). seaborn: statistical data visualization. *Journal of Open Source Software* 6, 3021. doi: 10.21105/joss.03021.

Weaver, S. C., and Lecuit, M. (2015). Chikungunya Virus and the Global Spread of a Mosquito-Borne Disease. *New England Journal of Medicine* 372, 1231–1239. doi: 10.1056/NEJMra1406035.

Weaver, S. C., Winegar, R., Manger, I. D., and Forrester, N. L. (2012). Alphaviruses: Population genetics and determinants of emergence. *Antiviral Research* 94, 242–257. doi: 10.1016/j.antiviral.2012.04.002.

Welsch, S., Müller, B., and Kräusslich, H.-G. (2007). More than one door - Budding of enveloped viruses through cellular membranes. *FEBS Letters* 581, 2089–2097. doi: 10.1016/j.febslet.2007.03.060.

Wigington, C. P., Williams, K. R., Meers, M. P., Bassell, G. J., and Corbett, A. H. (2014). Poly(A) RNA-binding proteins and polyadenosine RNA: new members and novel functions. *WIREs RNA* 5, 601–622. doi: 10.1002/wrna.1233.

Williams, F. P., Haubrich, K., Perez-Borrajero, C., and Hennig, J. (2019). Emerging RNA-binding roles in the TRIM family of ubiquitin ligases. *Biological Chemistry* 400, 1443–1464. doi: 10.1515/hsz-2019-0158.

Woodard, L. E., and Wilson, M. H. (2015). piggyBac-ing models and new therapeutic strategies. *Trends in Biotechnology* 33, 525–533. doi: 10.1016/j.tibtech.2015.06.009.

Xue, G., Braczyk, K., Gonçalves-Carneiro, D., Dawidziak, D. M., Sanchez, K., Ong, H., Wan, Y., Zadrozny, K. K., Ganser-Pornillos, B. K., Bieniasz, P. D., and Pornillos, O. (2022). Poly(ADP-ribose) potentiates ZAP antiviral activity. *PLoS Pathogens* 18, e1009202. doi: 10.1371/journal.ppat.1009202.

Yan, N., Cherepanov, P., Daigle, J. E., Engelman, A., and Lieberman, J. (2009). The SET Complex Acts as a Barrier to Autointegration of HIV-1. *PLoS Pathogens* 5, e1000327. doi: 10.1371/journal.ppat.1000327.

Yang, E., and Li, M. M. H. (2020). All About the RNA: Interferon-Stimulated Genes That Interfere With Viral RNA Processes. *Frontiers in Immunology* 11, 605024. doi: 10.3389/fimmu.2020.605024.

Yang, Z., Lasker, K., Schneidman-Duhovny, D., Webb, B., Huang, C. C., Pettersen, E. F., Goddard, T. D., Meng, E. C., Sali, A., and Ferrin, T. E. (2012). UCSF Chimera, MODELLER, and IMP: An integrated modeling system. *Journal of Structural Biology* 179, 269–278. doi: 10.1016/j.jsb.2011.09.006.

Yao, H., Lee, M. W., Waring, A. J., Wong, G. C. L., and Hong, M. (2015). Viral fusion protein transmembrane domain adopts β-strand structure to facilitate membrane topological changes for virus–cell fusion. *PNAS* 112, 10926–10931. doi: 10.1073/pnas.1501430112.

Ye, P., Liu, S., Zhu, Y., Chen, G., and Gao, G. (2010). DEXH-Box protein DHX30 is required for optimal function of the zinc-finger antiviral protein. *Protein Cell* 1, 956–964. doi: 10.1007/s13238-010-0117-8.

Youn, J.-Y., Dunham, W. H., Hong, S. J., Knight, J. D. R., Bashkurov, M., Chen, G. I., Bagci, H., Rathod, B., MacLeod, G., Eng, S. W. M., Angers, S., Morris, Q., Fabian, M., Côté, J.-F., and Gingras, A.-C. (2018). High-Density Proximity Mapping Reveals the Subcellular Organization of mRNA-Associated Granules and Bodies. *Molecular Cell* 69, 517-532. doi: 10.1016/j.molcel.2017.12.020.

Zaccara, S., Ries, R. J., and Jaffrey, S. R. (2019). Reading, writing and erasing mRNA methylation. *Nature Reviews Molecular Cell Biology* 20, 608–624. doi: 10.1038/s41580-019-0168-5.

Zang, H., Ren, S., Cao, H., and Tian, X. (2017). The ubiquitin ligase TRIM25 inhibits hepatocellular carcinoma progression by targeting metastasis associated 1 protein. *IUBMB Life* 69, 795–801. doi: 10.1002/iub.1661.

Zeng, W., Sun, L., Jiang, X., Chen, X., Hou, F., Adhikari, A., Xu, M., and Chen, Z. J. (2010). Reconstitution of the RIG-I Pathway Reveals a Signaling Role of Unanchored Polyubiquitin Chains in Innate Immunity. *Cell* 141, 315–330. doi: 10.1016/j.cell.2010.03.029.

Zhang, R., Kim, A. S., Fox, J. M., Nair, S., Basore, K., Klimstra, W. B., Rimkunas, R., Fong, R. H., Lin, H., Poddar, S., Crowe, J. E., Doranz, B. J., Fremont, D. H., and Diamond, M. S. (2018). Mxra8 is a receptor for multiple arthritogenic alphaviruses. *Nature* 557, 570–574. doi: 10.1038/s41586-018-0121-3.

Zhang, X.-Z., Li, F.-H., and Wang, X.-J. (2021). Regulation of Tripartite Motif-Containing Proteins on Immune Response and Viral Evasion. *Frontiers in Microbiology* 12:794882. doi: 10.3389/fmicb.2021.794882.

Zheng, X., Wang, X., Tu, F., Wang, Q., Fan, Z., and Gao, G. (2017). TRIM25 Is Required for the Antiviral Activity of Zinc Finger Antiviral Protein. *Journal of Virology* 91, e00088-17. doi: 10.1128/JVI.00088-17.

Zhu, Y., Chen, G., Lv, F., Wang, X., Ji, X., Xu, Y., Sun, J., Wu, L., Zheng, Y.-T., and Gao, G. (2011). Zinc-finger antiviral protein inhibits HIV-1 infection by selectively targeting multiply spliced viral mRNAs for degradation. *PNAS* 108, 15834–15839. doi: 10.1073/pnas.1101676108.

Zhu, Y., Wang, X., Goff, S. P., and Gao, G. (2012). Translational repression precedes and is required for ZAP-mediated mRNA decay: ZAP-mediated translational repression versus mRNA decay. *EMBO Journal* 31, 4236–4246. doi: 10.1038/emboj.2012.271.

- **This study presents a mechanism for ZAP translational inhibition via its interference with the translation initiation factors eIF4A and eIF4G.**

Zimmerberg, J., and Kozlov, M. M. (2006). How proteins produce cellular membrane curvature. *Nature Reviews Molecular Cell Biology* 7, 9–19. doi: 10.1038/nrm1784.